RICHARD ALAN BRAGG
Ph. D.

103
024
THS

Ph. D.

103
024
THS

Ph. D.

MATERIAL PROPERTIES FOR SAND-ICE STRUCTURAL SYSTEMS

Dissertation for the Degree of Ph. D.

MICHIGAN STATE UNIVERSITY
RICHARD ALAN BRAGG

1980

THESIS

3 1293 10211 7201

LIBRARY
Michigan State
University

OVERDUE FINES:
25¢ per day per item

RETURNING LIBRARY MATERIALS:
Place in book return to remo
charge from circulation reco

X-1234

ABSTRACT

MATERIAL PROPERTIES FOR
SAND-ICE STRUCTURAL SYSTEMS

By

Richard Alan Bragg

Controlled ground freezing has been profitably used as a construction aid to provide temporary support for excavations, tunnels, mine shafts, buildings experiencing severe settlement distortions, and to provide an impermeable barrier to seepage into excavations. More widespread application of frozen soil as a structurally effective material has been limited by difficulty in predicting the mechanical behavior of the soil-ice material and the influence of temperature on this behavior.

Experimental data has been obtained in an effort to define the material properties of frozen sand required for design of frozen soil structures subject to flexure. The effects of strain rate, temperature, and sample size on the compressive and tensile properties of frozen silica sand have been determined from uniaxial compression and split cylinder tests. Data are presented which describes the temperature and strain rate effects on the elastic modulus, strength, failure strain, and failure mode. Observations are presented relating the influence of machine stiffness and test system errors on the observed frozen soil behavior. Test methods used are reviewed with respect to possible standardization of test procedures for frozen soils.

To eliminate the influence of mineral composition, ice content, and soil density on the observed mechanical properties, all tests were

conducted on frozen saturated Wedron (silica) sand. Samples were prepared with a sand volume fraction of 64 percent in split aluminum molds. Uniaxial compression test samples ranging from 1.13 to 2.40 inches in diameter (length:diameter ratio of 2.0) were tested at strain rates ranging from $5 \times 10^{-7} sec^{-1}$ to $8 \times 10^{-4} sec^{-1}$ (at temperatures from -2°C to -15°C). Several uniaxial compression creep tests were conducted on 1.13 inch diameter samples. Split cylinder samples ranging from 1.94 to 4.00 inches in diameter (length: diameter ratios of 0.5), were tested at vertical deformation rates varying from 0.002 to 0.28 in/min, and temperatures ranging from -2°C to -15°C.

Results of constant strain rate compression tests indicated that the frozen sand stress-strain behavior was dependent on the applied strain rate. There was an observed transition from plastic to brittle failure as the applied strain rate increased. The stress-strain curves, at low to moderate strain rates, exhibited an initial yield corresponding to yield in the ice matrix. At high strain rates this yield coincides with the peak stress. The initial tangent modulus, initial yield stress, and the peak stress were observed to increase with increasing strain rate and temperature. The initial yield strain and the failure strain were independent of temperature, but the failure strain was observed to increase with decreasing strain rate.

Uniaxial constant stress creep tests were conducted for comparison with constant strain rate tests. Comparison of creep parameters obtained from the two tests suggests that constant strain rate tests may be used to define the creep strength of frozen sand and the time dependent strain during secondary creep. Volume change measurements for constant stress creep tests show that dilatancy influences the creep deformation

process. The observed increase in volumetric strain during secondary creep also increased Poisson's ratio. This contradicts the usual assumption of volume constancy during the creep process.

Results for the split cylinder tests show that the tensile strength and tensile failure strain of frozen sand was significantly less than the corresponding values in compression. The tensile strength and elastic modulus were also observed to increase with temperature and strain rate in a fashion similar to the compression properties. Application of the split cylinder test to frozen sand was limited by the material behavior and difficulties in interpreting results.

Machine stiffness altered the observed strain rate in constant strain rate compression tests. Material parameters did not appear to be significantly effected, but the phenomenon would suggest a source of test system error and differences in results reported by difference investigators.

The Mohr-Coulomb failure theory was examined with respect to data obtained in the current investigation. A parabolic failure envelope helps describe the time dependent strength of frozen sand in terms of the compression:tension strength ratio.

The final section presents a simplified analysis of a frozen soil beam to consider the time dependent strength and deflection of the beam. The analysis serves to demonstrate how tensile strengths can be utilized to resist bending stresses (at least for short periods of time) and how other mechanical properties obtained from the investigation may be used in design of frozen sand structural elements.

MATERIAL PROPERTIES FOR SAND-ICE STRUCTURAL SYSTEMS

By

Richard Alan Bragg

A DISSERTATION

Submitted to
Michigan State University
in partial fulfillment of the requirements
for the degree of

DOCTOR OF PHILOSOPHY

Department of Civil and Sanitary Engineering

1980

I would like to dedicate this dissertation to my wife, Kris. Without her encouragement, I would not have undertaken a Ph.D. program. Without her love, understanding, and hard work, completion of this study would not have been possible.

ACKNOWLEDGMENTS

I would like to express my sincere gratitude to my major professor, Dr. Orlando B. Andersland, Professor of Civil Engineering, for his guidance and encouragement and for the time he generously devoted to discussions and consultations. His genuine interest and concern was constantly evident and I feel fortunate to have been a recipient of his experience and knowledge.

Appreciation is also due to my doctoral committee: Dr. W. A. Bradley, Professor of Civil Engineering; Dr. R. K. Wen, Professor of Civil Engineering; and Dr. C. O. Horgan, Professor of Metallurgy, Mechanics, and Material Science. Further appreciation is expressed to the Department of Civil and Sanitary Engineering and to the Division of Engineering Research for their financial assistance during this study.

I would also like to express special thanks to the Dwornik family (Dad, Mom, Karen and David) for their love and support. Without them and my wife, Kris, obtaining my doctorate would not have had such special meaning.

TABLE OF CONTENTS

Page

LIST OF TABLES vi

LIST OF FIGURES vii

CHAPTER

I. INTRODUCTION 1

II. LITERATURE REVIEW 5

2.1 Creep Behavior of Sand-Ice Materials 6

2.1.1 Power Law Relationships 9
2.1.2 Vyalov's Hereditary Creep Law 14

2.2 Constant Strain Rate Tests 16

2.2.1 Compressive Strength 17
2.2.2 Tensile Strength 18
2.2.3 Factors Affecting Uniaxial Strength 19

2.3 Temperature Effects On Creep Rate And Strength. . . 22

2.4 Tensile Tests For Sand-Ice Materials 24

2.4.1 Theory Of The Split Cylinder Test 27
2.4.2 Factors Influencing The Split Cylinder Test 31

2.5 Flexural Behavior 34

2.5.1 Elastic Materials 34
2.5.2 Time Dependent Plastic Materials 39

III. MATERIAL AND SAMPLE PREPARATION 61

3.1 Uniaxial Compression Test Samples 62

3.2 Split Cylinder Test Samples 64

IV. EQUIPMENT AND TEST PROCEDURES 66

4.1 Equipment 66

4.2 Test Procedures 70

CHAPTER Page

V. EXPERIMENTAL RESULTS 79

5.1 Constant Strain Rate Uniaxial Compression Tests . . 79

5.1.1 Strain Rate Effects 80
5.1.2 Temperature Effects 86
5.1.3 Sample Size Effects 89

5.2 Constant Stress Uniaxial Compression Creep Tests. . 91

5.3 Split Cylinder Tests 93

5.3.1 Strain Rate Effects 93
5.3.2 Temperature Effects 96
5.3.3 Sample Size Effects 97

VI. DISCUSSION AND ANALYSIS 156

6.1 Mechanical Behavior Of Frozen Sand 156

6.1.1 Material Properties In Compression 156
6.1.2 Material Properties In Tension 172

6.2 Standardization And Evaluation Of Test Methods . . 177

6.2.1 Influence Of Machine Stiffness 178
6.2.2 Sample Size Effects 180
6.2.3 Evaluation Of Test Methods 183

6.3 Material Property Selection 186

6.3.1 Material Properties For Design In Tension And Compression 187
6.3.2 Failure Criterion 191

6.4 Simplified Analysis 193

6.4.1 Stress Distribution 194
6.4.2 Time Dependent Deformation 196

VII. SUMMARY AND CONCLUSIONS 226

7.1 Material Behavior 226

7.2 Standardization And Evaluation Of Test Methods . . 229

7.3 Material Property Selection 231

7.4 Recommended Additional Research 233

APPENDIX 235

BIBLIOGRAPHY 278

LIST OF TABLES

TABLE		Page
2-1	Equations for Calculation of Tensile Properties	43
5-1	Physical Properties Summary for Constant Strain Rate Uniaxial Compression Test Samples	99
5-2	Test Results for Constant Strain Rate Uniaxial Compression Tests	101
5-3	Physical Properties Summary for Constant Stress Uniaxial Creep Tests	105
5-4	Uniaxial Compression Constant Stress Creep Tests . . .	105
5-5	Physical Properties Summary for the Split Cylinder Samples	106
5-6	Test Results for Split Cylinder Tests	107
6-1	Comparison of Material Constants σ_c and m for Several Frozen Silica Sands	200
6-2	Comparison of Temperature Effects on Initial Yield Stress With Effects on Compressive Strength	201
6-3	Comparison of Tensile Strength of Frozen Silica Sands .	202
6-4	Influence of System Stiffness on Material Properties. .	203
6-5	Comparison of Material Constants from Uniaxial Constant Strain Rate Compression Tests with Split Sylinder Tests	204
A-1	Constant Strain Rate Uniaxial Compression Test Data . .	235
A-2	Constant Stress Uniaxial Compression Creep Test Data. .	266
A-3	Split Cylinder Test Data	269

LIST OF FIGURES

FIGURE		Page
2-1	Constant Stress Creep Test; (a) Creep Curve Variations, (b) Classical Creep Curve, (c) Strain Rate versus Time	44
2-2	Linearized Creep Curves with $\sigma_1 < \sigma_2 < \sigma_3 < \sigma_4$	45
2-3	Log-Log Plot of Pseudoinstantaneous Strain versus Stress for Determination of σ_k and k	46
2-4	Log-Log Plot of Stress versus Strain Rate for Determination of n and σ_c	47
2-5	Primary Creep Curves	48
2-6	Curves Showing Relationships Between Stress and Deformation; (a) Creep Curves, (b) Isocurves	49
2-7	Creep Tests on Polycrystalline Ice; (a) Strain Rate versus Strain, (b) Creep Curves	50
2-8	Effect of Volume Concentration of Sand on Peak Strength	51
2-9	Stress versus True Strain Rate Curves for Specimans with Different Slenderness Ratios, Compressed Between Smooth Platens, at e = 0.77, T = -5°C	52
2-10	Temperature Dependence of Unconfined Compressive Strength	53
2-11	The Indirect Tensile Test	54
2-12	Loading Conditions for the Indirect Tensile Test	55
2-13	Stress Distribution Along the Principal Axes for Loading STrip Width, a, Less Than D/10	56
2-14	Typical Failure Modes; (a) No Loading Strip, (b) Ideal Loading Strip, (c) Wide Loading Strip	57
2-15	Elastic and Inelastic Stress Distributions in a Homogeneous Beam; (a) Stress-Strain Curve, (b) Elastic Stresses, (c) Plastic Stresses	58

FIGURE Page

2-16 Pure Bending of a Bisymmetric Beam 59

2-17 Frozen Soil Beam; (a) Diagram of Simply Supported Beam; (b) Stress Distribution 60

4-1 Diagram of Triaxial Cell Used for Uniaxial Compression Tests 74

4-2 Modified Triaxial Cell 75

4-3 Diagram of Split Cylinder Test Equipment 76

4-4 Diagram of Test System 77

4-5 Split Cylinder Loading Jig with Lateral Deformation Transducer (LADT) in Place 78

5-1 Frame Stiffness Effect on the Observed Strain Rate for Sample No. 44 109

5-2 Frame Stiffness Effect on the Observed Strain Rate for Sample No. 45 110

5-3 Typical Stress-Strain Curves for Unconfined Compression Tests 111

5-4 Typical Failure Modes for the Stress-Strain Curves Shown in Figure 5-3; (a) Low Strain Rate, Sample 63, (b) Intermediate Strain Rate, Sample 59, (c) High Strain Rate, Sample 58 112

5-5 Typical Stress-Strain Curves Showing the Offset Method Used to Determine the Initial Yield Point. . . . 113

5-6 Effect of Strain Rate on the Initial Yield Stress. . . . 114

5-7 Initial Yield Stress versus Average Axial Strain Rate. . 115

5-8 Compressive Strength versus Nominal Strain Rate 116

5-9 Compressive Strength versus Average Strain Rate to Failure 117

5-10 Axial Strain at Failure (Peak Stress) versus the Average Axial Strain Rate 118

5-11 Initial Tangent Modulus versus Average Strain Rate to Failure 119

5-12 Stress-Strain Curves for Samples 87, 88 and 89 at -2°C 120

FIGURE Page

5-13 Stress-Strain Curves for Samples 84, 85 and 86 at -6°C 121

5-14 Stress-Strain Curves for Samples 82 and 83 at -15°C . . 122

5-15 Volumetric Strain versus Axial Strain for Samples 87, 88 and 89 at -2°C 123

5-16 Volumetric Strain versus Axial Strain for Samples 84, 85 and 86 at -6°C 124

5-17 Volumetric Strain versus Axial Strain for Samples 82 and 83 at -15°C 125

5-18 Tangent Poisson's Ratio versus Axial Strain for Samples 87, 88 and 89 at -2°C 126

5-19 Tangent Poisson's Ratio versus Axial Strain for Samples 84, 85 and 86 at -6°C 127

5-20 Tangent Poisson's Ratio versus Axial Strain for Samples 82 and 83 at -15°C 128

5-21 Test Temperature Effect on the Stress-Strain Behavior of Frozen Sand in Compression 129

5-22 Initial Yield Stress versus Degrees Below Freezing . . . 130

5-23 Temperature Effect on Initial Tangent Modulus 131

5-24 Temperature Effect on Compressive Strength 132

5-25 Temperature Effect on Volumetric Strain 133

5-26 Sample Diameter Effect on; (a) the Initial Yield Stress, (b) Initial Yield Strain 134

5-27 Sample Diameter Effect on; (a) Compressive Strength, (b) Failure Strain 135

5-28 Sample Diameter Effect on the Initial Tangent Modulus. . 136

5-29 Creep Curves for Constant Stress Compression Creep Tests 137

5-30 Uniaxial Compressive Stress versus Creep Rate for Constant Stress Creep Tests 138

5-31 Axial Strain at Failure (Tertiary Creep) versus Axial Stress for Constant Stress Creep Tests 139

FIGURE Page

5-32 Volumetric Strain versus Time for the Constant Stress Creep Tests 140

5-33 Tangent Poisson's Ratio versus Time for the Constant Stress Creep Tests 141

5-34 Typical Vertical Deformation versus Time Plots (Split Cylinder Tests) Straight-Line Approximation for Determination of Vertical Deformation Rates 142

5-35 Typical Load versus Vertical Deformation Curves for Split Cylinder Tests 143

5-36 Vertical Deformation Rate Effect on the Indirect Tensile Strength 144

5-37 Log-Log Plot of Vertical Deformation Rate versus Indirect Tensile Strength 145

5-38 Typical Load versus Horizontal Deformation Plots for the Split Cylinder Tests 146

5-39 Typical Vertical Deformation versus Horizontal Deformation Plots (Split Cylinder Tests) for Determination of DR 147

5-40 Poisson's Ratio versus Applied Vertical Deformation Rate for the Split Cylinder Tests 148

5-41 Typical Horizontal Deformation versus Time Plots (Split Cylinder Tests) showing Straight-Line Approximations to Determine Horizontal Deformation Rate 149

5-42 Tensile Strain Rate Effect on the Tensile Strain at Failure 150

5-43 Tensile Strain Rate Effect on Indirect Tensile Strength 151

5-44 Tensile Strain Rate Effect on Young's Modulus 152

5-45 Temperature Effect on the Indirect Tensile Strength . . 153

5-46 Temperature Effect on Young's Modulus Determined from Split Cylinder Tests 154

5-47 Sample Diameter Effect on the Indirect Tensile Strength 155

FIGURE Page

6-1 Comparison of Initial Yield Stress of Frozen Wedron Sand with the Compressive Strength of Polycrystalline Ice 205

6-2 Comparison of Initial Yield Strain in Frozen Wedron Sand with Failure Strain in Polycrystalline Ice 206

6-3 Comparison of Initial Tangent Modulus Values; Frozen Wedron Sand versus Polycrystalline Ice 207

6-4 Initial Tangent Modulus for Frozen Sands 208

6-5 Comparison of Compressive Strength for Wedron Sand with Other Sand Types 209

6-6 Comparison of Initial Yield Stress with Uniaxial Compressive Strength 210

6-7 Comparison of Constant Strain Rate Compression Test Results with Constant Stress Compression Creep Tests at -6°C 211

6-8 Comparison of Failure Strains obtained from Constant Strain Rate Tests with Constant Stress Creep Tests 212

6-9 Volumetric Strain versus Axial Strain for Constant Stress Uniaxial Compression Tests 213

6-10 Comparison of Indirect Tensile Strength of Frozen Wedron Sand with the Tensile Strength of Polycrystalline Ice 214

6-11 Tensile Strength of Frozen Sand 215

6-12 Comparison of Young's Modulus from Split Cylinder Tests with Initial Tangent Modulus for Ice in Tension 216

6-13 Comparison of Computed Tensile Strains at Failure for Split Cylinder Tests with Failure Strains for Polycrystalline Ice in Tension 217

6-14 Comparison of Uniaxial Compressive Strength with Indirect Tensile Strength 218

6-15 Elastic Modulus in Tension and Compression 219

6-16 Tangent Poisson's Ratio versus Axial Strain for Unconfined Uniaxial Compression Creep Tests 220

FIGURE		Page
6-17	Time Dependence of Failure Envelopes	221
6-18	Frozen Sand Backfill Simulating an Unreinforced Beam for Partial Support of Pipeline in Areas of Differential Frost Heave Action	222
6-19	Simply supported Frozen Soil Beam	223
6-20	Simply supported Beam; (a) Assumed Strain Distribution, (b) Computed Stress Distribution	224
6-21	Determination of Temperature Correction Factor	225

CHAPTER I

INTRODUCTION

Controlled ground freezing is a viable and competitive alternative for providing temporary ground support and groundwater control for large open excavations. Geometry of the structure and available space help determine the structural system for the frozen earth wall. Relatively high compressive and low tensile strengths of frozen soil generally limit the structural system to curved or circular arch walls. Gravity and/or anchored walls are used when restrictions prevent the use of curved structural elements. Use of reinforcement in the frozen soil structural elements and design methods which account for available tensile strengths would greatly increase potential applications.

The major limitation to greater use of frozen soil as a structural or static effective material has been the difficulty in predicting its mechanical behavior and the influence of temperature on its behavior. In particular, little information has been available concerning the flexural behavior of soil-ice materials and the influence of time and temperature on the tensile strength of frozen soils has not been well defined. Since frozen soils have a distinct time-dependent strength, the temporal development of stress and strain in soil-ice structural systems is of interest.

The mechanical properties of frozen soils are gradually being defined through the independent efforts of various researchers. Interpretation of data concerning the influence which strain rate, temperature, sample size or shape, and test conditions have on the stress-strain behavior, time dependent strength in compression or tension,

failure strain, and failure mode has been limited by differences in sample preparation and test procedures. Standardization of test procedures would permit a more accurate comparison of data for the material properties obtained by different researchers. Selection of sample preparation techniques and test procedures must insure consistency in test results, ease in interpretation, and define the properties of interest without significant experimental error. Of common concern are test procedures to determine the long term compressive and tensile strength of frozen soils from laboratory tests on a limited number of soil samples.

The primary objective of this research was to investigate those mechanical properties of frozen soils required for design of frozen soil barriers or structures subject to flexural stresses. A number of variables which have been observed to influence the mechanical behavior of frozen soils include mineral composition, percent ice saturation, and the dry density of the soil. To eliminate these variables all tests were conducted on frozen saturated Wedron silica sand samples at a sand volume content of approximately 64 percent.

The initial phase of the research was directed at defining the mechanical properties of the sand-ice material in compression and observing the physical mechanisms responsible for the material behavior. The effects of temperature and strain rate on the compressive strength, initial tangent modulus, failure strain, and failure mode were determined experimentally over a range of strain rates from $5 \times 10^{-7} sec^{-1}$ to $8 \times 10^{-4} sec^{-1}$ and temperatures from -2°C to -15°C. Volumetric strain measurements were obtained for several samples to observe the influence of strain on the value of Poisson's ratio and to provide insight into

the deformation mechanisms during strain.

Several authors (Andersland, et al, 1978; Baker, 1980; Sayles, 1972; Parameswaran, 1980) have suggested that constant strain rate tests may be used to determine the creep behavior of frozen sand. To investigate the relationship between constant strain rate tests and the creep behavior of frozen sand, several constant stress uniaxial compression (creep) tests were conducted. Volume measurements were taken to observe the volumetric strain during creep and to compute a time (or strain) dependent Poisson's ratio. Comparison of results obtained from the two test methods indicates that the constant strain rate compression tests may be related to secondary creep of the frozen sand, but may in essence neglect deformations during initial phases of the creep process.

The second part of the study was directed at determining mechanical properties of the frozen sand in tension. The Brazilian or split cylinder test was used in this capacity. Tests were conducted at various loading rates and temperatures, and the vertical and horizontal deflections monitored. The theory of elasticity was used to compute Poisson's ratio, Young's modulus, the tensile strength, tensile strain rate, and the tensile strain at failure from test results. The data was analyzed with respect to the influence of tensile strain rate (range from $1.4 \times 10^{-5} sec^{-1}$ to $2 \times 10^{-4} sec^{-1}$) and temperature (range from -2°C to -6°C) on the sample response and on the various material properties. Since the split cylinder test had not previously been conducted on frozen sand, an evaluation is presented by comparison of test results with those obtained for various test methods reported by other investigators on similar sand materials.

Emphasis was also placed on a discussion of standardization of test

procedures. Comparisons were made between the mechanical properties of frozen sand in tension and compression to determine if the creep parameters and long term strength in tension may be determined from the uniaxial compression tests (preferably the constant strain rate compression test). The influence of sample diameter on the mechanical properties obtained from both the constant strain rate uniaxial compression tests and split cylinder tests was investigated over a size range suitable for field investigations. This data aids in selection of sample geometry for the tests considered. Observations are also presented with respect to the influence which machine stiffness has on the stress-strain behavior and the mechanical properties of the frozen soil.

Selection of material properties for design of frozen soil structures is discussed with respect to this investigation and data reported in the literature. A failure criterion suitable for biaxial (or multiaxial) stress states, based on the Mohr-Coulomb theory, is presented in terms of the compression:tensile strength ratio and the time dependent behavior of the material. Computations are included to demonstrate the ability of frozen sand to resist flexural deformation and to illustrate in a simplified manner how flexural design may account for the time dependent strength of the frozen sand.

CHAPTER II

LITERATURE REVIEW

Frozen soils consist of a multi-phase system composed of polycrystalline ice, crystal hydrates, unfrozen pore water, solids consisting of mineral and/or organic matter, and entrapped air. The ice component of frozen soil forms when the temperature of the free water in the mineral pores is lowered below the normal freezing point of water. It is now generally accepted that an unfrozen water phase exists between the ice and the mineral grains. The quantity of unfrozen water is related to the physio-chemical properties of the soil mineral and in particular the specific surface area of the soil particles. This unfrozen water content may be determined calorimetrically (Lovell, 1957; Leonards and Andersland, 1960; William, 1963) or may be estimated on the basis of certain measurable soil properties (Dillon and Andersland, 1966; Anderson and Tice, 1972; Anderson, et al, 1978). Various investigators (Tsytovich, 1960; Anderson, 1967; and Anderson and Tice, 1972) have shown that clays have unfrozen quantities of pore water at temperatures as low as -30°C. However, for clean sands, because of their low specific surface area, nearly all available water in the sand pores is frozen at temperatures slightly below 0°C.

Frozen sand, as a result of the ice component, is clearly characterized by rheological properties. The effect of creep deformations in frozen sand subject to stresses is significant and may greatly exceed the elastic deformations developed immediately after application of a load. Engineering design of structures placed on frozen sand or constructed of sand-ice materials must consider this time dependent

behavior of the material.

This chapter examines available information and theories which account for the creep deformation of frozen soils with respect to engineering applications. It is also necessary to evaluate and discuss test procedures for the measurement of the tensile properties of frozen sand. A review of flexure theory, with respect to elastic and creep deformation, is presented prior to discussion of flexural design.

2.1 Creep Behavior of Sand-Ice Materials

The mechanical properties of frozen sand are significantly influenced by the ice content. The strength of sand-ice mixtures is derived from cohesion, interparticle friction, and particle interlocking. The interparticle friction and particle interlocking contribute to the shear strength of frozen sand in the same fashion as they influence unfrozen soils. The cohesion component of the shear strength is derived from the ice matrix. The behavior of ice-rich soil at low solids concentrations may nearly approximate that of ice. As the sand particle concentration increases the interaction of the sand grains begins to contribute to the strength and deformation characteristics of the mixture.

When a constant load is applied to a frozen sand, the deformation curve is characterized by an instantaneous elastic-plastic deformation followed by a time dependent creep deformation. Deformations which develop with time may be hundreds of times greater than the initial ones, while the continuous strength is from 5 to 15 times less than the instantaneous value (Vyalov, 1963). Engineering design of frozen soil structures should, therefore, be based on an analysis of the time dependent or creep deformations which occur over the service life of the structure.

The creep process in frozen sand may be explained as presented by

Tsytovich (1955). Frozen soils are in a state of dynamic equilibrium between the liquid and solid phases of water. Application of a constant load to the soil mass causes concentrations of stress at points of contact between the soil particles and the ice. These stress concentrations induce pressure-melting of the ice. As a result the dynamic equilibrium is disturbed and the amount of pore water increases. Differences in water surface tensions are produced and the unfrozen water migrates to regions of lower stress where it refreezes. This process of ice melting and water migration is accompanied by a breakdown of the ice and the structural bonds between the ice and the soil grains. Simultaneously, there is a readjustment in particle orientation. These processes take time and are also accompanied by reorientation of the ice crystals, which tend to orient their basal planes parallel to the slide direction. This structural deformation leads to a denser packing of the soil particles, which in turn causes a strengthening of the material due to the increased interlocking and interparticle contact with a consequent increase in interparticle friction. During the creep process there is also a weakening associated with reduced structural cohesion caused by pressure melting of the ice and possibly an increase in the unfrozen water content (especially for fine-grained soils, i.e. clays). If the strengthening process exceeds the weakening, the creep behavior is damped or the rate of deformation decreases with time. This implies that for low stress levels, the creep deformation approaches a limiting value with time. However, if applied load exceeds the long-term strength of the frozen soil or if the ice content is high, the breakdown of internal bonds is not fully compensated by the strengthening process and the rate of deformation increases with time. The net result is undamped creep which develops into plastic flow and

and terminates in collapse of the frozen soil structure.

Experimental data (Vyalov, 1962; Sayles, 1968, 1972; and Goughnour, 1968) show that the creep characteristics of frozen sand are similar to those depicted by the classical creep curve. Figure 2-1a shows typical creep curve variations for frozen soils as a function of stress level or ice content under an applied step load and at constant temperature. Figure 2-1b shows the basic undamped creep curve common for frozen soils and metals at high temperatures. The corresponding creep rate ($d\varepsilon/dt$) versus time is shown in Figure 2-1c. The classical creep curve is generally considered to consist of four parts: (1) instantaneous elastic-plastic strain resulting from application of the uniaxial stress (step loading); (2) Period I in which the creep rate is decreasing; (3) Period II in which the creep rate is nearly constant; and (4) Period III in which the creep rate is increasing with time resulting in brittle, or viscous failure. These periods are normally referred to as primary, secondary, and tertiary creep, respectively.

Vyalov (1962) describes the four parts of the creep curve in terms of deformation processes. Part (1) is termed elasto-plastic since a portion of the strain, depending on the stress level, may not be recoverable upon load removal. The primary creep region includes both a time delayed plastic and elastic deformation. The secondary creep region is described as a plastic-viscous strain, since the deformation is completely residual and the constant strain rate with time is analogous to viscous flow. The third period of the classical creep curve (tertiary creep) is considered a region of progressive flow leading to instability.

In general the total strain, ε, (Figure 2-1) may be expressed as

an instantaneous strain, ε_0, and a time dependent creep strain $\varepsilon(t)$;

$$\begin{aligned}\varepsilon &= \varepsilon_0 + \varepsilon(t) \\ &= \varepsilon_0 + \varepsilon_1^c + \varepsilon_2^c + \varepsilon_3^c \\ &= \varepsilon_0 + \int_0^{t_1} \frac{\partial \varepsilon_1^c}{\partial t}\, dt + \int_{t_1}^{t_2} \frac{\partial \varepsilon_2^c}{\partial t}\, dt + \int_{t_1}^{t_f} \frac{\partial \varepsilon_3^c}{\partial t}\, dt\end{aligned} \qquad (2\text{-}1)$$

where ε_0, ε_1^c, ε_2^c, and ε_3^c are defined in Figure 2-1. Normally, tertiary creep (ε_3^c) is not considered in design since it leads to instability. Engineering design requires that a constitutive equation describing the stress-strain-time relationship for the remaining terms be developed and related to the creep strength of the frozen sand. Two common theories used to describe stress-strain-time behavior include the power law relationships (Ladanyi, 1972) and the hereditary creep law proposed by Vyalov (1962).

2.1.1 Power Law Relationships

The purpose of a constitutive creep equation is to provide the engineer with suitable means for calculating stresses and strains in a structure subject to creep. The proposed service life of the structure is of importance in determining the form of the constitutive relationship. If the service life is close to the duration of primary creep period of the material then the constitutive equation must describe the decrease in creep rate (Figure 2-1b). If the service life extends into the secondary creep period, then the straight-line approximation of Figure 2-1b may be appropriate.

For the creep curves shown in Figure 2-2 ($\sigma_1 < \sigma_2 < \sigma_3 < \sigma_4$), Hult (1966) has described a convenient method of establishing the constitutive equation for stress-strain-time relationships during secondary

creep based on the straight-line approximations of the creep curves. Note that the strain predicted using this approximation will over estimate the creep strain during primary creep, but the error will decrease steadily during the creep process and approach the actual creep strain at the beginning of the secondary (steady state) creep period.

According to Hult (1966), for constant stress and temperature, the straight-line approximations may be described by:

$$\varepsilon = \varepsilon^{(i)} + \frac{d\varepsilon^{(c)}}{dt}(t) = \varepsilon^{(i)} + \varepsilon^{(c)}$$
$$= F(\sigma, T) + t\, G(\sigma, T) \qquad (2\text{-}2)$$

where $\varepsilon^{(i)}$ is the pseudoinstantaneous strain, dependent on stress (σ) and temperature (T), and $\varepsilon^{(c)}$ is the time dependent creep strain as a function of stress and temperature. The pseudoinstantaneous strain ($\varepsilon^{(i)}$) may be separated into an elastic strain, $\varepsilon^{(ie)}$, and a plastic strain, $\varepsilon^{(ip)}$:

$$\varepsilon^{(i)} = \varepsilon^{(ie)} + \varepsilon^{(ip)} \qquad (2\text{-}3)$$

The elastic portion can be expressed as:

$$\varepsilon^{(ie)} = \frac{\sigma}{E(T)} \qquad (2\text{-}4)$$

where E(T) is a fictitious Young's modulus, smaller than the modulus corresponding to the instantaneous elastic modulus. The plastic portion may be written as a pure power expression of the form presented by Ladanyi (1972):

$$\varepsilon^{(ip)} = \varepsilon_k \left[\frac{\sigma}{\sigma_k(T)}\right]^{k(T)} \qquad (2\text{-}5)$$

where σ_k is a temperature dependent deformation modulus, the exponent $k > 1$ is usually little dependent on temperature, and ε_k is an arbitrary small strain introduced for convenience in calculation and

plotting data. For a given constant temperature, the numerical values of σ_k and k are determined from a log-log plot of $\varepsilon^{(ip)}$ vs stress (σ) since Equation 2-5 linearizes on a log-log plot. (Figure 2-3)

Similarly, the time dependent creep strain may be written as a simple power expression (Hult, 1966; Odqvist, 1966; Landanyi, 1972; and Andersland, et al, 1978) of the form:

$$\varepsilon^{(c)} = t\, G(\sigma, T)$$
$$= t\dot{\varepsilon}_c \left[\frac{\sigma}{\sigma_c(T)}\right]^{n(T)} \qquad (2\text{-}6)$$

where $\sigma_c(T)$ and $n(T)$ are defined as temperature dependent creep parameters (n much less dependent than σ_c). The quantity $\dot{\varepsilon}_c$ is an arbitrary standard strain rate introduced for normalization. The quantity $\sigma_c(T)$ is the uniaxial stress necessary to cause the secondary creep rate of $\dot{\varepsilon}_c$ and was described by Hult (1966) as the creep proof stress. The magnitude of $\sigma_c(T)$ is dependent on the value of $\dot{\varepsilon}_c$ ($\dot{\varepsilon}_c = 10^{-5}\text{min}^{-1}$ or $1.67 \times 10^{-7}\text{sec}^{-1}$ is normally chosen for frozen soils; Landanyi, 1972). For a constant temperature, the numerical values of σ_c and n are obtained from a log-log plot of experimental stress vs strain rate data as shown in Figure 2-4.

The constitutive equation of the frozen soil may now be written in terms of a step load as:

$$\varepsilon = \varepsilon^{(i)} + \varepsilon^{(c)}$$
$$= \frac{\sigma}{E} + \varepsilon_k \left[\frac{\sigma}{\sigma_k}\right]^k + \dot{\varepsilon}_c \left[\frac{\sigma}{\sigma_c}\right]^n t \qquad (2\text{-}7)$$

In frozen soils, according to Vyalov (1959), the immediate strains considered in the first two terms of this equation may be less than 10 percent of the total creep strain for time intervals greater than 24 hours. Thus, for time intervals greater than 1 day the last term may be

considered sufficient to estimate the creep strain at constant stress and temperature.

The creep strength of a frozen soil may be defined using Equation 2-7 (Ladanyi, 1972; Andersland, et. al, 1978). Creep strength is defined as the stress level, at which, after a finite time interval, instability or rupture of the material occurs. In constant stress compression creep testing, the beginning of the tertiary creep period (increasing strain rate) is generally accepted as the first sign of instability for ductile materials such as frozen soils. In tension creep testing, the creep strength is usually taken as the stress at which rupture actually occurs.

According to Ladanyi, experimental data (Sayles and Epanchin, 1966; Vyalov, 1962) shows that axial strain at the beginning of instability (tertiary creep) is approximately constant for compression creep testing at a given temperature. Ladanyi (1972) adopted the constant permanent strain at the onset of tertiary creep as the creep-failure criterion. If the service life of the structure is known, the steady state creep rate may be estimated as:

$$\dot{\varepsilon}^{(c)} = \frac{\varepsilon_f - \varepsilon^{(i)}}{t_f} \qquad (2\text{-}8)$$

where ε_f is the strain at creep failure and t_f is the service life of the structure. Substitution of Equation (2-7) into (2-8) gives:

$$\dot{\varepsilon}^{(c)} = \dot{\varepsilon}_c \left[\frac{\sigma_f}{\sigma_c}\right]^n = \frac{\varepsilon_f - \varepsilon_k(\sigma_f/\sigma_k)^k - (\sigma_f/E)}{t_f} \qquad (2\text{-}9)$$

For time intervals greater than approximately 24 hours the immediate deformation may be neglected and for a constant temperature and a large time interval or service life Equation (2-9) becomes:

$$\dot{\varepsilon}_c \left[\frac{\sigma}{\sigma_c}\right]^n = \frac{\varepsilon_f}{t_f}$$

$$\text{or} \qquad \sigma_f = \sigma_c \left[\frac{\varepsilon_f}{t_f \dot{\varepsilon}_c}\right]^{1/n} = \text{creep strength} \qquad (2\text{-}10)$$

When the service life of a structure coincides roughly with the duration of primary creep, the constitutive equation, based on the linearized creep curves, will over estimate the strain with time. The constitutive equation must then describe the decrease in strain rate with time in order to more accurately estimate the creep strain. Figure 2-5 shows characteristic creep curves for most materials (including frozen soils) during the primary creep phase. Immediately after application of a constant uniaxial stress the strain ε_0 develops, followed by a gradual development of the creep strain, $\varepsilon^{(c)}$.

The immediate strain, ε_0, contains both a plastic and an elastic deformation. For small stresses, the plastic deformation is small and if neglected (Hult, 1966; Andersland, et. al, 1978), the immediate deformation may be approximated by:

$$\varepsilon_0 = \frac{\sigma}{E_0(T)} \qquad (2\text{-}11)$$

where $E_0(T)$ is the temperature, (T), dependent instantaneous Young's modulus.

The creep strain, $\varepsilon^{(c)}$, is a function of stress, time, and temperature:

$$\varepsilon^{(c)} = f(\sigma, t, T) \qquad (2\text{-}12)$$

Hult (1966) presents a strain hardening creep law corresponding to the constant stress condition:

$$\varepsilon^{(c)} = K\sigma^a t^b \quad , \qquad b < 1 \qquad (2\text{-}13)$$

The constants K, a, and b are material and temperature dependent. Differentiation with respect to time and elimination of t results in a creep law of the form presented by Hult (1966) and Andersland, et al (1978):

$$\varepsilon^{(c)} = \left(\frac{\dot{\varepsilon}_c}{b}\right)^b \left(\frac{\sigma}{\sigma_c}\right)^n t^b \qquad (2\text{-}14)$$

with b, n, and σ_c temperature and material dependent creep parameters determined from a set of creep curves obtained at a constant temperature. The constant $\dot{\varepsilon}_c$ is an arbitrarily selected strain rate. Note that the constants n and σ_c are the same for both steady state and primary creep (Andersland, et al, 1978).

2.1.2 Vyalov's Hereditary Creep Law

Vyalov (1962) proposed that the Volterra-Boltzman nonlinear hereditary creep theory was suitable for describing the time-dependent deformations in frozen soil. The theory assumes that the strain at any time depends not only on the applied stress and temperature, but also on the prior strain history. Vyalov (1962) introduced parameters, derived from experimentation, into the equations to characterize the behavior of actual soils.

The total strain may be expressed as a function of the instantaneous strain, primary creep, and secondary creep, as was presented by Equation 2-1. The initial strain ε_0 can be completely recoverable or can include a residual nonrecoverable strain depending on the stress level. The strain ε_1^c includes both recoverable and residual strains and ε_2^c and ε_3^c are completely residual strains (ε_3^c is not normally taken into consideration).

As the deformation at any time (t_i) consists of an elastic strain,

linearly related to the stress level, and a plastic strain, which is nonlinear, the relationship between stress and strain may be written as (Vyalov, 1962):

$$\varepsilon_i = \frac{\sigma}{E_i} + \left(\frac{\sigma}{A_i}\right)^{1/m} \qquad (2\text{-}15)$$

where E_i and A_i are moduli of linear and nonlinear deformation, respectively. To simplify calculations, one common law can be used for the entire stress range:

$$\varepsilon_i = f(\sigma) \quad \text{or} \quad \sigma = f(\varepsilon_i) \qquad (2\text{-}16)$$

As strain increases with time, every t_i is characterized by its own stress-strain curve or isocurve (figure 2-6). The curve at $t = 0$ corresponds to the initial deformation, while the curve at $t =$ infinity represents the strain with unlimited time duration of the stress (σ). The intermediate curves represent the strain at some time t_i.

Vyalov (1963) indicates that experimental data shows that all the curves are similar and may be described by a power law of the form:

$$\varepsilon = \left(\frac{\sigma}{A(t)}\right)^{1/m} \quad \text{or} \quad \sigma = A(t)\varepsilon^m \qquad (2\text{-}17)$$

in which A(T) is the modulus of total deformation. The value of A(t) is dependent on temperature and test duration (changes with time). The strengthening factor $m \leq 1$ is independent of both time and temperature.

In compliance with the theory of nonlinear hereditary creep, the small initial strain (ε_0) can be neglected and the expression rewritten as (Vyalov, 1963):

$$\varepsilon = \left[\frac{\sigma\, t^{\lambda}}{\omega(\theta+1)^k}\right]^{1/m} \qquad (2\text{-}18)$$

The parameters ω, λ, k, and m are constants representative of the frozen soil and $\theta° = 273 - T(°K)$. These constants must be evaluated

experimentally from a set of creep curves.

The long-term strength of the frozen soil for uniaxial stress conditions may also be obtained from an expression proposed by Vyalov (1959):

$$\sigma_f = \frac{\sigma_0}{\ln[(t_f + t^*)/t_o]} \simeq \frac{\sigma_0}{\ln(t_f/t_0)} \qquad (2\text{-}19)$$

in which σ_0 and t_0 are parameters dependant on soil type and temperature. The time to failure is given by t_f and σ_f is the long-term strength. The parameter $t^* = t_0 \exp(\sigma_0/\sigma_i)$, where σ_i is the instantaneous strength, may be neglected (Vyalov, 1963).

Equation (2-19) results in $\sigma_f = 0$ when t_f = infinity, which is not consistent with the idea of continuous strength at some finite stress. However, Vyalov (1963) indicated that in engineering practice, after some long period of time the strength reduction is so insignificant and so slow that it can be neglected in engineering calculations.

2.2 Constant Strain Rate Tests

The constant strain **rate compression** test is commonly used to test a number of materials including unfrozen soils and would seem to be readily adaptable to frozen soils. The test is conducted by deforming cylindrical samples along the longitudinal axis at a constant rate. This test method results in a constant engineering strain rate ($\dot{\varepsilon} = (d/dt)(\Delta L/L_0)$) or a true strain rate ($\dot{\xi} = (d/dt)[\ln(L/L_0)]$) which increases linearly with time.

Andersland, et al (1978) suggest that the stress-strain curves obtained from constant uniaxial strain rate tests may be used to determine both a time dependent deformation modulus (or initial tangent modulus) and the time dependent strength of frozen soils The peak

strength is plotted against either time to failure strain or the applied axial strain rate on a log-log plot. The latter plot is believed to be equivalent to the relationship between secondary creep rates and the corresponding stress levels in constant axial stress creep tests (Figure 2-4). However, the primary advantages of the constant strain rate test, with respect to the constant stress creep test, are the reduction in dynamic effects due to the sudden initial stress condition required in the uniaxial creep tests and the relatively short test duration.

2.2.1 Compressive Strength

Experimental data obtained by a number of investigators (Sayles and Epanchin, 1966; Perkins and Ruedrich, 1972; Sayles, 1974; Baker, 1978; and Parameswaran, 1980) would seem to support the use of the constant uniaxial strain rate test to obtain the time dependent strength in compression. The linear relationship between the peak compressive stress and applied axial strain rate may be expressed as:

$$\sigma = \sigma_c(\dot{\varepsilon})^m \qquad (2\text{-}20)$$

or

$$\dot{\varepsilon} = (\sigma/\sigma_c)^n \qquad (2\text{-}21)$$

where m is the slope of a straight-line through the data on a log-log plot, $n = 1/m$, and σ_c is a temperature dependent proof stress evaluated at a strain rate of 1 sec^{-1}. Equation 2-21 is of the same form as the steady state creep law given by Ladanyi (1972). This observation suggests that constant uniaxial strain rate tests may be used to determine the creep parameters needed to predict the secondary creep deformation of frozen soils subject to constant uniaxial stresses (when using the linearized approximation to the creep curves shown in Figure 2-2).

The relationship between constant stress creep tests and constant

strain rate compression tests can be visualized from the data for polycrystalline ice, obtained by Goughnour (1967) and presented in Figure 2-7. According to Andersland, et al (1978), a horizontal section across the plot in Figure 2-7a corresponds to a particular constant strain rate test. The corresponding stress-strain curve for a given strain rate may be deduced by reading the stresses as a function of strain at all intersection points with the curves. These stress-strain curves are quite different from the isocurves described by Vyalov (1963), which correspond to the total strains attained at a given time. The isocurves are obtained from vertical sections through the creep curves in Figure 2-7b.

2.2.2 Tensile Strength

At present very little data is available from constant strain (or deformation) rate tensile tests conducted on frozen soils. Ladanyi (1972) summarizes data from other investigators which indicates that the compression:tensile strength ratio for Ottawa sand varies from greater than 5 to less than 8. Vyalov (1962) presented limited data suggesting that the momentary strength of sandy loam was approximately 1.7 times the corresponding tensile strength and the continuous strength in compression was about 2.8 times the continuous tensile strength at -4.5°C. Offensend (1966) conducted direct tensile tests at constant deformation rates on frozen Manchester fine sand using briquette-shaped samples. The tensile strength was observed to be temperature dependent, but independent of the deformation rate for rates between 0.1 and 10 inches per minute. Haynes, Karalius, and Kalifut (1975) conducted constant strain rate tensile tests on dumbbell shaped samples of frozen silt at a temperature of -9.5°C. The tensile strength was observed to be

relatively independent of strain rate, while the compressive strength was very sensitive to strain rate. The compressive strength increased by 10 times over a range of strain rates (2.9×10^{-4} to 2.9 sec^{-1}). The tensile strength was observed to only double over this range. However, for strain rates below approximately $10^{-2} sec^{-1}$ the tensile strength was approximatley equal to the compressive strength. Consequently, there is some evidence to indicate that the strength of frozen soils may differ in tension and compression at high strain rates and be approximately the same at lower strain rates. This would also imply that test rates could influence the creep parameters (σ_c and n) determined in the laboratory.

2.2.3 Factors Affecting Uniaxial Strength

Several factors influence the compressive behavior of frozen sand. Goughnour (1967) investigated the effect of sand density on the compressive strength of saturated frozen Ottawa sand. Figure 2-8 shows the relationship between sand volume fraction and peak axial stress at the same temperature and strain rate. A bilinear relationship appeared to be appropriate. For low volume fractions of sand, the shear strength increased linearly with increasing sand content. At a critical volume fraction of approximately 42 percent, a rapid increase in the compressive strength was observed. Interparticle friction and dilatancy are believed to significantly influence the shear strength for sand volume fractions above this critical value (Goughnour and Andersland, 1968). As the sand volume fraction increases the dry density of the sand increases proportionally. The net result is an increase in the number of interparticle contacts and the amount of particle interlocking.

Data presented by Alkire and Andersland (1973) indicates that the

shear strength of frozen sand decreased with decreasing ice saturation (ratio of ice volume to sand pore volume). The reduction in peak stress was proportional to the volume of ice in the sand voids and was primarily the result of a decrease in cohesion in the ice matrix and adhesion between the ice and the sand particles.

Ladanyi and Arteau (1978) investigated experimentally the effect of speciman shape on the creep response of frozen sand. Uniaxial constant stress and constant strain rate compression tests were conducted on cylindrical samples with slenderness ratios (Height/Diameter) varying from 0.5 to 2.0. When the strength of the frozen sand was expressed in terms of strain rate (by the power law creep equation), it was concluded that, for smooth loading platens, the apparent strength of the frozen sand increased with increasing slenderness ratio for any given strain rate. The value of the creep parameter n (Equation 2-6) also increased with increasing slenderness ratio as shown in Figure 2-9.

Baker (1978a) considered the effects of end conditions on the uniaxial compressive strength of frozen sand. Four different loading platen configurations were used to determine the uniaxial compressive strength of Ottawa sand at temperatures from -5°C to -6°C and at a strain rate of $0.7 \times 10^{-3} min^{-1}$. A compliant platen was designed to reduce friction between the sample and platen, to distribute the load uniformly, and to minimize stress gradients produced by eccentric loading. Experimental results indicated that at large slenderness ratios (greater than 2.0) aluminum end caps, aluminum disk platens, and aluminum disk platens with rubber inserts gave about the same average compressive strength. The compressive strength determined using the compliant platens was about 25 percent higher than with the other

platens at slenderness ratios greater than 2.0. He attributed this higher strength to reductions in stress concentrations resulting from rough specimen ends in contact with the platens. In addition, the compressive strength was found to be relatively independent of the slenderness ratio for the compliant platens (for ratios between 0.75 and 2.6). This would suggest that smaller slenderness ratios could be used to determine the compressive strength while eliminating the possibility of buckling or tilting.

In a later publication, Baker (1978b) considered the influence of end conditions on the creep parameters and compressive strength of Ottawa sand. Cylindrical specimens with a slenderness ratio of 2.0 were tested at constant axial strain rates between 2×10^{-7} and 2×10^{-3} sec^{-1} at a temperature of -5.5°C. Neither the unconfined compressive strength nor the axial strain at failure was observed to depend significantly on platen type. However, the value of the exponent m (Equation 2-20) obtained from log-log plots of strain rate versus compressive strength was observed to vary from 0.09 for aluminum disk platens to -0.06 for Maraset compliant platens.

Similar studies considering the influence of testing conditions on the tensile behavior of frozen sand have not yet been conducted. However, Offensend (1966) encountered problems in direct tensile tests on frozen Manchester fine sand using briquette shaped samples (ASTM specified shape and gripping clamp). Rather than failing at the neck of the briquette, the samples broke at the points where the clamps gripped the samples. Apparently, stress concentrations at contact points caused the specimens to fail in a complex interaction of shear and tension. Pads of various materials were inserted between the clamps

and the samples in an attempt to reduce the stress concentrations. These efforts were unsuccessful and it was necessary to reduce the cross-sectional area of the briquettes in order to insure that they would break in the middle section. Additional research is needed to develop and evaluate test methods for determination of the tensile strength and behavior of frozen sand.

2.3 Temperature Effects On Creep Rate And Strength

Experimental data summarized by Sayles (1966), Figure 2-10, indicates a substantial increase in uniaxial compressive strength with decreasing temperature for frozen soils. Other researchers (Andersland and AlNouri, 1970; Parameswaran, 1978; Perkins and Reudrich, 1973; and Sayles and Epanchin, 1966) have also presented data which shows an increase in compressive strength with decreasing temperature at constant strain rate or an increase in strain rate with decreasing temperature at a constant compressive stress.

Several investigators have proposed relationships to describe the effects of temperature on strength and creep rate. Andersland and AlNouri (1970) suggested that the temperature dependence of the creep rate was related to the thermal activation energy by an expression of the form:

$$\dot{\varepsilon}^{(c)} = A \exp(-L/T) \qquad (2\text{-}22)$$

where L = U/R with units of temperature, U is the apparent activation energy, T is the absolute temperature, and R is the universal gas constant. Landanyi (1972) combined this relationship with Equation 2-6 and eliminated the constant A to obtain:

$$\sigma_{c\theta} = \sigma_{c0} \exp \frac{L\theta}{273n(273-\theta)} = \sigma_{c0} f(\theta) \qquad (2\text{-}23)$$

or

$$\dot{\varepsilon}^{(c)} = \dot{\varepsilon}_c \left(\frac{\sigma}{\sigma_{co} f(\theta)} \right)^n \qquad (2\text{-}24)$$

where $\sigma_{c\theta}$ is the temperature dependent proof stress in Equation 2-6, σ_{co} is the proof stress for uniaxial compression tests extrapolated to 0°C, θ is the absolute value of the temperature in °C, and n is assumed relatively independent of temperature.

Equation 2-24 indicates that the compression strength should increase exponentially with decreasing temperature. The data presented in Figure 2-10 only partially supports this prediction. It appears that an exponential relationship between strength and temperature is limited primarily to clays. For coarser grained materials (silts and sands) the relationship between strength and temperature is more nearly parabolic or linear. According to Ladanyi (1972) there would appear to be some justification in selecting the power law relationship proposed by Vyalov (1962), which can be written in the following normalized form (Assur, 1963):

$$\sigma_{c\theta} = \sigma_{co}(1 + \theta/\theta_c)^{\omega} = \sigma_{co} f(\theta) \qquad (2\text{-}25)$$

where θ_c is an arbitrary temperature (1°C usually) and θ is the absolute value of the temperature in degrees Celsius. The value of the exponent ω can be obtained by plotting $\sigma_{c\theta}$ versus $(1 + \theta/\theta c)$ on a log-log scale, where ω is the slope of a straight-line drawn through the data points and σ_{co} is the intercept on the $\sigma_{c\theta}$ axis at 0°C.

$$\omega = \frac{\Delta \log \sigma_{c\theta}}{\Delta \log(1 + \theta/\theta_c)} \qquad (2\text{-}26)$$

For sm

Equati

where

const

at

T is

in

wh

c

t

For small temperature intervals, ω is approximately equal to one and Equation (2-26) reduces to a linear expression of the form:

$$\sigma_{c\theta} = \sigma_{c0}(1 + \theta/\theta_o) = \sigma_{c0}\, f(\theta) \qquad (2\text{-}27)$$

where σ_{c0} and θ_0 are determined from a plot of $\sigma_{c\theta}$ versus θ. The constant θ_o is the intercept on the axis and σ_{c0} is the proof stress at $\theta = 0$.

The uniaxial compressive creep strength at a given temperature T is obtained by substituting σ_c (Equations 2-23, 25 or 27) for σ_c in Equation 2-10.

$$\sigma_f = \sigma_{c0}\left(\frac{\dot{\varepsilon}_f}{\dot{\varepsilon}_c}\right)^{1/n} f(\theta) \qquad (2\text{-}28)$$

where $\dot{\varepsilon}f = \varepsilon_f/t_f$ (Ladanyi, 1972).

The validity of the expressions presented above have not yet been clearly demonstrated for the tensile behavior of frozen sand. Experimental data obtained by Offensend (1966) from direct tensile tests indicates that the tensile strength of Manchester fine sand increases with decreasing temperature. However, temperature-strength relationships were not developed and no comparison was made of the compressive strength-temperature variation.

2.4 Tensile Tests For Sand-Ice Material

Analysis of sand-ice structures subject to bending requires an understanding of the tensile behavior of the frozen sand. Various test methods have been developed and used to determine the tensile strength of brittle and composite materials. These tests can be classified as (1) direct tensile tests, (2) bending tests, or (3) indirect tensile tests.

The direct tensile test is simple in theory. It consists of applying an axial tensile force directly to a sample of the material and measuring the stress-strain behavior. A variety of speciman configurations and gripping devices exist. While the direct tensile test seems simple, several difficulties have been encountered in practical applications of the method. The major problems have concerned the influence of bending stress due to misalignment of the applied load and stress concentrations near the gripping devices. Any eccentricity of the applied load results in bending stresses which introduce errors in the assumed uniform tensile stress distribution over the cross-sectional area. This problem is particularly serious in brittle materials, which can not relieve bending stresses by plastic flow. Since it is believed that the behavior of frozen sand in tension will be governed by the ice matrix, the frozen sand may exhibit brittle fractures (at least at the higher loading rates).

The second major problem in direct tension testing is that of gripping the specimen. Use of the common briquette, which is the accepted tension test for mortar, is complicated by stress concentrations. Mitchell (1961) indicates that the maximum stress at the central cross-section is about 1.75 times the average stress, and photoelastic studies indicated large stress concentrations at the loading grips. The tests conducted on frozen sand by Offensend (1966) using standard mortar briquettes often failed in shear adjacent to the gripping device. The sample shape was modified to reduce the minimum cross-sectional area, but stress concentrations undoubtedly still existed.

A second method of determining the tensile strength is to find the modulus of rupture by testing beams in flexure. The modulus of rupture

is calculated by the standard flexure formula using the dimensions of the beam and the applied bending moment at the point where the beam fails. This analysis assumes that the neutral axis is at the centroid of the cross-sectional area and that the stress is linearly proportional to the distance from the neutral axis. These assumptions are valid only if the stress-strain behavior of the material is linear and the material behavior is the same in both tension and compression. Grieb and Werner (1962) estimated that the modulus of rupture for concrete may be equal to or greater than two times the tensile strength. A conversion factor from the rupture modulus to tensile strength does not appear to be successful. Mitchell (1961) indicates that the conversion factor for concrete seems to be a variable that decreases as the tensile strength increases and most studies have attempted to determine a constant conversion factor. If frozen soil may be assumed analogous to concrete, this test method does not appear too promising. In addition, development of a conversion factor would seem to require some prior knowledge of the true strength in tension.

The indirect tensile or split cylinder test was developed simultaneously by Carniero and Bacelleros (1953) in Brazil and Akazawa (1953) in Japan. The test consists of compressing a disc or cylinder along diametrically opposite generators (Figure 2-11). This loading condition creates a nearly uniform tensile stress perpendicular to and along the loaded axis of the cylinder. Failure occurs by splitting of the speciman along this axis.

It has been demonstrated that the split cylinder test gives reasonable values for the tensile strength of a variety of materials. Mitchell (1961) concluded that the split cylinder test appears to be superior in

most aspects to other tension tests on Portland cement concrete and that the indirect tensile strength compared favorably with data obtained by others using direct tensile tests on cylindrical shaped specimens. Mellor and Hawkes (1971) evaluated the split cylinder test with respect to the determination of the tensile strength of several materials (including rocks). Their conclusion was that the split cylinder test appeared to provide a good measure of the tensile strength for brittle materials when it was carefully performed, with special attention paid to control of contact stresses and accurate load readout. Hudson and Kennedy (1968) reviewed existing information and conducted a testing program with the conclusion that the split cylinder test appeared to be the best test currently available for evaluating the tensile characteristics of stabilized subbase materials (asphaltic concrete and cement treated gravel) for pavement design. The viscous behavior of asphalt is not unlike that of ice, suggesting the potential suitability of the split cylinder test for the determination of the tensile strength of frozen sand.

2.4.1 Theory Of The Split-Cylinder Test

Timoshenko (1934) and Frocht (1948) developed relationships for the stress distributions in circular elements subjected to concentrated forces applied at the boundaries based on the theory of elasticity and photo-elastic studies, respectively. A complete stress solution for the case of a circular element subjected to distributed loads applied over finite arcs for both plane strain and plane stress conditions was given by Hondros (1959). The stresses on the vertical and horizontal axes are given by the following equations (see Figure 2-12):

(1) Stresses Along the Horizontal Axis (OX)

a. Tangential stress (parallel to the loaded axis)

$$\sigma_{\theta X} = \frac{-2P}{\pi at}\left[\frac{\left(1-\frac{r^2}{R^2}\right)\sin 2\sigma}{\left(1+\frac{2r^2}{R^2}\cos 2\sigma+\frac{r^4}{R^4}\right)}+\tan^{-1}\left[\frac{\left(1-\frac{r^2}{R^2}\right)}{\left(1+\frac{r^2}{R^2}\right)}\tan\sigma\right]\right] \quad (2\text{-}29)$$

b. Radial stress (perpendicular to the loaded axis)

$$\sigma_{rX} = \frac{+2P}{\pi at}\left[\frac{\left(1-\frac{r^2}{R^2}\right)\sin 2\sigma}{\left(1+\frac{2r^2}{R^2}\cos 2\sigma+\frac{r^4}{R^4}\right)}-\tan^{-1}\left[\frac{\left(1-\frac{r^2}{R^2}\right)}{\left(1+\frac{r^2}{R^2}\right)}\tan\sigma\right]\right] \quad (2\text{-}30)$$

c. Shear stress

$$\tau_{\theta X} = 0 \quad (2\text{-}31)$$

(2) Stresses Along the Vertical Axis (OY)

a. Tangent stress (perpendicular to the loaded axis)

$$\sigma_{\theta Y} = \frac{+2P}{\pi at}\left[\frac{\left(1-\frac{r^2}{R^2}\right)\sin 2\sigma}{\left(1-\frac{2r^2}{R^2}\cos 2\sigma+\frac{r^4}{R^4}\right)}-\tan^{-1}\left[\frac{\left(1+\frac{r^2}{R^2}\right)}{\left(1-\frac{r^2}{R^2}\right)}\tan\sigma\right]\right] \quad (2\text{-}32)$$

b. Radial stress (parallel to the loaded axis)

$$\sigma_{rY} = \frac{-2P}{\pi at}\left[\frac{\left(1 - \frac{r^2}{R^2}\right)\sin 2\sigma}{\left(1 - \frac{2r^2}{R^2}\cos 2\sigma + \frac{r^4}{R^4}\right)} - \tan^{-1}\left\{\frac{\left(1 + \frac{r^2}{R^2}\right)}{\left(1 - \frac{r^2}{R^2}\right)}\tan\sigma\right\}\right] \quad (2\text{-}34)$$

c. Shear stress

$$\tau_{r\theta} = 0 \quad (2\text{-}35)$$

where tensile stresses are taken as positive, P is the applied load, and a, t, R, r and σ are defined in Figure 2-12. The stress distributions along these principal axes for a loading strip width less than D/10 are shown in Figure 2-13 (where D is the diameter of the sample).

According to the Griffith criterion for fracture in brittle materials, the exact center of the disc is the only point at which the conditions for tensile failure at a value equal to the uniaxial strength are met (Mellor and Hawkes, 1971). The principal stresses at the center of the speciman are given by:

$$\sigma_\theta = \frac{P}{\pi Rt}\left(\frac{\sin 2\sigma}{\sigma} - 1\right) \simeq \frac{P}{\pi Rt} \quad (2\text{-}36)$$

$$\sigma_r = \frac{-P}{\pi Rt}\left(\frac{\sin 2\sigma}{\sigma} + 1\right) \simeq \frac{-P}{\pi Rt} \quad (2\text{-}37)$$

If the arc of contact is less than or equal to 15°, the error introduced by use of the approximate formula for σ_θ (the tensile strength) is less than 2 percent (Mellor and Hawkes, 1971).

Hadley, Hudson, and Kennedy (1971) presented techniques for estimating the modulus of elasticity, Poisson's ratio, and the tensile strain assuming that the material tested behaved as a homogeneous,

istropic, and elastic (obeying Hooke's Law) material. This method requires that the total horizontal and vertical deformation be monitored during testing. The relationships for Young's modulus and Poisson's ratio are obtained from application of Hooke's Law and integration of the unit stresses over the vertical and horizontal diametrical axes giving:

$$\nu = \frac{\left[\int_{-r}^{r} \sigma_{rY} + R\int_{-r}^{r} \sigma_{rX}\right]}{\left[DR\int_{-r}^{r} \sigma_{\theta X} + \int_{-r}^{r} \sigma_{\theta} Y\right]} \qquad (2\text{-}38)$$

and

$$E = \frac{P}{X_T}\left[\int_{-r}^{r} \frac{\sigma_{rX}}{P} - \nu\int_{-r}^{r} \frac{\sigma_{\theta X}}{P}\right] \qquad (2\text{-}39)$$

where ν is Poisson's ratio, E is Young's modulus, P/X_T is the slope of the least squares line of best fit between the load (P) and the total horizontal deformation (X_T), and DR is the absolute value of the slope of the least squares line of best fit between the total vertical deformation (Y_T) and the corresponding total horizontal deformation up to the failure load.

Integration of the theoretical relationships presented above was performed by Anagnos and Kennedy (1972) for 4-inch and 6-inch diameter samples. The simplified relationships for calculating Poisson's ratio, the modulus of elasticity, and the total tensile strength at failure are presented in Table 2-1. The loading strip width

for both size samples was assumed to be 0.5 inches.

2.4.2 Factors Influencing the Split-Cylinder Test

Several factors appear to influence the indirect tensile strength determined from the split-cylinder test. Characteristics and properties of the loading strip may have a definite effect on the type of failure and test results. It is also possible that the desirable characteristics of the loading strip may vary with the type of material being tested. In addition, theoretical evidence indicates that the compression:tension strength ratio of the material may influence the value of the indirect tensile strength.

In conducting a split-cylinder test, it is beneficial to apply a distributed load to the sample since it reduces the magnitude of the maximum compressive and shear stresses and causes the stress acting perpendicular to the loaded diameter to change from tension to compression just below the strip, thus minimizing the effect of surface irregularities in the specimen. Mitchell (1961) investigated experimentally the influence of the composition and width of the loading strip. Concrete cylinders were tested using cardboard strips of varying sizes. The size of the loading plate was found to influence the type of rupture observed. Large strips usually resulted in double-cleft failures with large pieces, which in some cases did not split completely to a central fracture (Figure 2-14a). Small strips caused shattering of material immediately adjacent to the applied load as shown in Figure 14c. Intermediate size plates produced fractures ranging from ideal (Figure 2-14b) to extreme. However, the failure mode did not seem to produce any significant effect on the computed tensile strength provided the specimen ultimately failed in tension. Tests conducted

on concrete cylinders (with strain gages mounted on their faces) using cardboard and masonite strips, indicated differences in the load-strain behavior of the cylinders. With the cardboard strips, the strain increased constantly up to failure. Using the masonite strips, the strain increased constantly and, for the same load, were similar to those with the cardboard strips. At the failure strain of the first cylinder, there was a strain reversal in the speciman tested with masonite and the speciman failed from the bottom. The author concluded that the masonite strips did not provide good bearing over the entire width of the strip and that cardboard strips were preferred.

Other investigators have also looked at the influence of the loading strips. Wright (1955) conducted tests on Portland cement concrete using wood, steel, and rubber strips. He found that the strength results did not differ significantly for wood and rubber strips, but that the steel strips resulted in lower and somewhat less uniform results. Hudson and Kennedy (1968) investigated the influence of platen width and composition on the compressive strength of asphaltic concrete. Tests were conducted on 4-inch diameter samples using neoprene and steel loading strips 0.5 and 1.0 inches wide. It was recommended that steel strips be used for future work with asphalt concrete because of its practical advantage in determining vertical deformation of the sample even though experimental results indicated the scatter in the tensile strength data to be slightly less for the neoprene. They also recommended that the 1.0-inch wide strip ($\simeq$ 30 degree loading arc) be selected on the basis of reduced data dispersion. Mellor and Hawkes (1971) reviewed existing experimental and theoretical evidence and concluded that an acceptable upper bound of 15 degrees for the loading

arc was appropriate for testing brittle materials.

Both Wright (1955) and Mitchell (1961) state that a nonlinear stress-strain relationship tends to relieve stress concentrations. This would tend to increase the load required to cause failure in the specimen and to give higher strength values. Chen and Chang (1978) examined the validity of using the elasticity solution for computing the tensile strength of concrete as compared with solutions obtained from the theory of plasticity. Three types of analysis were considered for the plane strain condition: (1) Limit analysis assuming the material to be perfectly plastic, (2) slip-line field based on perfect plasticity, and (3) finite element analysis of work-hardening theory of plasticity. The relevant formulas for computing the tensile strength based on the various plasticity analyses were found to be similar to that of the elasticity solution. It was concluded that the elasticity solution gave a fairly good estimate of the tensile strength for materials such as rocks and concrete. Since these materials exhibit more elastic (or linear) stress-strain curves at high loading rates, it seems reasonable to select loading rates which are sufficiently high to suppress nonlinearity for best agreement with elastic theory.

For materials with low compression:tension strength ratios, there is some concern regarding where fracture initiates in the cylinder. Fairhurst (1964) examined theoretically the dependence of the computed tensile strength using the Hondros solution as a function of the compression:tension strength ratio. Based on an empirical generalization of the Griffith criterion, he concluded that for low values of the ratio and for narrow contact strips there was a tendency for off-center fracture initiation. This was accompanied by a systematic underestimation of the

tensile strength. The dependence of the indicated tensile strength on the strip angle was determined to decrease with increasing values of the compression:tension strength ratio. However, for a constant value of the ratio, the critically stressed region was increased with increasing loading arcs.

2.5 Flexural Behavior

The deformation response of frozen sand to static loading is characterized by immediate and time dependent deformations. The immediate deformation consists of both an elastic and a plastic component which are stress dependent for a given temperature. Time dependent creep deformations are predominantly a plastic deformation resulting from ice flow and particle reorientation as a function of stress and temperature.

The response of a frozen sand structure to stress induced by bending would then consist of both immediate and time dependent strains. Analysis of the beam behavior would require that the stress distribution both immediately after load application and during the creep process be known. Design for flexure must consider both rupture and allowable deflection over the service life of the structure.

2.5.1 Elastic Materials

At any cross-section of a beam subject to external loading there exist internal forces which may be resolved into components normal and tangential to the cross-section. Those components which are normal to the section include bending stresses. Their function is to resist the bending moment at the section. The tangential components are known as shear stresses, and they resist the transverse or shear forces applied

to the beam.

According to Popov (1968), the strength of materials approach to relating applied bending moments to the cross-sectional properties of a member, the internal stresses, and deformations, requires three fundamental steps: a plausible deformation assumption is required to reduce the statically indeterminate problem to a determinate one, the deformations causing strains must be related to stresses through appropriate stress-strain relationships, and equilibrium must be satisfied.

The fundamental assumption in flexure theory is that plane sections through a beam taken normal to the axis of the beam remain plane after the beam is subjected to bending. This condition implies that in a beam subjected to bending, fiber strains (ε) vary linearly as their respective distances from the neutral axis of the beam.

Based on these assumptions the bending stress at any point depends on the strain at that point in a manner determined by the stress-strain curve for the material. For a homogeneous material whose stress-strain curve in tension and compression is similar to that shown in Figure 2-15a, the strain is proportional to the distance from the neutral axis (Figure 2-15b) if the maximum strain in the outer fibers is less than the limit of proportionality (ε_p). If the strain at the outer fibers exceeds ε_p this is no longer true. Where the strain is greater than ε_p the magnitude of the stress is no longer proportional and depends on the stress-strain curve above the limit of proportionality (Figure 2-15c). Thus, for a given strain, the stress at a point is the same as that given by the stress-strain diagram.

When the stresses in the outer fibers are smaller than the

proportional limit σ_p, the beam behaves elastically. In this case, the neutral axis passes through the center of gravity of the cross-section. The intensity or magnitude of the bending stress normal to the section increases directly with the distance from the neutral axis according to the elastic flexure formula:

$$\sigma = -\frac{Mz}{I} \tag{2-40}$$

where M is the applied bending moment, z is the distance from the neutral axis, and I is the moment of inertia of the cross-section about the neutral axis. This expression satisfies the condition of equilibrium (Popov, 1968) and indicates that the maximum stress occurs in the external fibers (where $z = z_{max}$).

The distribution of shear stresses over the beam cross-secion depends on the shape of the cross-section and of the stress-strain curve. For bending stresses below the limit of proportionality, the fundamental strength of materials equation defines the shear stress (v) at any point in the beam cross-section as:

$$v = \frac{VQ}{Ib} \tag{2-41}$$

where V is the total shear force at the section, I is the moment of inertia about the neutral axis, b is the width of the beam at the given point, and Q is the static moment about the neutral axis of that portion of the cross-section lying between a line through the point of interest parallel to the neutral axis and the nearest outer fiber of the beam. The shear stress is largest at the neutral axis and equal to zero at the outer fibers. Shear stresses on horizontal and vertical planes through any point are equal as required to satisfy equilibrium.

Due to the combined action of shear stresses and bending stresses,

at any point in the beam there are inclined stresses of tension and compression. The largest of these stresses form an angle of 90 degrees with each other. The intensity of the inclined stresses (principal stresses) at any point is given by:

$$t = \frac{\sigma}{2} \pm \sqrt{\frac{\sigma^2}{4} + v^2} \qquad (2\text{-}42)$$

where σ and v are as previously defined. The inclination of the stress makes an angle α with the horizontal, where $\tan 2\alpha = 2v/\sigma$ (Popov, 1968). If an element of the beam is chosen at the neutral axis (where $\sigma = 0$) the tensile and compressive stresses are inclined at 45 degrees to the horizontal and are of the same magnitude as the shear stress.

Based on the fundamental hypothesis that plane sections remain plane during deformation, one may express the fundamental relationship between the curvature (κ) of the beam and the linear strain distribution across the beam section as (Popov, 1968):

$$\kappa = \frac{1}{\rho} = -\frac{\varepsilon}{z} \qquad (2\text{-}43)$$

where κ is the curvature, ρ is the radius of curvature of the neutral axis, and z is the distance from the neutral axis to the point of interest. According to Popov (1968) the derivation of this expression requires no use of material properties, and therefore, the expression can be used for inelastic problems as well as for elastic. In the case of elastic problems, the strain may be related to the bending moment as follows:

$$\varepsilon = \frac{\sigma}{E} = \frac{Mz}{IE} = \frac{z}{\rho} \qquad (2\text{-}44)$$

so that

$$\frac{1}{\rho} = \frac{M}{IE} \qquad (2\text{-}45)$$

This equation relates the bending moment M at a section of an elastic beam, having a moment of inertia I about the neutral axis, to the curvature $1/\rho$.

For small deflections the curvature is approximately equal to the second derivative of the deflection with respect to the x coordinate of the beam (the x-axis coincides with the longitudinal axis of the beam)

$$\frac{1}{\rho} \simeq \frac{d^2y}{dx^2} \qquad (2\text{-}46)$$

where y is the transverse deflection of the beam (in the z-direction) at point x. Equating expressions (2-45) and (2-46) yields the governing differential equation for the deflection of an elastic beam:

$$\frac{d^2y}{dx^2} = \frac{M}{EI} \qquad (2\text{-}47)$$

This treatment of beam deflections neglects shear deformations. If shear stresses exist, according to the theory of elasticity shearing strains must also exist. These shear strains warp the initially plane sections of the beam, which contradicts the basic assumption. However, for slender beams, it can be shown that these shear distortions are negligible (Popov, 1968) and that the bending theory is adequate provided the length of a beam is at least two to three times greater than the total depth of the member.

It has also been assumed that the deflections are small in comparison to the length of the beam. Popov (1968) indicates that for deflections on the order of one-twentieth of the length, the error with respect to the exact solution for deflections is approximately one percent. If the deflection is increased to one-tenth the length the error is increased to approximately 4 percent.

2.5.2 Time Dependent Plastic Materials

The time dependent plastic deformation of beams may be considered on the basis of linearized creep curves shown in Figure 2-2. Hult (1966) indicates that for materials whose creep curves may be approximated in this manner a state of stationary creep will always be approached. The term stationary creep here describes a creep process in which the spacial distribution of stresses remain constant.

Hult (1966) and Odqvist (1966) consider the stationary creep stress distribution in a beam subject to pure bending using the elastic analogue. For a structure where a constant state of stress prevails during the creep process the creep strain may be written as:

$$\varepsilon^{(c)} = \phi(\sigma,T)\ \Psi(t) \qquad (2\text{-}48)$$

where $\Psi(t)$ is a monotonically increasing function of time. If, as time progresses, the creep strain, $\varepsilon^{(c)}$, tends to dominate the immediate strain, ε_0, Equation (2-48) provides a estimate of the total strain. If the Bernoulli assumption of plane sections is made, the ratio of strains between any two arbitrary points on the section must be a constant. This same ratio also prevails in a beam if the material is elastic according to:

$$\varepsilon = \Phi(\sigma,T)C \qquad (2\text{-}49)$$

where C is a constant.

Therefore, the stress and strain distributions subject to stationary creep can be formed by analyzing a corresponding problem of nonlinear elasticity. The elastic analogy simply implies that the elastic strain is made to correspond to a plastic creep strain rate. In this fashion the time element is eliminated from the analysis. The elastic analogy is then expressed as (Hult, 1966; Odqvist, 1966):

$$\varepsilon = \left| \frac{\sigma}{\sigma_c} \right|^n \text{sgn } \sigma = \dot{\varepsilon}^{(c)} \qquad (2\text{-}50)$$

where the signum function (sgn σ) is -1.0 for $\sigma < 0$, 0 for $\sigma = 0$, and +1.0 for $\sigma > 0$ (σ is taken as positive in tension). Equation (2-50) corresponds to the secondary creep law (Equation 2-6) when $\dot{\varepsilon}_c = 1.0$. A similar expression can be written for the strain-hardening creep law given by Equation (2-14) by equating $\varepsilon^{(c)}$ to ε.

For the case of a beam in pure bending, as shown in Figure 2-16, Hult (1966) gives the stress distribution as:

$$\sigma_x = \frac{M}{I_n} |z|^{1/n} \text{sgn } z \qquad (2\text{-}51)$$

where

$$I_n = \int |z|^{1 + 1/n} \, dA = \int_{-H/2}^{H/2} |z|^{1 - 1/n} \, b(z) dz \qquad (2\text{-}52)$$

The positive sense of the bending moment M is taken as shown in Figure 2-16 and the quantity I_n is characteristic of the cross-section and reduces to the ordinary moment of inertia for n = 1. Since the above expression for the stress is based on the assumption that the stress-strain-time relationship is the same for both tension and compression, the neutral axis of the beam must pass through the centroid of the cross-section. Consequently, the stress distribution is symmetric about the neutral axis. The maximum stress occurs in the outer fibers and is a function of the geometry of the cross-section and the creep parameter n. As the value of n decreases the magnitude of the maximum stress increases.

Hult (1966) and Odqvist (1966) present the governing differential equation for the time dependent deflection of the beam in pure bending as:

$$\frac{d^2\dot{y}}{dx^2} = -\left|\frac{M}{\sigma_c I_n}\right|^n \text{sgn } M \qquad (2\text{-}53)$$

where $\dot{y}$ is the rate of deflection of the beam in the z direction and $(\sigma_c I_n)^n$ corresponds to the bending stiffness EI in linearly elastic bending. The total deflection of the beam at any time t may be obtained by solution of the nonlinear differential equation for $\dot{y}$ with respect to the boundary conditions and integrating with respect to time.

The creep equations (2-51 and 2-53) for the bending stresses and deflections of the beam are based on the Bernoulli assumption of plane strain. Consequently, they are most applicable when beam deflections are small. As in the case of elastic deformations, the error should not be large for deflections, on the order of 1/10 the beam length.

Klein and Jesseberger (1978) presented a method of transforming the power law given by Equation 2-6 from the uniaxial case to multi-axial states of stress based on the Prandtl-Reuss equation and the Von Mises flow rule. A finite element computer program was developed to consider an incremental treatment of creep in frozen ground assuming that the stress-strain behavior was the same in tension and compression. The computer program was used to compute the stress distribution and deflection rate of the simply supported frozen soil beam shown in Figure 2-17a. Both the rate of deflection and the stress distribution were in close agreement with the analytical solutions presented by Hult (1966) and Odqvist (1966). Figure 2-17b shows the stress distribution at a cross-section as computed from Equation (2-51) and with the finite element computer program. For a beam loaded as

shown in Figure 2-17a and composed of Karlsruher sand at -33°C, the finite element program predicted a deflection rate at the midpoint of the beam of 3.56×10^{-6} m/hr and the analytical solution gave a deflection rate of 4.11×10^{-6} m/hr. Thus, the analytical solution and the finite element analysis were shown to be in good agreement.

Table 2-1: Equations For Calculation Of Tensile Properties (Anagnos and Kennedy, 1972)

Tensile Property	Diameter of Specimen	
	4-Inch	6-Inch
Tensile Strength S_T, psi	$0.156 \frac{P_{Fail}}{h}$	$0.105 \frac{P_{Fail}}{h}$
Poisson's ratio ν	$\frac{0.0673DR - 0.8954}{-0.2494DR - 0.0156}$	$\frac{0.04524DR - 0.68040}{-0.16650DR - 0.00694}$
Modulus of Elasticity E, psi	$\frac{S_H}{h} [0.9976\nu + 0.2692]$	$\frac{S_H}{h} [0.9990\nu + 0.2712]$
Total Tensile Strain At Failure ε_T	$X_{TF}\left[\frac{0.1185\nu + 0.03896}{0.2494\nu + 0.06730}\right]$	$X_{TF}\left[\frac{0.0529\nu + 0.0175}{0.1665\nu + 0.0452}\right]$

P_{Fail} = total load at failure (maximum load P_{max} or load at first break point), in pounds

h = height of specimen, in inches

X_{TF} = total horizontal deformation at failure (deformation at the maximum load or at first break point), in inches

DR = deformation rate $\frac{Y_T}{X_T}$ (the slope of line of best fit between vertical deformation Y_T and the corresponding horizontal deformation X_T up to failure load P_{Fail})

S_H = horizontal tangent modulus $\frac{P}{X_T}$ (the slope of the line of best fit between load P and total horizontal deformation X_T for loads up to failure load P_{Fail})

Strain Rate, $\dot{\varepsilon}$
Strain, ε

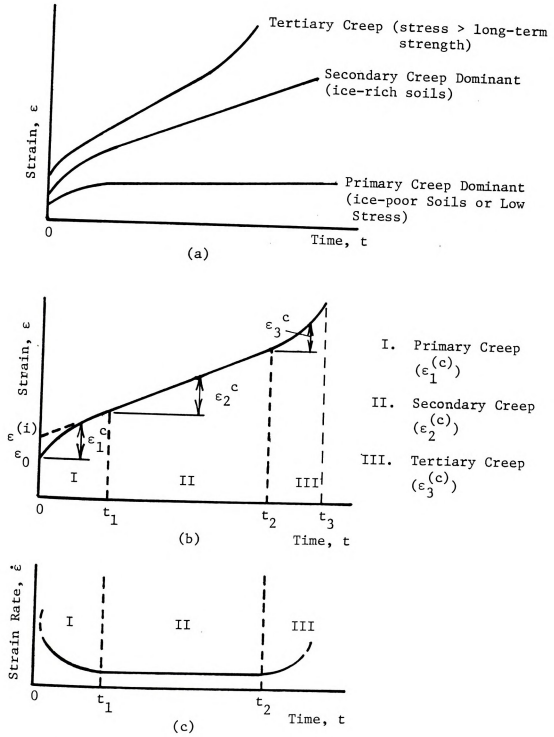

Figure 2-1: Constant Stress Creep Test; (a) Creep Curve Variations, (b) Classical Creep Curve, (c) Strain Rate versus Time (Andersland, et al, 1978).

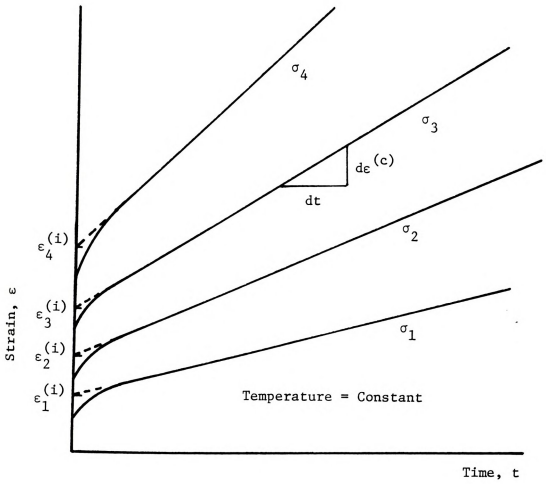

Figure 2-2: Linearized Creep Curves with $\sigma_1 < \sigma_2 < \sigma_3 < \sigma_4$ (Hult, 1966).

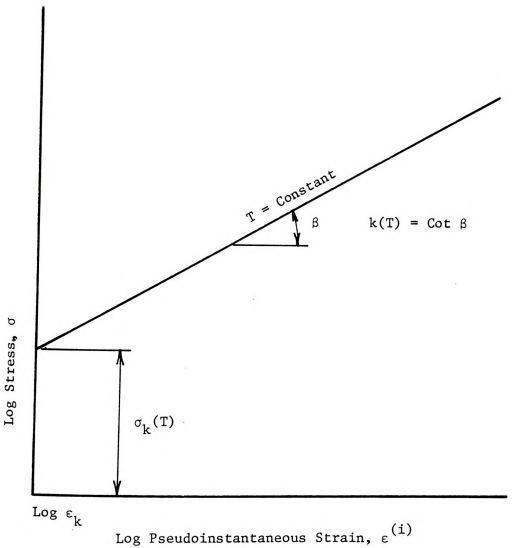

Figure 2-3: Log-Log Plot of Pseudoinstantaneous Strain versus Stress for Determination of σ_k and k.

For Sistas Only

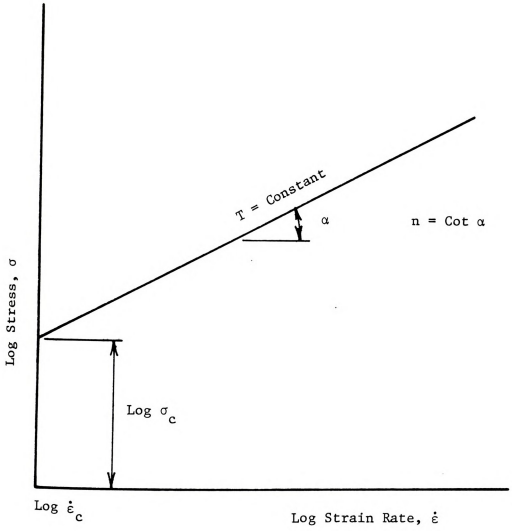

Figure 2-4: Log-Log Plot of Stress versus Strain Rate for Determination of n and σ_c.

Strain, ε

Figure

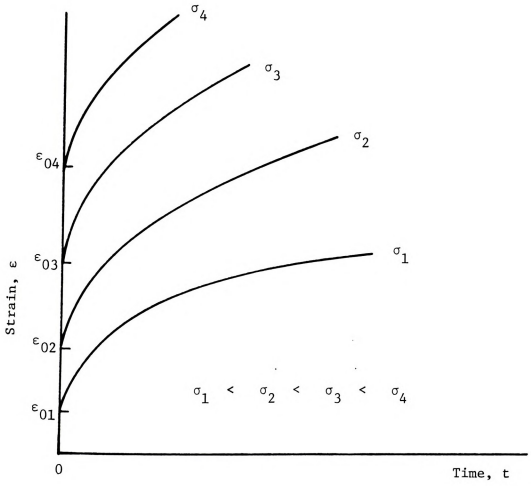

Figure 2-5: Primary Creep Curves (Hult, 1966).

Figure 2

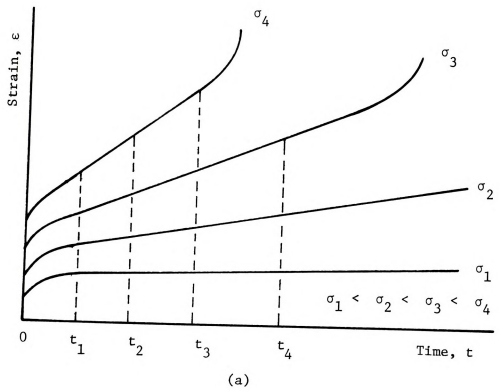

(a)

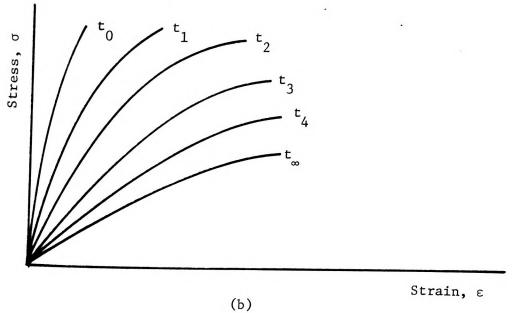

(b)

Figure 2-6: Curves Showing Relationship Between Stress and Deformation; (a) Creep Curves, (b) Isocurves (After Vyalov, 1963).

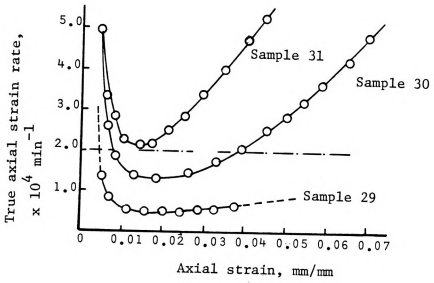

(a)

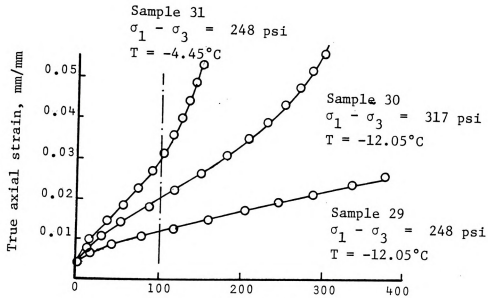

(b)

Figure 2-7: Creep Tests on Polycrystalline Ice; (a) Strain Rate versus Strain, (b) Creep Curves (Goughnour, 1967).

Peak axial stress (psi)

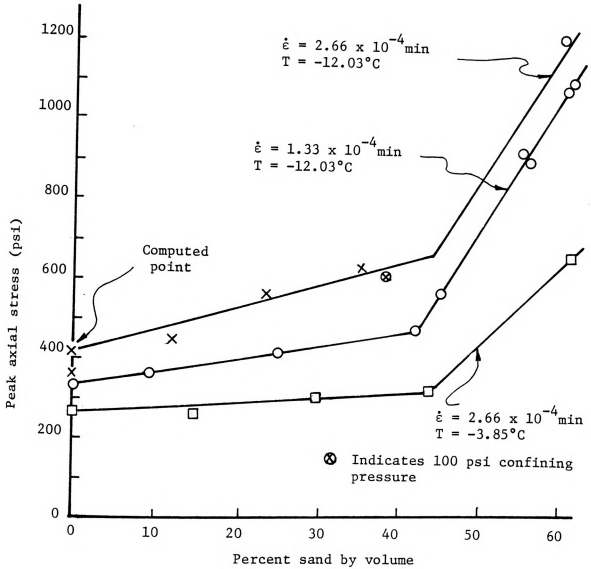

Figure 2-8: Effect of Volume Concentration of Sand on Peak Strength (Goughnour, 1967).

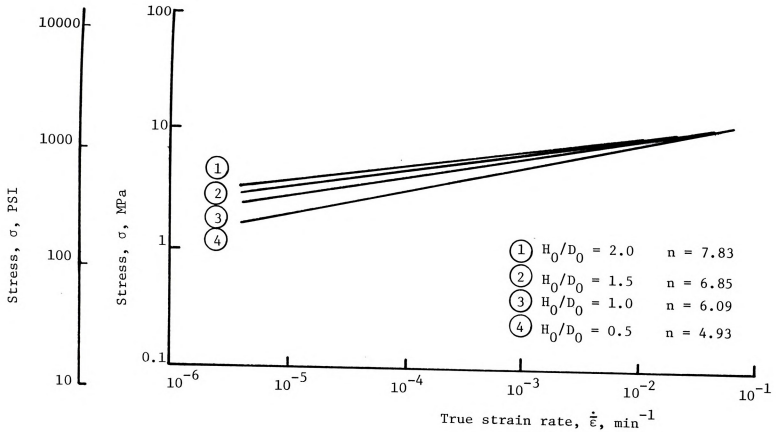

Figure 2-9: Stress versus True Strain Rate Curves for Specimens with Different Slenderness Ratios, Compressed Between Smooth Platens, at e = 0.77, and T = -5°C. (Ladanyi and Arteau, 1978).

Unconfined Compressive Strength, psi

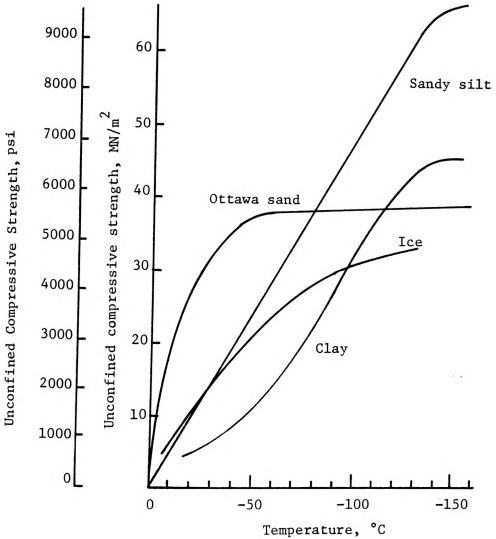

Figure 2-10: Temperature Dependence of Unconfined Compressive Strength (After Sayles, 1966).

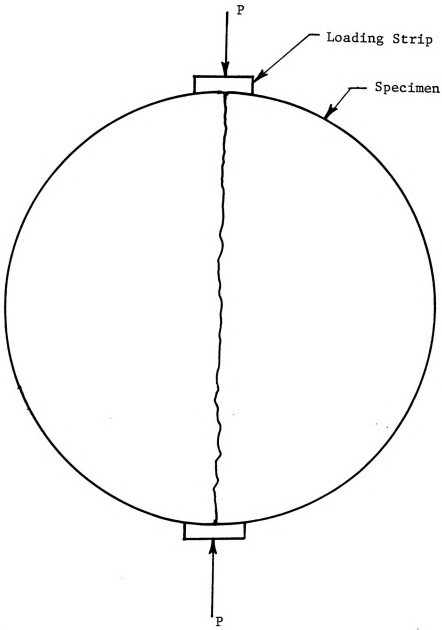

Figure 2-11: Indirect Tensile Test.

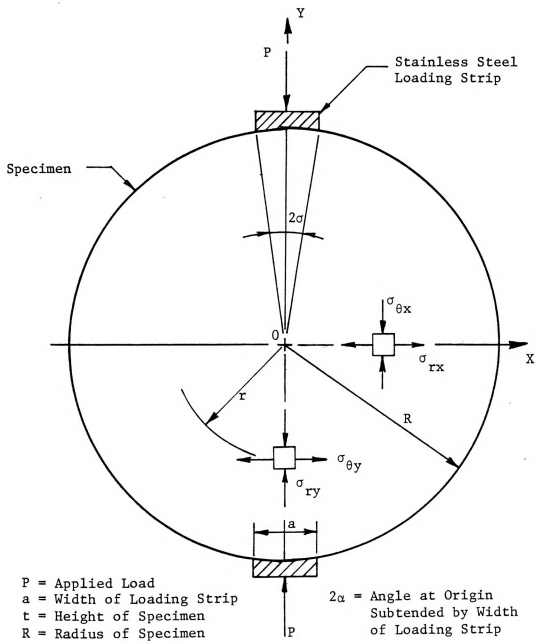

Figure 2-12: Loading Conditions for the Indirect Tensile Test (After Hondros, 1959).

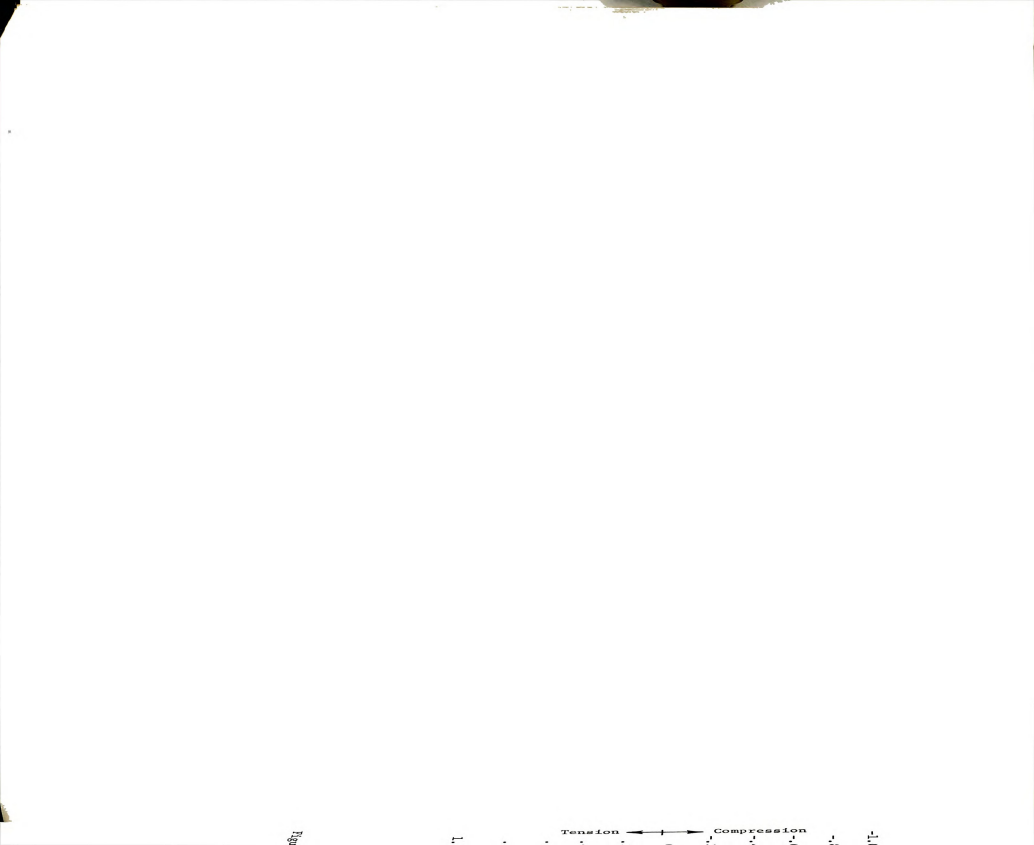
Tension
Compression

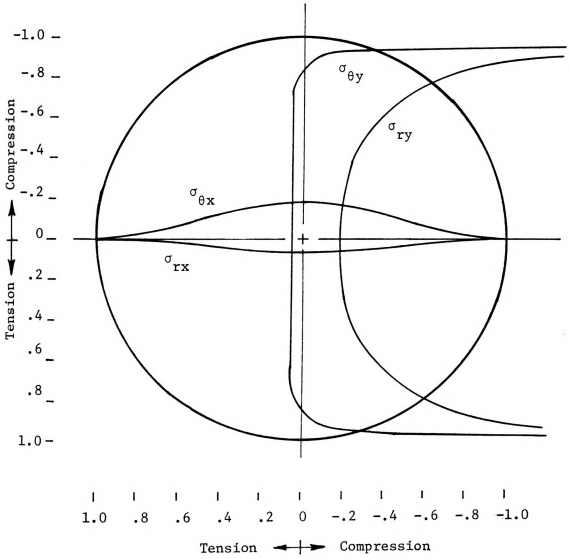

Figure 2-13: Stress Distribution Along the Principal Axes for Loading Strip Width, a, Less Than D/10 (Hudson and Kennedy, 1978).

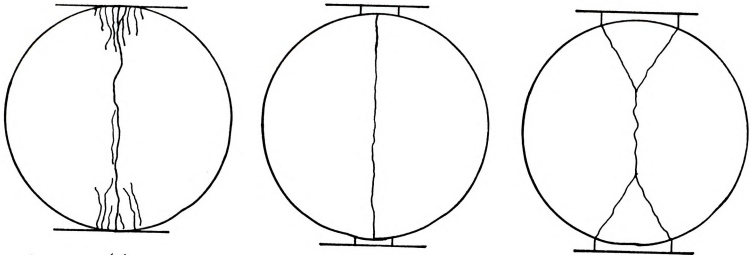

Figure 2-14: Typical Failure Modes; (a) No Loading Strip, (b) Ideal Loading Strip, (c) Wide Loading Strip (Mitchell, 1961).

Figure 2

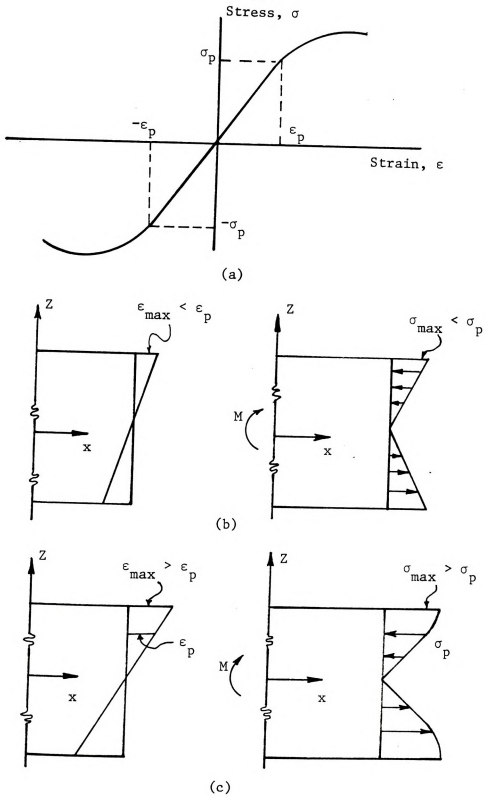

Figure 2-15: Elastic and Inelastic Stress Distributions in a Homogeneous Beam; (a) Stress-Strain Curve, (b) Elastic Stresses, (c) Plastic Stresses.

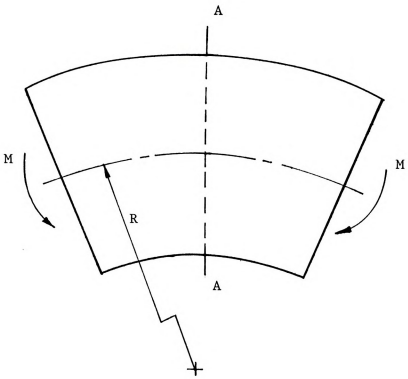

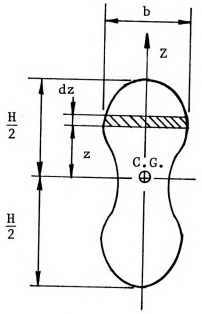

Section A-A

Figure 2-16: Pure Bending of a Bisymmetric Beam.

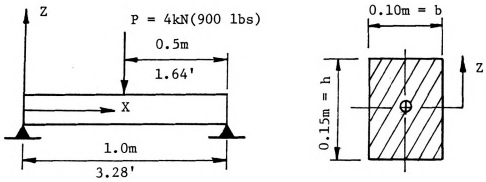

(a)

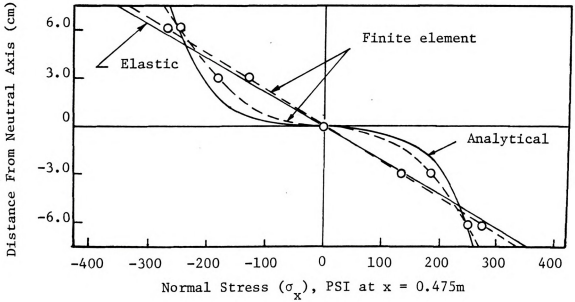

(b)

Figure 2-17: Frozen Soil Beam; (a) Diagram of Simply Supported Beam; (b) Stress Distribution (After Klein and Jessberger, 1978).

CHAPTER III

MATERIAL AND SAMPLE PREPARATION

A commercially available silica sand produced by the Wedron Division of the Pebble Beach Corporation of Wedron, Illinois was selected for this investigation. The 40-40 Wedron sand consisted of sub-angular quartz particles with a specific gravity of 2.65. The sand gradation was uniform with all material passing the number 30 U.S. standard sieve and retained on the number 140 sieve. The coefficient of uniformity was approximately 1.50.

A sand volume fraction of 64 percent was selected to give a dense soil mass. This volume fraction was selected for ease of compaction and is comparable to values normally encountered in the field. It is also well above the critical volume fraction of 42 percent determined by Goughnour (1968) to be the point where interparticle friction and dilatancy contribute significantly to the compressive strength of frozen sand. The actual sand volume fractions for all samples tested varied from 63.1 to 64.9 percent. These values correspond to void ratios varying from 58.5 to 54.1 percent, respectively.

All samples were prepared in split aluminum molds. Extensions, 0.375 inches high, were attached to the open end of each mold to aid in compaction. The molds were disassembled and cleaned prior to compacting each sample. A thin coat of silicone grease was applied to the inner mold surfaces to reduce adhesion at the sample-mold interface and to aid in sample removal after freezing.

The correct amount of oven dried sand, to provide a volume fraction of 64 percent, was predetermined using mold volumes (with extensions

attached

degree c

demineral

into the

degree c

from 96

-12°C (

mold si

the mol

Th

allowed

assumed

were fi

sharpen

platens

enclos

3.1 U

U

and at

sample

height

sample

of st

const

and a

sampl

at -6

attached) and the specific gravity of the sand. To insure a high degree of saturation, the molds were partially filled with distilled demineralized water and the sand was slowly poured through a funnel into the molds, allowing air bubbles to escape to the surface. The degree of ice saturation for samples prepared in this manner ranged from 96.1 to 99.9 percent based on an ice density of 0.9185 gm/cm^3 at -12°C (Pounder, 1967). Sample compaction was achieved by tapping the mold sides and bottom sufficiently to level the sand with the top of the mold.

The mold and samples were then placed in a cold box at -12°C and allowed to freeze for at least 12 hours. After this period it was assumed that essentually all of the water was frozen. Mold extensions were first removed and the exposed sample surface was trimmed with a sharpened paint scraper giving a uniform seating area for the loading platens. Samples were then removed from the molds, weighed, and enclosed in rubber membranes to prevent sublimation during storage.

3.1 Uniaxial Compression Test Samples

Uniaxial constant strain rate compression tests conducted at -6°C and at a strain rate of approximately $1.2 \times 10^{-4} sec^{-1}$ on cylindrical samples (diameters of 1.13, 1.41, 1.94 and 2.40 inches with a 2:1 height to diameter ratio) were used to investigate the influence of sample size on the mechanical properties of frozen sand. The effects of strain rate and temperature were determined from tests conducted at constant strain rates ranging from $5.69 \times 10^{-7} sec^{-1}$ to $1.78 \times 10^{-3} sec^{-1}$ and at temperatures of -2, -6, -10, and -15°C using 1.41 inch diameter samples. Constant axial stress compression creep tests were conducted at -6°C using samples 1.13 inches in diameter. These sample diameters

were se

for co

availa

as a s

was ap

ventio

necess

stress

tertia

P

(disk)

of the

reduce

sample

The l

of th

plate

sampl

conta

trans

water

for t

what

to th

atta

load

were selected to stay within the capacity of the test equipment and for convenience, since molds in most of these sizes were already available in the laboratory. The 1.41-inch diameter sample was chosen as a standard for comparison of rate and temperature effects since it was approximately the same diameter as samples normally tested in conventional triaxial cells. For the constant stress creep tests, it was necessary to use the smaller 1.13-inch diameter sample size to obtain stress levels (using a dead weight hanger system) high enough to reach tertiary creep in less than eight hours.

Prior to mounting samples in the triaxial cell, stainless steel (disk) loading platens were placed on each end of the sample. Surfaces of the loading platens were coated with a thin layer of Teflon to reduce end effects. Two protective membranes were placed over the samples and fastened securely to the loading platens with rubber bands. The 1.13 and 1.41-inch diameter samples were then mounted on the base of the triaxial cell (inside a cold box) by screwing the bottom loading platen onto the loading pedestal. The triaxial cell was placed over the sample, attached to the cell base, and the loading ram was brought into contact with the top loading platen. The entire triaxial cell was then transferred to a low temperature circulating bath of ethylene glycol and water and the cell was allowed to fill with coolant.

In order to use available equipment, the mounting procedure required for the larger diameter samples (1.94 and 2.40 inch diameters) was somewhat different. After the loading platens and membranes had been applied to the samples, they were transferred to the low temperature bath and attached to the base of the cell by screwing the bottom platen onto the loading pedestal. A cylindrical aluminum cell was placed over the sample

and the ram of the loading frame was lowered into contact with the top loading platen.

These mounting procedures protected the samples from any contact with the coolant fluid which contained ethylene glycol. While sample trimming and mounting took approximately one hour, the samples were exposed to temperatures above 0°C for only a few seconds while being transferred from the cold box to the low temperature bath.

Sample temperatures were allowed to adjust to the cold bath temperature prior to testing. A period of at least 6 hours was allowed for the smaller samples (1.13 and 1.41-inch diameters) and at least 12 hours was allowed for temperature equilibration for the larger samples (1.94 and 2.40-inch diameters).

After the sample had been tested the triaxial cell was disassembled and the sample removed. The membrane and sample were inspected for leaks and the failure mode was noted and sketched (in most cases the samples were also photographed). The oven dry weights were then determined and the volume fraction and degree of ice saturation computed based on the mold volume.

3.2 Split Cylinder Test Samples

The influence of sample size on the indirect tensile strength of the frozen sand was determined using disk shaped samples prepared in split aluminum molds with a height to diameter ratio of 0.5 and diameters of 1.94, 2.40 and 4.00 inches. The test temperature was maintained at -6°C and the applied vertical deformation rate was adjusted to give an average vertical strain rate of $6 \times 10^{-4} sec^{-1}$ for each size sample (average strain rate = vertical deformation rate ÷ sample diameter). Samples for investigation of rate and temperature effects were prepared in the

4.00-

rangi

and -

for u

devic

The 4

later

of th

loadi

consi

the s

lower

rubbe

lower

clamp

rods

stre

defo

just

then

leas

briu

was

was

weig

and

vol

4.00-inch diameter molds and tested at vertical deformation rates ranging from 0.002 to 0.280 in/min at temperatures of -2, -6, -10, and -15°C. The 1.94 and 2.40-inch diameter samples were selected for use since they compared roughly with the diameters of coring devices (BX and NX sizes) normally used in field investigations. The 4.00 inch diameter sample provided a convenient size for measuring lateral deformations and represented an upper bound on the dimensions of the samples to remain within the testing capacity of the available loading frame and load transducer.

The mounting procedure for the split cylinder samples was considerably simpler than for the uniaxial compression tests. After the samples had been trimmed and weighed, they were mounted on the lower half of the loading jig (described in Chapter IV). A rubber membrane was placed over the sample and fastened securely to the lower circular loading plate with a rubber o-ring and a steel hose clamp. The top half of the loading jig was then aligned with the guide rods and brought into contact with the sample. The membrane was stretched over the top loading plate and secured as before. The lateral deformation transducer was then attached to the jig assembly and adjusted to rest against the sample sides. The loading jig assembly was then transferred from the cold box to the low temperature bath. At least 12 hours was allowed for the sample temperature to reach equilibrium with the bath before testing. Immediately after testing the jig was disassembled and the sample inspected for leaks. The failure mode was sketched and the sample was oven dried at 110°C to determine the weight of sand. As with the uniaxial tests, the sand volume fraction and the degree of ice saturation were computed based on the mold volume and the weight of the sand.

CHAPTER IV

EQUIPMENT AND TEST PROCEDURES

The influence of sample diameter on the compressive strength of the frozen sand was investigated using samples varying in size from 1.13 inch to 2.40 inches in diameter. Since conventional triaxial cells available in the laboratory were not large enough to accompany the larger sample sizes, existing equipment was modified for use in the testing program. Similarly, the loading apparatus used to determine the indirect tensile behavior of the frozen sand was designed and built expressly for this investigation. This chapter presents a description of the equipment and test procedures used to determine the mechanical properties of the sand-ice material.

4.1 Equipment

A standard triaxial cell was used for the uniaxial compression tests and for the constant strain rate compression tests conducted on the 1.13 and 1.41-inch diameter samples. The samples rested on a stainless steel platen which screwed onto the end of a loading pedestal attached directly to a Strainsert Model FL5U-2SPKT flat load cell (rated capacity of 5,000 pounds). Figure 4-1 presents a schematic diagram of the triaxial cell assembly.

The uniaxial compression tests (constant strain rate) on the 1.94 and 2.40-inch diameter samples were conducted using the modified triaxial cell shown in Figure 4.2. The samples rested on a stainless steel platen which screwed directly onto the end of a 15,000 pound capacity stud type load transducer (Strainsert Model Q-1096). The cell consisted

of a 5.0

The loadi

cell. S

due to c

construc

ram of t

directly

a hemisp

lubricat

and the

The

jig show

opposite

with a

was adj

of the

sample

Model F

A co

the tes

circula

mixture

using a

with s

bath.

sample

voltme

of a 5.0 inch O.D. aluminum pipe capped with a circular aluminum plate. The loading ram of the test frame served as the piston for the triaxial cell. Since the cell served only to reduce the temperature variation, due to cycling of the refrigeration coolant bath, the cell was not constructed to apply confining pressures. The sample and the loading ram of the test frame were aligned by centering the base of the cell directly under the ram. The load was transmitted to the sample through a hemispherical piston cap attached to the upper loading platen. A lubricated hardened steel washer was placed between the loading ram and the piston cap in an attempt to minimize any eccentricity.

The indirect tensile strength was determined using the loading jig shown schematically in Figure 4-3. The load was applied to opposite sides of the sample through two stainless steel loading strips with a radius matching that of the sample. The width of the loading strips was adjusted such that the angle at the origin subtended by the width of the strips was approximately 15 degrees. The load applied to the sample was measured using a 10,000 pound capacity load cell (Strainsert Model FL10U-2SPKT) attached to the end of the loading ram.

A constant temperature was maintained during testing by immersion of the test apparatus (triaxial cell or split cylinder loading jig) in a circulating low temperature bath of ethylene glycol and water (50-50 mixture). The temperature of the coolant fluid was maintained to $\pm$ 0.1°C using a micro-regulated refrigeration unit and circulator. A thermometer with scale divisions of 0.1°C was used to monitor the temperature of the bath. The temperature of the coolant immediately adjacent to the samples was determined to $\pm$ 0.05°C using a thermistor and digital voltmeter. Figure 4-4 shows a diagram of the testing equipment and

coolant

Tw

All co

using

with a

loadin

Result

slight

load h

tests

a 10,(

displ

split

screw

testi

that

rates

a deg

bath.

the p

(for

the

samp

form

eith

atta

coolant circulation system.

Two different load frames were used during the testing program. All constant strain rate uniaxial compression tests were conducted using a Wykeham-Farrance (Model WF 10050) variable speed testing machine with a 10,000 pound capacity. This frame had a 30 speed gear box with loading rates varying from 0.225 to 0.00024 inches per minute. Results indicate that the cross-head displacement rate increased slightly during testing, reaching the selected rate only after the peak load had been reached. The uniaxial creep tests and the split cylinder tests were conducted using a Soiltest load frame (Model T-118-X) with a 10,000 pound capacity and Graham variable speed gear box. The displacement rates were also observed to vary slightly during the split cylinder test. The transmission on this test frame was of the screw type which permitted displacement rates to be corrected during testing, but the split cylinder tests were of such short duration that insufficient time was available for correction of the displacement rates. The uniaxial constant stress creep tests were performed using a dead-weight hanger which straddled the test frame and low temperature bath. The electric motor and gear box were used to raise and lower the hanger.

Axial displacement of the uniaxial compression test samples (for both constant strain rate and constant stress creep tests) and the deformation across the loaded diameter of the split cylinder samples were monitored using a Sanborn Linearsyn differential transformer (Model 585DT-1000). When used with the triaxial cells to conduct either the creep or constant strain rate tests, the transformer was attached to the loading ram with the core element bearing on the top

of the triaxial cell as shown in Figures 4-1 and 4-2. The transformer was also attached to the loading ram during the split cylinder tests, with the core element resting on a stationary portion of the loading apparatus as shown in Figure 4-3. All deformation measurements obtained in this fashion contained elastic deflections of the loading ram. These deflections were determined by placing steel cylinders in the test equipment and monitoring the deflections as a function of the applied loads. The measured sample deformations were than corrected by subtracting the elastic deflection of the ram.

The lateral deformation along the diametrical axis perpendicular to the axis of the split cylinder samples was recorded using a specially designed transducer. The Lateral Deformation Transducer (LADT) consisted of two cantilever bars fitted with four resistance strain gages (Micro-Measurements, Type EA-06-125PC-350) arranged in a full Wheatstone bridge circuit. The cantilever bars were fixed to the sides of two aluminum adjustment blocks resting on a rack and pinion device. Movements or deflections of the beams at the points of contact with the specimen were calibrated with the output of the bridge circuit. Figure 4-5 shows a photograph of the split cylinder loading jig and LADT with a sample in place.

The outputs from the various transducers were recorded using two different strip chart recorders. A Sanborn 2 channel recorder (model 7702B) and preamplifier (Model 8805A) was used to record the load and axial deformation for all constant strain rate uniaxial compression tests. At maximum sensitivity, one centimeter needle deflection on this recorder represented 0.0053 inches axial deflection for the differential transformer, 99.26 pounds for the 5,000 pound capacity

flat

stud

and u

Sanbo

1100)

needl

diffe

defor

capac

strai

a bu

burr

in t

volu

bure

chan

4.2

test

the

test

of

seq

flat load cell, and 150.18 pounds for the 10,000 pound capacity stud transducer. The load and deformation data from the split cylinder and uniaxial constant stress creep tests was recorded using a Sanborn 4 channel recorder (Model 150) and preamplifiers (Model 150-1100). At maximum sensitivity for this recorder one centimeter of needle deflection represented 0.0032 inches deflection for the differential transformer, 0.0066 inches deflection for the lateral deformation transducer, and 138.21 pounds for the 10,000 pound capacity flat load cell.

Sample volume change measurements were obtained for 8 constant strain rate compression tests and 3 constant stress creep tests, using a burette and flexible tube connected to the triaxial cell. The burrette was fixed to the side of the coolant tank. The fluid level in the burette was only slightly above the coolant surface to minimize volume changes in the fluid due to any temperature differential. The burette, calibrated with scale divisions of 0.1 cm^3, permitted volume changes to be estimated to the nearest 0.01 cm^3.

4.2 Test Procedures

Test procedures for the constant strain rate uniaxial compression tests and the split cylinder tests were essentually the same. After the sample had been mounted in the triaxial cell or loading jig, the test apparatus was submerged in the cold bath. When a sufficient period of time had elapsed for temperature stabilization, the following test sequence was followed:

1. The transducer circuits were connected to the recorder, which was allowed to warm up for approximately one-half hour prior to testing. After the warm-up period, the transducers were

2.

3.

4.

5.

6

adjusted to a zero reading.

2. The loading ram of the test frame was brought into contact with the test apparatus, but with no applied load. For constant strain rate uniaxial compression samples 27 through 90, a small seating stress of approximately 100 psi was applied to the samples prior to testing. The manual loading feature of the Wykeham-Farrance test frame was used to apply the seating load and the magnitude was monitored with the load transducer. The speciman was not tested until the seating stress had been decreased to nearly zero by sample relaxation. This procedure was intended to provide a more uniform contact surface between the sample and the loading platens and served to minimize data scatter. Prior to use of this procedure, several samples (23 through 26) exhibited failure surfaces through the trimmed end of the sample, indicating the presence of small surface irregularities.
3. The temperature of the cold bath adjacent to the sample (inside the triaxial cell for the uniaxial compression tests) was observed and recorded.
4. The gear box controls for the loading ram were adjusted to give the desired loading rate and the loading ram was engaged.
5. The deflection of the stylus needles on the recorder were observed as the test progressed. The attenuation of the recorder was adjusted, as needed, to keep the trace on the recording paper.
6. All constant strain rate uniaxial compression samples were strained to at least 7 percent (failure or peak stresses

7.

8.

T

conduc

of lea

100 ps

12 hou

sample

seatir

the ha

triax

frame

monit

inter

for t

remai

cases

normally occurred at less than 5 percent axial strain). Failure in the split cylinder tests was usually quite sudden, with the load dropping immediately to zero. The drive mechanisms for the recorder and test frame were then stopped and the temperature of the bath recorded.

7. Circuits from the transducers were then disconnected from the recorder and the test apparatus was removed from the cold bath. Samples were oven dried at 110°C to determine the dry weight of sand.
8. Recorder strips were labeled and filed until the data could be transcribed to data sheets.

The constant stress uniaxial compression (creep) tests were conducted using static loads applied by a hanger supporting a dead weight of lead bricks. Prior to testing, a seating stress of approximately 100 psi was applied and the samples allowed to creep for approximately 12 hours to minimize surface irregularities at the trimmed end of the samples. Axial strains observed in the samples, as a result of this seating stress, were less than 0.2 percent. To apply the test load, the hanger (and lead bricks) was lowered onto the loading ram of the triaxial cell using the fastest rate possible with the Soiltest loading frame. After the load was applied the deflection of the sample was monitored with the differential transformer and, at predetermined intervals, small increments of weight were added to the hanger to correct for the increased sample cross-sectional area. Weights were allowed to remain on the sample until initiation of tertiary creep (and in some cases, until rupture). The sample was then unloaded and the triaxial

cell

sketc

of sa

cell removed from the cold bath and disassembled. The failure mode was sketched and the sample was oven dried at 110°C to determine the weight of sand.

Figur

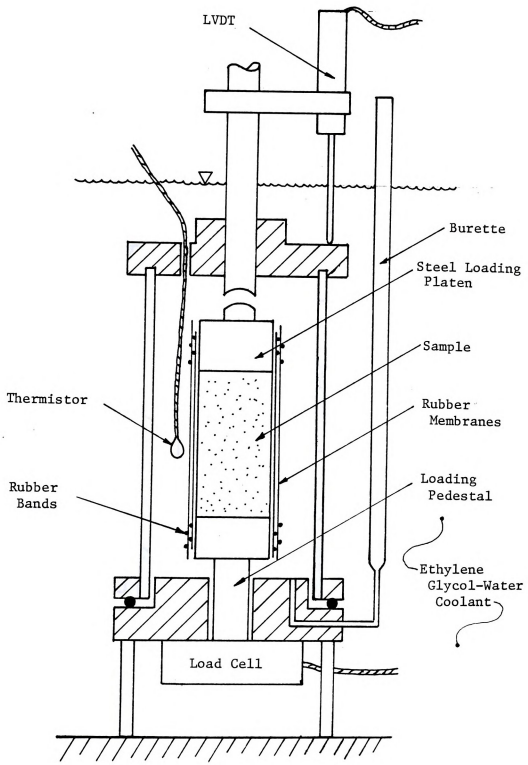

Figure 4-1: Diagram of Triaxial Cell Used for Uniaxial Compression Tests.

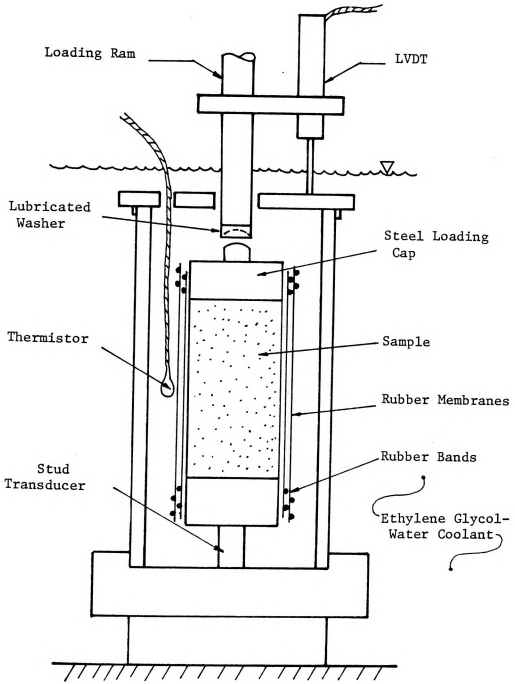

Figure 4-2: Modified Triaxial Cell.

Spl
Cyl
Loa
Jig

Eth
Gly
Coc

Fig

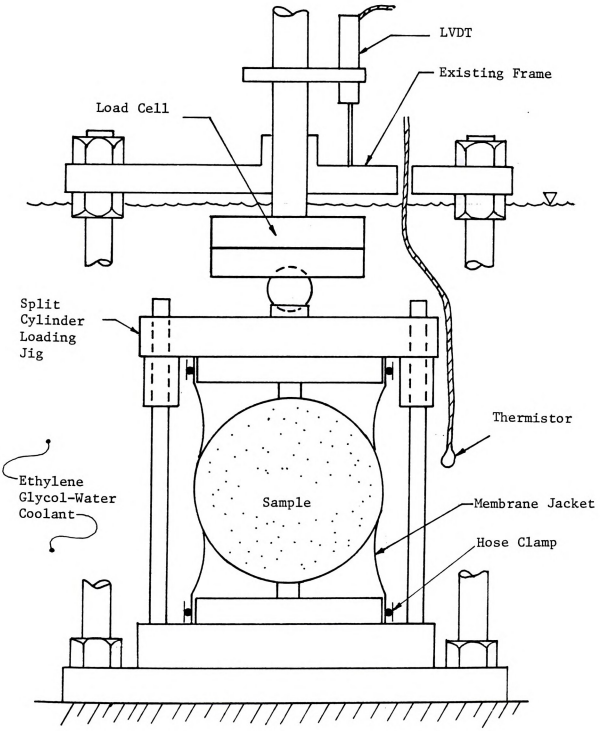

Figure 4-3: Diagram of Split Cylinder Test Equipment.

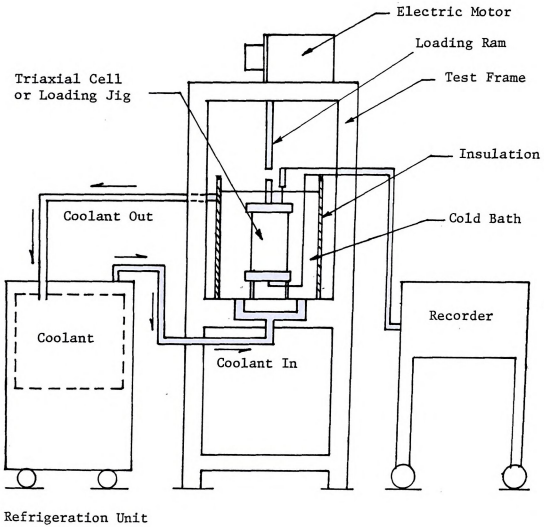

Figure 4-4: Diagram of Test System.

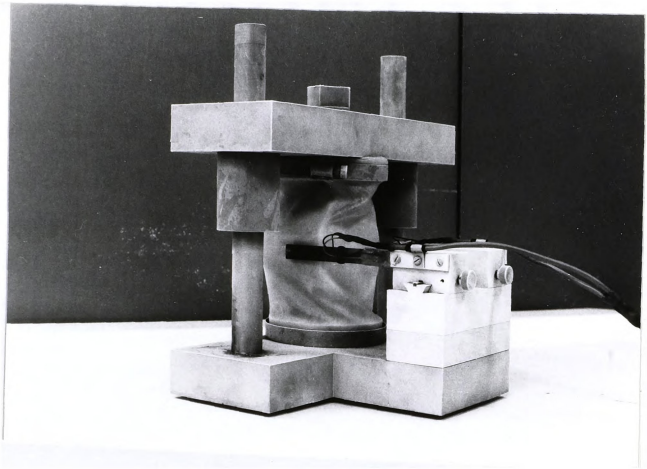

Figure 4-5: Split Cylinder Loading Jig with Lateral Deformation Transducer (LADT) in Place.

CHAPTER V

EXPERIMENTAL RESULTS

Experimental results along with a brief discussion of implications of these results are given in Chapter V. This material is presented in three parts: constant strain rate uniaxial compression tests, constant stress uniaxial compression creep tests, and split cylinder tests.

5.1 Constant Strain Rate Uniaxial Compression Tests

The constant strain rate (unconfined) uniaxial compression test provided information on the mechanical properties of frozen Wedron sand. Several investigators have noted that strain rate, temperature, and sample shape influence the compressive strength of frozen sand. In addition, constant strain rate compression tests have been suggested for determination of the creep parameters needed to predict time dependent deformation of frozen soils subject to constant stress loading conditions. However, the influence of temperature, strain rate, and sample diameter on the stress-strain behavior of frozen sand has not been fully assessed. Data is not available for a direct comparison between creep parameters obtained from constant stress creep tests and constant strain rate tests.

This section presents results from a series of constant strain rate uniaxial compression tests conducted to determine the influence of sample diameter, temperature, and strain rate on the stress-strain behavior of frozen Wedron sand. Table 5-1 summarizes the physical properties (dry density, sand volume fraction, and degree of ice saturation) of samples

used

summ

froz

5.1.

mate

stra

5.65

appr

-10

con

5-1

for

1.1

sho

dur

aft

wa

of

av

Fi

ti

sa

5.

a

used for the constant strain rate compression tests. Table 5-2 summarizes test results with respect to mechanical properties of the frozen sand in compression.

5.1.1 Strain Rate Effects

The strain rate effect on the stress-strain behavior of sand-ice materials in compression was investigated using a series of constant strain rate tests conducted at nominal strain rates between $5.69 \times 10^{-7} sec^{-1}$ and $1.78 \times 10^{-3} sec^{-1}$ and a sand volume fraction of approximately 64 percent. Temperatures were held constant at -2, -6, -10 and -15°C.

A Wykeham-Farrance variable speed testing machine was used to conduct all of the constant strain rate compression tests. Figures 5-1 and 5-2 present plots of stress versus time and strain versus time for samples 44 and 45 tested at -6°C and nominal strain rates ($\dot{\varepsilon}_n$) of $1.19 \times 10^{-4} sec^{-1}$ and $8.89 \times 10^{-4} sec^{-1}$, respectively. These figures show that the strain rate (or cross-head displacement rate) increased during testing, approaching the selected or nominal strain rate only after the peak stress was obtained. The variation in the strain rate was due to stiffness of the test apparatus and appears to be typical of all tests conducted on the Wykeham-Farrance loading frame. The average strain rate ($\dot{\varepsilon}_{ave}$) for each test was determined as shown in Figures 5-1 and 5-2; by dividing the axial strain at failure by the time to reach the peak stress (failure was assumed at the peak stress).

The stress-strain behavior and deformation modes for the frozen sand appear to be governed by the applied axial strain rate. Figure 5-3 presents stress-strain curves for samples 58, 59, and 63 tested at -10°C and at average strain rates ranging from 2.52×10^{-4} to

4.82

modes

froze

of fa

obser

sand

by a

was

the

valu

harv

2 x

the

at

2

us

al

th

st

cu

o

i

s

$4.82 \times 10^{-7} sec^{-1}$. The photographs in Figure 5-4 illustrate the failure modes associated with these samples. The deformation behavior of the frozen sand was observed to change from a ductile to a brittle type of failure as the strain rate increased. This general trend was also observed for samples tested at -2, -6, and -15°C.

At low average strain rates (less than $7 \times 10^{-6} sec^{-1}$), the frozen sand deformed elastically in the early stages of deformation followed by an initial yield or rapid change in slope. The initial yield point was followed by a prominent region of plastic strain hardening up to the peak stress (defined as failure). As the strain rate increased, the value of the initial yield stress increased and the region of strain hardening became less pronounced. At high average strain rates (above $2 \times 10^{-4} sec^{-1}$), the stress-strain curves remained nearly linear up to the peak stress.

In most cases, the initial yield point was not as clearly defined at the higher strain rates, as for average strain rates below $2 \times 10^{-4} sec^{-1}$. Consequently, the construction shown in Figure 5-6 was used to systematically estimate the initial yield stress and strain for all samples tested. A line parallel to the initial linear portion of the stress-strain curve (below the yield stress) was offset by a small strain value. The intersection of the offset line and the stress-strain curve was defined as the initial yield point. The value of the strain offset for each test temperature was selected to provide points of intersection near the visable yield in the stress-strain curves. A strain offset of 0.1 percent was used for samples tested at -2, -6 and -10°C, while a value of 0.2 percent was found to be more appropriate for samples tested at -15°C.

The results obtained from this construction procedure are presented on a log-log plot of initial yield stress versus average strain rate ($\dot{\varepsilon}_{ave}$) to failure in Figure 5-6. This plot implies that a straight-line relationship may be the most appropriate to describe the effect of strain rate on the initial yield stress (σ_y) of the material; suggesting a power expression of the form:

$$\sigma_y = \sigma_c(\dot{\varepsilon}_{ave})^m \qquad (5\text{-}1)$$

where σ_c and m are defined as in Equation (2-20). The initial yield strain was observed to be nearly independent of the applied strain rate as shown by Figures 5-3 and 5-7.

Samples tested at average strain rates less than $7 \times 10^{-6}\text{sec}^{-1}$ remained nearly cylindrical, with no visible shear planes or cracking, at strains well in excess of the peak stress (Figure 5-4a). For moderate average strain rates, between $7 \times 10^{-6}\text{sec}^{-1}$ and $2 \times 10^{-4}\text{sec}^{-1}$, the samples exhibited well defined shear planes inclined at an angle of approximately 60 degrees to the horizontal as shown in Figure 5-4b. At higher strain rates ($\dot{\varepsilon}_{ave} \geq 2 \times 10^{-4}\text{sec}^{-1}$), the samples developed multiple conjugate slip-lines or fractures inclined at angles of approximately 60 degrees to the horizontal. The inclination of the failure surfaces for both the moderate and high nominal strain rates suggests that the mobilized angle of internal friction was close to 30 degrees for these tests.

For average strain rates below $7 \times 10^{-6}\text{sec}^{-1}$, the peak stress or compressive strength (σ_f) was observed to be a function of the applied strain rate. Figure 5-8 shows a log-log plot of compressive strength versus the nominal axial strain rate and Figure 5-9 presents a log-log plot of the compressive strength versus the average strain rate up

to failu

sive str

law of t

where σ

($\dot{\varepsilon}_{ave}$ m

are def

7 x 10^{-}

strengt

rate fo

Th

decrea

curves

versus

strain

is nea

As the

brittl

than

below

rate

deter

analy

below

initi

linea

to failure. At average strain rates below $7 \times 10^{-6} sec^{-1}$ the compressive strength increased linearly with strain rate according to a power law of the form:

$$\sigma_f = \sigma_c (\dot{\varepsilon}_{ave})^m \qquad (5\text{-}2)$$

where σ_f is the compressive strength, $\dot{\varepsilon}_{ave}$ is the average strain rate ($\dot{\varepsilon}_{ave}$ may be replaced by $\dot{\varepsilon}_n$ for $\dot{\varepsilon}_n \leq 1 \times 10^{-5} sec^{-1}$) and σ_c and m are defined as in Equation (2-20). For average strain rates above $7 \times 10^{-6} sec^{-1}$ (nominal strain rates above $1 \times 10^{-5} sec^{-1}$), the compressive strength appears to be relatively independent of the applied strain rate for the range of strain rates considered.

The axial strain at failure (at peak stress) was observed to decrease with increasing strain rate as shown by the stress-strain curves in Figure 5-3. A log-log plot of the axial strain at failure versus the average axial strain rate, Figure 5-10, indicates that for strain rates less than about $10^{-5} sec^{-1}$ the axial strain at failure is nearly independent of strain rate and roughly equal to 4.5 percent. As the strain rate increased and the material behavior became more brittle, the axial strain at failure decreased rapidly to values less than 1 percent.

The slope of the initial linear portion of the stress-strain curves, below the initial yield stress, was observed to increase as the strain rate increased (see Figure 5-3). The initial tangent modulus was determined, for each sample tested, by a linear regression least squares analysis of the nearly straight-line portion of the stress-strain curves below the yield point. Figure 5-11 presents a log-log summary of the initial tangent modulus versus the average strain rate to failure. The linear increase in the initial tangent modulus with increasing strain

rate

Equa

wher

were

the

show

-15'

pon

at

find

app

obt

ini

met

in

a

th

co

mi

aq

cu

f

a

rate on the log-log plot suggests a power law relationship similar to Equations (5-1) and (5-2):

$$E_i = B(\dot{\varepsilon}_{ave})^b \qquad (5\text{-}3)$$

where B and b are temperature dependent constants.

Eight tests were conducted in which volume change measurements were made to examine the influence of strain rate and temperature on the volumetric strain of the frozen sand. Figures 5-12, 5-13 and 5-14 show the stress-strain curves for the tests conducted at -2, -6 and -15°C, respectively. Figures 5-15, 5-16 and 5-17 present the corresponding plots of volumetric strain versus axial strain. Initially, at low axial strain values, the volumetric strain was negative indicating a net decrease in the sample volume. As the axial strain approaches the initial yield strain value, the volumetric strain obtains its minimum value. As the axial strain increased beyond the initial yield strain and toward the axial strain at failure, the volumetric strain increases at an accelerating rate. The initial reduction in volume appears to be associated with pressure melting of the ice, a simultaneous densification of the sand particles, and compression of the ice matrix. As dilatancy and interparticle friction begin to contribute to the volumetric strain, the sample volume reaches its minimum value and begins to increase. The increase in sample volume appears to continue at axial strains in excess of the failure strain corresponding to the peak stress.

Poisson's ratio was computed (as a function of the axial strain) from the volumetric strain data as discussed by Duncan and Chang (1970) and Daniel and Olson (1974):

$$\nu_t = \frac{-\Delta(\varepsilon_v - \varepsilon)}{2\Delta\varepsilon} \qquad (5\text{-}4)$$

where ν_t is the tangent Poisson's ratio computed for increments of axial stress applied to the sample, ε_v is the volumetric strain, and ε is the axial strain (positive for compression). Figures 5-18, 5-19 and 5-20 present plots of the tangent Poisson's ratio versus axial strain for the samples corresponding to the stress-strain curves in Figures 5-12 through 5-13. As would be expected from the volumetric strain data, the value of the tangent Poisson's ratio was initially less than 0.5, indicating that the volume was decreasing with increasing strain. Poisson's ratio then increased rapidly to a value of approximately 0.5 at or near the initial yield strain, indicating a point of zero volume change in the stress-strain process. Beyond the initial yield strain, the value of Poisson's Ratio continued to increase at a somewhat slower rate with increasing axial strain. At axial strains in excess of the peak stress the value of tangent Poisson's ratio appears to approach a value of 1.0.

Both the volumetric strain and the tangent Poisson's ratio appear to increase somewhat with increasing strain rate. Figure 5-17 illustrates the apparent influence of strain rate on the volumetric strain. Samples 82 and 83 compare very favorably with respect to dry density and degree of ice saturation (dry densities equal to 105.8 and 106.2 pcf, respectively, and degree of ice saturation equal to 96.4 97.3 percent, respectively). However, sample 82, tested at an average strain rate of $8.34 \times 10^{-5} sec^{-1}$, experienced a greater volume reduction at low strain values as compared to sample 83 tested at an average strain rate of $5.63 \times 10^{-6} sec^{-1}$ and at the same temperature of

-15°

volu

stra

tang

stra

tang

(te

in

(Fi

val

con

sup

ave

re

st

at

re

Sa

th

sa

a

S

o

5

-15°C. Sample 82 also exhibited a significantly greater increase in volume at axial strain values equal to or greater than the failure strain. The same trend is also observed in Figure 5-20 for tangent Poisson's ratio as a function of axial strain. At the higher strain rate (Sample 82, $\dot{\varepsilon}_{ave} = 8.34 \times 10^{-5} sec^{-1}$), the value of tangent Poisson's ratio initially is less than that for Sample 83 (tested at $\dot{\varepsilon}_{ave} = 5.63 \times 10^{-6} sec^{-1}$), indicating a more rapid decrease in volume. Above the initial yield point on the stress-strain curves (Figure 5-14), the higher strain rate results in significantly greater values of Poisson's ratio for Sample 82 than for Sample 83, as is consistent with the volume change data presented in Figure 5-17.

The data shown in Figures 5-17 and 5-18 at a temperature of -2°C supports the general trend described above. Sample 87 tested at an average strain rate of $9.42 \times 10^{-5} sec^{-1}$ experienced greater volume reduction prior to initial yield and greater volumetric expansion at strains above this initial yield point than Samples 88 and 89, tested at average strain rates of $6.19 \times 10^{-6} sec^{-1}$ and $8.74 \times 10^{-7} sec^{-1}$, respectively. However, a greater volume increase was observed for Sample 89 than for Sample 88. Figure 5-18 indicates that the values of the tangent Poisson's ratio for these two samples are very close for the same strain levels. Since the sand volume fractions for the two samples are nearly the same (64.05 percent for Sample 88 and 64.10 percent for Sample 89) this would suggest that volumetric strain is less dependent on strain rate as the applied strain rate decreases.

5.1.2 Temperature Effects

The influence of test temperature on the compression mechanical properties of the frozen sand was investigated by conducting a series of

constant strain rate compression tests at constant temperatures of -2, -6, -10 and -15°C. Figure 5-21 illustrates the effect of temperature on the stress-strain behavior of frozen Wedron sand. For samples tested at the same nominal strain rate, but different temperatures, there was no significant change in the general shape of the stress-strain curves.

However, as may be noted in Figure 5-21 and Figure 5-5, the value of the initial yield stress increases with decreasing temperature. This phenomenon suggests that the ice matrix within the frozen sand increases in strength as the temperature decreases, since the soil structure and density of the samples tested was held relatively constant. Figure 5-22 presents a log-log plot of the initial yield stress versus the number of degrees below freezing (freezing assumed at 0°C) for several strain rates. To eliminate data scatter at the selected strain rates, values of the initial yield stress for a given strain rate were obtained from a least squares linear regression analysis of the data shown in Figure 5-5. For temperatures below -2°C, the initial yield stress increased linearly with decreasing temperature for a given average strain rate on the log-log plot (Figure 5-22). Thus, a power law of the form:

$$\sigma_y = C(\theta)^s \qquad (5\text{-}5)$$

would be appropriate to relate the number of degrees below freezing (θ) to the initial yield stress (σ_y); where s is a strain rate dependent constant.

The initial yield strain was observed to remain relatively independent of the test temperature as shown in Figure 5-7 and 5-21. Since the initial yield stress increased with decreasing temperature, the net effect was to increase the initial tangent modulus as the temperature

decre

to th

incre

init

temp

of t

temp

modu

stra

prov

(E_i

tha

mod

inc

li

is

ti

to

w

r

decreased. Because the stress-strain curves remained nearly linear up to the yield point, an increase in the yield stress results in an increase in the tangent modulus. This temperature dependence of the initial tangent modulus may be clearly observed from Figure 5-11. For temperatures below -2°C, there is a significant increase in the value of the initial tangent modulus, at a given strain rate, with decreasing temperature. Figure 5-23 presents a log-log plot of the initial tangent modulus versus the number of degrees below freezing for several average strain rates. A power expression similar to Equation (5-5) appears to provide a reasonable relationship between the initial tangent modulus (E_i) and the number of degrees below freezing (θ) for temperatures less than or equal to -6°C. There was no apparent decrease in the tangent modulus between -6°C and -2°C.

The compressive strength or peak stress was also observed to increase with decreasing temperature (see Figures 5-9 and 5-21). A linear increase in the compressive strength with decreasing temperature is shown on a log-log plot in Figure 2-24. This suggests the application of an expression of the form given by Equation (5-5) and similar to Equation (2-25):

$$\sigma_f = C(\theta)^s \qquad (5\text{-}6)$$

where σ_f is the compressive strength and the constants C and s are strain rate dependent.

The influence of temperature on the volumetric strain may be observed in Figure 5-25. There appears to be a greater initial decrease in volume (for axial strains below the initial yield strain) as the temperature decreases. For axial strains above about 1.5 percent, the volumetric strain appears to be relatively independent of the test

tempera

may be

inspect

strain

tempera

strain

closely

5.1.3

Th

ties in

nomina

sample

ratio

on the

T

diamet

A leas

only a

of sam

stress

14 pe

squar

sizes

sampl

the d

depen

temperature. The net effect on the value of the tangent Poisson's ratio may be deduced from the above observation and verified from a close inspection of Figures 5-18, 5-19 and 5-20. At low values of the axial strain (< 1.0 percent) tangent Poisson's ratio is less at the lower temperatures, as a result of the greater volume decrease. As the axial strain increased, values of tangent Poisson's ratio appear to more closely agree.

5.1.3 Sample Size Effects

The influence of sample size (diameter) on the mechanical properties in compression was investigated at a temperature of -6°C and a nominal strain rate of approximately $1.2 \times 10^{-4} sec^{-1}$ using cylindrical samples 1.13, 1.41, 1.94 and 2.40 inches in diameter (length: diameter ratio of 2.0). Figure 5-26 summarizes the influence of sample diameter on the initial yield stress and strain.

The initial yield stress obtained for the 1.41, 1.94 and 2.40 inch diameter samples appears to be relatively independent of sample diameter. A least squares linear regression analysis (Figure 5-26a) indicates only a 0.23 percent decrease in the initial yield stress over a range of sample sizes from 1.41 to 2.40 inches. However, the average yield stress obtained from the 1.13 inch diameter samples is approximately 14 percent less than the value predicted from an extension of the least squares line fitted through the data points for the three larger sample sizes (Figure 5-26a).

Figure 5-26b presents the initial yield strain as a function of sample diameter. A least squares linear regression analysis through the data points indicates that the initial yield strain is somewhat dependent on the sample diameter. There is approximately a 9.30 percent

decr

test

for

of t

This

Prio

seat

the

samp

rel

uni

sam

is

lir

1.4

Fig

in

co

A

th

re

a

o

s

a

decrease in the initial yield strain over the range of sample sizes tested (1.13 inches to 1.41 inches in diameter). However, the data for the 1.41 inch diameter sample gives a significantly higher value of the initial yield strain, as may be observed from Figure 5-26b. This probably results from higher strains associated with sample seating. Prior to testing the 1.13, 1.94 and 2.40 inch diameter samples, a small seating stress of approximately 100 psi was placed on each sample using the manual loading option of the Wykeham-Farrance test machine. The sample was then allowed to creep for a sufficient period of time to relax the applied load. This procedure was intended to provide a more uniform application of load to the sample. The 1.41 inch diameter samples were tested without the application of a seating stress. Thus, is would seem reasonable to expect somewhat higher yield strains. A linear regression analysis through the data points, neglecting the 1.41 inch diameter samples, results in a slope reversal, as shown in Figure 5-26b. Consequently, there appears to be an 11 percent increase in ε_y over a range in sample diameters from 1.13 to 2.40 inches.

Figure 5-27 summarizes the effect of sample diameter on the compressive strength (peak stress) and the axial strain at failure. A least squares line through the strength data in Figure 5-27a shows that an increase in sample diameter from 1.13 inches to 2.40 inches results in a 0.65 percent decrease in the compressive strength. The axial strain at failure (shown in Figure 5-27b) appears to be independent of the sample size for the range in diameters considered.

The initial tangent modulus, summarized in Figure 5-28, shows significant data scatter at each sample diameter. A linear regression analysis of the data indicates a 31 percent increase in E_i for sample

diame

samp

stres

5.2

comp

froz

stre

test

110

phy

deg

sum

of

an

a

th

of

sl

(s

le

wh

a

E

a

diameters over the range considered. This data suggests that the sample diameter significantly influences the initial slope of the stress-strain curve.

5.2 Constant Stress Uniaxial Compression Creep Tests

To investigate the suitability of constant strain rate uniaxial compression tests to determine the time dependent behavior of the frozen sand under constant stress conditions, a series of constant stress creep tests were conducted for comparison. A total of seven tests were conducted at -6°C and at uniaxial stresses ranging from 1100 psi to approximately 1500 psi. Table 5-3 summarizes the samples' physical properties (including volume fraction, dry unit weight and degree of ice saturation) for the constant stress creep tests. A summary of the test results related to the time dependent deformation of the frozen sand is contained in Table 5-4.

The creep curves are summarized in Figure 5-29. Each curve shows an instantaneous strain immediately after load application followed by a region of decreasing strain rate (primary creep). Beyond this region the curves approach linearity (secondary creep) prior to development of instability or an accelerating creep rate (tertiary creep). The slope of the linear or constant strain rate portion of the creep curve (secondary creep rate) was observed to increase with increasing stress level as shown in Figures 5-29. This increase appears to be linear when plotted on a log-log scale, as suggested by Ladanyi (1972) and as shown in Figure 5-20. An expression of the form presented by Equation (2-6) appears appropriate to relate the secondary creep rate and the uniaxial stress.

The total axial strain at failure (at the initiation of instability

or te

Figur

the b

Howev

with

proce

the

5-32

vers

volu

in F

proc

in

was

sam

sam

app

the

dat

of

of

0.

ra

in

or tertiary creep) was determined from the creep curves shown in Figure 5-29. As shown in Figure 5-31, the total axial strain at the beginning of tertiary creep increased as the stress level increased. However, the time required to reach tertiary creep decreased rapidly with increasing stress (Figure 5-29).

To investigate the volumetric strain behavior during the creep process, volume change data was obtained using a burette to measure the fluid expelled from the triaxial cell during testing. Figure 5-32 presents a plot of volumetric strain (ε_v) and volume change (ΔV) versus time for samples 3c, 5c, and 6c. The result is a series of volumetric creep curves similar in shape to the creep curves presented in Figure 5-29. The increase in sample volume during the creep processes denotes the influence of dilatancy and interparticle friction in resisting deformation.

The failure mode for those samples reaching instability or rupture was similar to that observed in the constant strain rate tests for samples tested at moderate strain rates. Once in tertiary creep the samples generally developed a well defined shear plane oriented at approximately 60 degrees to the horizontal; suggesting as before that the mobilized angle of internal friction was close to 30 degrees.

The tangent Poisson's ratio was computed from the volumetric strain data using Equation (5-4). Tangent Poisson's ratio (ν_t) as a function of time is summarized in Figure 5-33. Immediately after application of the uniaxial stress, Poisson's ratio is approximately equal to 0.5. However, as the creep process proceeds the value of ν_t increases rapidly as dilatancy contributes to the volumetric strain. The rate of increase in ν_t is greatest at the higher stress levels as would be

expe

5.3

and

sand

cond

a s

com

the

5.3

in

loa

inv

me

di

ra

te

ve

co

s

t

o

T

d

r

expected from the volume change data presented in Figure 5-32.

5.3 Split Cylinder Tests

The influence of temperature, deformation rate (or strain rate), and sample diameter on the mechanical properties of frozen Wedron sand in tension was evaluated from a series of indirect tensile tests conducted using the split cylinder test method. Table 5-5 presents a summary of sample densities, ice saturation, and dimensions. A complete summary of test results related to the tensile behavior of the sand-ice material is presented in Table 5-6.

5.3.1 Strain Rate Effects

The split cylinder tests were conducted as shown schematically in Figures 2-11 and 2-12. A compressive load was applied over a narrow loading arc and across the vertical diameter of the sample. To investigate the influence of the vertical deformation rate ($\dot{Y}_T$) on the mechanical properties in tension, 4.00 inch diameter samples (height: diameter ratio of 0.5) were tested at constant vertical deformation rates varying from 0.002 in/min to approximately 0.28 in/min (at constant temperatures of -2, -6, -10, and -15°C). Figure 5-34 presents typical vertical deformation (Y_T) versus time plots for the split cylinder tests conducted using the Soiltest loading frame. The deformation rate varies slightly with time up to the point of rupture. Therefore, the deformation rates were computed using a least squares linear regression analysis of the vertical deformation versus time curve for each test conducted. This procedure results in the straight-time approximation for the deformation-time plots shown in Figure 5-34. The maximum deformation rate achieved by the test machine was also observed to decrease with

decr

the

Cons

appa

at -

cyl

and

cur

typ

shi

was

of

rat

de

ap

ra

be

fc

fa

a

w

t

c

decreasing test temperature. As the stiffness of the sample increased the recorded deformation rate at a selected transmission speed decreased. Consequently, the maximum deformation rate possible with the test apparatus varied from approximately 0.28 in/min at -2°C to 0.22 in/min at -15°C.

Typical load versus vertical deformation curves for the split cylinder tests are given in Figure 5-35 for a temperature of -10°C and several different vertical deformation rates. The load-deformation curves remain nearly linear up to the rupture load, indicating a brittle type of deformation behavior and a nearly linear stress-strain relationship for the frozen sand up to failure.

The indirect tensile strength (σ_t) or the tensile stress at rupture was computed using Equation (2-36) given by Hondros (1959). The value of σ_t was observed to increase with increasing vertical deformation rate, as shown in Figure 5-36. The rate of increase in σ_t appears to decrease as the deformation rate increases and may asymtotically approach a constant value for some deformation rate above the maximum rate achieved in the present study. A linear relationship (log-log plot) between deformation rate and indirect tensile strength may be appropriate for the range of deformation rates shown in Figure 5-37.

For vertical deformation rates above 0.002 in/min the samples failed by splitting along the loaded diametrical axis, with wedges formed at each loading strip as shown in Figure 2-14c. A total of four samples were tested at a deformation rate of 0.002 in/min and temperatures of -6°C and -15°C. Both of the samples tested at -6°C failed to develop tensile splits even at large vertical deformations. Only a local compression deformation adjacent to the steel loading strip was observed.

At -1

while

This

sand

trans

defo

was

Chap

tota

plot

Pois

in T

a le

The

appl

val

cer

hor

by

to

exp

wh

sl

de

At -15°C, one sample split at tensile stress (computed) of 407 psi, while the second deformed plastically under the applied loading. This implies that the split cylinder test may be applicable to frozen sand only at high deformation rates and that a ductile-brittle transition occurs with respect to the split cylinder test at a deformation rate of approximately 0.002 in/min.

The total horizontal deformation of most samples (4-inch diameter) was measured using the horizontal deformation device described in Chapter IV (see Figure 4-5). Figure 5-38 shows typical load versus total horizontal deformation (X_T) plots and Figure 5-39 gives typical plots of total vertical deformation versus total horizontal deformation. Poisson's ratio for each sample was computed using the expression given in Table 2-1, where DR is deformation ratio (Y_T/X_T) determined from a least squares linear regression analysis as shown in Figure 5-39. The computed values of Poisson's ratio are plotted as a function of the applied vertical deformation in Figure 5-40. The computed numerical values varied from approximately -0.21 to 0.03. There was no discernable dependence of Poisson's ratio on the vertical deformation rate.

The total tensile strain at rupture was computed from the total horizontal deformation at failure (X_{TF}) and Poisson's ratio as indicated by the appropriate equation in Table 2-1. The tensile strain rate up to rupture was also computed by taking the time derivative of this expression as shown below:

$$\dot{\varepsilon}_t = \dot{X}_T \left[\frac{0.1185\nu + 0.03896}{0.2494\nu + 0.06730}\right] \qquad (5\text{-}7)$$

where ν is considered constant with time and $\dot{X}_T$ is the slope of the least squares line fitted through the total horizontal deformation versus time curves (shown in Figure 5-41). Over the range

of de

to be

versu

of -

σ_t a

wher

data

from

The

as

load

rup

in

lin

in

5.

fr

cy

5-

st

pr

di

deformation rates considered, the tensile strain at failure appears be independent of the computed tensile strain rate (Figure 5-42).

Figure 5-43 presents a log-log plot of indirect tensile strength rsus the computed tensile strain rate. The data at temperatures -15°C and -10°C seems to indicate a linear relationship between and $\dot{\varepsilon}_t$ (on a log-log scale) of similar form as Equation (2-20):

$$\sigma_t = \sigma_c(\dot{\varepsilon}_t)^m \qquad (5\text{-}8)$$

ere σ_c and m are material constants defined as before. The limited ta at -2°C and -6°C also appear to support this observation.

The modulus of elasticity, E_t, (Young's modulus) was computed om the expression given in Table 2-1 for the 4-inch diameter samples. e value of S_H, the horizontal tangent modulus (P/X_T) was determined the slope of the least squares line of best fit between the applied ad (P) and the total horizontal deformation (X_T) for the loads up to pture (typical load versus horizontal deformation plots are shown Figure 5-38). The modulus of elasticity was observed to vary nearly (log-log plot) with increasing tensile strain rate as shown Figure 5-44.

3.2 Temperature Effects

The influence of test temperature on the mechanical properties of ozen Wedron sand in tension was obtained from a series of split linder tests conducted at -2, -6, -10, and -15°C. Figures 5-40 and 42 suggest that the computed values of Poisson's ratio and the tensile rain at failure are relatively independent of test temperature. Both operties exhibited considerable data scatter and there was no scernable relationship with the test temperature.

from

chan

Log-

the

5-45

seve

show

and

whe

5.3

of

cyl

(wi

for

was

0.(

th

or

ra

te

ov

wa

s

Both the indirect tensile strength and Young's modulus, determined from the split cylinder test, appear to be significantly influenced by changes in temperature, as seen in Figures 5-43 and 5-44, respectively. Log-log plots of indirect tensile strength and Young's modulus versus the number of degrees below freezing (0°C) are presented in Figures 5-45 and 5-46, respectively. The data points shown were computed for several strain rates from the equations for the least squares lines shown in Figures 5-43 and 5-44. Both the indirect tensile strength and Young's modulus may be expressed as a power function of temperature:

$$\sigma_t \text{ or } E_t = C(\theta)^s \qquad (5\text{-}9)$$

where C and s are constants for a given strain rate.

5.3.3 Sample Size Effects

The influences of sample diameter on the indirect tensile strength of the frozen sand was determined from tests conducted at -6°C on cylindrical samples with diameters of 1.94, 2.40, and 4.00 inches (with a height to diameter ratio of 0.5). Two specimens were tested for each sample diameter. The deformation rate for each sample diameter was selected to give an average vertical compression strain rate of 0.035 min^{-1} (vertical deformation rate divided by aample diameter) over the loaded diameter of the speciman. For no variation in Young's modulus or Poisson's ratio, this procedure would produce the same tensile strain rate for all sample diameters. As indicated in Figure 5-47, the indirect tensile strength was observed to be independent of the sample diameter over the range of sample sizes considered.

The lateral deformation of the 1.94 and 2.40 inch diameter samples was not measured. Based on results obtained from the 4.00 inch diameter samples, the horizontal deformation in the 1.94 and 2.40 inch diameter

samples

of the

mation

tensile

samples was estimated to be approximately equal to the resolution of the LADT and Sanborn 4 channel recorder. Consequently, no information was obtained related to the effect of sample diameter on the tensile strain at failure, Young's modulus, or Poisson's ratio.

Table

Sample No.
1
2
3
4
5
6
7
8
9
10
11
12
13
14
15
16
17
18
19
20
21
22
23
24
25
26
27
28
29
30
31
32
33
34
35
36
37
38
39
40
41
42
43
44
45

Table 5-1: Physical Properties Summary for Constant Strain Rate Uniaxial Compression Test Samples

Sample No.	Sample Diameter (in)	Percent Sand by Volume	Dry Unit Wt. (pcf)	Degree Ice Saturation (%)
1	1.40	63.26	104.4	98.27
2	1.40	63.17	104.3	99.22
3	1.40	63.97	105.6	98.83
4	1.40	64.44	106.4	97.03
5	1.40	63.39	104.7	99.99
6	1.40	63.69	105.2	98.56
7	1.40	63.69	105.2	98.79
8	1.40	63.78	105.3	98.16
9	1.40	64.91	107.2	98.39
10	1.40	63.50	105.3	98.50
11	1.40	63.73	105.2	97.91
12	1.40	63.37	104.6	98.80
13	1.40	63.01	104.0	99.03
14	1.40	63.62	105.0	97.88
15	1.40	63.39	104.7	97.24
16	1.40	63.73	105.2	97.78
17	1.40	63.40	104.7	97.75
18	1.40	63.61	105.0	98.23
19	1.40	63.94	105.6	98.99
20	1.40	63.88	105.5	98.88
21	1.40	63.80	105.3	97.78
22	1.40	-------- Membrane Leak ----------		
23	1.13	63.54	104.9	98.29
24	1.13	63.39	104.7	97.82
25	1.13	63.37	104.6	98.14
26	1.13	63.34	104.6	98.06
27	1.94	64.81	107.0	98.75
28	1.94	63.35	104.6	98.48
29	1.94	64.28	106.1	98.11
30	1.94	64.16	105.9	99.07
31	1.94	63.44	104.7	98.38
32	1.94	63.38	104.6	98.53
33	1.94	63.38	104.6	98.54
34	1.13	63.42	104.7	98.04
35	1.13	-------- Membrane Leak ----------		
36	1.13	63.62	105.0	98.27
37	1.13	64.51	106.6	98.60
38	1.13	63.83	105.4	98.36
39	1.13	63.45	104.8	98.04
40	1.13	63.92	105.5	99.15
41	1.40	63.81	105.3	99.71
42	1.40	63.93	105.6	97.32
43	1.40	63.68	105.1	98.19
44	1.40	63.54	104.9	97.03
45	1.40	64.07	105.8	97.43

Table 5

Sample No.
46
47
48
49
50
51
52
53
54
55
56
57
58
59
60
61
62
63
64
65
66
67
68
69
70
71
72
73
74
75
76
77
78
79
80
81
82
83
84
85
86
87
88
89
90

ble 5-1 (cont'd.)

mple No.	Sample Diameter (in)	Percent Sand by Volume	Dry Unit Wt. (pcf)	Degree Ice Saturation (%)
46	2.40	64.33	106.2	98.15
47	2.40	63.91	105.5	98.13
48	2.40	63.98	105.6	97.57
49	2.40	63.99	105.7	98.36
50	2.40	63.86	105.4	98.66
51	2.40	64.05	105.7	98.42
52	1.94	64.23	106.0	98.27
53	1.94	64.31	106.2	98.33
54	1.94	64.27	106.1	96.11
55	1.94	64.29	106.1	99.41
56	1.94	63.96	105.6	98.04
57	1.40	64.03	105.7	97.41
58	1.40	64.12	105.9	96.69
59	1.40	64.17	105.9	97.39
60	1.40	63.65	105.1	97.06
61	1.40	64.18	106.0	97.40
62	1.40	64.18	105.9	97.05
63	1.40	63.60	105.0	96.96
64	1.40	64.10	105.7	98.90
65	1.40	64.10	105.7	98.06
66	1.40	63.28	104.5	99.43
67	1.40	63.08	104.2	99.30
68	1.40	64.00	105.7	96.99
69	1.40	63.57	105.0	98.96
70	1.40	64.45	106.4	98.39
71	1.40	64.80	107.7	97.66
72	1.40	64.70	106.9	97.00
73	1.40	63.81	105.4	97.22
74	1.40	64.18	106.0	97.88
75	1.40	64.20	106.0	97.22
76	1.40	63.96	105.6	98.51
77	1.40	64.26	106.1	98.98
78	1.40	64.02	105.7	96.16
79	1.40	64.25	106.1	98.98
80	1.40	64.85	107.1	97.37
81	1.40	63.56	105.0	98.77
82	1.40	64.10	105.8	97.30
83	1.40	64.32	106.2	96.40
84	1.40	63.89	105.5	96.69
85	1.40	64.41	106.4	96.39
86	1.40	64.16	105.9	99.69
87	1.40	64.22	106.0	96.13
88	1.40	64.05	105.8	98.30
89	1.40	64.10	105.8	98.90
90	1.40	64.92	107.2	96.20

Table 5-2: Test Results for Constant Strain Rate Uniaxial Compression Tests

Sample No.	Sample Dia. (in)	Test Temp. (^{o}C)	a-Nominal Strain Rate (sec^{-1})	b-Average Strain Rate (sec^{-1})	Peak Stress (psi)	c-Failure Strain (in/in)	Yield Stress (psi)	Yield Strain (in/in)	Initial Tangent Modulus (psi)
1	1.40	-6.08	1.19×10^{-4}	9.46×10^{-5}	1585	0.0293	1160	0.0047	2.85×10^{5}
2	1.40	-6.05	1.19×10^{-4}	1.02×10^{-4}	1546	0.0341	1140	0.0038	2.37×10^{5}
3	1.40	-6.05	1.19×10^{-4}	9.76×10^{-5}	1569	0.0275	1280	0.0066	2.44×10^{5}
4	1.40	-6.05	1.19×10^{-4}	9.29×10^{-5}	1582	0.0269	1260	0.0047	3.07×10^{5}
5	1.40	-6.05	1.19×10^{-3}	9.91×10^{-4}	1727	0.0367	1190	0.0060	2.31×10^{5}
6	1.40	-6.08	1.33×10^{-4}	3.69×10^{-4}	1741	0.0049	1500	0.0018	8.00×10^{5}
7	1.40	-6.05	5.93×10^{-4}	2.68×10^{-4}	1589	0.0075	1575	0.0060	2.36×10^{5}
8	1.40	-6.10	2.67×10^{-5}	2.04×10^{-5}	1679	0.0292	1320	0.0060	2.85×10^{5}
9	1.40	-6.05	5.34×10^{-5}	2.57×10^{-5}	1795	0.0338	1100	0.0055	2.41×10^{5}
10	1.40	-6.05	5.34×10^{-5}	4.36×10^{-5}	1660	0.0328	1120	0.0050	2.63×10^{5}
11	1.40	-6.05	1.07×10^{-5}	9.23×10^{-6}	1656	0.0424	800	0.0060	1.51×10^{5}
12	1.40	-6.05	2.37×10^{-3}	2.01×10^{-5}	1618	0.0392	875	0.0045	2.21×10^{5}
13	1.40	-6.05	1.78×10^{-6}	6.46×10^{-4}	1746	0.0051	1560	0.0028	5.15×10^{5}
14	1.40	-6.10	4.75×10^{-6}	4.05×10^{-6}	1662	0.0457	700	0.0065	1.29×10^{5}
15	1.40	-6.05	1.42×10^{-6}	1.23×10^{-6}	1442	0.0456	370	0.0035	2.02×10^{5}
16	1.40	-6.06	5.69×10^{-4}	4.90×10^{-4}	1292	0.0458	350	0.0050	9.61×10^{5}
17	1.40	-6.13	4.45×10^{-6}	2.26×10^{-6}	1600	0.0081	1350	0.0043	3.62×10^{5}
18	1.40	-6.06	2.14×10^{-5}	1.87×10^{-5}	1559	0.0490	420	0.0025	1.42×10^{5}
19	1.40	-6.08	1.42×10^{-4}	1.16×10^{-5}	1739	0.0400	870	0.0068	1.72×10^{5}
20	1.40	-6.08	1.19×10^{-4}	8.88×10^{-5}	1656	0.0314	1290	0.0067	2.27×10^{5}
21	1.40	-6.08	1.19×10^{-4}	9.59×10^{-5}	1705	0.0321	1380	0.0077	1.99×10^{5}
22	1.40	----------	----------	----------	Membrane Leak	----------	----------	----------	----------

a - selected strain rate based on machine speed
b - average strain rate to peak stress
c - strain at peak stress

See Table 5-1 for sample physical properties

Table 5-2 (cont'd.)

	Initial

Sample No.	Sample Dia. (in)	Test Temp. (°C)	a-Nominal Strain Rate (sec^{-1})	b-Average Strain Rate (sec^{-1})	Peak Stress (psi)	c-Failure Strain (in/in)	Yield Stress (psi)	Yield Strain (in/in)	Initial Tangent Modulus (psi)
23	1.13	-6.08	1.11×10^{-4}	1.13×10^{-4}	1606	0.0276	973	0.0055	2.07×10^{5}
24	1.13	-6.08	1.11×10^{-4}	9.32×10^{-5}	1658	0.0318	840	0.0039	2.08×10^{5}
25	1.13	-6.09	1.11×10^{-4}	8.23×10^{-5}	1582	0.0281	780	0.0022	2.96×10^{5}
26	1.13	-6.08	1.11×10^{-4}	9.78×10^{-4}	1582	0.0374	830	0.0049	1.41×10^{5}
27	1.94	-6.03	1.29×10^{-4}	1.00×10^{-4}	1694	0.0258	1270	0.0045	3.90×10^{5}
28	1.94	-6.00	1.29×10^{-4}	1.01×10^{-4}	1802	0.0269	1430	0.0037	6.02×10^{5}
29	1.94	-6.05	1.29×10^{-4}	9.20×10^{-4}	1790	0.0218	1350	0.0039	4.75×10^{5}
30	1.94	-6.00	1.29×10^{-4}	1.02×10^{-5}	1751	0.0309	1260	0.0037	4.72×10^{5}
31	1.94	-6.05	1.29×10^{-4}	9.40×10^{-4}	1775	0.0265	1410	0.0022	1.18×10^{6}
32	1.94	-6.02	1.29×10^{-4}	1.04×10^{-5}	1738	0.0285	1420	0.0035	4.81×10^{5}
33	1.94	-6.08	1.29×10^{-4}	9.67×10^{-5}	1788	0.0259	1430	0.0030	6.23×10^{5}
34	1.13	-6.08	1.11×10^{-4}	8.63×10^{-5}	1780	0.0327	1105	0.0035	4.14×10^{5}
35	1.13	----------	----------	----------	Membrane Leak	----------	----------	----------	----------
36	1.13	-6.06	1.11×10^{-4}	9.12×10^{-5}	1711	0.0319	1120	0.0022	4.81×10^{5}
37	1.13	-6.08	1.11×10^{-4}	8.62×10^{-5}	1721	0.0285	1110	0.0022	4.54×10^{5}
38	1.13	-6.05	1.11×10^{-4}	8.66×10^{-5}	1757	0.0298	1145	0.0035	4.18×10^{5}
39	1.13	-6.08	1.11×10^{-4}	8.43×10^{-5}	1745	0.0291	1110	0.0035	3.24×10^{5}
40	1.13	-6.03	1.11×10^{-4}	8.88×10^{-5}	1778	0.0315	1055	0.0045	2.52×10^{5}
41	1.40	-6.06	1.19×10^{-4}	9.42×10^{-5}	1778	0.0327	1220	0.0040	3.59×10^{5}
42	1.40	-6.10	1.19×10^{-4}	9.02×10^{-5}	1698	0.0288	1255	0.0040	3.64×10^{5}
43	1.40	-6.06	1.19×10^{-4}	9.13×10^{-5}	1732	0.0306	1290	0.0042	3.64×10^{5}
44	1.40	-6.06	1.19×10^{-4}	9.52×10^{-4}	1678	0.0329	1270	0.0050	3.08×10^{5}
45	1.40	-6.09	8.89×10^{-4}	3.80×10^{-4}	1781	0.0062	1570	0.0035	4.85×10^{5}

a - selected strain rate based on machine speed
b - average strain rate to peak stress
c - strain at peak stress

See Table 5-1 for sample physical properties

Table 5-2 (cont'd.)

Initial

Sample No.	Sample Dia. (in)	Test Temp. (^{o}C)	a-Nominal Strain Rate^{-1} (sec^{-1})	b-Average Strain Rate^{-1} (sec^{-1})	Peak Stress (psi)	c-Failure Strain (in/in)	Yield Stress (psi)	Yield Strain (in/in)	Initial Tangent Modulus (psi)
46	2.40	-6.09	1.04×10^{-4}	8.62×10^{-5}	1754	0.0317	1210	0.0030	4.78×10^{5}
47	2.40	-6.06	1.04×10^{-4}	8.71×10^{-5}	1731	0.0308	1330	0.0032	5.48×10^{5}
48	2.40	-6.09	1.04×10^{-4}	8.72×10^{-5}	1725	0.0344	1290	0.0035	5.53×10^{5}
49	2.40	-6.03	1.04×10^{-4}	9.24×10^{-5}	1656	0.0334	1220	0.0046	3.33×10^{5}
50	2.40	-6.00	1.04×10^{-4}	8.95×10^{-5}	1662	0.0299	1200	0.0045	3.96×10^{5}
51	2.40	-6.05	1.04×10^{-4}	8.74×10^{-5}	1724	0.0309	1310	0.0030	6.99×10^{5}
52	1.94	-5.99	1.29×10^{-4}	1.02×10^{-4}	1677	0.0322	1240	0.0050	3.03×10^{5}
53	1.94	-6.03	1.29×10^{-4}	1.04×10^{-4}	1664	0.0282	1350	0.0045	4.21×10^{5}
54	1.94	-6.06	1.29×10^{-4}	1.04×10^{-4}	1755	0.0269	1330	0.0042	4.39×10^{5}
55	1.94	-6.16	1.29×10^{-4}	1.08×10^{-4}	1796	0.0360	1225	0.0047	3.39×10^{5}
56	1.94	-6.16	1.29×10^{-4}	1.10×10^{-4}	1802	0.0329	1180	0.0045	3.23×10^{5}
57	1.40	-10.05	1.78×10^{-3}	7.20×10^{-4}	2480	0.0071	2180	0.0046	5.35×10^{5}
58	1.40	-10.05	5.93×10^{-4}	2.52×10^{-4}	2231	0.0073	2050	0.0045	5.03×10^{5}
59	1.40	-10.05	1.19×10^{-4}	9.06×10^{-5}	2063	0.0295	1700	0.0050	4.28×10^{5}
60	1.40	-10.05	2.37×10^{-5}	2.15×10^{-5}	2213	0.0424	1200	0.0055	3.16×10^{5}
61	1.40	-10.05	4.75×10^{-6}	4.35×10^{-6}	2177	0.0531	680	0.0035	2.70×10^{5}
62	1.40	-10.05	1.42×10^{-6}	1.28×10^{-6}	1894	0.0484	580	0.0032	2.30×10^{5}
63	1.40	-10.00	5.69×10^{-7}	4.82×10^{-7}	1542	0.0442	435	0.0037	1.65×10^{5}
64	1.40	-10.05	2.14×10^{-6}	1.84×10^{-6}	1916	0.0473	640	0.0055	1.48×10^{5}
65	1.40	-10.00	1.07×10^{-5}	8.77×10^{-6}	2188	0.0427	1020	0.0040	3.02×10^{5}
66	1.40	-10.09	5.34×10^{-5}	4.18×10^{-5}	2170	0.0344	1440	0.0045	4.07×10^{5}
67	1.40	-10.06	2.67×10^{-4}	1.30×10^{-4}	2038	0.0087	1830	0.0050	4.44×10^{5}

a - selected strain rate based on machine speed
b - average strain rate to peak stress
c - strain at peak stress

See Table 5-1 for sample physical properties

Table 5-2 (cont'd.)

Sample No.	Sample Dia. (in)	Test Temp. (°C)	a-Nominal Strain Rate (sec^{-1})	b-Average Strain Rate (sec^{-1})	Peak Stress (psi)	c-Failure Strain (in/in)	Yield Stress (psi)	Yield Strain (in/in)	Initial Tangent Modulus (psi)
68	1.40	-10.00	1.33×10^{-3}	5.04×10^{-3}	2500	0.0065	2130	0.0036	9.37×10^{5}
69	1.40	-15.00	1.33×10^{-3}	4.75×10^{-3}	2863	0.0065	2500	0.0042	7.76×10^{5}
70	1.40	-15.00	5.93×10^{-4}	1.95×10^{-4}	2700	0.0055	2620	0.0045	1.06×10^{5}
71	1.40	-15.00	2.67×10^{-5}	1.14×10^{-5}	2453	0.0076	2200	0.0048	7.12×10^{5}
72	1.40	-15.00	7.12×10^{-5}	5.32×10^{-5}	2350	0.0292	1800	0.0050	5.68×10^{5}
73	1.40	-15.00	5.34×10^{-5}	4.02×10^{-5}	2362	0.0317	1800	0.0048	6.44×10^{5}
74	1.40	-14.98	3.56×10^{-5}	2.86×10^{-5}	2522	0.0370	1600	0.0040	5.62×10^{5}
75	1.40	-15.00	2.38×10^{-5}	1.79×10^{-5}	2558	0.0353	1500	0.0038	6.52×10^{5}
76	1.40	-15.00	1.42×10^{-5}	1.15×10^{-5}	2462	0.0388	1340	0.0048	5.93×10^{5}
77	1.40	-14.98	2.14×10^{-6}	1.82×10^{-6}	2297	0.0461	820	0.0040	4.64×10^{5}
78	1.40	-15.00	1.07×10^{-5}	8.53×10^{-5}	2341	0.0379	1410	0.0052	3.98×10^{5}
79	1.40	-15.00	1.42×10^{-6}	1.21×10^{-6}	2198	0.0411	830	0.0032	3.25×10^{5}
80	1.40	-14.98	5.69×10^{-7}	4.83×10^{-7}	2051	0.0439	670	0.0037	3.87×10^{5}
81	1.40	-14.98	4.75×10^{-6}	3.77×10^{-6}	2361	0.0348	1160	0.0040	5.57×10^{5}
82	1.40	-14.96	1.19×10^{-4}	8.34×10^{-4}	2309	0.0256	1970	0.0045	8.44×10^{5}
83	1.40	-14.96	7.12×10^{-6}	5.63×10^{-6}	2550	0.0405	1260	0.0048	5.11×10^{5}
84	1.40	-5.96	1.19×10^{-4}	9.64×10^{-4}	1890	0.0319	1225	0.0036	4.89×10^{5}
85	1.40	-5.95	7.12×10^{-6}	6.10×10^{-6}	1749	0.0451	550	0.0020	4.49×10^{5}
86	1.40	-5.95	9.94×10^{-7}	8.12×10^{-7}	1429	0.0443	360	0.0020	3.55×10^{5}
87	1.40	-2.03	1.19×10^{-4}	9.42×10^{-4}	1319	0.0331	920	0.0040	2.94×10^{5}
88	1.40	-2.02	7.12×10^{-6}	6.19×10^{-6}	1321	0.0448	340	0.0025	1.67×10^{4}
89	1.40	-2.02	9.94×10^{-7}	8.74×10^{-7}	738	0.0431	180	0.0027	9.05×10^{5}
90	1.40	-2.02	3.56×10^{-6}	3.02×10^{-6}	1161	0.0404	250	0.0016	1.61×10^{5}

a - selected strain rate based on machine speed
b - average strain rate to peak stress
c - strain at peak stress

See Table 5-1 for sample physical properties

Table

Sample No.
1c
2c
3c
4c
5c
6c
7c

Table

Sample No.
1c
2c
3c
4c
5c
6c
7c

* Fa

Al

Table 5-3: Physical Properties Summary for Constant Stress Uniaxial Creep Tests

Sample No.	Percent Sand by Volume	Dry Unit Wt. (pcf)	Degree Ice Saturation (%)
1c	63.69	105.2	98.22
2c	63.08	104.1	97.42
3c	63.62	105.0	97.30
4c	63.74	105.2	97.30
5c	63.58	104.9	96.87
6c	63.57	104.9	97.16
7c	63.89	105.5	98.36

Table 5-4: Uniaxial Compression Constant Stress Creep Test

ample No.	Stress (psi)	Secondary Creep Rate (sec^{-1})	Immediate Strain, $\varepsilon^{(i)}$ (in/in)	*Failure Strain, ε_f (in/in)
1c	1350	5.55×10^{-6}	0.0246	0.060
2c	1350	1.08×10^{-5}	0.0242	0.061
3c	1140	7.55×10^{-7}	0.0209	---
4c	1503	3.53×10^{-4}	0.0125	0.060
5c	1244	1.58×10^{-6}	0.0231	0.050
6c	1296	3.60×10^{-6}	0.0228	0.055
7c	1100	6.02×10^{-7}	0.0213	0.051

* Failure Strain taken as strain at beginning of tertiary creep period.

All samples were tested at -6°C.

Table 5-5: Physical Properties Summary for the Split-Cylinder Samples

Sample No.	Test Temp. °C	Percent Sand by Volume	Degree Ice Saturation (%)	Dry Unit Wt. (pcf)	Sample Dia. (in)
1s	-6.06	64.57	97.90	106.6	4.00
2s	-5.96	63.68	96.56	105.1	4.00
3s	-5.99	65.21	97.10	107.6	4.00
4s	-5.96	65.27	97.66	107.8	4.00
5s	-5.99	64.58	97.18	106.6	4.00
6s	-5.99	64.53	97.63	106.5	4.00
7s	-5.96	65.29	97.49	107.8	4.00
8s	-5.93	65.70	97.58	108.5	4.00
9s	-5.93	65.21	97.48	107.6	4.00
10s	-6.00	63.86	97.14	105.4	4.00
11s	-5.90	64.17	96.65	105.9	4.00
12s	-5.90	64.49	97.01	106.5	4.00
13s	-6.09	64.58	97.00	106.6	4.00
14s	-10.09	64.63	97.23	106.7	4.00
15s	-10.09	64.54	97.53	106.6	4.00
16s	-10.10	64.67	97.19	106.7	4.00
17s	-9.99	64.93	98.45	107.2	4.00
18s	-9.99	64.18	97.42	105.9	4.00
19s	-10.08	64.95	98.37	107.2	4.00
20s	-10.01	64.45	97.13	106.4	4.00
21s	-15.05	64.15	96.89	105.9	4.00
22s	-15.05	64.81	98.09	106.9	4.00
23s	-15.05	64.58	97.61	106.6	4.00
24s	-14.95	64.75	∿100	106.9	4.00
25s	-14.93	64.69	98.02	106.8	4.00
26s	-14.95	64.67	96.92	106.8	4.00
27s	-14.95	64.69	98.44	106.8	4.00
28s	-14.95	64.80	98.09	106.9	4.00
29s	-1.96	64.28	96.95	106.1	4.00
30s	-1.96	65.31	98.55	107.8	4.00
31s	-1.98	64.88	99.37	107.1	4.00
32s	-6.03	64.42	99.36	106.3	2.40
33s	-5.99	64.07	98.48	105.7	2.40
34s	-6.00	64.04	97.72	105.7	1.94
35s	-5.96	64.10	98.75	105.8	1.94

Table 5-6: Test Results for Split-Cylinder Tests

Table 5-6: Test Results for Split-Cylinder Tests

Sample No.	Temp. (°C)	Sample Dia. (in)	Deform. Rate (in/min)	Tensile Strain Rate (sec^{-1})	Tensile Strength (psi)	Elastic Modulus (psi)	Poisson's Ratio	Tensile Failure Strain (%)
*1s	-6.06	4.00	0.250	---	345	---	---	---
2s	-5.96	4.00	0.256	7.02×10^{-5}	330	3.23×10^{5}	-0.033	0.047
3s	-5.99	4.00	0.050	2.49×10^{-5}	321	2.75×10^{5}	0.036	0.132
4s	-5.96	4.00	0.002	----------	----------	No Tensile Split	----------	----------
5s	-5.99	4.00	0.002	----------	----------	No Tensile Split	----------	----------
6s	-5.99	4.00	0.083	5.24×10^{-5}	364	3.68×10^{5}	-0.084	0.096
*7s	-5.96	4.00	0.143	---	386	---	---	---
*8s	-5.93	4.00	0.144	---	395	---	---	---
*9s	-5.93	4.00	0.092	---	367	---	---	---
*10s	-6.00	4.00	0.053	---	326	---	---	---
*11s	-5.90	4.00	0.100	---	386	---	---	---
*12s	-5.90	4.00	0.192	---	384	---	---	---
*13s	-6.09	4.00	0.256	---	398	---	---	---
14s	-10.09	4.00	0.250	1.17×10^{-4}	367	4.99×10^{5}	-0.071	0.066
15s	-10.09	4.00	0.178	1.46×10^{-4}	474	5.73×10^{5}	0.028	0.096
16s	-10.10	4.00	0.146	8.81×10^{-5}	457	4.41×10^{5}	-0.036	0.095
17s	-9.99	4.00	0.100	5.48×10^{-5}	447	4.99×10^{5}	-0.047	0.079
18s	-9.99	4.00	0.072	3.19×10^{-5}	431	3.88×10^{5}	-0.104	0.069
19s	-10.08	4.00	0.039	1.81×10^{-5}	363	2.68×10^{5}	-0.086	0.089
20s	-10.01	4.00	0.230	2.03×10^{-4}	442	6.05×10^{5}	-0.026	0.094
21s	-15.05	4.00	0.222	8.59×10^{-5}	517	8.18×10^{5}	-0.069	0.055
22s	-15.05	4.00	0.133	6.67×10^{-5}	533	6.31×10^{5}	-0.113	0.064
23s	-15.05	4.00	0.160	1.06×10^{-4}	507	6.06×10^{5}	0.033	0.096
*24s	-14.95	4.00	0.106	---	517	---	---	---
25s	-14.93	4.00	0.035	1.52×10^{-5}	470	4.11×10^{5}	-0.123	0.083

* Lateral Deformation Transducer not operating
** Lateral Deformation Transducer not used

Table 5-6 (cont'd.)

Sample No.	Temp. (°C)	Sample Dia. (in)	Deform. Rate (in/min)	Tensile Strain Rate (sec^{-1})	Tensile Strength (psi)	Elastic Modulus (psi)	Poisson's Ratio	Tensile Failure Strain (%)
26s	-14.95	4.00	0.075	3.76×10^{-5}	485	4.59×10^{5}	-0.164	0.086
27s	-14.95	4.00	0.002	3.00×10^{-6}	407	2.40×10^{5}	0.531	0.376
28s	-14.95	4.00	0.002	----------	----------	No Tensile Split	----------	----------
29s	-1.96	4.00	0.163	9.42×10^{-5}	237	1.83×10^{5}	-0.069	0.098
30s	-1.96	4.00	0.280	9.22×10^{-5}	242	9.99×10^{4}	-0.178	0.111
31s	-1.98	4.00	0.058	1.36×10^{-5}	226	1.12×10^{5}	-0.207	0.067
**32s	-6.03	2.40	0.085	---	391	---	---	---
**33s	-5.99	2.40	0.070	---	392	---	---	---
**34s	-6.01	1.94	0.069	---	387	---	---	---
**35s	-6.03	1.94	0.066	---	396	---	---	---

* Lateral Deformation Transducer not operating
** Lateral Deformation Transducer not used

20
5

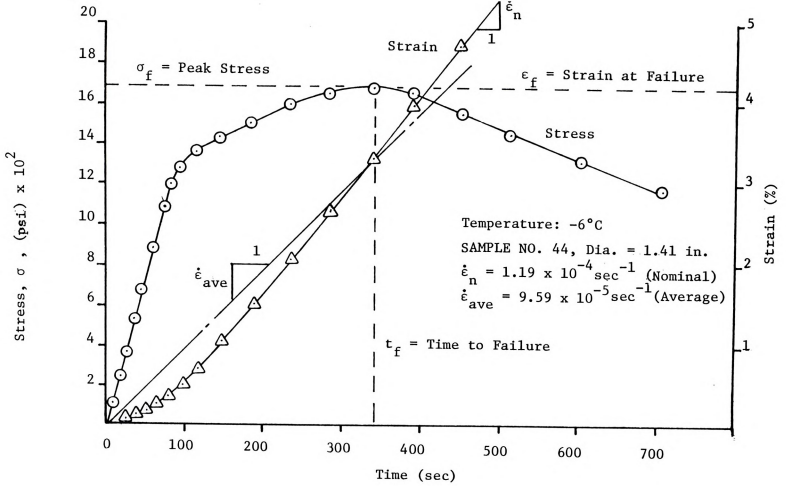

Figure 5-1: Frame Stiffness Effect on the Observed Strain Rate for Sample No. 44.

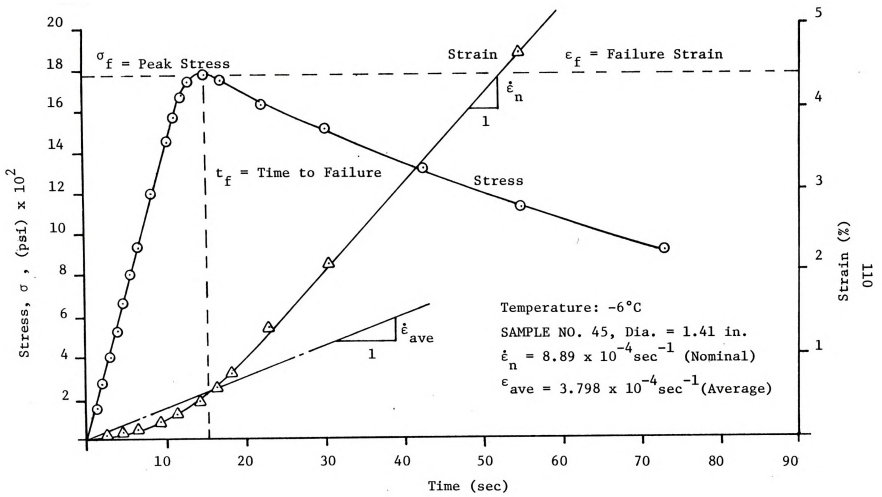

Figure 5-2: Frame Stiffness Effect on the Observed Strain Rate for Sample No. 45.

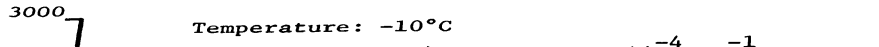
3000
Temperature: -10°C
-4
-1

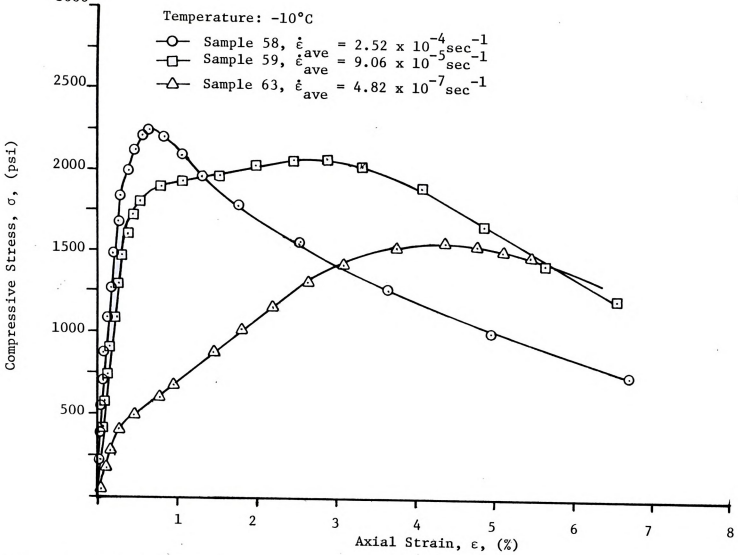

Figure 5-3: Typical Stress-Strain Curves for Unconfined Compression Tests.

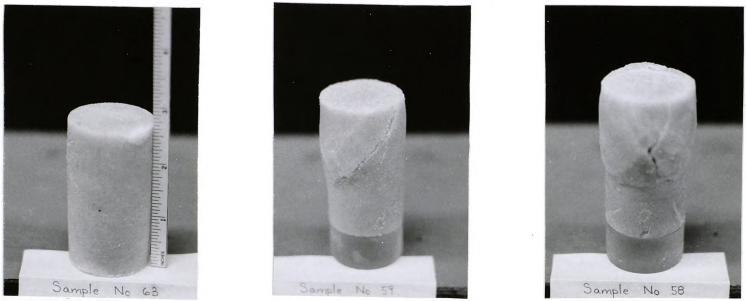

(a) (b) (c)

Figure 5-4: Typical Failure Modes for the Stress-Strain Curves Shown in Figure 5-3;
(a) Low Strain Rate, Sample 63,
(b) Intermediate Strain Rate, Sample 59,
(c) High Strain Rate, Sample 58.

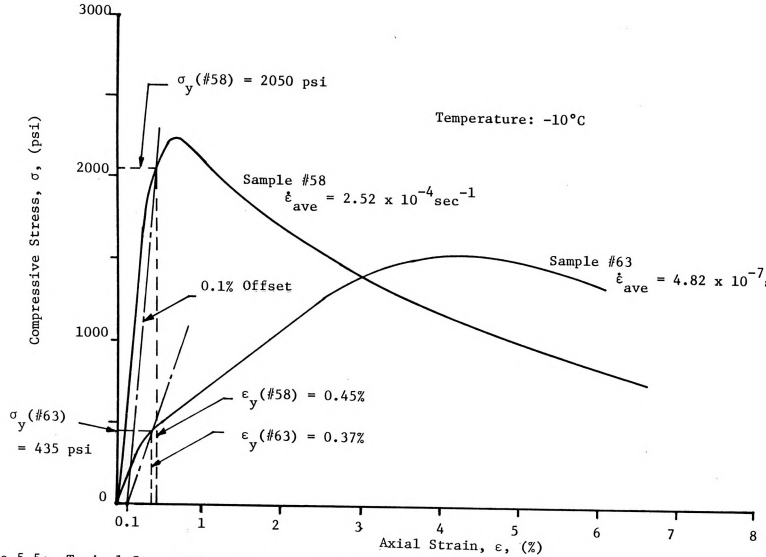

Figure 5-5: Typical Stress-Strain Curves Showing the Offset Method Used to Determine the Initial Yield Point.

10000

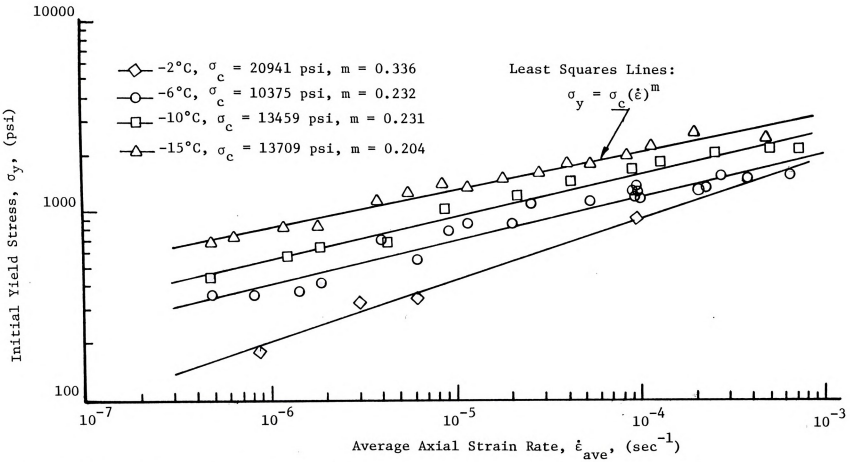

Figure 5-6: Effect of Strain Rate on the Initial Yield Stress.

10.0

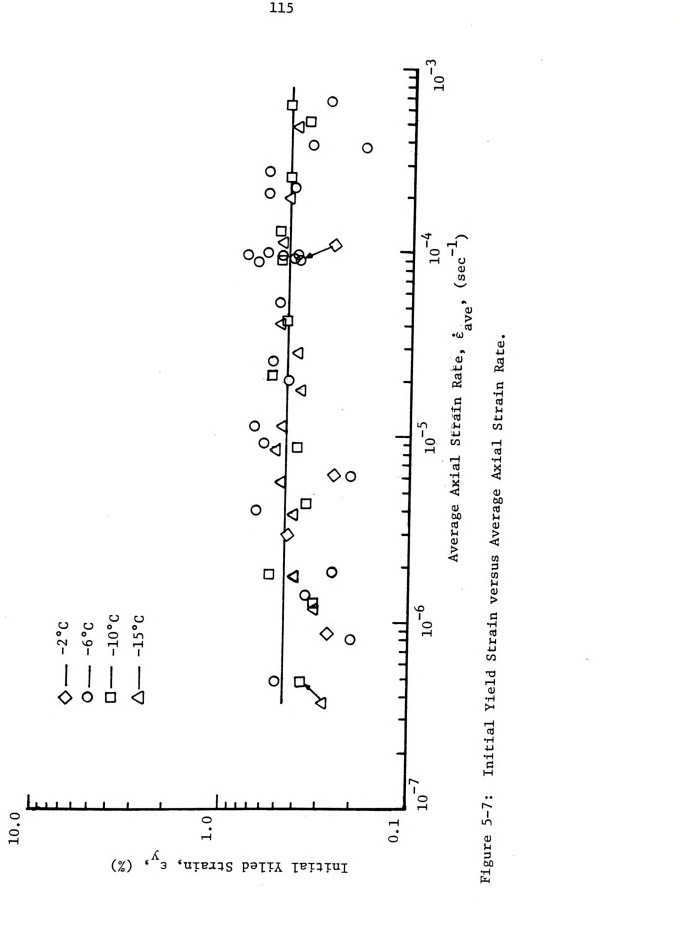

Figure 5-7: Initial Yield Strain versus Average Axial Strain Rate.

10000 E

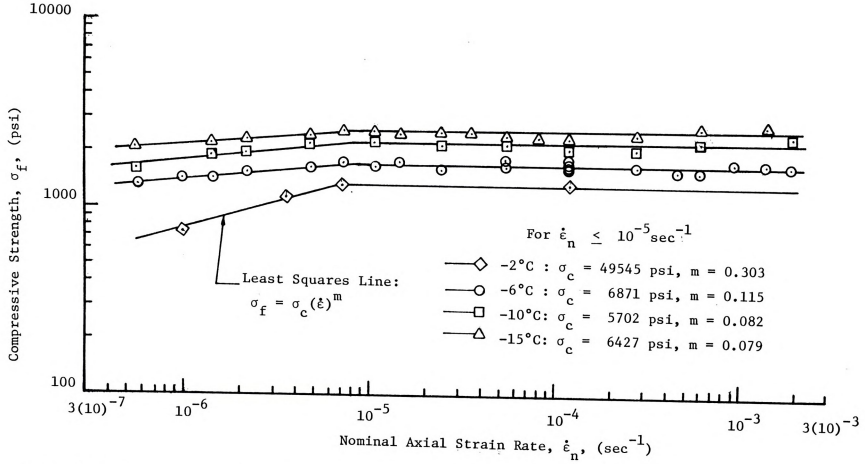

Figure 5-8: Compressive Strength versus Nominal Strain Rate.

10000
E
Least Squares Line:

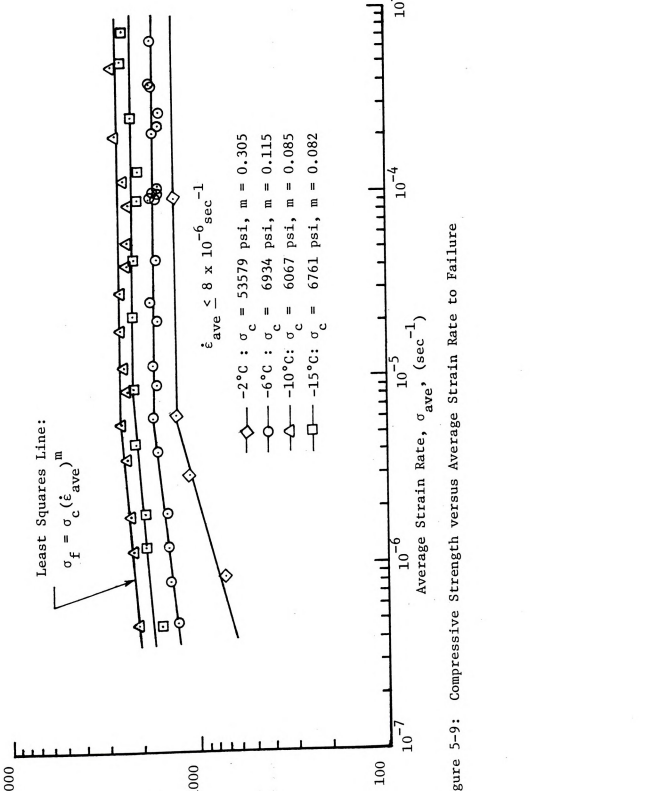

Figure 5-9: Compressive Strength versus Average Strain Rate to Failure

10.0 F

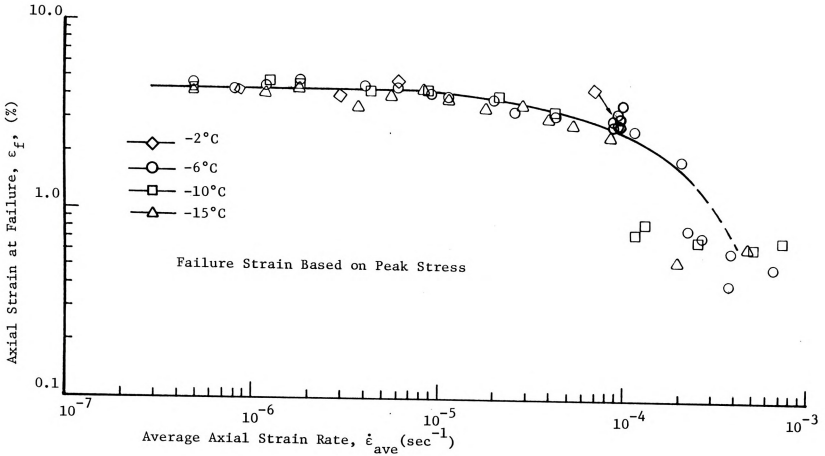

Figure 5-10: Axial Strain at Failure Peak Stress versus the Average Axial Strain Rate.

$2(10)^6$
10^6
Least Squares Line:
$E_i = B(\dot{\varepsilon}_{ave})^b$

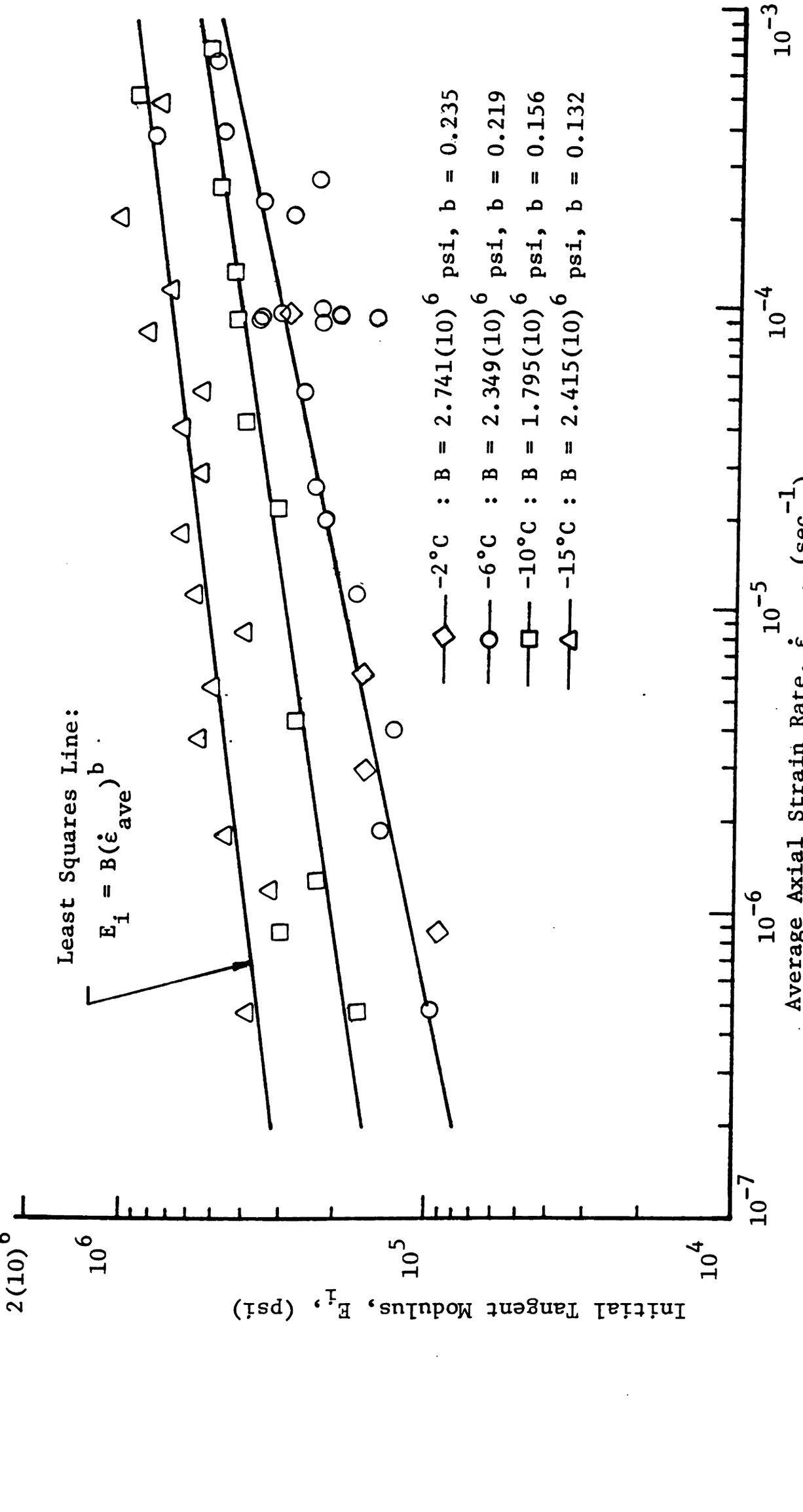

Figure 5-11: Initial Tangent Modulus versus Average Strain Rate to Failure.

1.8
Temperature: -2.02°C

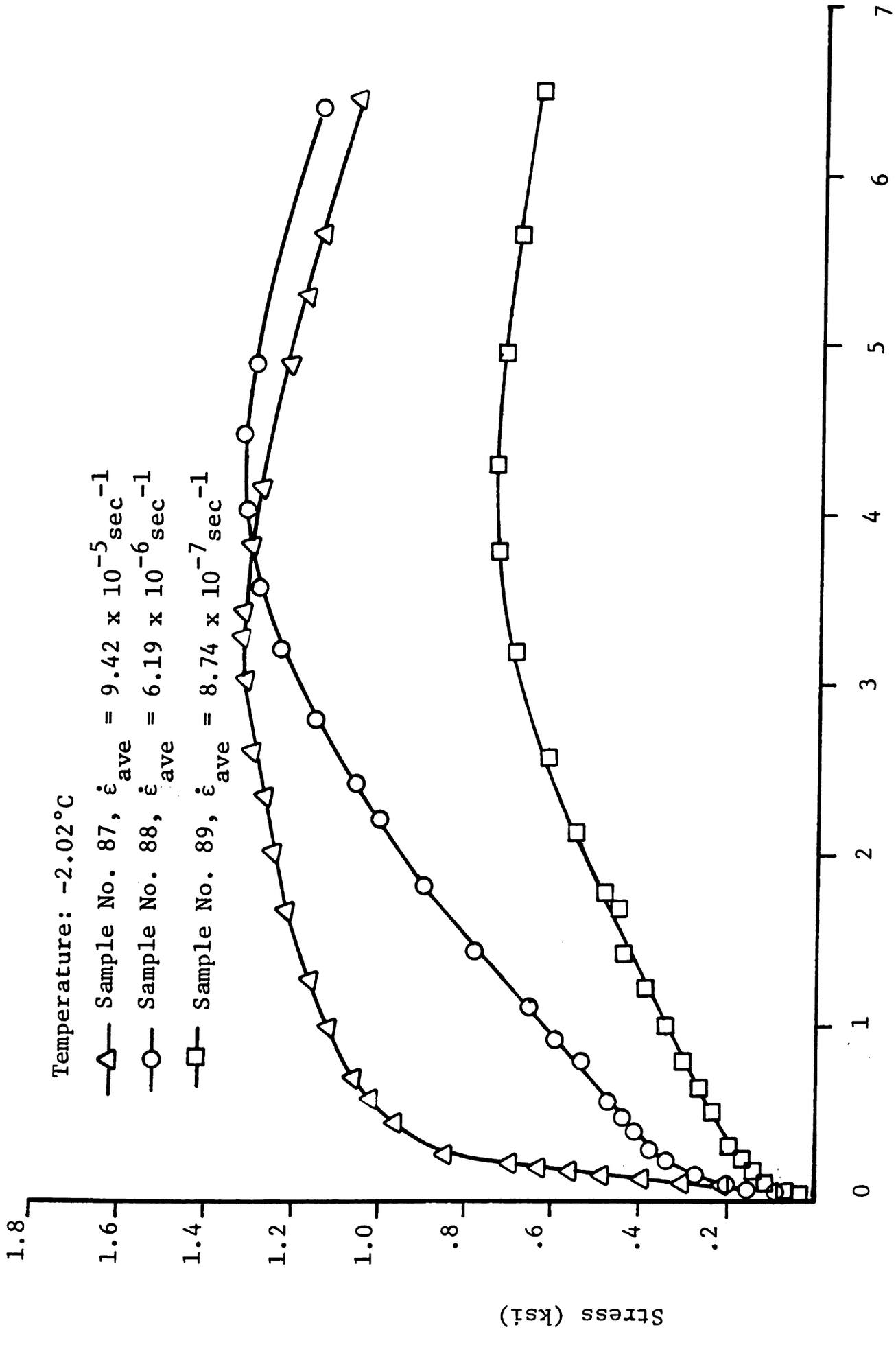

Figure 5-12: Stress - Strain Curves for Samples 87,88, and 89 at -2°C

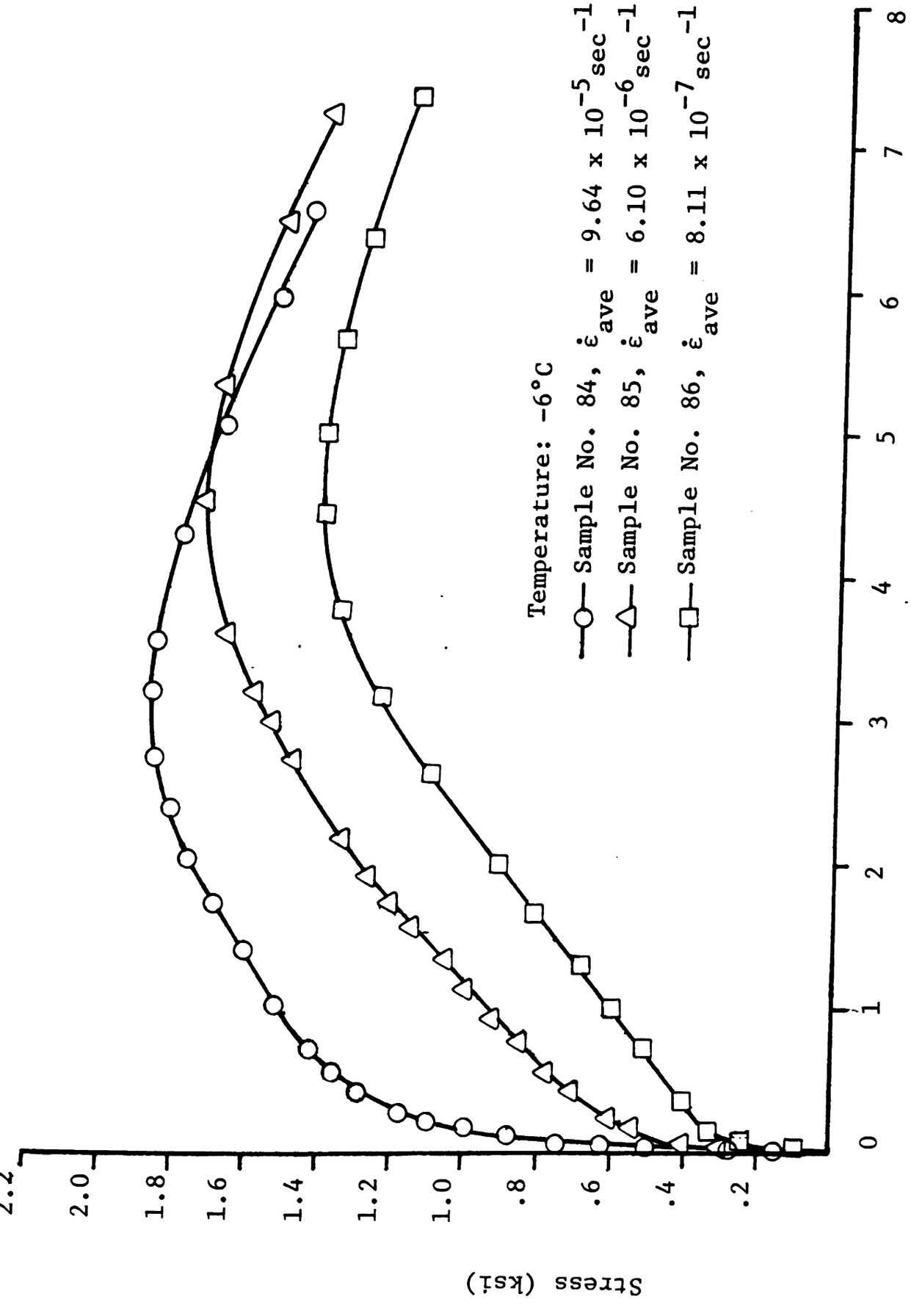

Figure 5-13: Stress-Strain Curves for Samples 84, 85, and 86 at -6°C.

2.

2

2

2

1

1

1

Stress (ksi)

Figur

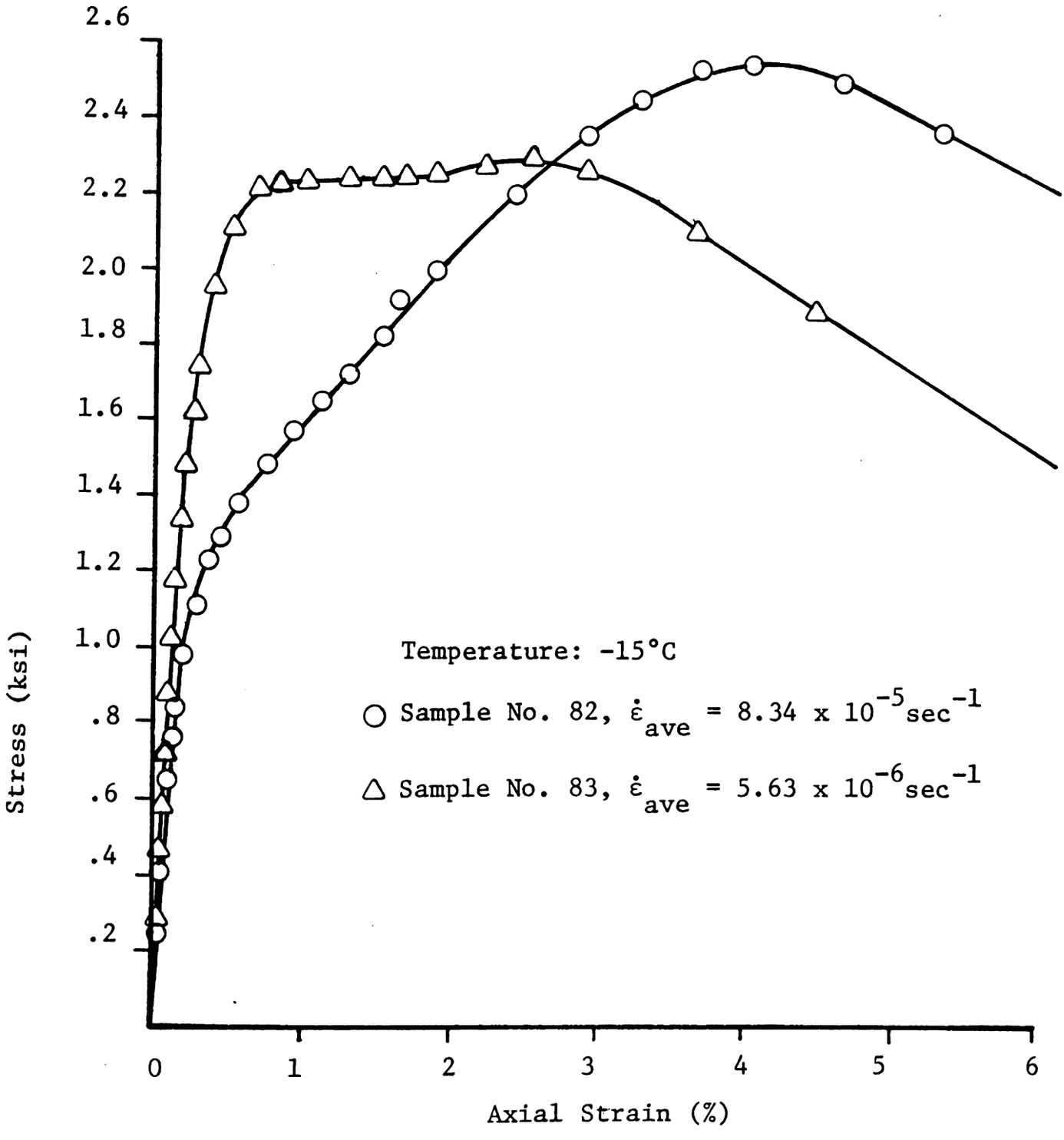

Figure 5-14: Stress-Strain Curves for Samples 82 and 83 at -15°C.

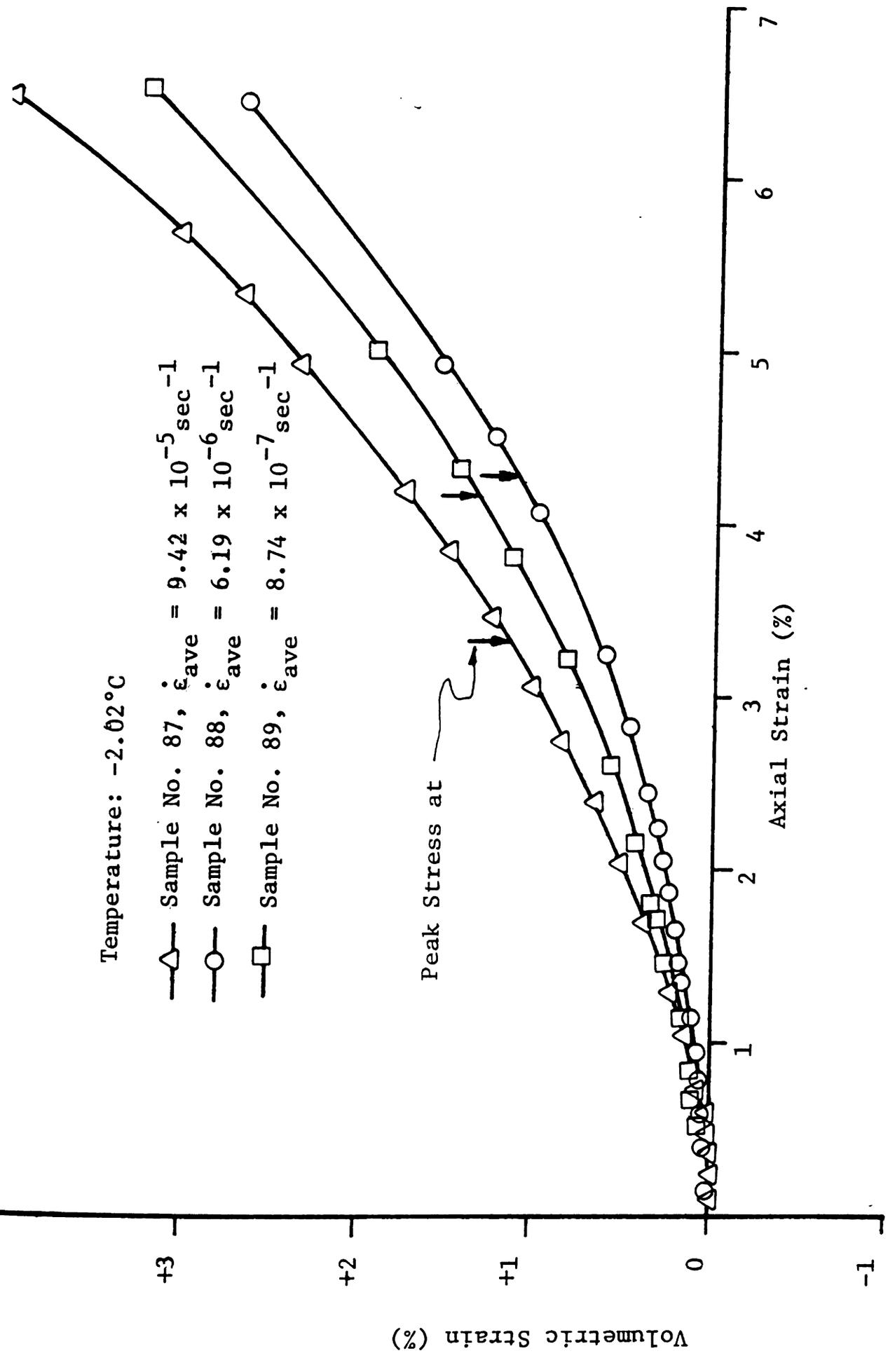

Figure 5-15: Volumetric Strain versus Axial Strain for Samples 87, 88, and 89 at -2°C.

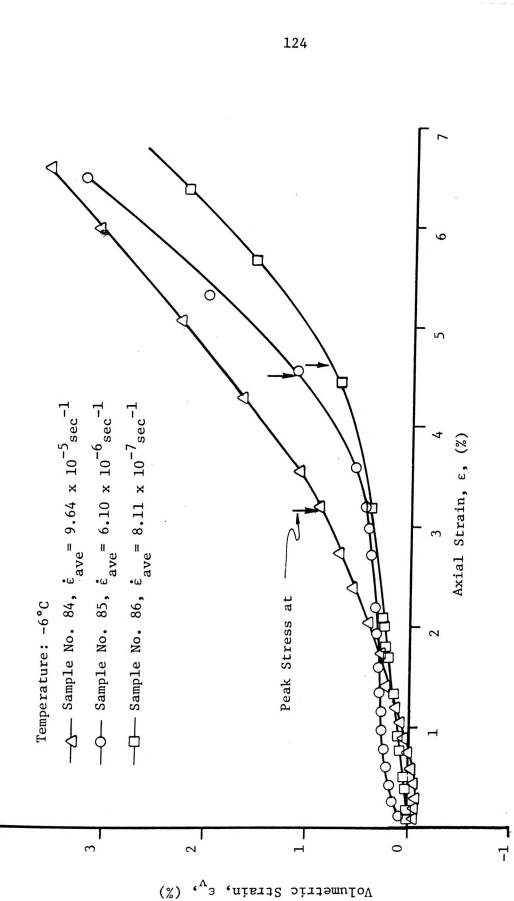

Figure 5-16: Volumetric Strain versus Axial Strain for Samples 84, 85, and 86 at -6°C

Temperature: -15°C

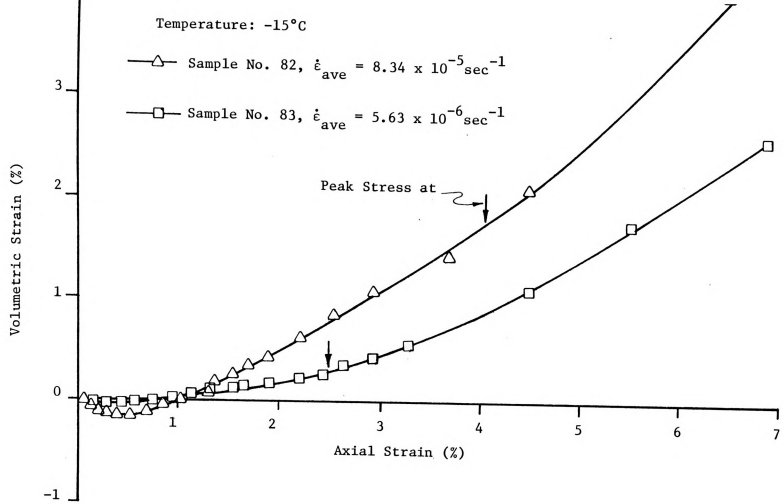

Figure 5-17: Volumetric Strain versus Axial Strain for Samples 82 and 83 at -15°C.

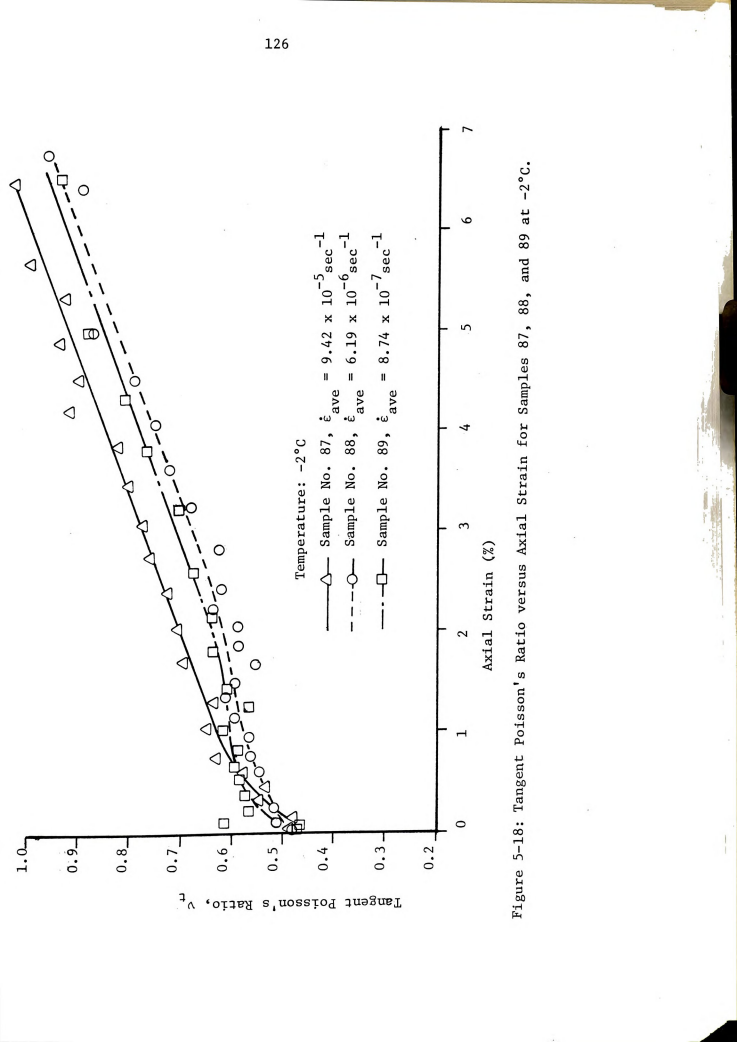

Figure 5-18: Tangent Poisson's Ratio versus Axial Strain for Samples 87, 88, and 89 at -2°C.

1.0

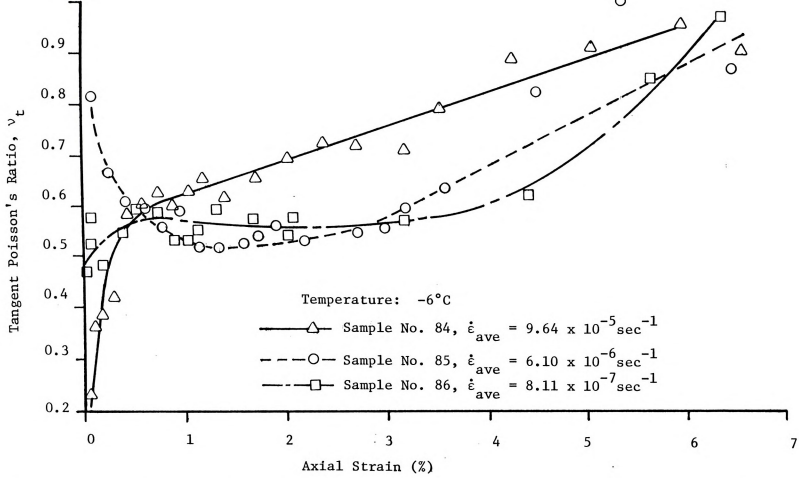

Figure 5-19: Tangent Poisson's Ratio versus Axial Strain for Samples 84, 85, and 86 at -6°C.

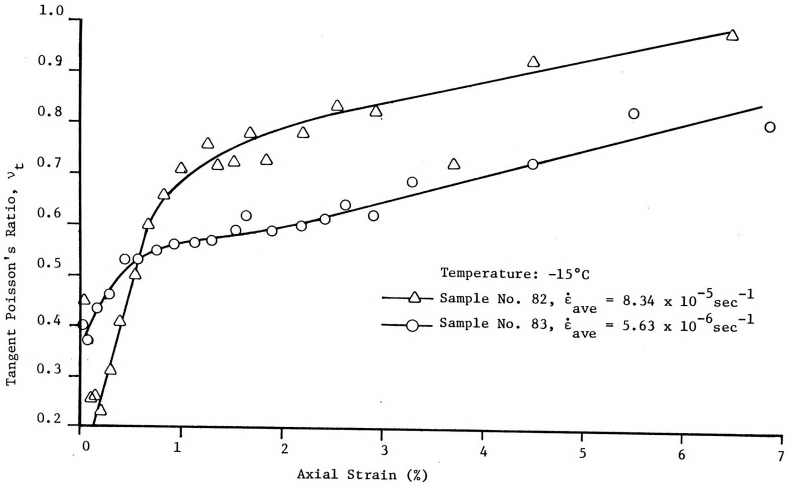

Figure 5-20: Tangent Poisson's Ratio versus Axial Strain for Samples 82 and 83 at -15°C.

2400

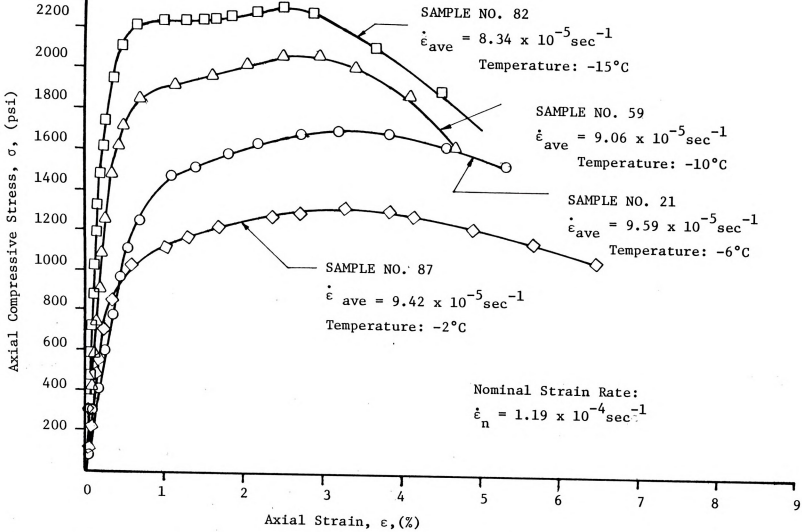

Figure 5-21: Temperature Effect on the Stress-Strain Behavior of Frozen Sand in Compression.

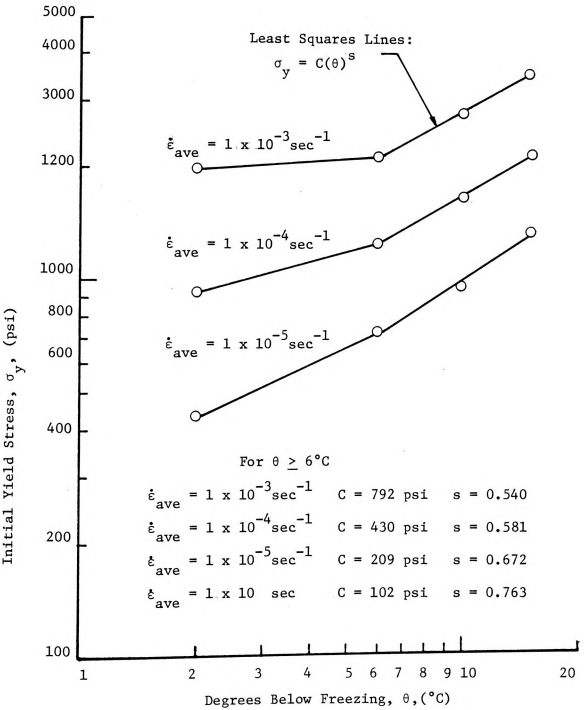

ure 5-22: Initial Yield Stress versus Degrees Below Freezing.

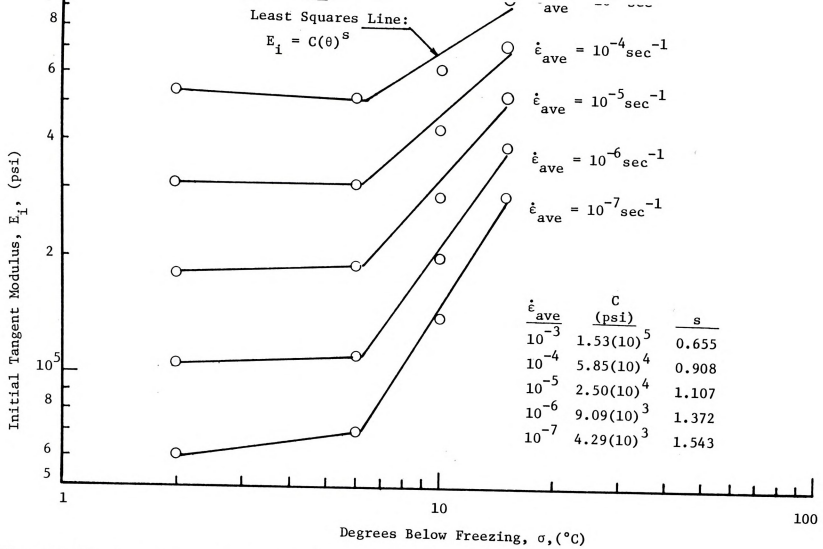

$\dot{\varepsilon}_{ave}$	C (psi)	s
10^{-3}	$1.53(10)^5$	0.655
10^{-4}	$5.85(10)^4$	0.908
10^{-5}	$2.50(10)^4$	1.107
10^{-6}	$9.09(10)^3$	1.372
10^{-7}	$4.29(10)^3$	1.543

Figure 5-23: Temperature Effect on Initial Tangent Modulus.

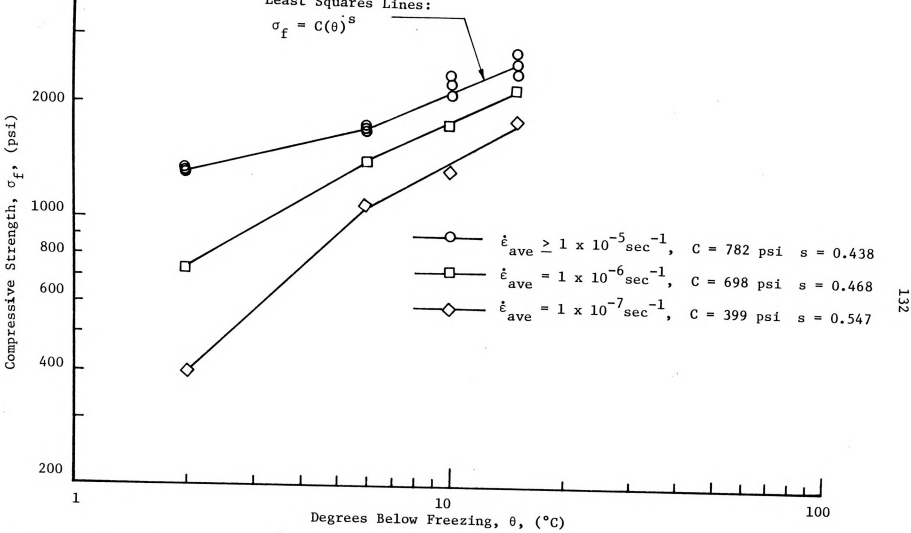

Figure 5-24: Temperature Effect on Compressive Strength.

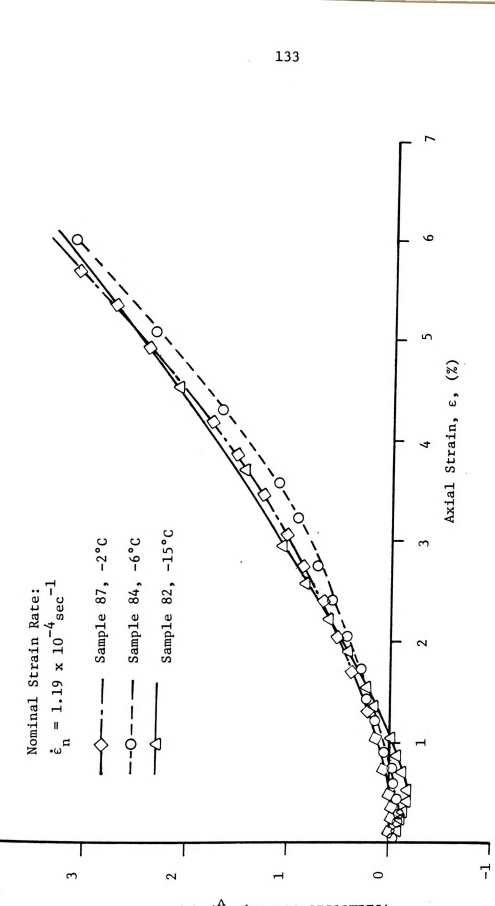

Figure 5-25: Temperature Effect on Volumetric Strain.

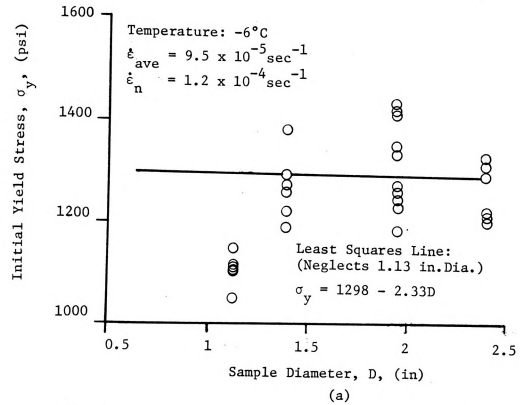

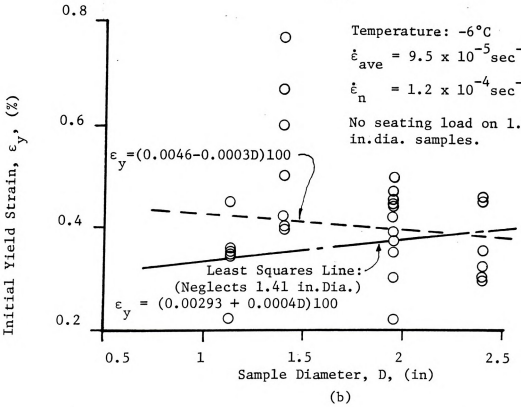

ure 5-26: Sample Diameter Effect on (a) Initial Yield Stress
(b) Initial Yield Strain

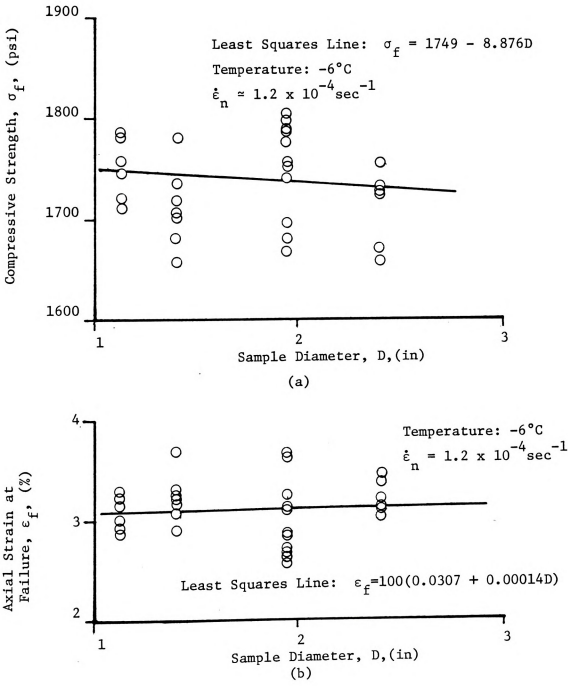

gure 5-27: Sample Diameter Effect on;(a) Compressive Strength, (b) Failure Strain.

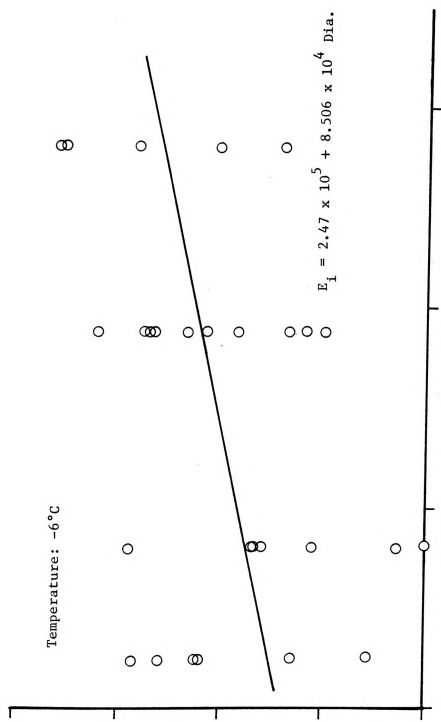

Figure 5-28: Sample Diameter Effect on the Initial Tangent Modulus.

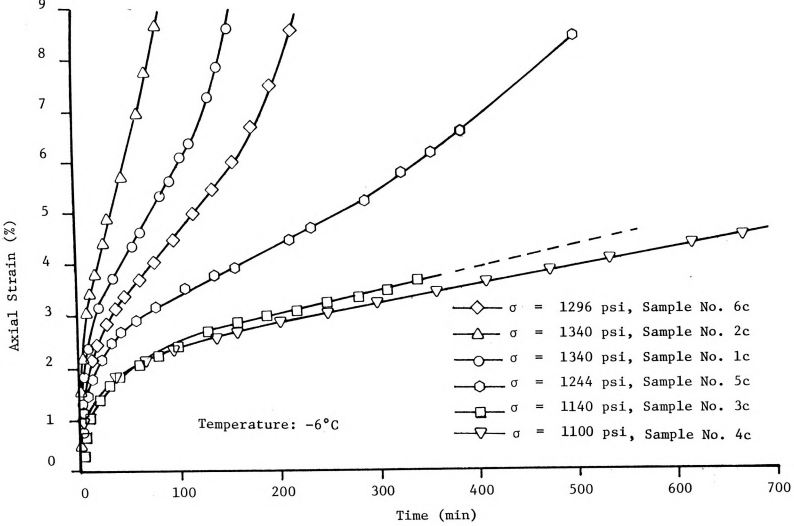

Figure 5-29: Creep Curves for Constant Stress Compression Creep Tests.

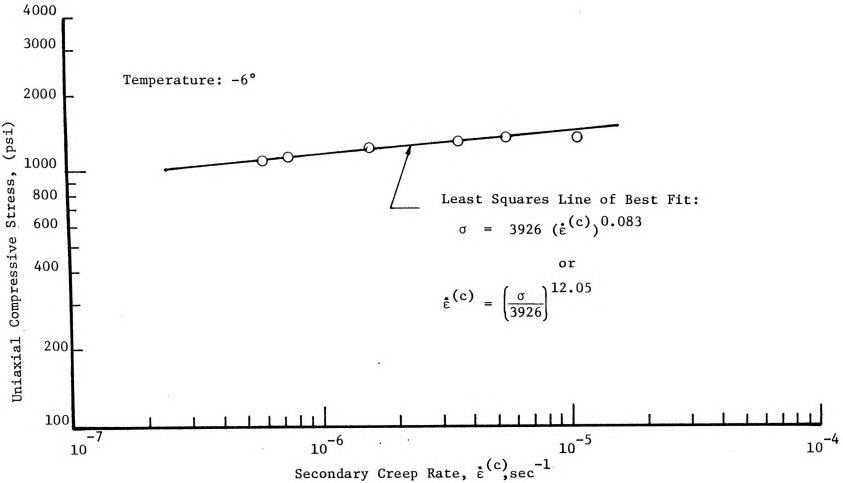

Figure 5-30: Uniaxial Compressive Stress versus Creep Rate for Constant Stress Creep Tests.

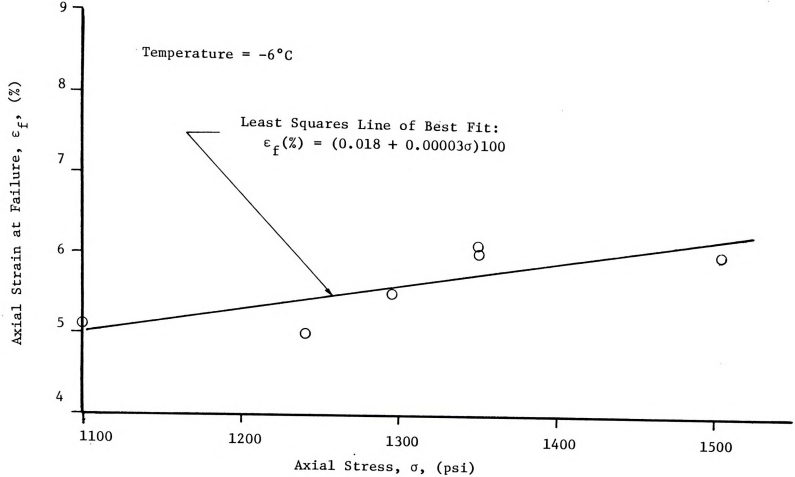

Figure 5-31: Axial Strain at Failure (Tertiary Creep) versus Axial Stress for Constant Stress Creep Tests.

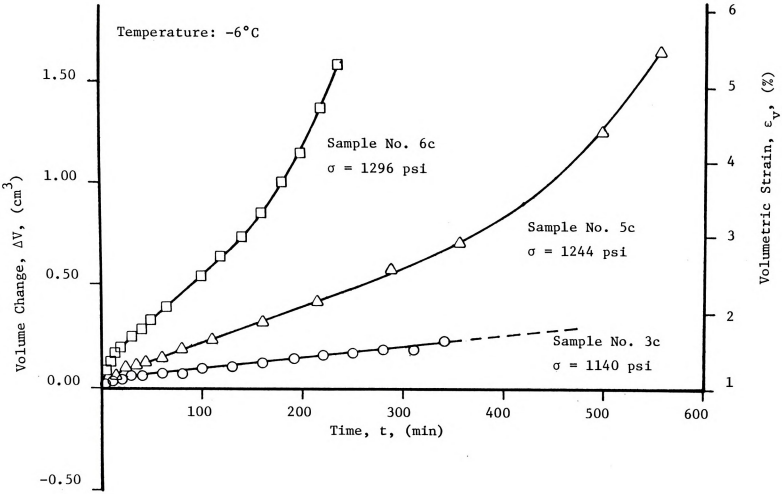

Figure 5-32: Volumetric Strain versus Time for the Constant Stress Creep Tests.

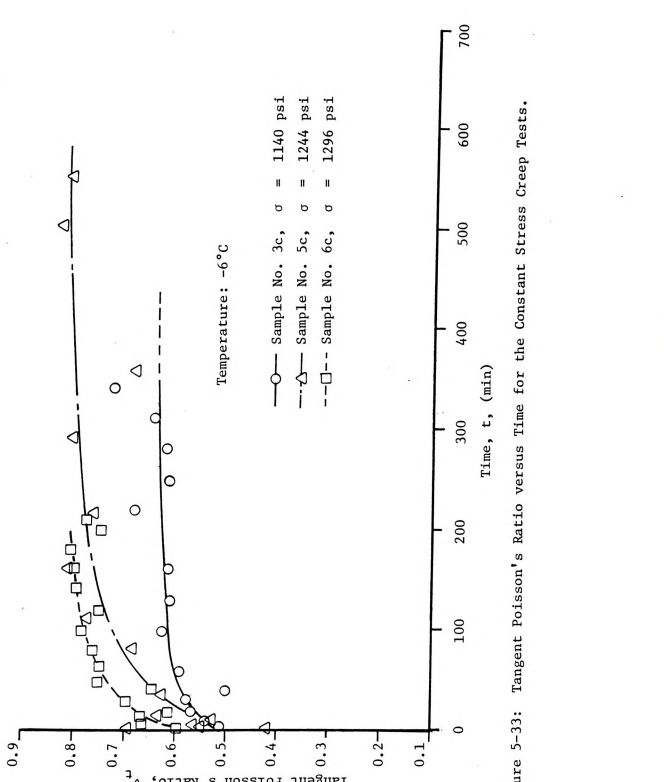

Figure 5-33: Tangent Poisson's Ratio versus Time for the Constant Stress Creep Tests.

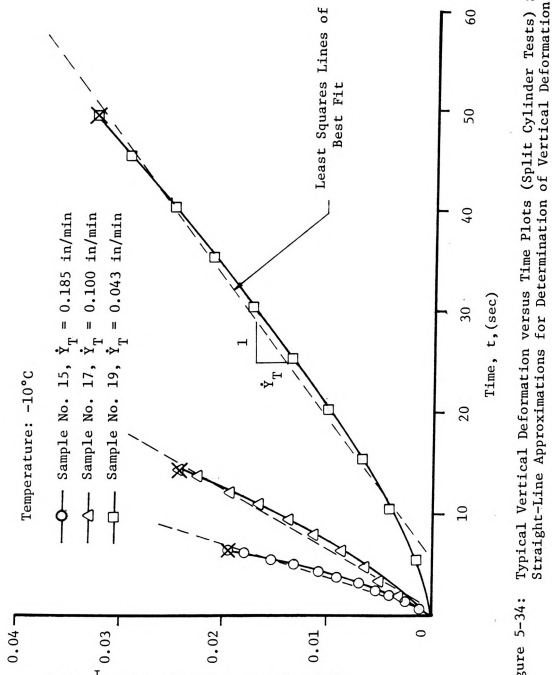

Figure 5-34: Typical Vertical Deformation versus Time Plots (Split Cylinder Tests) Showing Straight-Line Approximations for Determination of Vertical Deformation Rates.

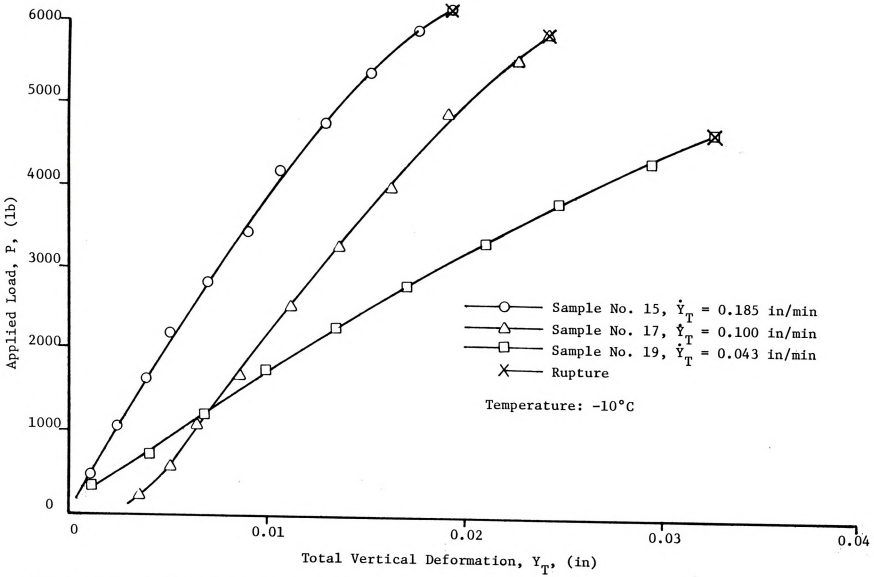

Figure 5-35: Typical Load versus Vertical Deformation Curves for Split Cylinder Tests

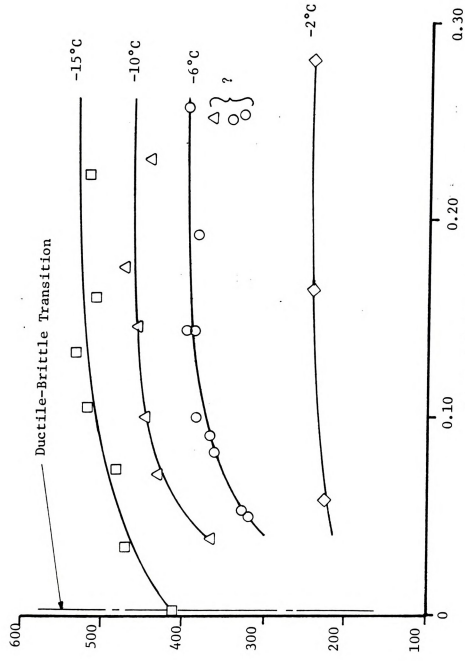

Figure 5-36: Vertical Deformation Rate Effect on the Indirect Tensile Strength.

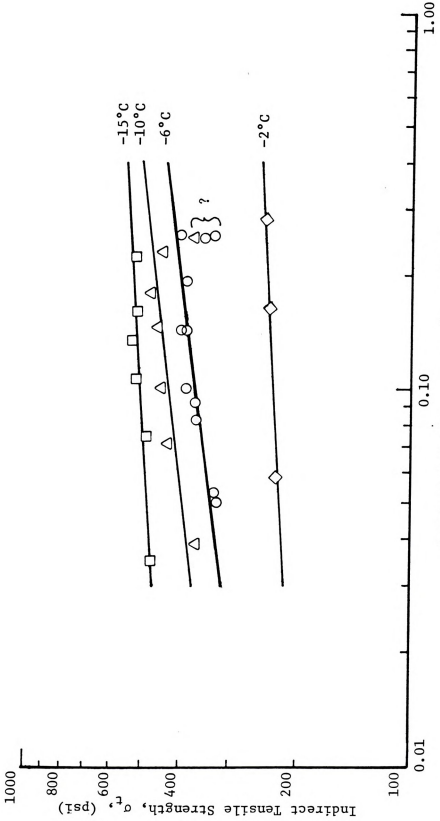

Figure 5-37: Log-Log Plot of Vertical Deformation Rate versus Indirect Tensile Strength.

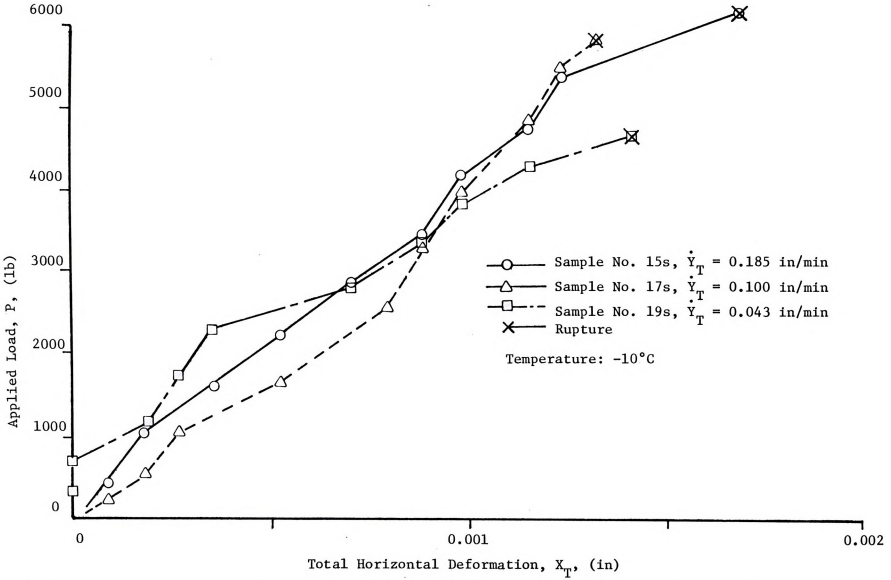

Figure 5-38: Typical Load versus Horizontal Deformation Plots for the Split Cylinder Tests.

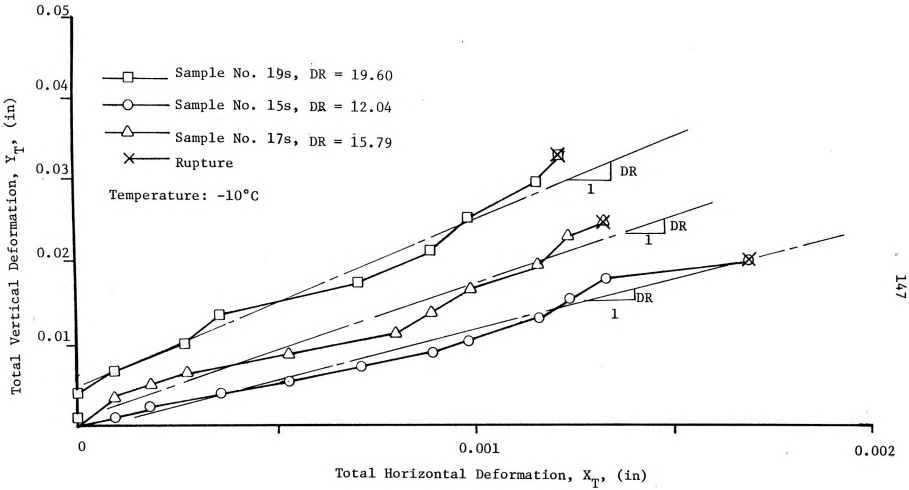

Figure 5-39: Typical Vertical Deformation versus Horizontal Deformation Plots (Split Cylinder Tests) for Determination of DR.

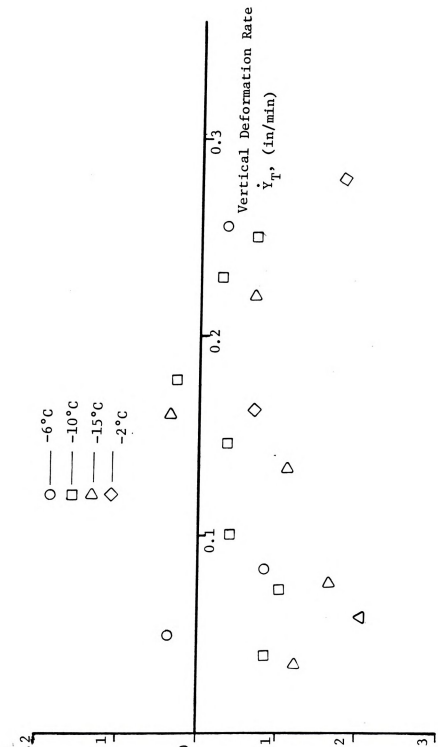

Figure 5-40: Poisson's Ratio versus Applied Vertical Deformation Rate for the Split Cylinder Tets.

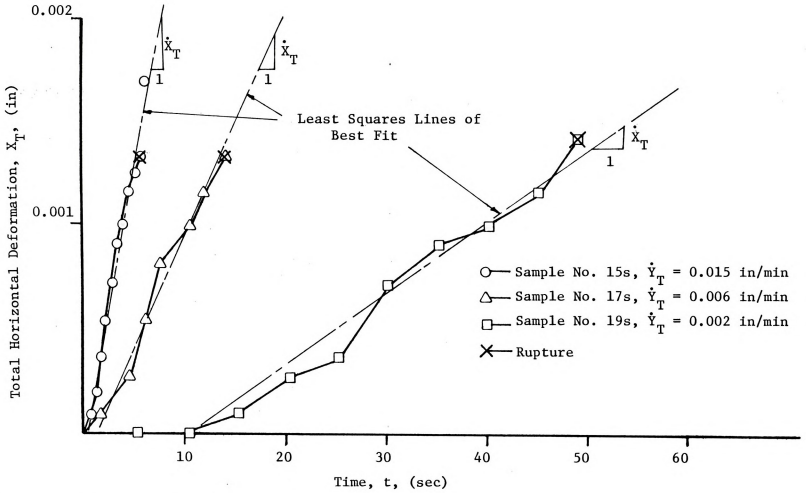

Figure 5-41: Typical Horizontal Deformation versus Time Plots (Split Cylinder Tests) Showing Straight-Line Approximations to Determine Horizontal Deformation Rate.

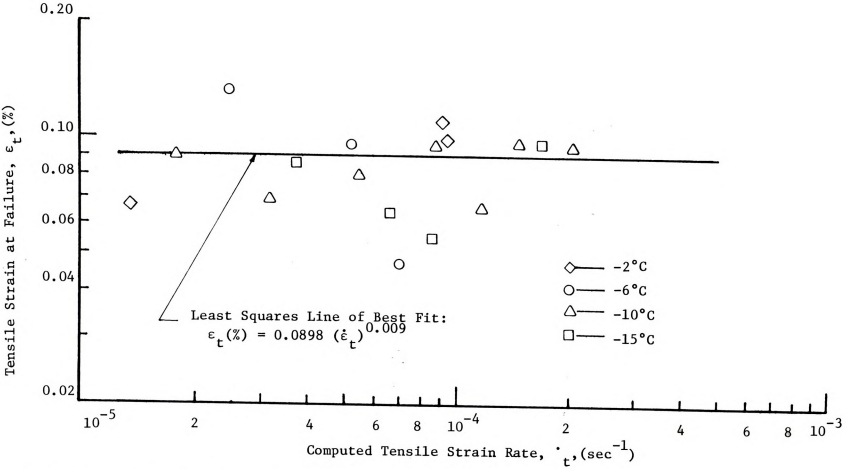

Figure 5-42: Tensile Strain Rate Effect on the Tensile Strain at Failure.

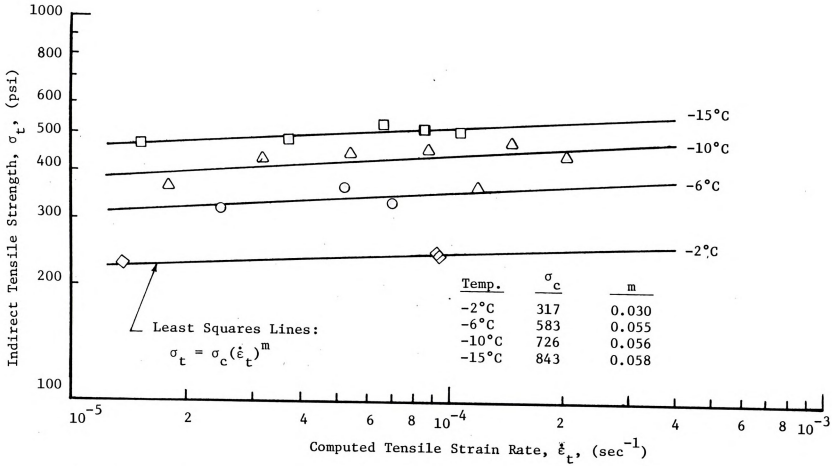

Figure 5-43: Tensile Strain Rate Effect on Indirect Tensile Strength.

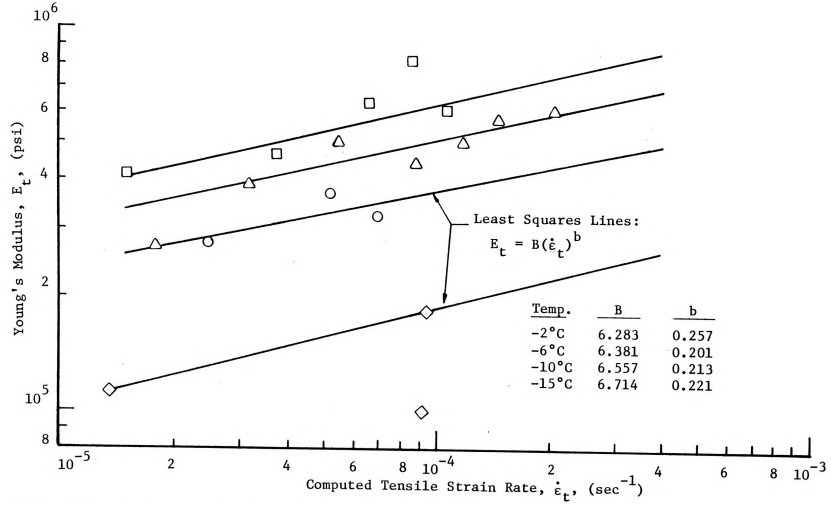

Figure 5-44: Tensile Strain Rate Effect on Young's Modulus.

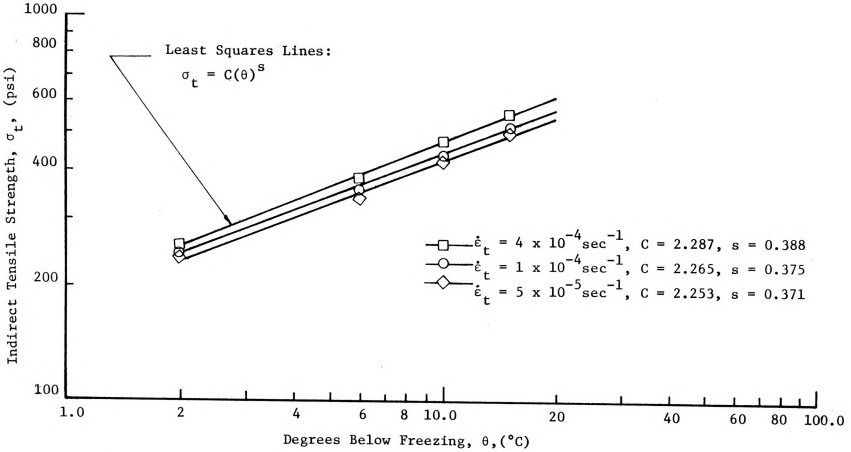

Figure 5-45: Temperature Effect on the Indirect Tensile Strength.

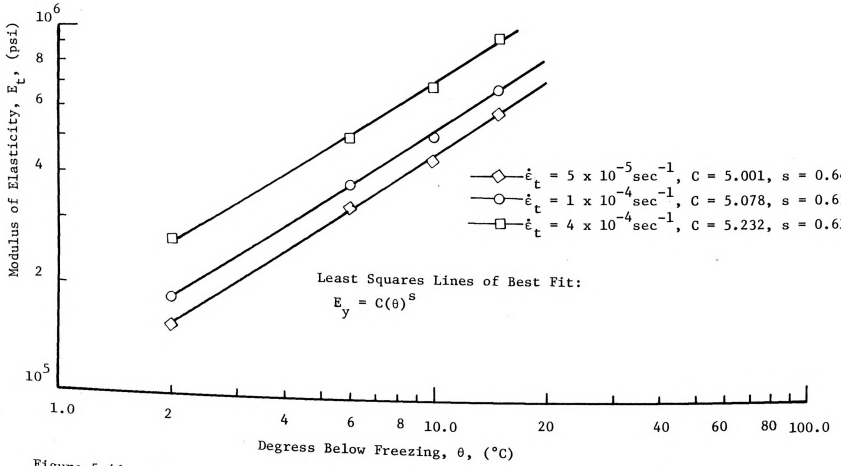

Figure 5-46: Temperature Effect on Young's Modulus Determined from Split Cylinder Tests.

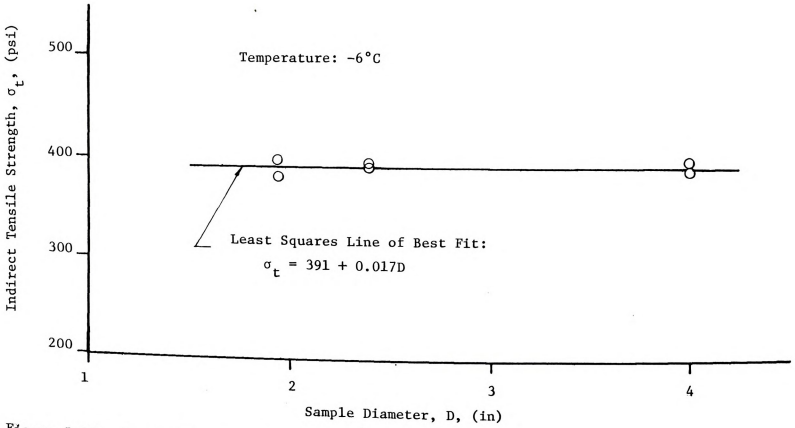

Figure 5-47: Sample Diameter Effect on the Indirect Tensile Strength.

CHAPTER VI

DISCUSSION AND ANALYSIS

The analysis and design of frozen soil structures requires information on the soil-ice mechanical properties and the influence of test methods and service variables on the material behavior. The experimental results presented in Chapter V are analyzed and discussed in Chapter VI with respect to defining the mechanical frozen sand properties, standardization of test procedures, and selection of material properties for design. The final section presents discussion of a preliminary design procedure which considers time dependent response of a simply supported frozen sand beam.

6.1 Mechanical Behavior Of Frozen Sand

The mechanical behavior of frozen Wedron sand was investigated experimentally to determine both the tensile and compressive properties of the sand-ice material relative to engineering design. Material properties in tension and compression are considered in separate sections.

6.1.1 Material Properties In Compression

As observed in Chapter V, the applied strain rate governs the stress-strain behavior and deformation modes of the frozen sand in compression (see Figure 5-3 and 5-4). The deformation behavior clearly changes from a plastic to a brittle type of failure as the applied strain rate increases. At high average strain rates, above $2 \times 10^{-4} sec^{-1}$, the stress-strain curve remains nearly linear up to the peak stress. At lower strain rates the stress-strain curves are characterized by an abrupt transition from elastic to plastic deformation. The frozen sand

deforms elastically for strains less than one percent and stresses up to the initial yield stress. A prominent region of plastic strain hardening occurs beyond the initial yield point and up to the peak stress.

The transition from ductile to brittle behavior is primarily the result of influence from the ice matrix. Data obtained by Hawkes and Mellor (1972) from constant strain rate compression tests on polycrystalline (granular) ice indicates a similar transition in the stress-strain curves for ice. Alkire (1974) conducted constant strain rate compression tests on unconfined samples of frozen sand over a limited range of strain rates ($4.4 \times 10^{-6} sec^{-1}$ to $4.4 \times 10^{-5} sec^{-1}$). The results of these tests indicated that as the strain rate increased the initial yield stress and the peak strength increased, while strain at the peak stress decreased. Consequently, the net effect was to increase the elastic response of the frozen sand with increasing strain rate. Since the soil structure and volume of sand for the samples were constant, Alkire (1974) concluded that the strain rate primarily affects the ice matrix. The transition in the shape of the stress-strain curves for the frozen sand appears to result from a ductile to brittle transition in the ice matrix.

Several other authors have suggested that the initial yield stress observed in the frozen sand samples is the result of yielding in the ice matrix. Sayles (1974) conducted a series of triaxial tests on frozen Ottawa sand at constant axial strain rates with hydrostatic confining pressures varying from 50 psi to 1200 psi. For strains exceeding 0.1, two peak stresses were observed when the confining pressure was above 400 psi. The first peak occurred at strains less than

0.01 and the second at a strain of about 0.10. Comparison of the first yield point with the failure strain of columnar grained ice indicated that the two occurred at approximately the same strain value. This observation suggested that the initial yield or first peak results as a consequence of the yielding of the ice matrix. The second peak was then attributed to development of friction between sand grains and/or ice crystals as the strain progresses. Sayles (1974) concluded that these two sources of strength were nearly independent of each other for strain rates greater than $3.3 \times 10^{-4} sec^{-1}$. After the ice matrix had failed at a strain less than 0.01, the soil resistance became a function of the normal stress and the apparent angle of internal friction (as described by the Mohr-Coulomb failure theory).

Parameswaran (1980) presented experimental data from a series of unconfined compression tests conducted at strain rates from 10^{-7} to $10^{-2} sec^{-1}$. The transition from elastic to plastic deformation for a given stress-strain curve was not well defined at high temperatures and low strain rates. As the strain rates increased, the specimens showed an initial yield point at the end of the elastic region followed by a small drop in the stress before plastic deformation started. This initial yield point was attributed to yielding of the ice matrix. The stress drop was believed due to a decrease in stress required to maintain the strain rate from that required to initiate the yield. The increase in the stress after the yield drop was proposed to be due to the development of the frictional component of strength (even at zero confining pressure.)

The initial yield stresses, determined from the stress-strain curves described in Chapter V, were observed to increase with increasing

strain rate as shown in Figure 5-6. The initial yield stress, for the Wedron sand as a function of strain rate, is replotted and compared with the compressive strength of polycrystalline ice at -7°C (Hawkes and Mellor, 1972) in Figure 6-1. Both values appear to be reasonably well described by a straight-line relationship on the log-log plot, suggesting power laws of the form given by Equation (5-1). Least squares linear regression analyses of the data results in values for the constant σ_c of 10,357 psi and 5,773 psi and the constant m of 0.232 and 0.214 for the Wedron sand and the ice, respectively (where σ_c is the proof stress defined at $\dot{\varepsilon}_{ave} = 1.0\ sec^{-1}$ and m is the slope of the lines on the log-log plot). The large difference in σ_c values denotes a significant discrepancy between the values of the initial yield stress of the frozen sand and the compressive strength of the granular ice. However, some portion of the total stress applied to the frozen dense sand must be carried by the soil structure up to the yield stress. Consequently, the total stress required to induce yielding in the ice matrix of a frozen sand would be expected to be greater than the compressive strength of pure ice due to the stress carried by the sand particles. The values of the exponents (m) are in close agreement, indicating that the strain rate dependency of the initial yield stress and the strength of ice are very similar. This correlation supports the hypothesis that yielding of the ice matrix results in the initial yield point observed in the stress-strain traces of the frozen sand.

Values for the initial yield strain of the frozen Wedron sand also compare relatively well with the compressive strain at the peak stress for the polycrystalline ice. Figure 6-2 presents a comparison of the

initial yield strain for the sand with the failure strains in granular ice (Hawkes and Mellor, 1972). The failure strain of the ice was observed to decrease from 1.1 percent to 0.13 percent over a range of strain rates from 6 x 10^{-6} sec^{-1} to approximately 1 x 10^{-3} sec^{-1}. Over this same range in strain rates the initial yield strain of the sand decreased from approximately 0.70 to 0.18 percent as the strain rate decreased. These observations also suggest the initial yield is essentually the consequence of the yield of the ice matrix.

Figure 6-3 compares the initial tangent modulus of the frozen sand with the initial tangent modulus of polycrystalline ice. A comparison of the initial tangent modulus of the frozen Wedron sand with initial tangent modulus of Ottawa sand (passing No. 30 and retained on No. 100 sieve), as determined by Parameswaran (1980), is presented in Figure 6-4. As may be observed from Figure 6-4, the initial tangent modulus values compare reasonably well. The data for the Ottawa sand (approximately the same gradation as the Wedron sand) appears to lie nearly in the mid-range of the values for the Wedron sand and both appear to vary linearly with strain rate on a log-log plot (for temperatures less than -2°C) as described by Equation 5-3. A least squares linear regression analysis of the data obtained by Parameswaran (1980) for temperatures below -2°C results in a value of b of 0.130 while the value of the exponent b for Wedron sand varied from 0.121 at -15°C to 0.230 at -2°C. The two investigations appear to provide consistent results with respect to strain rate dependency of the initial tangent modulus. However, data for the Wedron sand indicates a greater temperature dependence for the elastic modulus than does the data from Parameswaran (1980).

The initial tangent modulus of frozen sand appears to be somewhat less than the initial tangent modulus of ice as shown in Figure 6-3. Since the data for the tangent modulus of Wedron and Ottawa sands appear to agree relatively well, it must be concluded that the elastic modulus of frozen sand is indeed less than that for polycrystalline ice. This seems to be somewhat of a contradiction in that the initial tangent moduli for the Wedron sand was determined from the portion of the stress-strain curve below the initial yield point. This portion of the curve is thought to be dominated by the behavior of the ice matrix. Imperfections in the contact surfaces may partially explain the observed difference in modulus values. The sand samples are more difficult, due to their granular nature, to trim and seat against the loading platens. Initial seating loads were applied to the Wedron sand samples tested at -2, -10, and -15°C to minimize this problem. The data shown in Figure 5-6 does exhibit less scatter for these temperatures than for -6°C. However, it is doubtful that the procedure completely eliminated the strains associated with sample seating. In addition, the stress-strain curves for the frozen sand were not truely linear up to the initial yield. Since the initial tangent moduli were computed from a linear regression analysis of the portion of the stress-strain curves below initial yield and since the initial yield strain of the frozen sand was approximately equal to the failure strain of ice, it is suspected that the initial tangent modulus values for the ice were determined over a much smaller range of strains. This would also explain the significantly higher values of E_i for ice as compared with the frozen sand.

The region of plastic strain hardening which follows initial yield

in the samples (see Figure 5-3) appears to result from dilatancy of the sand and mobilization of internal friction between sand grains and ice crystals. Figures 5-15, 5-16, and 5-17 present several plots of volumetric strain versus axial strain. In general, the samples exhibit a small initial decrease in volume. As the axial strain approaches the initial yield strain the volumetric strain decreases to a minimum value. This decrease in volume corresponds to compression of the ice matrix, pressure melting at points of contact between sand particles and ice crystals, and densification of the sand packing structure. As the axial strain increases above the initial yield point, the volume of the sample increases. Similar behavior was also observed by Goughnour (1967) from tests conducted on frozen Ottawa sand. His comparison of stress-strain curves for the frozen sand with those of ice (multipled by a stress factor to account for the additional stiffness of the sand structure) indicated that the curves diverged at a strain level close to that at which the volume change reversed its initial decrease and began to increase. The additional strengthening observed in the frozen sand above the initial yield was attributed to dilatancy of the sand material.

At low confining pressures and low strain rates cohesion of the ice matrix and frictional resistance of the sand grains can not be considered to act independently as observed by Sayles (1974) for high strain rates and confining pressures. At low strain rates (average less than $7 \times 10^{-6} sec^{-1}$ in the present study) ice flow appears to govern the initial deformation process. Compression forces between sand particles and ice crystals at points of contact induce pressure melting. Sufficient time is available at the low strain rates for water migration

to regions of lower stress where it refreezes. This water migration is accompanied by compression of the ice matrix and densification of the sand. The initial yield occurs as the pore ice reaches its final yield stress and as dilatancy begins to contribute to the shear strength. A prominent region of plastic strain hardening occurs above the yield point with the samples tending to remain nearly cylinderical up to failure (see Figure 5-4a). This period of strain hardening represents dilatancy and mobilization of interparticle friction.

With increasing strain rates the ice matrix strength increased giving higher yield stresses. For moderate strain rates ($7 \times 10^{-6} sec^{-1} < \dot{\varepsilon}_{ave} < 2 \times 10^{-4} sec^{-1}$) the stress-strain curves exhibit a smaller region of strain hardening and a well defined shear plane inclined at approximately 60 degrees to the horizontal. At higher average strain rates (above $2 \times 10^{-4} sec^{-1}$), the stress-strain curves remained nearly linear up to the peak stress. Samples tested at average strain rates above $2 \times 10^{-4} sec^{-1}$ showed multiple slip lines (Figure 5-4c). The formation of slip surfaces at moderate and high strain rates suggest that the mobilized angle of internal friction was close to 30 degrees.

The total shear strength, as a function of strain rate, must consist of both cohesion of the ice matrix and mobilized friction in the sand. Figure 5-9 presents a plot of compressive strength versus average strain rate on a log-log scale. The compressive strength of the frozen sand was observed to increase linearly with increasing strain rate for average strain rates below about $7 \times 10^{-6} sec^{-1}$, suggesting a power law of the form given by Equation (5-2). At average strain rates above about $7 \times 10^{-6} sec^{-1}$, the unconfined compressive strength was essentually independent of the applied strain rate.

Table 6-1 contains values for the constant σ_c (proof stress at an average strain rate of 1 sec^{-1}) and the exponent m based on a linear regression analysis of the data. Values reported by other researchers for silica sand with similar gradation and density are included. Unconfined compression test results for Wedron sand at -6°C are compared with results of several other investigations in Figure 6-5.

Data presented in Table 6-1 and summarized in Figure 6-5 shows that the compressive strength of Wedron sand, for average strain rates less than about 7 x $10^{-6}sec^{-1}$, is in good agreement with the data reported by Parameswaran (1980), Baker (1978), and Sayles and Epanchin (1966). However, these earlier investigations do not always report a transition or change in slope for strength versus strain rate data. Parameswaran (1980) noted that the peak strength was independent of strain rate for samples tested at -2°C and strain rates above approximately $10^{-5}sec^{-1}$. He presumed that the low strain rate behavior at -2°C was governed by the unfrozen water content in the frozen sand specimens. Parameswaran (1980) estimated the unfrozen water content of Ottawa sand at -2°C to be approximately 0.14 percent by weight based on the specific surface area. The amount of unfrozen water at contact points would be increased considerably due to pressure melting of the ice as a result of stress concentrations. At a temperature of -2°C and at low strain rates the unfrozen water may migrate within the soil sample and reduce the compressive strength. This behavior would explain the drop in strength for -2°C below a strain rate of $10^{-5}sec^{-1}$.

For the data shown in Figure 5-9, the drop in compressive strength occurs at about the same strain rate where visable cracking or shearing was first observed. This would imply that the change in slope

corresponds to an upper limit where pressure melting, water migration, and refreezing have time to occur during soil deformation. This hypothesis is in general agreement with the explanation offered by Parameswaran (1980). However, it does not explain why other investigators did not observe the change in slope over the same range of temperatures and strain rates, while the mode of deformation of the samples was reported to change from plastic flow to brittle failure (cracking) as the strain rate increased.

A second possible explanation can be based on a comparison of the compressive strength with the initial yield stress (Figure 6-5). At average strain rates below about $7 \times 10^{-6} sec^{-1}$, the difference between the compressive strength and initial yield stress at a given temperature was nearly independent of strain rate. If the initial yield may be attributed to yield in the ice matrix, this suggests that contribution of dilatancy and interparticle friction to the sample shear strength was nearly constant for the lower strain rates. As the average strain rate increased above $7 \times 10^{-6} sec^{-1}$, the difference between the initial yield stress and the peak stress decreases until the initial yield stress approaches the unconfined compressive strength. The contribution from dilatancy and interparticle friction would then decrease with increasing strain rate. At the point where the initial yield stress approaches the peak stress, the contribution of the frictional and dilatancy components of shear strength is zero. As the applied strain rate increases the ice matrix becomes less effective in confining the movement of sand particles.

At low strain rates, the samples remained nearly cylindrical with no visable cracking or shearing at strains well in excess of the peak

stress. Deformation of the frozen sand was governed primarily by ice flow. At high strain rates cracking and shear planes were observed. If cracking occurred at the initial yield, then the absence of a confining pressure would allow some of the cracks to open and prevent full mobilization of friction along the crack surface (a large crack was observed in Sample 58, Figure 5-4c).

The volume change data presented in Figure 5-17 lends support to this explanation. Samples 82 and 83, tested at -15°C, compare very well with respect to density and degree of ice saturation (see Table 5-1). However, Sample 82 (tested at an average strain rate of $8.34 \times 10^{-5} sec^{-1}$) shows greater variation in volume change with axial strain than does Sample 83 (tested at an average strain rate of $5.63 \times 10^{-6} sec^{-1}$). This behavior is comparable to the influence of confining pressure on the volume change of unfrozen sand during shearing. As the confining pressure increases, the amount of dilatancy in an unfrozen sand decreases (Perloff and Baron, 1976). This implies that the effective confinement was greater at the lower strain rates. However, this effect should also have influenced the results reported by other investigators.

The observed change in slopes shown in Figure 6-5 could also have resulted from surface irregularities at the trimmed end of the sand-ice samples. For average strain rates close to $7 \times 10^{-6} sec^{-1}$, the development of shear planes, slip surfaces, and sample bulging was generally observed to be nearer the trimmed sample ends. Surface irregularities could induce stress concentrations at the platen sample contact points and may have initiated premature failures in the samples as the sand-ice material became more brittle with increasing strain rate.

Samples 23 through 26 exhibited significantly lower strength values (see Tables 5-2) than did other samples of the same diameter (1.13 inches) tested at the same nominal strain rate ($1.29 \times 10^{-4} sec^{-1}$). These samples exhibited either shear planes passing through the trimmed end of the sample or cracking parallel to the longitudinal axis of the sample. Application of a seating load prior to testing subsequent samples was effective in increasing the compressive strength and reducing scatter, but may not have completely eliminated all surface irregularities or premature failures. At low average strain rates (less than $7 \times 10^{-6} sec^{-1}$), the effects of irregularities or surface roughness at the trimmed ends would be minimized. Sufficient time is allowed at these strain rates for relaxation of stress concentrations due to plastic flow in the ice.

The reasons for other investigators not observing the transition in log-log plots of compressive strength versus axial strain rate are not clear from the present study, but may be related to test conditions and sample prepartion techniques. Baker (1978b) observed that values of the exponent m (slope of compressive strength versus axial strain rate lines on a log-log plot), in Equation (2-20), varied significantly with the type of loading platen used. Differences in trimming and preparing loading surfaces, as well as sand gradation, could produce significant differences in surface roughness and compressive strength.

Regardless of the mechanism responsible for the break in slope shown in Figure 6-6, it is apparent that the drop in compressive strength occurs at about the same strain rate that a transition in the deformation mode of the samples was observed (see Figure 5-4).

Samples tested at rates below 7 x 10^{-6} sec^{-1} deformed plastically with no visable cracking. It is also apparent from Figure 6-6, that the mechanism controlling the change in slope effects primarily the deformation process after yield occurs in the ice matrix, since no change in slope was observed for the initial yield stress.

Figure 6-6 also indicates that both the initial yield stress and the compressive strength increase with decreasing temperature. Log-log plots of initial yield stress and compressive strength versus degrees below freezing are presented in Figures 5-22 and 5-24, respectively. For temperatures of -6°C or more below freezing (assuming freezing occurs at 0°C), the data for either value seems to vary linearly with temperature on the log-log scales. Consequently, an expression of the form given by Equation (5-3) is most appropriate. Table 6-2 provides a comparison of the material constants C and s for the initial yield stress and compressive strength for several average strain rates. The temperature dependency of both stress values increased as the strain rate decreased, as shown by the increase in exponent s. However, the initial yield stress increased more rapidly with decreasing temperature than did the compressive strength. This implies that contribution of the ice matrix to the total compressive strength increased in proportion to the friction component of strength as the temperature decreased. The frictional resistance mobilized by the sand-ice material must decrease with decreasing temperature.

The temperature dependence of compressive strength was also investigated by Parameswaran (1980) for Ottawa sand. A linear variation of compressive strength was observed as a function of degrees Celcius below freezing on a log-log scale. Parameswaran (1980)

obtained an s value of 0.44 (Equation 5-5), which compares very well with the s values presented in Table 6-2.

A comparison of results obtained from constant strain rate compression tests and results obtained from constant stress compression tests (creep tests) at -6°C is shown in Figure 6-7. Included in Figure 6-7 is a comparison of the creep parameters σ_c and n determined from least squares linear regression analyses of the data (Equations 2-6 and 2-21). Both sets of data show linear relationships between stress and strain rates on the log-log plot. The two lines shown (in Figure 6-7) are nearly parallel, indicating that the creep parameters n obtained from the two methods are in close agreement. However, there is a significant difference in the proof stresses σ_c obtained from the two methods.

Odqvist (1966) presents a theoretical discussion of the relationship between constant stress creep tests and constant strain rate tests. If engineering strain is considered equal to the true strain (i.e. for small strains) and if primary creep may be neglected, the rupture stress (peak or failure stress) determined from constant strain rate tests may be related to the creep parameters determined from constant stress tests as shown below:

$$\dot{\varepsilon} = \left(\frac{\sigma_f}{\sigma_c}\right)^n \qquad (6\text{-}1)$$

where σ_f is the rupture stress, σ_c and n are the creep parameters defined for Equation (2-6), and $\dot{\varepsilon}$ is the applied strain rate. Comparison of Equations (6-1) and Equation (2-21) indicates that the constant σ_c should be equivalent for constant strain rate and constant stress creep tests.

This statement is consistent with the discussion presented in Chapter II. In addition, Hawkes and Mellor (1972) presented data indicating that no significant difference existed between the results of constant stress creep tests and constant strain rate strength tests for ductile materials such as ice at low strain rates. The compressive strength data was obtained from constant strain rate tests on polycrystalline ice at -7°C and at strain rates between $10^{-6}sec^{-1}$ and $10^{-2}sec^{-1}$. Constant stress creep tests were conducted at stresses producing secondary creep rates between $10^{-11}sec^{-1}$ and $10^{-6}sec^{-1}$. On a log-log plot of stress versus strain rate, Hawkes and Mellor (1972) observed a smooth transition from creep data to unconfined compressive strength data. This supports the relationship given by Odqvist (1966) between constant stress and constant strain rate tests.

As shown in 5-1 and 5-2, the applied strain rate was not constant over the duration of a test. There was a noted increase in the strain rate after the initial yield in the sample and the test machine did not achieve the nominal strain rate until after the peak stress was reached. As a result, the average strain rate to failure was considered more representative of the test conditions and was selected for analysis purposes. However, the effects of the strain rate varying during a test can not be fully evaluated since suitable equipment was not available to conduct true constant (engineering) strain rate tests. This variation in strain rate may account, at least in part, for the difference in proof stress (σ_c) values determined from the constant stress and constant strain rate tests.

Surface irregularities at the trimmed sample ends may also

contribute to the observed difference. For constant strain rate tests (at average strain rates below 7 x 10^{-5}sec^{-1}), the load was applied to the sample at a relatively slow rate. Plastic flow in the ice matrix had time to occur as the strain progressed, relaxing stress concentrations due to surface irregularities. In constant stress creep tests, the load was applied very rapidly to the sample (less than 30 seconds), possibly inducing high stress concentrations and cracking or yielding in the vicinity of the trimmed end of the samples. A small seating load of approximately 100 psi was applied to the sample for approximately 12 hours prior to testing. The creep strains observed as a result of the seating stress were less than 0.2 percent. Since this strain corresponds to a sample deflection of only 0.004 inches (less than the maximum particle diameter), the seating stress should be considered ineffective in reducing surface irregularities. The high loading rate applied to the samples, coupled with resulting stress concentrations, could produce crack formation in the samples and increase the secondary creep strain rate. The net effect would be a decrease in the value of σ_c and the downward shift of the plot shown in Figure 6-7.

A comparison of total strains at failure for constant strain rate tests (strain at peak stress) and constant stress creep tests (strain at initiation of tertiary creep) is presented in Figure 6-8. For strain rates below approximately 10^{-5}sec^{-1}, the failure strains observed for constant strain rate tests were relatively constant at approximately 4.5 percent. The failure strain for constant stress creep tests was observed to increase with increasing secondary creep rate (or uniaxial stress). Values obtained from the two test methods differ by less than 2 percent at a strain rate of 10^{-5}sec^{-1} and appear to approach

the same value at strain rates below 10^{-6} sec^{-1}. Since the total strain at failure based on constant strain rate tests appears to always be less than or equal to the total strain at the beginning of tertiary creep, the strain at the peak stress in constant strain rate compression tests may be used to determine the creep strength of frozen Wedron sand (see Equation 2-10).

A series of volumetric strain creep curves (for Samples 3c, 5c, and 6c) are summarized in Figure 5-32. The increase in sample volume during creep indicates the influence of dilatancy and mobilization of interparticle friction. Volumetric strain for these samples is shown in Figure 6-9 as a function of axial strain. These plots are very similar to those obtained from constant strain rate tests (Figures 5-15 through 5-17), indicating that the volume change or dilatancy appears to be primarily a function of the axial strain. For the creep samples reaching rupture, a shear plane inclined at approximately 60 degrees to the horizontal was observed. This suggests, as for the constant strain rate tests, that the mobilized friction angle was approximately 30 degrees.

6.1.2 Mechanical Properties In Tension

The mechanical properties of frozen Wedron sand in tension were investigated using the indirect tensile or split cylinder tests. The applied vertical deformation rate was observed to control the mechanical behavior in tension. For deformation rates greater than 0.002 in/min the samples failed by splitting along the loaded diametrical axis. At deformation rates of 0.002 in/min or less only a local compression deformation adjacent to the steel loading strips was observed. The load increased to some maximum value and then decreased, but no tensile

cracking was observed. Since a biaxial state of stress existed in the sample, it appears that the samples failed in compression along the vertical loaded axis rather than in tension. The compressive stress at the center of the sample acting parallel to the loaded diameter is 3 times the tensile stress acting perpendicular to it. This would imply that the ratio of compressive strength to tensile strength was less than 3 (assuming failure occurred at the center of the sample) for deformation rates of 0.002 in/min or less.

At deformation rates above 0.002 in/min., the load versus vertical deformation plots remained nearly linear up to the fracture load (Figure 5-35). The linearity of the curves indicates a brittle deformation-fracture behavior with a nearly linear stress-strain relationship. Since the indirect tensile strength is based on the theory of elasticity (Hondros, 1959), assuming linear elastic isotropic materials, the results in Figure 5-35 would seem to infer at least partial compliance with the theoretical analysis. It was assumed that due to the presence of sand particles and since the direction of freezing was not explicitly controlled, the ice crystals were randomly oriented in the sand-ice material. Compaction of the sand prior to freezing was intended to produce a uniform density throughout the sample. Consequently, it was reasonable to assume that the samples were isotropic and homogeneous, thus, satisfying these aspects of the theoretical analysis. It is not certain that the stress-strain behavior was the same in tension and compression.

Plots of the indirect tensile strength computed from the elasticity solution as functions of vertical deformation rate and the computed tensile strain rate (log-log plot) are shown in Figures 5-36

and 5-43), respectively. As may be observed, the indirect tensile strength increased with increasing vertical deformation rate or tensile strain rate. Figure 6-10 presents a comparison of the indirect tensile strength of the frozen sand at -6°C with measured direct tensile strength of polycrystalline ice, as determined by Hawkes and Mellor (1972) from constant axial strain rate tests at -7°C. The indirect tensile strength of the frozen sand appears to be nearly equal to the tensile strength of the ice. Since the sand matrix is not cohesive when dry, the observed tensile strength may be attributed to the ice matrix. Consequently, the data shown in Figure 6-10 is consistent with the anticipated behavior of the frozen sand in tension.

While the split cylinder data presented in Figure 6-10 is very limited, the interpretation discussed above is supported by Figures 5-36 and 5-43. Additional split cylinder tests were conducted at -6°C in which the lateral deformation of the sample was not determined due to malfunctions in the lateral deformation transducer (LADT). These data are included in Figure 5-36 and the curve drawn through the data points is approximately parallel to those obtained at other temperatures. The least squares linear regression line fitted through the data points for -6°C in Figure 5-43 is also consistent with data obtained at other temperatures where problems with the LADT were not encountered.

The data presented in Figure 5-43 would imply a straight-line relationship (Equation 5-8) between the indirect tensile strength and strain rate on a log-log plot. Data shown in Figure 6-10 imply that the tensile strength of frozen sand is approximately equal to the

tensile strength of ice at the same strain rate. Since theoretically the creep parameters may be obtained from constant strain rate tests (Odqvist, 1966), Figure 6-10 suggests that the creep behavior of the frozen sand in tension is roughly that of the polycrystalline ice in tension.

A limited amount of direct tensile data for frozen silica sand is available in the literature for comparison. A comparison of test results obtained by different investigators is presented in Table 6-3. Offensend (1966) observed the tensile strength of frozen Manchester fine sand to be independent of the applied loading rate for the range of loading rates used (1 to 10 in/min). The results obtained from the split cylinder tests are somewhat lower than those obtained by Offensend, as seen in Table 6-3. It is probable that the indirect tensile data was obtained at significantly lower strain rates. Since the indirect tensile strength was observed to increase with increasing values of the computed strain rate, the difference in the two results would have been reduced had it been possible to conduct the split cylinder tests at higher loading rates.

A comparison of experimental results obtained from the split cylinder tests with direct tensile strength data obtained by Perkins and Ruedrich (1973) is shown in Figure 6-10. The direct tensile data give tensile strengths, over the same range of strain rates, that are twice as large as those obtained from the split cylinder tests. This would indicate that the split cylinder test may significantly under estimate the tensile strength of the frozen sand, as suggested by Hawkes and Mellor (1971) for material with low compression to tensile strength ratios. In addition, Haynes (1973) investigated the influence

of confining pressure on the direct tensile strength of polycrystalline ice. For a confining pressure equal to 3 times the tensile stress, the observed tensile strength was approximately 1/3 the value of the unconfined tensile strength at the same strain rate. Since a biaxial state of stress exists in the split cylinder test (with a tension: compression stress ratio of 3 at the center of the cylinder), this would also seem to explain the lower strengths obtained from the split cylinder tests.

The values of Young's modulus obtained from the split cylinder tests are compared with Young's modulus for polycrystalline ice from direct tensile tests (Hawkes and Mellor, 1972) in Figure 6-12. Over the same range in strain rates, Young's modulus for frozen Wedron sand (split cylinder tests) was considerably less than the values obtained for ice. If the tensile behavior is controlled by the ice matrix, one would have expected Young's modulus for ice and frozen sand to compare favorably. Perkins and Ruedrich (1973) estimated the initial tangent modulus, for high strain rate uniaxial tension tests, to range from approximately 2 to 3 x 10^5 psi. These values are also significantly below the values reported for ice, but agree more favorably with the values obtained from the split cylinder tests.

The computed tensile strains at failure are presented in Figure 5-42. These values were computed from the theory of elasticity using Young's modulus and Poisson's ratio obtained from the split cylinder test, as described in Chapter V. As determined from a least squares linear regression analysis, the tensile strain at failure appears to be independent of the applied strain rate (1.35 x $10^{-5}$$sec^{-1}$ to 2 x $10^{-4}$$sec^{-1}$). Perkins and Ruedrich (1973) observed the tensile

strains at peak stress for frozen silica sand in uniaxial tension to vary from 0.5 percent to 5.0 percent over a range of strain rates from $1.67 \times 10^{-6} sec^{-1}$ to $1.67 \times 10^{-3} sec^{-1}$. These values compare very well with the observed strain at the peak stress in uniaxial compression, but are much greater than the computed tensile strains at fracture obtained from the split cylinder tests on frozen Wedron sand. However, they compare much better with the failure strains observed in uniaxial constant strain rate tension tests conducted on polycrystalline ice over the same range of strain rates, as shown in Figure 6-13. Data reported by Offensend (1966) for Manchester fine sand indicates that the failure strain ranged from approximately 0.004 percent to 0.095 percent for tests conducted on briquette shaped samples at loading rates between 0.1 and 10 in/min. The data presented by Offensend (1966) limit interpretations as to the loading rate in terms of an applied tensile strain rate, but it appears that these low strain values at failure are associated with strain rates much higher than those considered in the present study.

6.2 Standardization and Evaluation Of Test Methods

Some consideration must be directed toward development and standardization of laboratory tests to investigate or determine the mechanical properties of frozen sand. Standardization of test procedures would permit more realistic comparisons of test results for frozen soils obtained by different investigators. This section considers several factors influencing test results and presents a brief evaluation of the test procedures used in this investigation.

6.2.1 Influence Of Machine Stiffness

There is little doubt that deformation history influences the development of yielding or cracking in the ice matrix and the strength properties of frozen sand. In laboratory testing, the deformation behavior is controlled by the test equipment. Consequently, an examination of the test systems influence on the experimental test results is desirable.

As shown in Figures 5-1 and 5-2, applied strain rate varied during the strain rate controlled uniaxial compression tests. The strain in the sample was determined by the cross-head displacement of the Wykeham-Farrance test machine. Prior to testing the cross-head displacement rate was observed to be constant and equal to the manufacturer's nominal rate. During testing the resistence or stiffness of the sample permitted development of the nominal strain rate only after the peak stress had been reached. There was also a marked increase in the observed strain rate immediately following the initial yield. The nominal strain rate and average strain rate to failure are presented for each sample tested in Table 5-2. The values for the average strain rate to failure are significantly less than those of the nominal strain rates.

This behavior may be attributed to stiffness of the test system. In turn, the test system stiffness is dependent on the rigidity of all system components and their connections. As the load increases, elastic strain energy is stored in the test system (i.e. the test frame, loading ram, load cells, etc.). Once the initial yield has been reached and the loading rate decreases, the rate at which energy is stored in the system is reduced and the corresponding increase in the strain rate was

observed, as shown in Figures 5-1 and 5-2. As the peak stress is achieved and the load begins to decrease, the stored energy in the test system is released. This release of strain energy results in an additional increase in the strain rate until the observed strain approaches the nominal value.

The influence of machine stiffness of test results was demonstrated in Figures 5-8 and 5-9. These figures present the compressive strength or peak stress observed in the unconfined compression tests as functions of the applied nominal strain rate and average strain rate to failure, respectively. Both plots indicate that at low strain rates the compressive strength increases linearly with increasing strain rate according to the power law:

$$\sigma_f = \sigma_c(\dot{\varepsilon})^m \qquad (6\text{-}2)$$

where σ_c is the stress intercept at a strain rate of 1 sec^{-1} and m is the slope of the line. Table 6-4 presents a comparison of the constants σ_c and m obtained using the nominal and average strain rates. Use of average strain rates results in higher values for the constants at each test temperature. This increase was also observed in other material properties such as the initial tangent modulus (given in Table 6-4). The maximum increase in the constant σ_c was computed to be 8.1 percent and m increased by a maximum of 3.8 percent when the average strain rate was used. These changes are not considered significant. They do indicate that the machine stiffness does influence the material constants. The total influence of the variation in strain rate could not be accessed since equipment capable of maintaining a constant strain was not available. Consequently, the effects of the machine stiffness can only be discussed qualitatively.

Any changes in test system components or specimen geometry should effect the systems stiffness, strain rate, and the material properties as discussed above. Any change in sample diameter or length would result in a change in the sample stiffness which would either increase or decrease the amount of strain energy in the test equipment depending on whether the stiffness increased or decreased. If there is no change in any of the components in the loading column or sample, then any test machine differing significantly in stiffness would influence the observed strain rate in the same fashion. A stiff machine would be more capable of achieving a constant strain rate during testing and result in higher strengths. For the same nominal strain rate, the average strain rate up to the peak stress would increase when using a stiffer test system. From the results in Figure 5-9, the increase in the average strain rate to failure would result in a high compressive strength.

6.2.2 Sample Size Effects

Standardization of test procedures should consider the influence of sample geometry on the mechanical properties of frozen soils. The above discussion indicates that sample stiffness may influence the response of the test frame and equipment during so called constant strain rate compression tests on cylinderical samples. Other investigators(Ladanyi and Arteau, 1978; Baker, 1978a; and Baker, 1978b) have observed from experimental results that end conditions and the length: diameter ratio of the sample influenced the creep behavior and compressive strength of frozen sand. The results of experimental data related to the effect of sample diameter (with length:diameter ratio of 2.0) on the stress-strain behavior of the frozen Wedron sand

in compression were summarized in Figures 5-26 through 5-28.

The uniaxial compressive strength (Figure 5-27a) and the axial strain at failure (Figure 5-27b) were observed to be essentially independent of the sample diameter over the range of sample diameters tested (1.13, 1.41, 1.94 and 2.40 inches) at a nominal strain rate of approximately $1.2 \times 10^{-4} sec^{-1}$. The initial yield strain was observed to increase by approximately 11 percent (when the 1.41 inch diameter samples were neglected) as determined from a least squares linear regression analysis. It was observed that the initial yield strain showed considerable data scatter for all sample sizes and ranged from approximately 0.22 percent to 0.50 percent for the 1.94 inch diameter samples. Initial yield strain values for the 1.13 and 2.40 inch diameter samples (Figures 5-26b) all fall within this range. Consequently, the linear regression analysis may be over-estimating the influence of sample diameter on the initial yield stress as a result of data scatter.

The initial yield stress was observed to be independent of sample diameter for samples 1.41, 1.94, and 2.40 inches in diameter. However, the 1.13 inch diameter samples reached the initial yield at stresses approximately 14 percent below the extension of the least squares line shown in Figure 5-26a. Since no decrease in compressive strength was observed for these samples, the data in Figure 5-26a implies that the initial yield occurs at an earlier stage in the deformation process when compared to larger sample sizes. The construction method used to determine the initial yield strain was not as well adapted to this sample size since the stress-strain curves were more nonlinear at stress levels below the initial yield point. In addition, the

stress-strain curves did not develop the well defined break in slope, which defined the initial yield point, but exhibited a more pronounced curvature up to the peak stress. It appears that the discrepancy in initial yield stress values may be due to the construction technique used to define the initial yield stress.

The initial tangent modulus (Figure 5-28) was observed to increase by approximately 31 percent over the range of sample diameters considered. This data would suggest that sample diameter significantly influences the initial slope of the stress-strain curve. An explanation for this apparent increase in E_i with increasing sample diameter can not be ascertained from the available data.

The effects of sample diameter on the indirect tensile strength was also investigated. Figure 5-47 presents the results of split cylinder tests conducted on samples 1.94, 2.40 and 4.00 inches in diameter. There was no observed effect on the indirect tensile strength due to the variation in sample diameter.

Consequently, the sample diameter did not effect test results for either the split cylinder test or the unconfined constant strain rate compression tests (with the possible exception of the initial tangent modulus) over the range of sample diameters considered. Some theoretical consideration of the minimum allowable sample diameter in terms of maximum particle size must be given. The speciman diameter should obviously be chosen to give a representative sample of the material. Hawkes and Mellor (1970) recommended, based on a theoretical analysis of the critically stressed volume, that the minimum linear dimension of the critical volume should be at least 10 times the maximum particle or grain size in the sample. This implies that the sample diameter in

uniaxial testing should be at least 20 times the maximum particle diameter. Extending this same reasoning to the split cylinder test, Mellor and Hawkes (1971)concluded that the minimum speciman diameter should also be on the order of 20 particle diameters. This would suggest that the minimum allowable sample diameter for the Wedron sand (maximum particle size of 0.023 in) would be on the order of 0.5 inches. Practical considerations would suggest larger samples comparable to field sampling equipment (1.5 to 3 nominal diameters) and for convenience in trimming and testing.

6.2.3 Evaluation of Test Methods

A brief discussion of the advantages and limitations of the split cylinder and constant strain rate tests is appropriate with respect to standardization. Several advantages and disadvantages of the two tests with respect to determination of strength and time dependent deformation properties have already been presented in previous sections and will not be repeated. However, several limitations should be discussed that have not been treated elsewhere.

The constant strain rate compression test has been shown in previous discussions to provide a reasonably good approximation of the creep parameters σ_c and m (or n = 1/m) for use in the third term of Equation (2-7), provided that the test results are not influenced by sample trimming techniques leading to premature failures in compression. It does in general provide a faster more convenient test method than uniaxial compression creep tests. The elastic and primary creep deformations are not considered in development of a theoretical relationship between the constant stress creep tests and the constant strain rate tests. Elastic strains, resulting from

constant stress conditions, maybe estimated using the initial tangent modulus obtained from the constant strain rate tests. However, consideration must be given to strain rate effects on the initial tangent modulus and field loading conditions when selecting a value for analysis. The plastic portion of the instantaneous strain, the second term in Equation 2-7, can not be determined from constant strain rate tests. Similarly, the material constants necessary to apply the primary creep expression, Equation (2-14), can not be obtained. If the service life of the structure is less than the duration of primary creep or if primary creep dominates the deformation process, constant stress creep tests are required. In order to use the results from constant strain rate tests, the assumption that the primary creep strain may be neglected, for time intervals greater than 24 hours, must be applied (Vyalov, 1959).

This investigation has also attempted to use the split cylinder, in conjunction with the theory of elasticity, to obtain the corresponding tensile strength and creep parameters in tension. The indirect tensile strength has been observed to compare reasonably well with the direct tensile strength of ice, but does not compare favorably with the very limited data available on frozen sand from other investigators. Based on a theoretical analysis using the Griffith criterion for brittle materials, Fairhurst (1964) indicates that the split cylinder test may significantly under estimate the tensile strength if the compression to tension strength ratio is less than 8. As observed in the present work, the compression:tension strength ratio is at most only 6. This mayin part explain the discrepancy between the observed results from the split-cylinder tests on Wedron sand and the results reported by others.

Interpretation of the results obtained from the split cylinder tests may be also complicated by the system behavior and the method of analysis. The tensile strain and tensile strain rate are both obtained based on the computed values of Poisson's ratio for each test (see Figure 5-40). In most cases, Poisson's ratio was observed to be less than zero. This would imply that in uniaxial tension tests the cross-sectional area of the sample would increase rather than decrease, as for other engineering materials.

Poisson's ratio was obtained from the expression given in Table 2-1, where DR is the ratio of the total vertical to horizontal deformation. The negative values of Poisson's ratio computed using this equation are the result of large DR ratios. These values may have resulted from several possiblities. Double cleft failures (Figure 2-14c) were observed for all samples exhibiting a tensile failure. Formation of the cleft wedges prior to tensile failure could have resulted in large vertical deformations and DR ratios. Compressive stresses acting parallel to the loaded axis of the sample would induce pressure melting. A reduction in the lateral expansion of the sample would result from the decrease in ice volume associated with phase change and a larger DR ratio would be observed. This phenomenon is probably not sufficient to explain the negative values of Poisson's ratio since the volume due to pressure melting would be small. Neither of these explanations could be verified during testing. The equipment used did not permit volume change measurements and visual observation of the sample was not possible since the test apparatus was submerged in the coolant tank during testing.

The split cylinder test method was found to be inappropriate

for determining strength parameters at low deformation rates (tensile failures were not observed). In addition, the negative values of Poisson's ratio raise questions concerning the validity of using the split cylinder test to determine tensile creep parameters and strength of frozen sand. It is not certain that the elastic theory presented in Chapter II is adequate to determine stress and strain distributions in the sample. Negative values of Poisson's ratio could also have resulted from anisotropy. The stress-strain behavior of the sand-ice material may not be the same in tension and compression. Significant differences may exist between the stress and strain distributions in the samples and those predicted by elastic theory for isotropic materials.

6.3 Material Property Selection

In order to use frozen sand structures as static effective elements for construction purposes, it is necessary to define the strength of the sand-ice material (tension and compression) and a constitutive equation governing the stress-strain-time behavior of the frozen sand. A constitutive equation governing the time dependent stress-strain behavior of uniaxial stress conditions was presented by Equation (2-7). The corresponding time dependent strength is given by Equation (2-10). Several authors (Odqvist, 1966; Ladanyi, 1972; and Klein and Jessberger, 1978) have proposed methods of analysis to extend these relationships to multiaxial states of stress based on the Von Mises plasticity rule, volume constancy, and the assumption that the stress-strain behavior in tension and compression are identical. Review of the experimental data obtained in this investigation with respect to such assumptions and selection of material

properties seem appropriate.

6.3.1 Material Properties For Design In Tension And Compression

The uniaxial unconfined compressive strength of frozen Wedron sand is compared with the indirect tensile strength obtained from the split cylinder test, as functions of strain rate, in Figure 6-14. For strain rates below $1.3 \times 10^{-5} sec^{-1}$, the indirect tensile data has been extrapolated for comparison with data obtained for the uniaxial compression tests below the observed break in slope. At strain rates less than about $7 \times 10^{-6} sec^{-1}$ and for temperatures less than -2°C, the measured compression strength was approximately 5 to 6 times the indirect tensile strength (based on extrapolated data). At -2°C the compressive:tensile strength ratio ranged from approximately 3 to 6 (also based on extrapolation) depending on the strain rate.

From the data contained in Figures 5-9 and 5-43, the frozen sand strength in both tension and compression appears to vary linearly with strain rate on a log-log plot (for low strain rates). Consequently, both may be related to the applied strain rate by a power law of the form given by Equation (2-20) or (2-21). Table 6-5 presents a comparison of the constants σ_c and m obtained from linear regression analyses of data for tensile and compressive strength. The substantial difference in σ_c proof stress values reflects the significant difference in tensile and compressive strength and to a lesser extent the difference in slope (m) of the lines. For the samples tested at -10 and -15°C, the m values (Table 6-5) obtained for the tensile strength are approximatley 25 percent less than those obtained for the compressive strength. In light of the

possible problems associated with computing the tensile strain rate (based on Poisson's ratio) for the split cylinder test, the difference in these values may be considered small. There is a much larger difference in the m values at -6°C. There were only three data points obtained for the split cylinder test at -6°C and the coefficient of correlation obtained from the least squares analysis of these data points is significantly less than for data at lower temperatures. It is assumed that additional data would have reduced this discrepancy.

Data obtained by other investigators for ice and frozen silt would seem to verify similar values in tension and compression for m at low strain rates. Hawkes and Mellor (1972) review available data for polycrystalline ice and suggest that for strain rates below about 10^{-6} sec^{-1}, there was no significant difference between creep rates in compression and tension (i.e. σ_c and m are the same for tension and compression). Data reported for frozen silt (Haynes, Karalius, and Kalafut, 1975) also indicates similar behavior in tension and compression. Tests conducted on dumbbell shaped specimens at constant machine speeds (cross-head displacement rates) indicated that at deformation rates below about 1.0 in/min the compressive and tensile strengths were equal.

It would appear reasonable to assume that the m values, from constant strain rate uniaxial compression tests may be used to describe the tensile behavior as well. At present it would also appear that the tensile strength of frozen sand is significantly less than the compressive strength. Since the indirect tensile strength obtained from the split cylinder tests appears to underestimate the direct tensile

strength, use of these values for design would be conservative. For strain rates below $10^{-5}sec^{-1}$, Figure 6-14 would suggest that the tensile strength is approximately 1/5 the compressive strength. If m is assumed to be the same for tension and compression, this would imply that the proof stress (σ_c, Equation (2-20)) in tensile is approximately 1/5 the value in compression.

A similar comparison of the initial tangent modulus from uniaxial constant strain rate compression tests with Young's modulus from the split cylinder tests is given in Figure 6-15. It appears that for temperatures below -2°C, the values of the elastic modulus correlate very well. At -2°C the frozen sand was close to the melting point, hence the lower value observed fro the split cylinder test may be attributed to pressure melting caused by the biaxial stress state (compression and temperature). If values for the elastic modulus from the split cylinder test are taken as the tensile modulus, then it would seem reasonable that the initial tangent modulus obtained from the constant strain rate uniaxial compression tests could be used to estimate the elastic modulus in tension. Since the initial tangent modulus is rate dependent, selection of a design value must be based on evaluation of loading or strain conditions associated with the engineering problem.

The effect of temperature on compressive and tensile strengths of the sand-ice material is shown in Figures 5-24 and 5-45. Both indirect tensile strength and uniaxial compressive strength may be related to temperature by a power law of the form given by Equations (5-6) and (5-9). For strain rates between $5 \times 10^{-5}sec^{-1}$ and $4 \times 10^{-4}sec^{-1}$ the average value of the exponent obtained from split

cylinder tests was 0.38. An average value for s of 0.47 was obtained from the uniaxial constant strain rate compression tests. Consequently, it would appear that the temperature dependency for the tensile and compressive strength may be considered approximately the same for design purposes and may be determined from constant strain rate compression tests.

Extension of the creep constitutive equation (Equation 2-7) for uniaxial stress to multiaxial stress conditions involves the assumption of constant volume (or Poisson's ratio equal to 0.5). Data presented in Figure 6-9 indicates that the volumetric strain may not be constant during steady state creep (secondary creep), but is a function of the axial strain. Similarly, Poisson's ratio, computed from Equation (5-4) and shown in Figure 5-33 as a function of time, may be replotted in terms of axial strain as shown in Figure 6-16. The data show that Poisson's ratio appears to be primarily dependent on the axial strain and is relatively independent of stress level. A least squares regression analysis indicates that an expression of the form given in Figure 6-16 may describe the relationship between Poisson's ratio and axial strain. Observed values of Poisson's ratio during creep were significantly greater than 0.5 for unconfined compression creep tests. The influence of confining pressure or multiaxial states of stress on Poisson's ratio was not investigated. It is suspected that confining pressure would substantially decrease the volumetric strain (volume increase) shown in Figure 6-9 and, consequently, the values of Poisson's ratio. Until additional data is available it appears that a value of 0.5 would be appropriate for creep deformations in multiaxial states of stress.

6.3.2 Failure Criterion

In structural applications, frozen soils may be subjected simultaneously to multiaxial stresses. For example, in frozen soil retaining structures much of the soil would be subject to compression or tension in two directions, in addition to shear stresses. By methods common to mechanics, such stress states may be resolved into principal stresses acting at right angles to each other. The strength properties of frozen sand are normally determined from simple tests such as unconfined compression tests, triaxial compression tests (with the intermediate and minor principal stresses equal) and the split cylinder tests (biaxial stress condition assumed). For triaxial or biaxial stress states, it would be desirable to predict the strength of the frozen soil, knowing only the unconfined uniaxial compressive strength.

The Mohr-Coulomb failure theory is commonly used to define failure conditions in unfrozen soils. The theory states that failure will occur along that plane for which the ratio of shear stress to normal stress reaches a critical value for a given state of stress. Mohr circles at failure based on uniaxial tension, uniaxial compression, and triaxial compression tests define a failure envelope for a given material.

Ladanyi (1972) indicated that a series of envelopes corresponding to different failure times may be representative of frozen sand (see Figure 6-17). This time equals the time required to reach peak stress in constant strain rate tests or the time to reach the onset of tertiary creep in a constant stress creep test. Ladanyi (1972) suggested that since the envelopes usually seem to have a parabolic

shape, they could be described by an equation of the form presented by Fairhust (1964) for rocks:

$$\tau = [(s-1)/r]\ \sigma_f\ [1 + r(\sigma/\sigma_f)]^{1/2} \qquad (6\text{-}3)$$

where r is the ratio of uniaxial compressive creep strength to uniaxial tensile creep strength, both of which are time and temperature dependent, and

$$s = (r + 1)^{1/2} \qquad (6\text{-}4)$$

Equation (2-28) suggests that for long time intervals the uniaxial compressive creep strength may be written as:

$$\sigma_f(t,\theta) = \sigma^c_{co}(\dot{\varepsilon}_f/\varepsilon_c)^{1/n}\ f(\theta) \qquad (6\text{-}5)$$

where σ^c_{co} is the compression creep proof stress extrapolated to 0°C and $f(\theta)$ is a temperature correction factor similar to Equation (2-25).

From the data for Wedron sand, it seems reasonable to express the time dependent tensile stress from split cylinder tests in the same form:

$$\sigma_t(t,\theta) = \sigma^t_{co}(\dot{\varepsilon}_f/\varepsilon_c)^{1/n}\ f(\theta) \qquad (6\text{-}6)$$

where σ^t_{co} denotes the proof stress obtained from tensile data extrapolated to 0°C and $f(\theta)$ is also a temperature correction factor similar to Equation (2-25).

If the value of m (m = 1/n) is the same for tension and compression and the same temperature-strength relationship applies, r will remain constant with time and temperature:

$$r = \frac{\sigma_f(t,\theta)}{\sigma_t(t,\theta)} = \frac{\sigma^c_{co}(\dot{\varepsilon}_f/\varepsilon_c)^m\ f(\theta)}{\sigma^t_{co}(\dot{\varepsilon}_f/\varepsilon_c)^m\ f(\theta)} = \frac{\sigma^c_{co}}{\sigma^t_{co}} = \text{a constant} \qquad (6\text{-}7)$$

Equation (6-3) may now be rewritten as:

$$\tau = \frac{(s-1)}{r} \sigma_f(t,\theta)\left[1 + r\left(\frac{\sigma}{\sigma_f(t,\theta)}\right)\right]^{1/2} \qquad (6\text{-}8)$$

The data presented in Figure 6-15 would suggest a value of r of approximately 1/5 for frozen Wedron sand.

6.4 Simplified Analysis

Ground freezing projects which involve frozen sand as a structural material include many diverse open excavations. One special application related to natural gas pipeline construction in discontinuous permafrost regions is illustrated in Figure 6-18. Operating temperatures for the natural gas pipeline will be in the range of -8 to -12°C. thus, granular bedding soils adjacent to the pipeline will remain continuously frozen. In areas where ground water and soil conditions are favorable, this procedure could result in the formation of ice lenses in the underlying unfrozen soil. Frozen sand backfill, simulating an unreinforced concrete beam, could provide some support for the pipeline in areas subject to differential frost heave.

A simple analogy to this application of frozen sand as a structural element considers the simply supported beam shown in Figure 6-19. To illustrate basic design concepts pertaining to time dependent strength and deflection behavior, an analysis of the beam response to the applied load P is presented in the following section. Beam dimensions and loading conditions have been selected to permit laboratory verification and use of analytical solutions for stress distribution and deflection.

6.4.1 Stress Distribution

The time dependent response of a beam subjected to pure bending, outlined in Section 2.5.2, was based on the assumption that the time dependent material behavior was the same in tension and compression. The frozen sand tensile strength (from the split cylinder tests) was approximately 1/5 the compressive strength from constant strain rate uniaxial compression tests. The parameter n in Equation (2-6) appears to be approximately the same for tension and compression. Therefore, the proof stress for tension (σ_c^t) should be approximately 1/5 the proof stress for compression (σ_c^c) determined from the constant strain rate uniaxial compression tests. Different stress-strain-time relationships for tension and compression requires that the stress distribution due to bending, given by Equation (2-5), be re-examined since the neutral axis will no longer be located at the centroid of the cross-section.

Applying the elastic analog described in Section 2.5.2, the strain rate is made to correspond to the elastic strain as given below:

$$z > 0: \quad \varepsilon = \dot{\varepsilon}_c \left| \frac{\sigma}{\sigma_c^c} \right|^n \operatorname{sgn}(\sigma)$$

$$z < 0: \quad \varepsilon = \dot{\varepsilon}_c \left| \frac{\sigma}{\sigma_c^t} \right|^n \operatorname{sgn}(\sigma) \qquad (6\text{-}8)$$

$$z = 0: \quad \varepsilon = 0$$

where z is the distance from the neutral axis (shown in Figure 6-20) and $\varepsilon = -z/\rho$ (ρ is the radius of curvature of the beam). The beam of the neutral axis may then be determined from equilibrium requirements:

$$\Sigma F = 0: \quad \int \sigma dA = 0 =$$

$$\int_0^{-z_1} \sigma_c^t \left| \frac{z}{\rho \dot{\varepsilon}_c} \right|^{1/n} \text{sgn}(z)\,bdy + \int_0^{h-z_1} \sigma_c^c \left| \frac{z}{\rho \dot{\varepsilon}_c} \right|^{1/n} \text{sgn}(z)\,bdy = 0 \qquad (6\text{-}9)$$

where z_1 is defined in Figure 6-20a and expressions for σ were obtained from Equations (6-8) in terms of the radius of curvature of the beam. Assuming the strain distribution shown in Figure 6-20a, ρ may be expressed as:

$$\rho = \frac{z_1}{\varepsilon_1} \qquad (6\text{-}11)$$

where ε_1 is the strain in the bottom fibers of the beam at some time t_1.

Substituting Equation (6-10) into Equation (6-9) and integrating yields:

$$\left(\frac{1}{z_1 \dot{\varepsilon}_c} \right) \frac{b}{1+n} \left[-\sigma_c^t \left| z_1 \right|^{1+1/n} + \sigma_c^c \left| h - z_1 \right|^{1+1/n} \right] = 0 \qquad (6\text{-}12)$$

If $\sigma_c^c = 5\sigma_c^t$, Equation 6-11 may be solved for z_1 in terms of h:

$$z_1 = \frac{h}{1 + (0.2)^{1/(1 + 1/n)}} \qquad (6\text{-}12)$$

For the beam shown in Figure 6-19, (h = 2.5in. and n = 11) z_1 may be determined to be 2.035 in.. Since Equation (6-12) is independent of the strain, the location of the neutral axis is independent of time for stationary creep conditions.

The spatial stress distribution may now be determined by considering equilibrium at a given cross-section in terms of the applied bending moment:

$$\Sigma M = 0: \quad M = \int z\sigma dA \qquad (6\text{-}13)$$

Substituting Equations 6-8 for σ and integrating yields:

$$z > 0: \quad \sigma = \frac{-M\,|z|^{1/n}}{\frac{b}{2+1/n}\left[\frac{\sigma_c^t}{\sigma_c^c}(z_1)^{2+1/n} + (h-z_1)^{2+1/n}\right]} \tag{6-14}$$

$$z < 0: \quad \sigma = \frac{M\,|z|^{1/n}}{\frac{b}{2+1/n}\left[(z_1)^{2+1/n} + \frac{\sigma_c^c}{\sigma_c^t}(h-z_1)^{2+1/n}\right]}$$

for the rectangular cross-section shown in Figure 6-20a. The maximum stresses in the beam due to bending are located in the outer fibers of the beam at x-coordinate where the bending moment is a maximum. For the simply supported beam shown in Figure 6-19, the maximum bending moment occurs at mid-span and equals $M_{max} = (PL/4)$. Figure 2-20b presents a plot of normal stress due to bending versus distance from the neutral axis in terms of the applied load P.

6.4.2 Time Dependent Deformation

The magnitude of the applied load may be determined so as to limit the maximum strain in the beam or the maximum deflection to an allowable value over the service life of the structure. Consider the beam shown in Figure 6-19 at a temperature of -20°C. Assume that the load is applied to the beam pseudo-instantaneously and that the dynamic response may be ignored. Assume also that a condition of stationary creep is developed in the beam within a short period of time and that plane sections through the beam remain plane during creep. If, as suggested by Vyalov (1959), the creep strain tends to dominate the deformation process, the total strain at any point in the beam

may be estimated from the stress distribution using Equation (2-6) as a function of time. The time dependent strength of the frozen sand may then be expressed in terms of a failure strain (or allowable strain) and a service life for the beam. With these conditions in mind; the allowable load P for a designated service life of the structure may be computed.

As shown in Figure 2-20a, the maximum strain in the beam occurs at $z = -z_1$. If the strain at failure in tension equals the failure strain in compression at the same applied strain rate, as suggested by Perkins and Ruedrich (1973), the allowable stress based on the failure strain and service life may be computed from Equations 6-8. The stress in the frozen sand beam at $z = -z_1$ based on the appropriate expression from Equations (6-14) becomes:

$$\sigma(z = -z_1) = 1.128P \tag{6-15}$$

If the failure strain (ε_f) in tension is taken as approximately 0.045 (Figure 5-10) and the service life (t_f) as 7 days (convenient for laboratory testing), the tensile stress required to reach the failure strain at t_f may be computed as:

$$\sigma = \frac{1}{5}\sigma_{co}^{c}\left(\frac{\varepsilon_f}{t_f \dot{\varepsilon}_c}\right)^{1/n} f(\theta) \tag{6-16}$$

$$= \frac{1}{5}(516)\left(\frac{0.045}{10^{-6}(6.05 \times 10^{5})}\right)^{0.091}(1 + 20)^{0.053} = 409 \text{ psi}$$

where σ_{co} is the compression proof stress extrapolated to 0°C and $f(\theta)$ and w are determined from a log-log plot (Figure 6-21) of σ_c^c versus the normalized temperature $(1 + \theta/\theta_c)$. The allowable load P

may be determined from Equations (6-15) and (6-16):

$$P = \frac{409}{1.128} = 363 \text{ lbs.} \tag{6-17}$$

The creep deflection at t_f may be obtained in a similar fashion to that presented by Odqvist (1966). The deflection rate $\dot{w}$ may be related to the radius of curvature and the strain rate as:

$$z > 0: \quad \frac{d^2\dot{w}}{dx^2} = \dot{w}'' = \frac{-\dot{\varepsilon}}{z} = \frac{\dot{\varepsilon}_c}{z}\left(\frac{\sigma}{\sigma_c^c}\right)^n \text{sgn}(\sigma)$$

$$z < 0: \quad \frac{d^2\dot{w}}{dx^2} = \dot{w}'' = \frac{-\dot{\varepsilon}}{z} = \frac{\dot{\varepsilon}_c}{z}\left(\frac{\sigma}{\sigma_c^t}\right)^n \text{sgn}(\sigma) \tag{6-18}$$

where $\dot{w}$ is the deflection rate. Solving for σ in terms of $\dot{w}''$ and substituting into Equation (6-13) one obtains:

$$M = \int(\sigma) z dA$$

$$= -\left(\frac{\dot{w}''}{\dot{\varepsilon}_c}\right)^{1/n} \sigma_c^c \left[\frac{b}{5(2 + 1/n)}(z_1)^{2+1/n} + \frac{b}{2 + 1/n}(h - z_1)^{2+1/n}\right] \tag{6-19}$$

$$= -\left(\frac{\dot{w}''}{\dot{\varepsilon}_c}\right)^{1/n} \sigma_c^c \, In$$

Solving for $\dot{w}''$ and integrating, the deflection rate at mid-span may be computed as:

$$\dot{w} = \dot{\varepsilon}_c \left(\frac{PL}{4\sigma_c^c \, In}\right)^n \frac{L^2}{4(n + 2)} \tag{6-20}$$

$$= 10^{-6}\left(\frac{364(22)}{4(2591)(1.038)}\right)^{11} \frac{(22)^2}{4(11 + 2)}$$

$$= 3.62 \times 10^{-7} \text{ in/sec}$$

At the anticipated service life of 7 days (6.05×10^5 sec) the deflection at mid-span is 0.219 inches. This deflection is only 0.99 percent of the length of the beam. Popov (1968) indicates that for elastic deflections less than approximately 1/10 of the beam length, the assumption of small deformations may be considered valid. If this criteria may be applied to the creep deflections, then the small deflection estimated would be consistant with the assumption of small deformations used in the development of creep equations (Odqvist, 1966).

The elastic and plastic deformations described by the first two terms of Equation (2-7) may also be included in an analysis similar to the one presented above. However, to avoid complexity in integrating Equation (6-19), these terms have been neglected in the example presented. The example does serve to demonstrate that small beams composed of frozen sand should support significant loads for limited periods of time and that the sand-ice material will resist bending moments (in agreement with field observations). The tensile strength of frozen sand may, therefore, be considered in the design of temporary engineering structures of sand-ice material.

Table 6-1: Comparison of Material Constants σ_c and m for Several Frozen Silica Sands

Material	Temp. (°C)	Strain Rate (sec^{-1})	*Material Constants σ_c(psi)	m	Sources
Saturated Wedron Sand	-2	6.2×10^{-6} to 8.7×10^{-7}	53579	0.305	Present Study
	-6	6.1×10^{-6} to 4.9×10^{-7}	6934	0.115	
	-10	8.8×10^{-6} to 4.8×10^{-7}	6067	0.085	
	-15	8.5×10^{-6} to 4.8×10^{-7}	6761	0.082	
Saturated 20-30 Ottawa Sand	-3.9	1.7×10^{-5} to 1.7×10^{-2}	2408	0.100	Sayles (1974)
Saturated 20-30 Ottawa Sand	-3	1.67×10^{-4} to 2.0×10^{-2}	---	0.105	Sayles and Epanchin (1966)
	-6.5	1.67×10^{-4} to 2.0×10^{-2}	---	0.092	
	-10	1.67×10^{-4} to 2.0×10^{-2}	---	0.094	
Saturated Fine Ottawa Sand	-5.5	2.0×10^{-3} to 2.0×10^{-7}	4200	0.090	Baker (1978b)
Saturated Fine Ottawa Sand	-2	1.0×10^{-5} to 1.0×10^{-7}	16502	0.190	Parameswaran (1980)
	-6	1.0×10^{-5} to 1.0×10^{-7}	4098	0.073	
	-10	1.0×10^{-5} to 1.0×10^{-7}	5143	0.071	
	-15	1.0×10^{-5} to 1.0×10^{-7}	6793	0.079	

*Material Constants for Equation 5-2: $\sigma_f = \sigma_c(\dot{\varepsilon})^m$ where σ_f is in psi and $\dot{\varepsilon}$ in sec^{-1}.

Table 6-2: Comparison of Temperature Effects on Initial Yield Stress with Effects on Compressive Strength

Strain Rate (sec^{-1})	Material Constants			
	Initial Yield Stress		Compressive Strength	
	c	s	c	s
1×10^{-3}	792	0.540	782	0.438
1×10^{-4}	430	0.581	782	0.438
1×10^{-5}	209	0.672	782	0.438
1×10^{-6}	102	0.763	608	0.468
1×10^{-7}	54	0.828	399	0.547

Constants for Equations 5-5 and 5-6: σ_f or $\sigma_y = C(\theta)^s$ where σ is in psi and θ is the number of degrees below freezing in °C.

Constants determined from Least Squares Linear Regression Analysis.

Table 6-3: Comparison of Tensile Strength of Frozen Silica Sands

Material and Test Method	Temp. (°C)	Deformation or Strain Rate	Tensile Strength (psi)	Source
Wedron Sand; Split Cylinder Tests	-2	*1.5×10^{-5} to 2×10^{-4} sec^{-1}	226 to 237	Present Study
	-6	*1.5×10^{-5} to 2×10^{-4} sec^{-1}	321 to 398	
	-10	*1.5×10^{-5} to 2×10^{-4} sec^{-1}	363 to 474	
	-15	*1.5×10^{-5} to 2×10^{-4} sec^{-1}	407 to 533	
Penn Sand; Constant Strain Rate Tests	-2.2	1.7×10^{-6} to 1.7×10^{-3} sec^{-1}	65 to 310**	Perkins and Ruedrich (1973)
	-6.6	1.7×10^{-6} to 1.7×10^{-3} sec^{-1}	280 to 820**	
	-13.3	1.7×10^{-6} to 1.7×10^{-3} sec^{-1}	540 to 920**	
Manchester Fine Sand; Constant Head Speed, Briquette Samples	-3.9	1 to 10 in/min	475	Offensend (1966)
	-9.4	1 to 10 in/min	550	
	-17.8	1 to 10 in/min	650	

*Strain rates computed from theory of elasticity.

**Data from curves presented in Reference: Perkins and Ruedrich, 1973; Mechanical Behavior of Synthetic Permafrost, Society of Petroleum Engineers Journal (Aug.).

Table 6-4: Influence of System Stiffness on Material Properties

Strain Rate	Temp. (°C)	Compressive Strength		Initial Tangent Modulus	
		σ_c	m	B ($\times 10^6$)	b
Nominal	-2	49545	0.303	2.483	0.230
	-6	6871	0.115	1.820	0.202
	-10	5702	0.082	1.422	0.139
	-15	6427	0.079	2.089	0.121
Average to Failure	-2	53579	0.305	2.741	0.235
	-6	6934	0.115	2.349	0.219
	-10	6067	0.085	1.795	0.156
	-15	6761	0.082	2.415	0.132

-Constants for Equations 5-2 and 5-3: $\sigma = \sigma_c(\dot{\varepsilon})^m$ where σ is in psi and $\dot{\varepsilon}$ is in sec^{-1}.

$E_i = B(\dot{\varepsilon})^b$ where E_i is in psi and $\dot{\varepsilon}$ is in sec^{-1}.

-Constants obtained from least squares linear regression analyses of data for 1.41 inch diameter samples.

Table 6-5: Comparison of Material Constants From Uniaxial Constant Strain Rate Compression Tests with Split Cylinder Tests

Test Type	Temp. (°C)	Strain Rate (sec^{-1})	Material Constants σ_c	Material Constants m	Coefficient of Correlation
Uniaxial Compression	-2	6.2×10^{-6} to 8.7×10^{-7}	53579	0.30	0.99
	-6	6.1×10^{-6} to 4.9×10^{-7}	6934	0.11	0.99
	-10	8.8×10^{-6} to 4.8×10^{-7}	6067	0.08	0.95
	-15	8.5×10^{-6} to 4.8×10^{-7}	6761	0.08	0.98
Indirect Tensile	-2	1.3×10^{-5} to 2.0×10^{-4}	316	0.03	0.95
	-6	1.3×10^{-5} to 2.0×10^{-4}	583	0.06	0.44
	-10	1.3×10^{-5} to 2.0×10^{-4}	726	0.06	0.86
	-15	1.3×10^{-5} to 2.0×10^{-4}	843	0.06	0.82

Equation relating strength and strain rate: $\sigma = \sigma_c(\dot{\varepsilon})^m$ where strength σ is in psi and strain rate $\dot{\varepsilon}$ is in sec^{-1}.

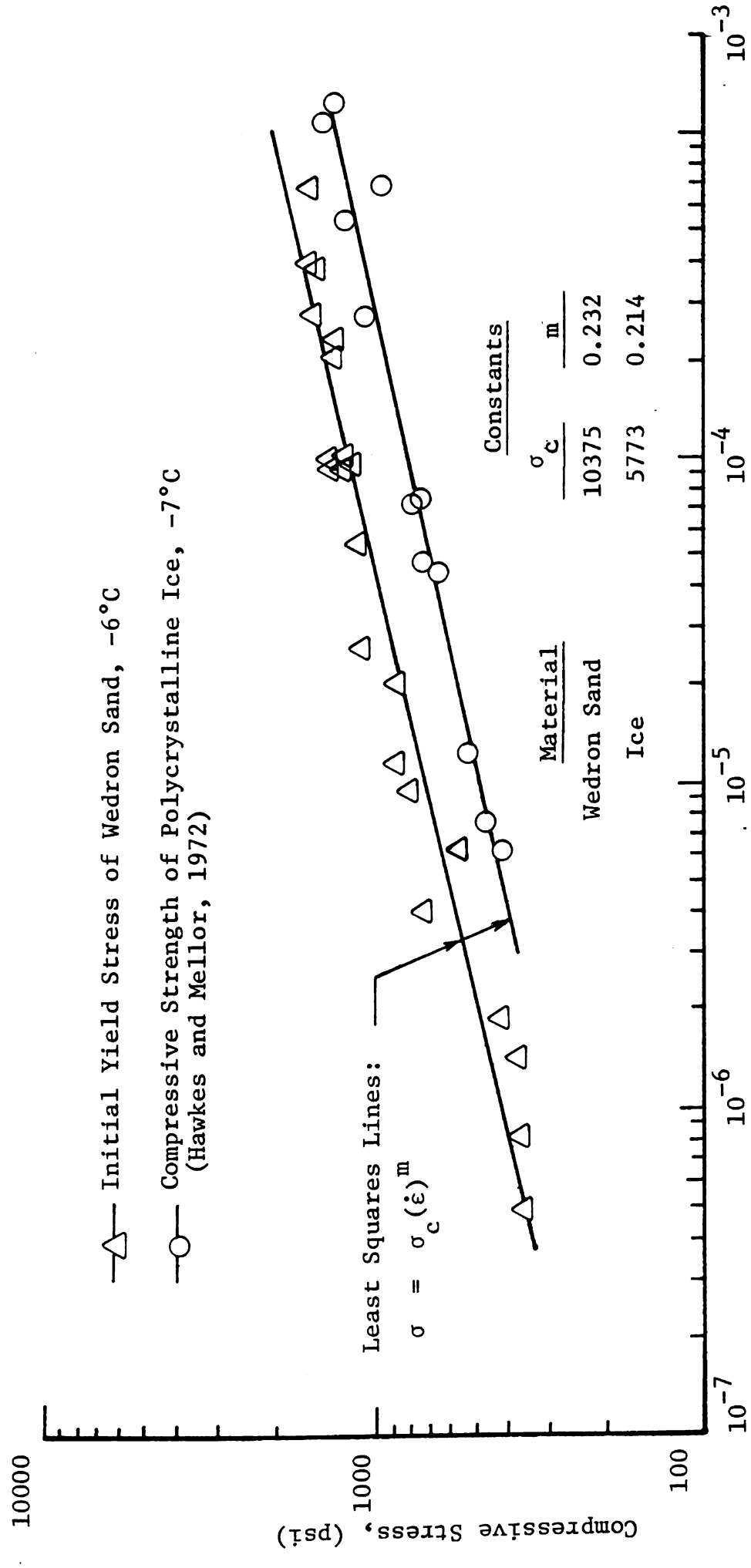

Figure 6-1: Comparison of Initial Yield Stress of Frozen Wedron Sand with Compressive Strength of Polycrystalline Ice.

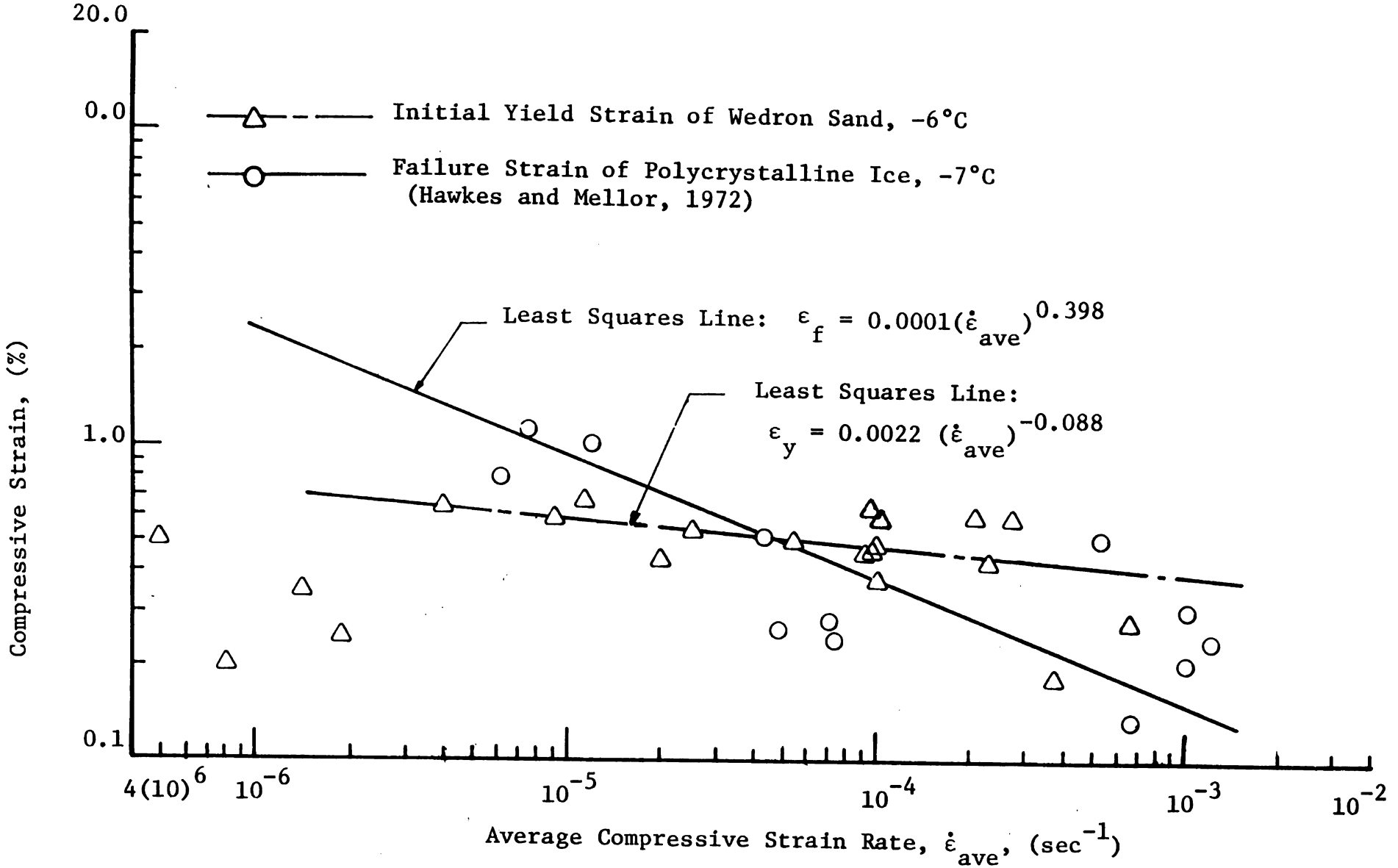
20.0
0.0
1.0
0.1
Initial Yield Strain of Wedron Sand, -6°C
Failure Strain of Polycrystalline Ice, -7°C
(Hawkes and Mellor, 1972)
Least Squares Line: $\varepsilon_f = 0.0001(\dot{\varepsilon}_{ave})^{0.398}$
Least Squares Line:
$\varepsilon_y = 0.0022\ (\dot{\varepsilon}_{ave})^{-0.088}$
Compressive Strain, (%)
$4(10)^6$
10^{-6}
10^{-5}
10^{-4}
10^{-3}
10^{-2}
Average Compressive Strain Rate, $\dot{\varepsilon}_{ave}$, (sec^{-1})

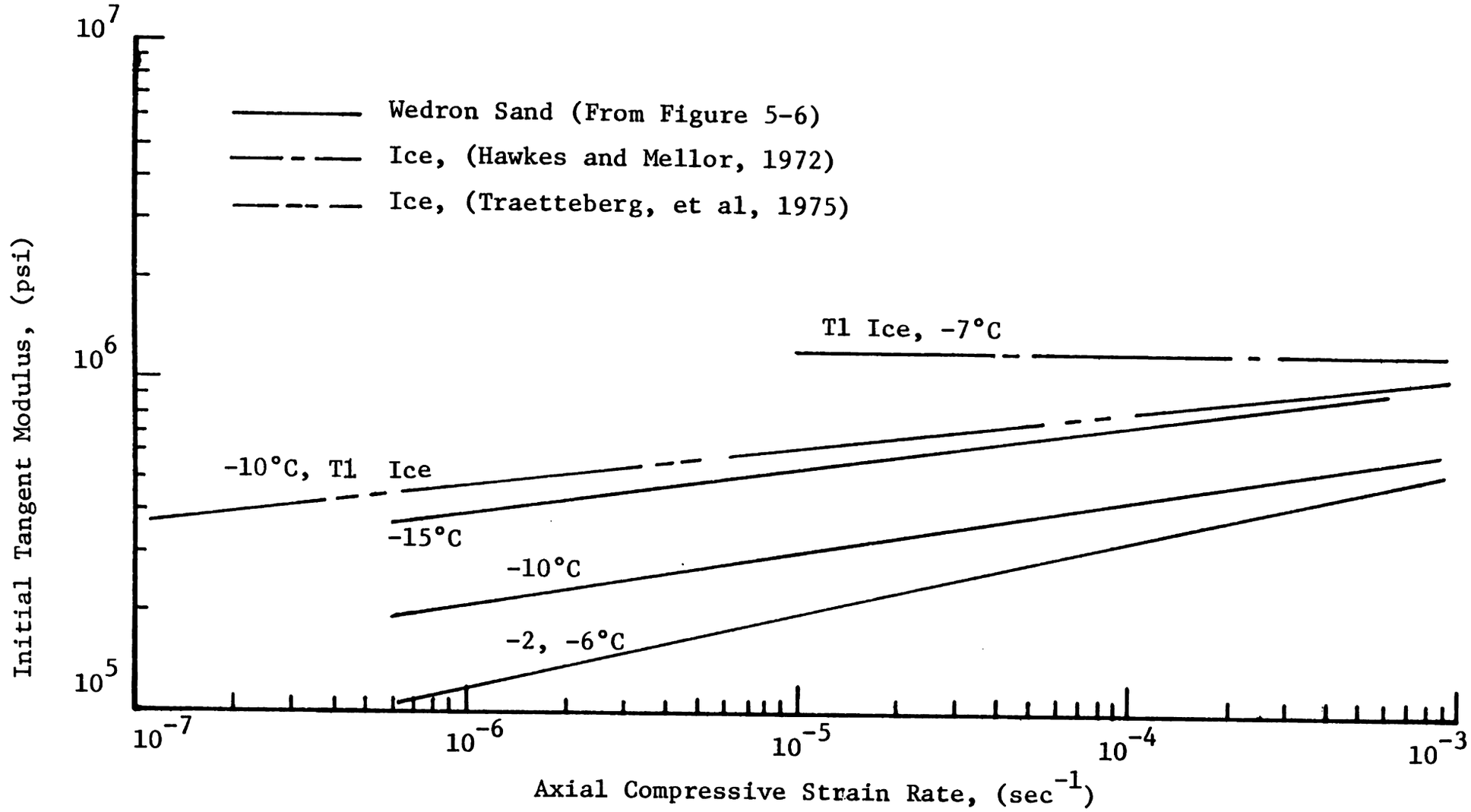

Figure 6-3: Comparison of Initial Tangent Modulus Values; Frozen Wedron Sand versus Polycrystalline Ice.

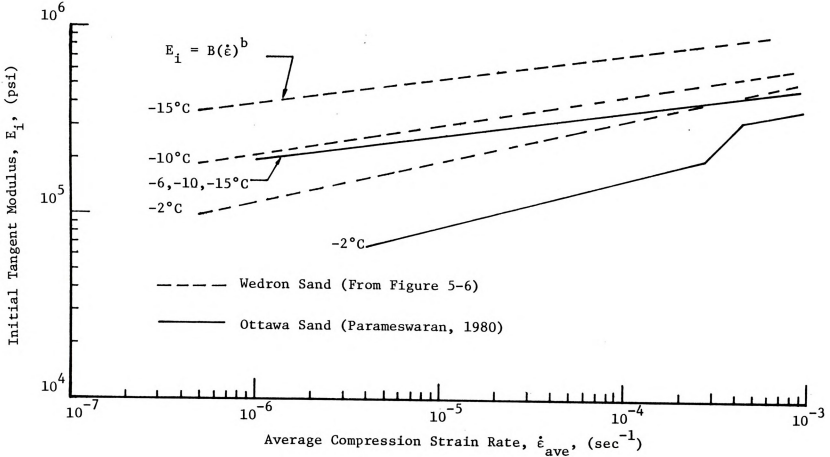
10^6
10^5
10^4
$E_i = B(\dot{\varepsilon})^b$
-15°C
-10°C
-6,-10,-15°C
-2°C
-2°C
Wedron Sand (From Figure 5-6)
Ottawa Sand (Parameswaran, 1980)
Initial Tangent Modulus, E_i, (psi)
10^{-7}
10^{-6}
10^{-5}
10^{-4}
10^{-3}
Average Compression Strain Rate, $\dot{\varepsilon}_{ave}$, (sec^{-1})

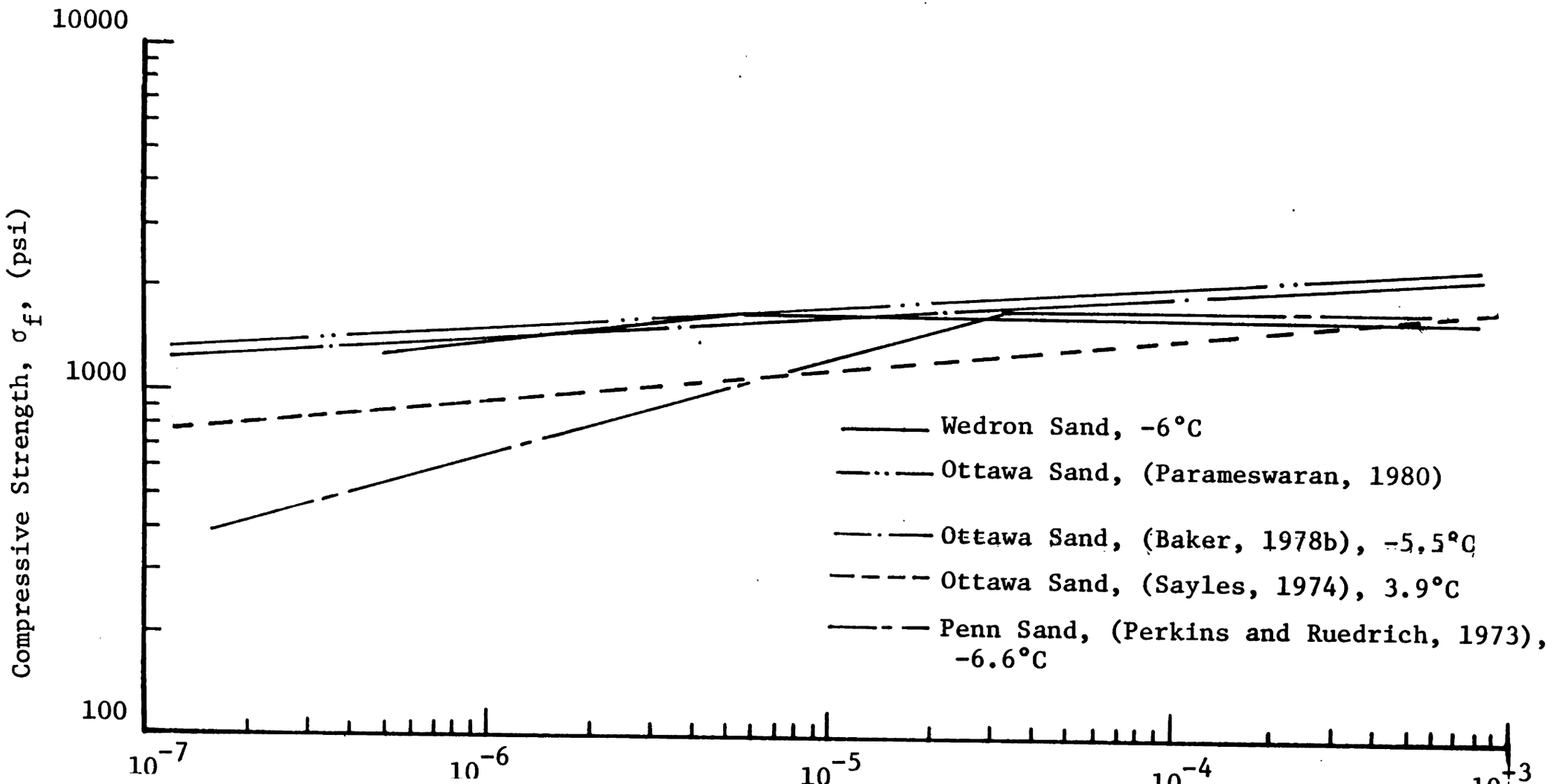
10000
1000
100
Compressive Strength, σ_f, (psi)
10^{-7}
10^{-6}
10^{-5}
10^{-4}
Wedron Sand, -6°C
Ottawa Sand, (Parameswaran, 1980)
Ottawa Sand, (Baker, 1978b), -5.5°C
Ottawa Sand, (Sayles, 1974), 3.9°C
Penn Sand, (Perkins and Ruedrich, 1973), -6.6°C

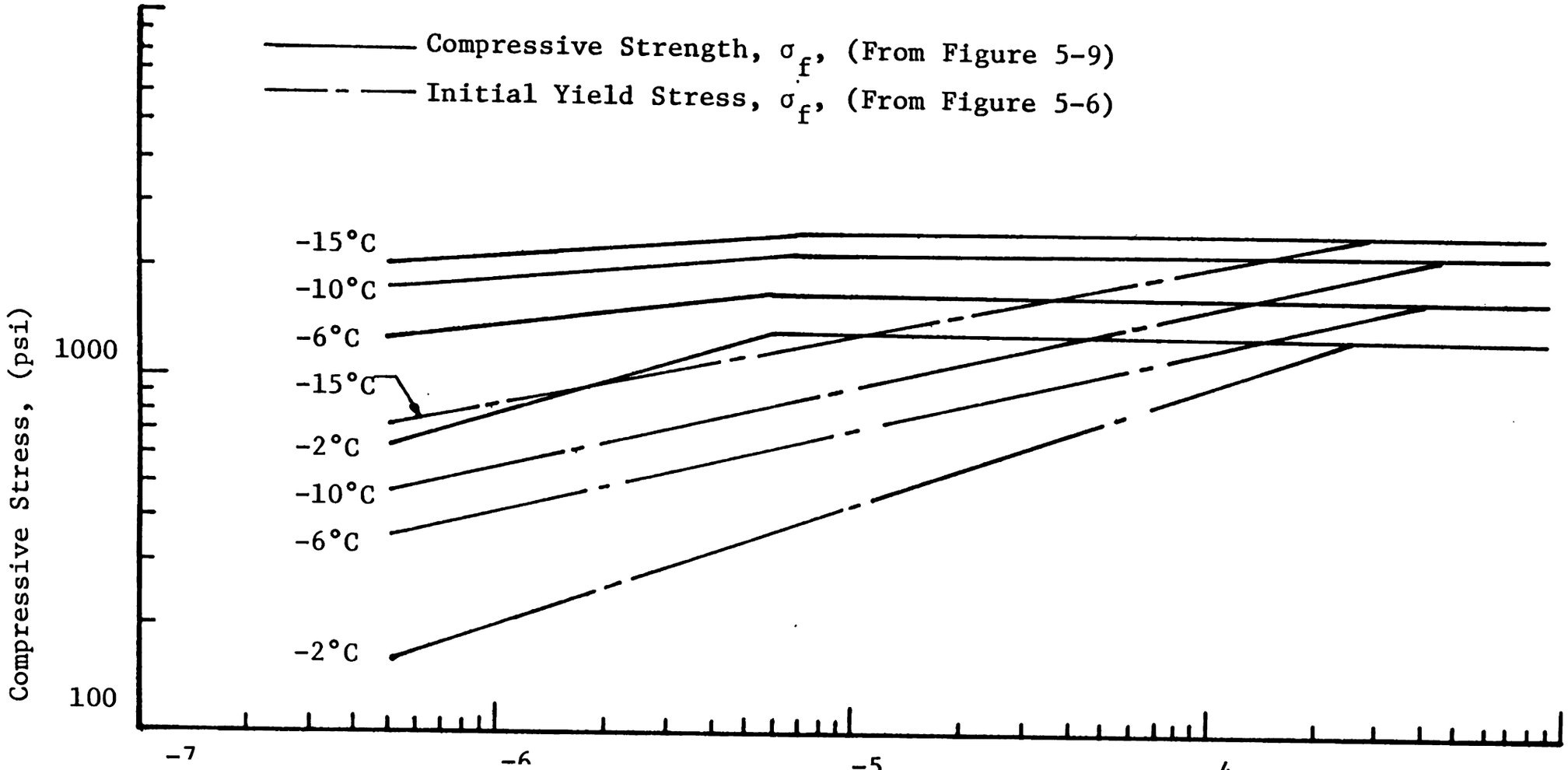
10000
1000
100
Compressive Stress, (psi)
Compressive Strength, σ_f, (From Figure 5-9)
Initial Yield Stress, σ_f, (From Figure 5-6)
-15°C
-10°C
-6°C
-15°C
-2°C
-10°C
-6°C
-2°C
-7
-6
-5

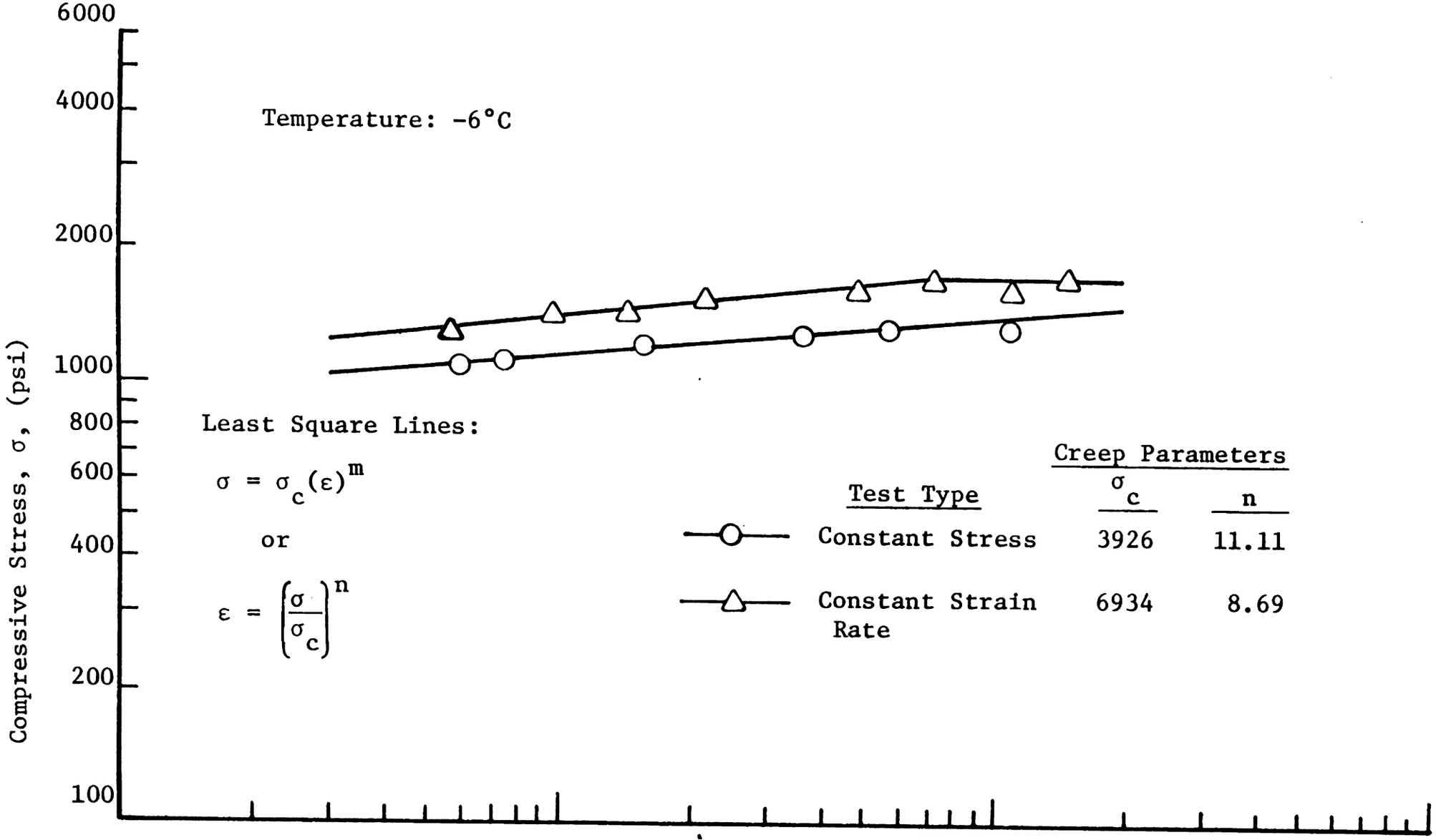
6000
4000
2000
1000
800
600
400
200
100
Compressive Stress, σ, (psi)
Temperature: -6°C
Least Square Lines:
σ = σc(ε)^m
or
ε = (σ/σc)^n
Test Type
Creep Parameters
σc
n
Constant Stress
3926
11.11
Constant Strain Rate
6934
8.69

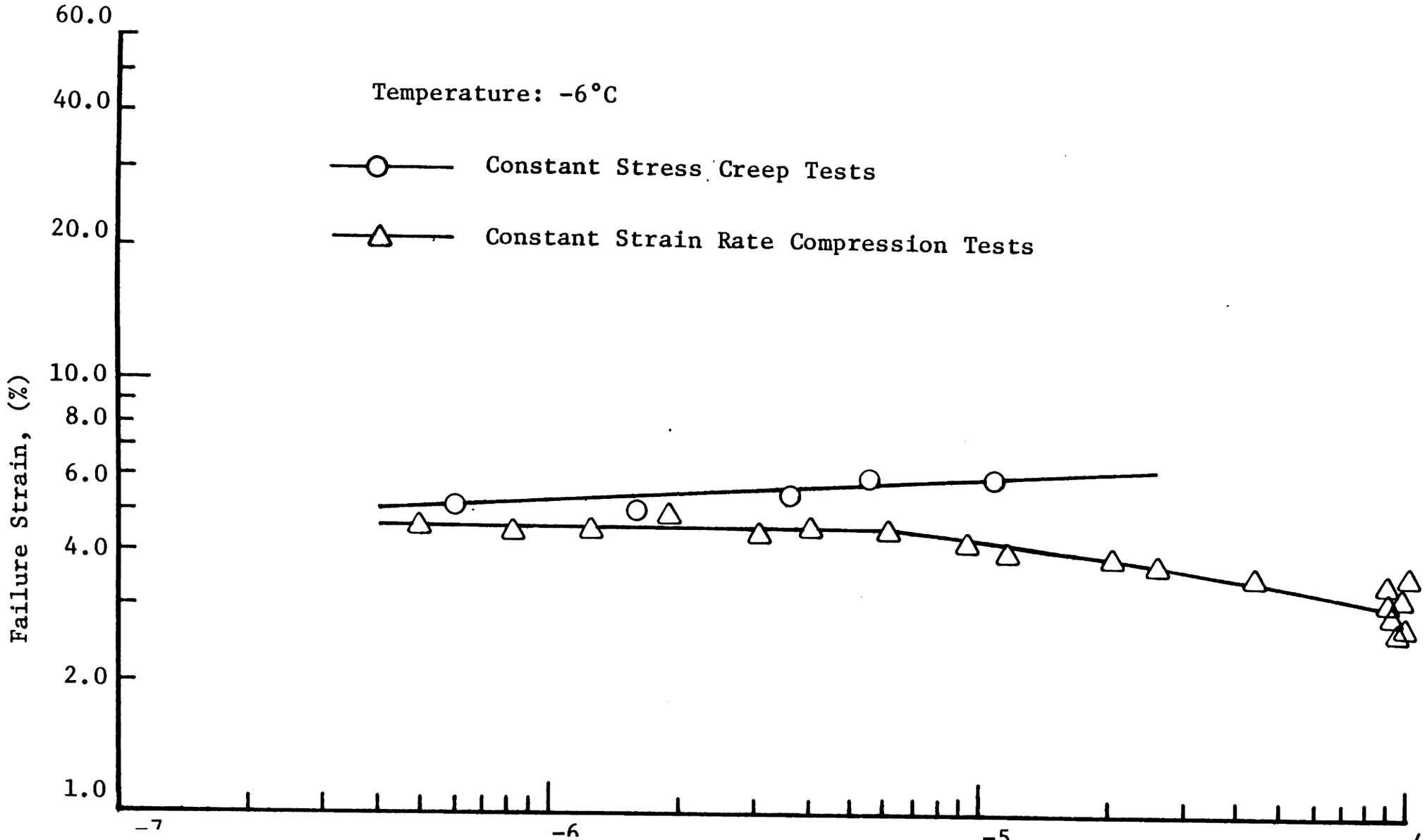
Temperature: -6°C
Constant Stress Creep Tests
Constant Strain Rate Compression Tests
Failure Strain, (%)
60.0
40.0
20.0
10.0
8.0
6.0
4.0
2.0
1.0
-7
-6
-5

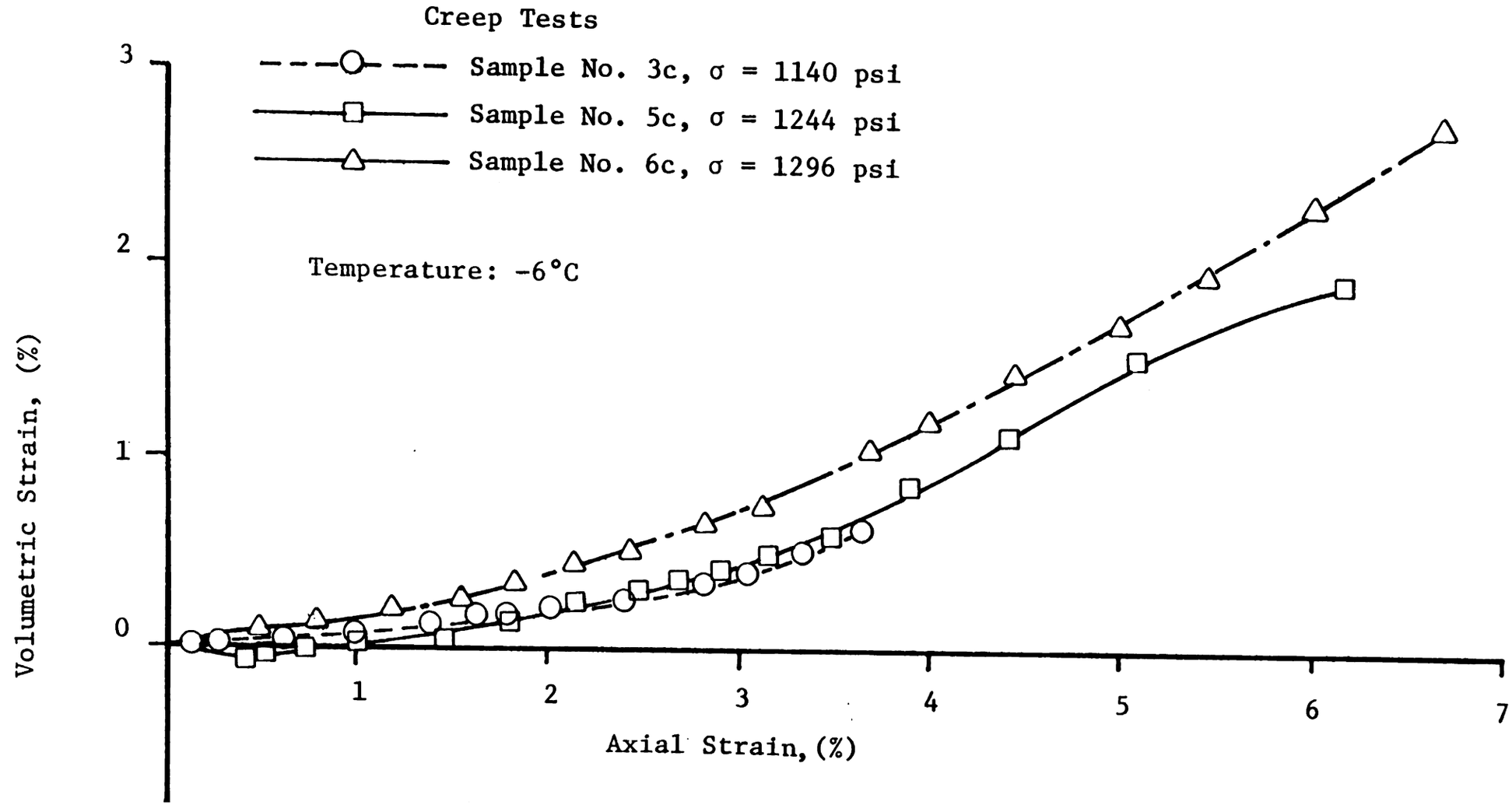
Creep Tests
Sample No. 3c, σ = 1140 psi
Sample No. 5c, σ = 1244 psi
Sample No. 6c, σ = 1296 psi
Temperature: -6°C
Volumetric Strain, (%)
Axial Strain, (%)
0
1
2
3
1
2
3
4
5
6
7

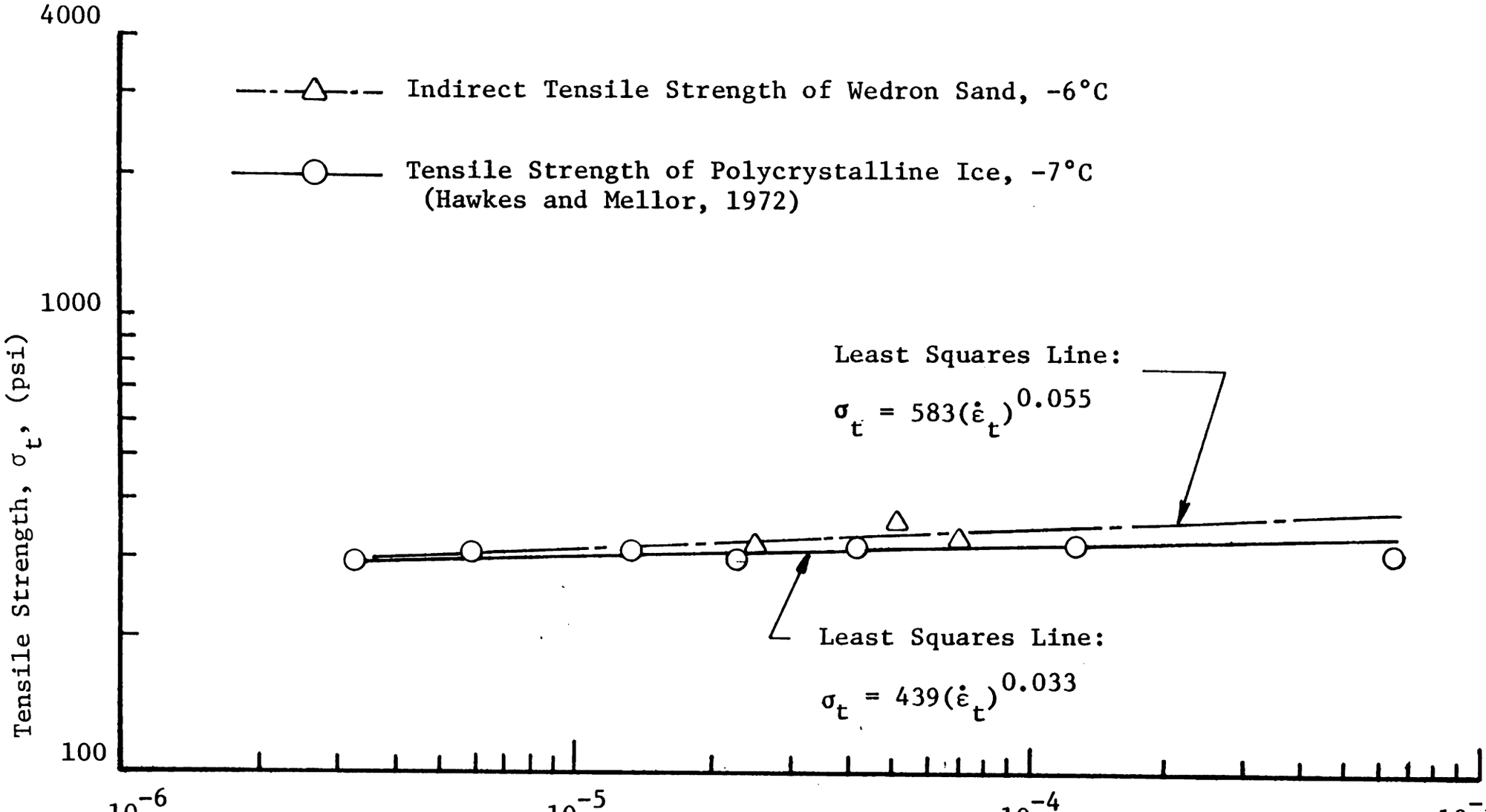
4000
1000
100
Tensile Strength, σ_t, (psi)
Indirect Tensile Strength of Wedron Sand, -6°C
Tensile Strength of Polycrystalline Ice, -7°C
(Hawkes and Mellor, 1972)
Least Squares Line:
$\sigma_t = 583(\dot{\varepsilon}_t)^{0.055}$
Least Squares Line:
$\sigma_t = 439(\dot{\varepsilon}_t)^{0.033}$
10^{-6}
10^{-5}
10^{-4}
10^{-3}

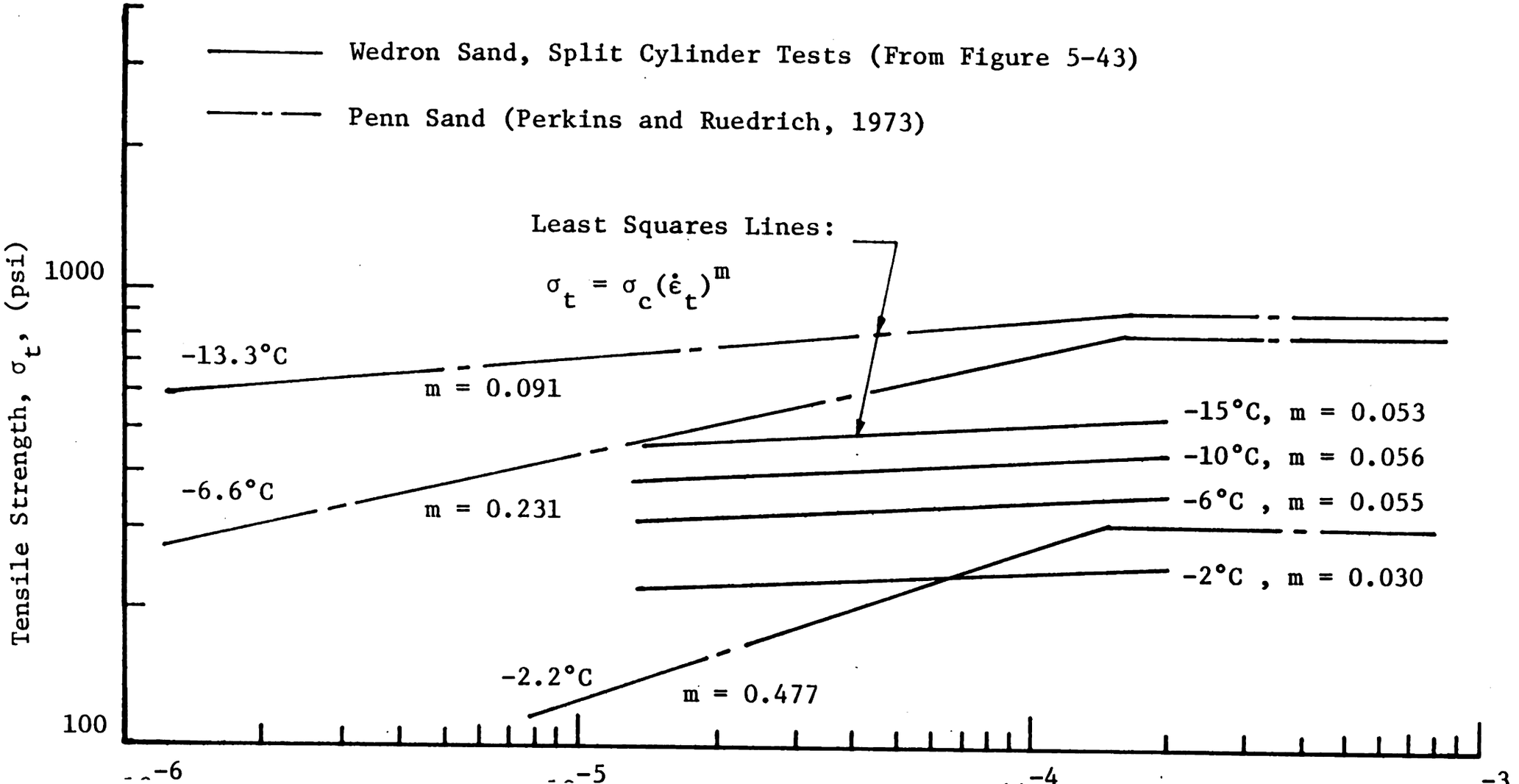
10000
1000
100
Tensile Strength, σ_t, (psi)
Wedron Sand, Split Cylinder Tests (From Figure 5-43)
Penn Sand (Perkins and Ruedrich, 1973)
Least Squares Lines:
$\sigma_t = \sigma_c(\dot{\varepsilon}_t)^m$
-13.3°C
m = 0.091
-6.6°C
m = 0.231
-2.2°C
m = 0.477
-15°C, m = 0.053
-10°C, m = 0.056
-6°C , m = 0.055
-2°C , m = 0.030
-6
-5
-4
-3

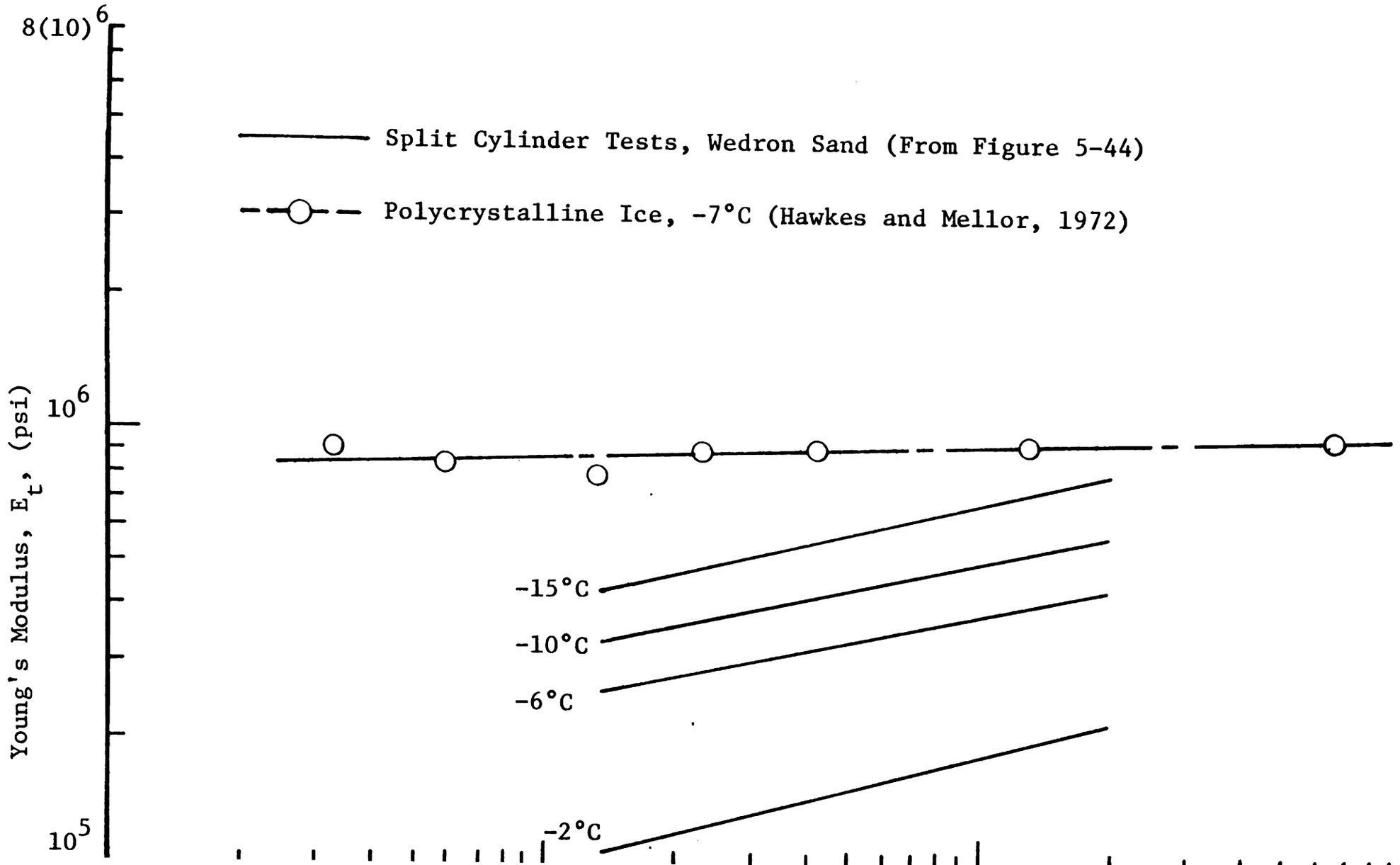
8(10)6
10^6
10^5
Young's Modulus, Et, (psi)
Split Cylinder Tests, Wedron Sand (From Figure 5-44)
Polycrystalline Ice, -7°C (Hawkes and Mellor, 1972)
-15°C
-10°C
-6°C
-2°C

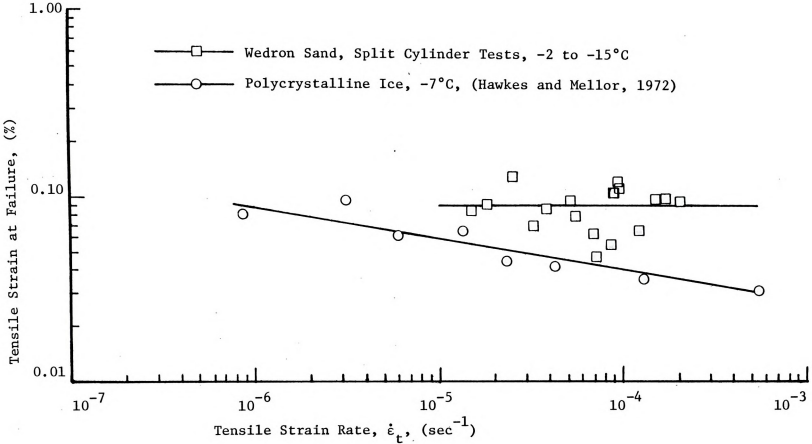
1.00
0.10
0.01
Tensile Strain at Failure, (%)
Wedron Sand, Split Cylinder Tests, -2 to -15°C
Polycrystalline Ice, -7°C, (Hawkes and Mellor, 1972)
10^{-7}
10^{-6}
10^{-5}
10^{-4}
10^{-3}
Tensile Strain Rate, $\dot{\varepsilon}_t$, (sec^{-1})

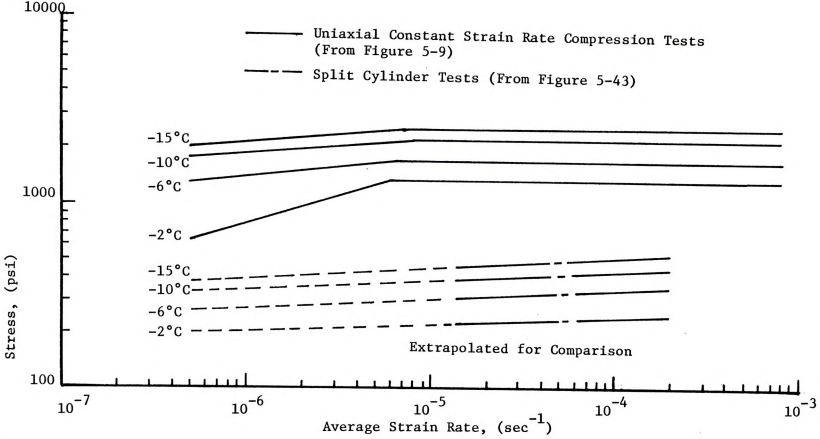

Figure 6-14: Comparison of Uniaxial Compressive Strength with Indirect Tensile Strength.

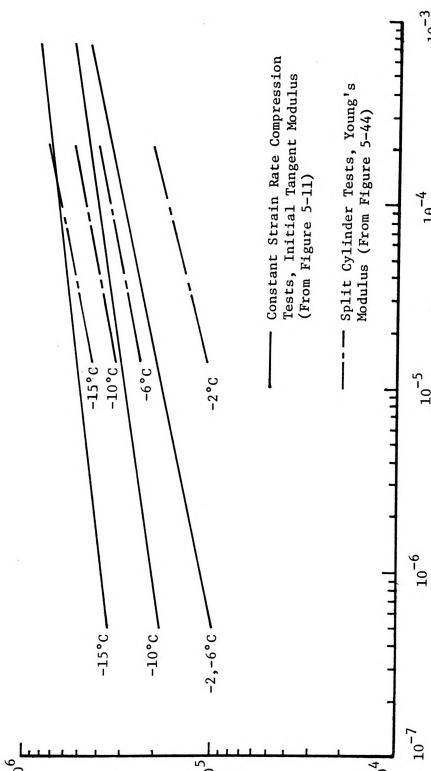

Figure 6-15: Elastic Modulus in Tension and Compression.

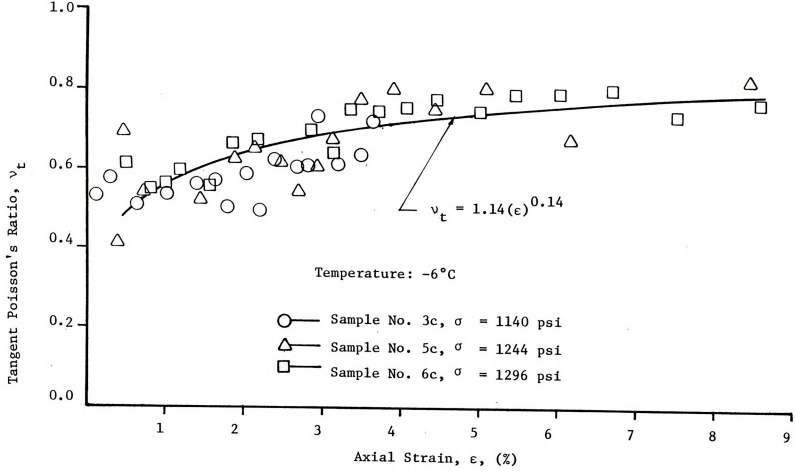

Figure 6-16: Tangent Poisson's Ratio versus Axial Strain for Unconfined Uniaxial Compression Creep Tests.

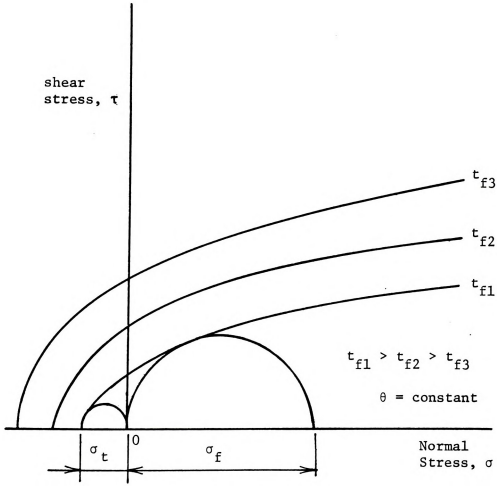

Figure 6-17: Time Dependence of Failure Envelopes.

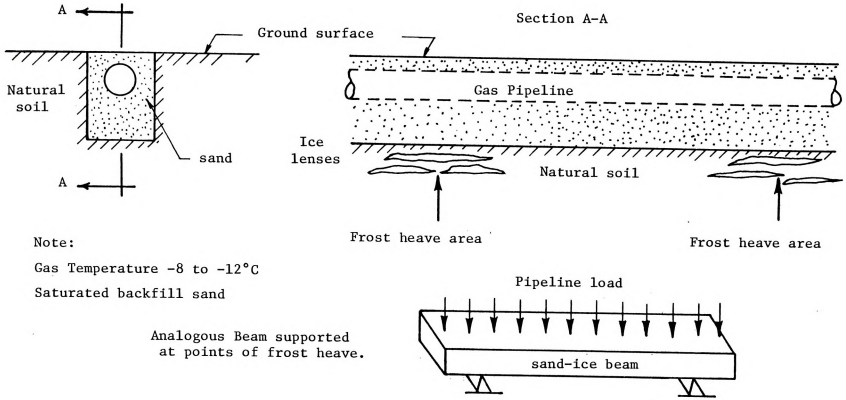

Figure 6-18: Frozen Sand Backfill Simulating an Unreinforced Beam for Partial Support of Pipeline in Areas of Differential Frost Heave Action.

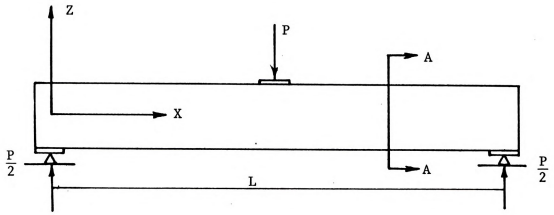

Material Properties

Tension: $\dot{\varepsilon}_c = 10^{-6}\,sec^{-1}$

σ_c^t (-20°C) = 518 psi

n = 11

Compression: $\dot{\varepsilon}_c = 10^{-6}\,sec^{-1}$

σ_c^c (-20°C) = 2591 psi

n = 11

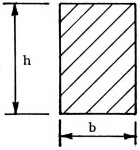

Section A-A

Beam Dimensions

b = 2.0 in

h = 2.5 in

L = 22.0 in

Figure 6-19: Simply Supported Frozen Soil Beam.

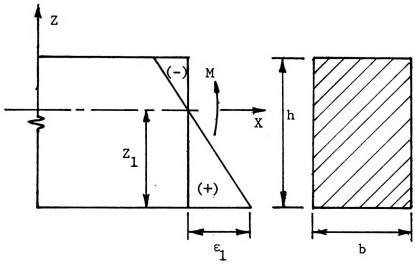

(a)

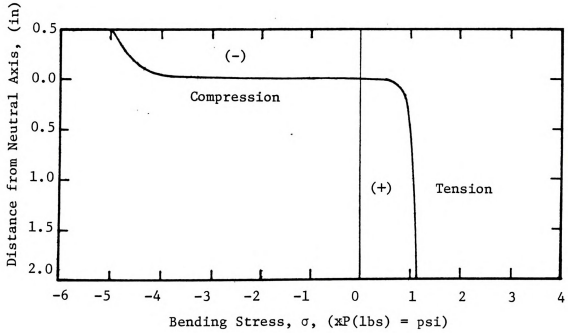

(b)

Figure 6-20: Simply Supported Beam; (a) Assumed Strain Distribution (b) Computed Stress Distribution

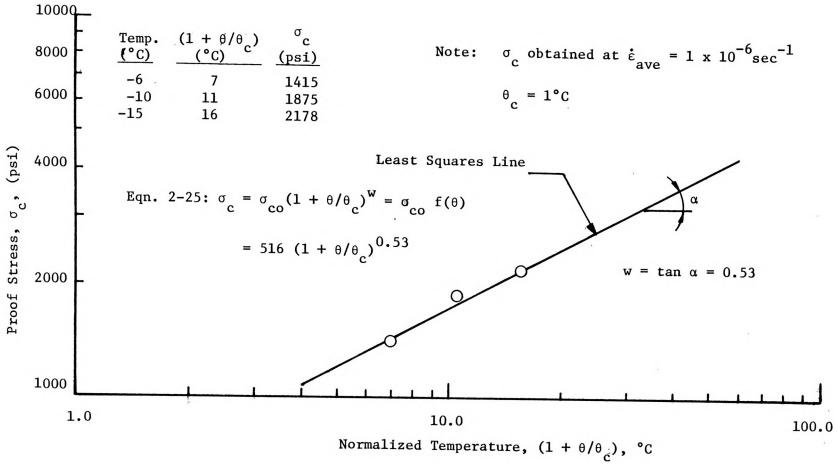

Figure 6-21: Determination of Temperature Correction Factor.

CHAPTER VII

SUMMARY AND CONCLUSIONS

The results and conclusions derived from this investigation are summarized in the following sections: material behavior, standardization and evaluation of test methods, material property selection, and recommended additional research.

7.1 Material Behavior

The material behavior of frozen Wedron sand was examined with respect to mechanical properties required for design of frozen soil structural elements subject to bending meoments. Of primary interst was the stress-strain-time relationships governing deformation in tension and compression.

Constant strain rate uniaxial compression tests conducted on the sand-ice material indicated that the stress-strain behavior of the material was governed by the applied strain rate. The deformation behavior changed from a plastic to a brittle failure as the applied strain rate increased. At average strain rates below $2 \times 10^{-4} sec^{-1}$, the stress-strain curves exhibited an initial yield followed by a period of plastic strain hardening. At high strain rates (average above $2 \times 10^{-4} sec^{-1}$), the stress-strain curves were nearly linear up to the failure, with the initial yield stress approximately equal to the peak stress. The initial portion of the stress-strain curves appears to be dominated by the behavior of the ice matrix. Yield in the ice is believed to be responsible for the initial yield point observed in the stress-strain curves. The plastic strain hardening occuring after the initial yield, has been attributed to dilatancy and mobilization

of interparticle friction (as supported by the volume change measurements).

The compressive strength of the frozen sand obtained,from the constant strain rate tests,was observed to increase uniformly with increasing strain rates, up to an average strain rate of about $7 \times 10^{-6} sec^{-1}$. At higher strain rates the compressive strength appears to be independent of the applied strain rate. This transition was observed to occur close to the strain rate at which the mode of failure changed from plastic (no visable cracking) to brittle (shear planes or multiple cracks). The decrease in plasticity coupled with surface irregularities at the sample ends may have produced premature failure at the higher strain rates. Data obtained at low strain rates increased uniformly with increasing strain rate according to a power law which, in turn, permits computation of the long term strength.

A similar relationship was observed for the indirect tensile strength determined from the split cylinder tests. The exponents in the two power law relationships were observed to be approximately the same. However, the indirect tensile strength appears to be roughly 1/5 the compressive strength of the frozen sand and approximately equal to the tensile strength of ice. There was some evidence which suggests that the split cylinder test may significantly underestimate the true tensile strength. However, data obtained by other investigators does seem to confirm that the tensile strength (as a function of strain rate) is much less than the compressive strength for frozen sand.

Both indirect tensile strengths and uniaxial compressive strengths increased with decreasing temperature (for temperatures less than -6°) according to a power law similar to that given by Ladanyi (1972). The indirect tensile strength increased in proportion to the compressive

strength with decreasing temperatures in such a fashion as to maintain a compression:tension strength ratio of approximately 5. At higher temperatures the compressive strength was observed to be more dependent on the applied strain rate.

The axial strain at failure in compression increased from less than one percent at high strain rates to greater than 4 percent at low strain rates. The slower rates appear to permit more pressure melting and water migration, refreezing and particle readjustments to occur prior to the development of the peak load. The computed tensile strains reported for the split cylinder tests were in most cases less than 0.1 percent, which compares favorably with the failure strain in tension reported for ice by other investigators. However, data presented for direct tensile tests on frozen sand (Perkins and Reudrich, 1973) indicates that the tensile strain at failure is approximately equal to the compressive failure strain, at the same strain rates. The failure strains observed for both the indirect tensile tests and the constant strain rate compression tests were determined to be independent of temperature.

The initial tangent modulus for constant strain rate compression tests was observed to be approximately equal to the computed value of Young's modulus from the split cylinder tests. Both values were observed to increase uniformly with strain rate and temperature. This suggests that power expressions similar to those used to relate temperature and strain rate to the strength of the frozen sand might be applied to the elastic modulus.

7.2 Standardization and Evaluation Of Test Methods

The applied strain rate during the so-called constant strain rate compression tests was observed to vary over the duration of the test. Variation in the applied strain rate may be attributed directly to the stiffness of the test apparatus. Elastic strain energy stored in the test system was released as the sample reached the initial yield and peak stress, accounting for the increase in strain rates observed at these points. The observed strain rates did not reach the nominal strain rate until after the sample had reached the peak stress.

Differences between material constants obtained from analyses using the average strain rate to failure and the nominal strain were not considered to be significant in this study. The differences do indicate that the test system stiffness will influence test results. The effect of machine stiffness on test results would obviously increase as the stiffness of the test system decreases. In addition, if the same test system were used, changes in the sample geometry, which influences the stiffness of the sample, will also effect the response of the test system during testing. Differences in test frames or sample geometry could result in significant differences in test results obtained by various investigators, if nominal strain rates were used by some for analysis.

The effect of sample diameter on the mechanical properties in tension and compression was observed for the same average strain rate to failure. The indirect tensile strength was observed to be independent of sample diameter for the range of sample sizes (1.94 to 4.00 inches) tested. The mechanical properties of the frozen sand determined from the constant strain rate compression tests were also observed to be

independent of the sample diameter, with the possible exception of the initial tangent modulus. Data obtained suggests that the initial tangent modulus increased by approximately 31 percent over a range of sample diameters (1.13 to 2.40 inches) which could be encountered in field investigations. The explanation for this apparent increase in E_i can not be ascertained from available data. A reasonable requirement, based on theoretical considerations, is that the minimum linear dimension of the sample should be 10 to 20 times the maximum particle diameter (Hawkes and Mellor, 197). The sample length should be at least twice the diameter for uniaxial compression tests (Baker, 1978a).

Comparison of results obtained from constant strain rate and constant stress compression (creep) tests indicates that the constant strain rate compression tests may be used to provide a reasonable estimate of the time dependent deformation during secondary creep. The material parameters necessary to define the creep strain prior to secondary creep can not be obtained from the constant strain rate tests. If the service life of a structure were less than the duration of primary creep, then constant stress creep tests are needed to define the parameters necessary for predication of the creep strain as a function of time. Application of constant strain rate tests are limited to situations where the elastic and primary creep deformations are small in comparison to the secondary creep strain.

It would also seem reasonable that constant strain rate compression tests could be used to determine the time dependent strength of the frozen sand. The failure strain obtained from the constant strain rate compression tests (for strain rates less than $10^{-5}sec^{-1}$) was observed to be approximately equal to the strain at the onset of tertiary creep in the constant stress creep tests. The long term strength of the

frozen sand may be determined as indicated by Equation 2-10.

Several problems were observed with respect to applying the split cylinder test to frozen sand. At low vertical deformation rates tensile failures did not occur in the samples, only an apparent compression in the area of the loading strips. As a result, it was not possible to obtain data for tensile strain rates below about $1.4 \times 10^{-5} sec^{-1}$. The computed values of Poisson's ratio were usually less than zero. Since Poisson's ratio was used to compute Young's modulus, the tensile strain at failure, and the tensile strain rate, there is some question as to the accuracy of the relationships between tensile strength or Young's modulus and tensile rate. In addition, there is some evidence to indicate that the split cylinder test may significantly underestimate the true tensile strength. These problems would suggest that emphasis should be placed on developing another test method to determine the material properties of frozen sand in tension.

7.3 Material Property Selection

Selection of material properties defining the stress-strain-time behavior of frozen sand in tension and compression is required for engineering design of sand-ice structural elements. The constitutive equations governing the time dependent strain of frozen sand in tension or compression appears to be reasonably approximated by power law relationships which are functions of stress and time.

Data obtained in this investigation and supported by the work of other researchers, indicates that the uniaxial constant strain rate compression test may be used to estimate the creep parameters in compression and tension. The creep parameter n (the exponent in the power law) appears to be approximately the same for tension and

compression (with respect to the uncertainty of computing tensile strain rates for the split cylinder test). The tensile strength of frozen Wedron sand was observed to be approximately 1/5 the compressive strength of the same range of strain rates. It appears that the creep proof stress σ_c^t for tension may be obtained from the constant strain rate compression tests as 1/5 the value of compression creep proof stress σ_c^c.

Young's modulus from the split cylinder tests was found to be in close agreement with values obtained from constant strain rate compression tests at the same temperature and strain rate. Values of the elastic modulus for tension and compression may be obtained as a function of strain rate from the constant strain rate compression test. Both the elastic modulus and strength were observed to increase with decreasing temperature according to similar power expressions, which may be evaluated from the constant strain rate compression data.

Extension of the uniaxial creep (power) expression to multiaxial states of stress has been considered by several other investigators. The von Mises flow law and the assumption of volume constantancy have usually been assumed. Volume change data obtained from uniaxial compression creep tests at zero confining pressure indicates that dilatancy results in a significant volume increase during the creep process. The value of Poisson's ratio during creep was computed to be greater than 0.5 (constant volume value) and was observed to vary with strain according to a power law relationship. Influence of confining pressure on Poisson's ratio was not investigated and may justify using a value of approximately 0.5 for design.

The Mohr-Coulomb failure theory may be extended to multiaxial states

of stress (ignoring the possible influence of the intermediate principal stress on failure) and to consider the time dependent strength of frozen sand. Assuming that the tensile strength of frozen sand may be estimated from the uniaxial compressive strength, a parabolic representation of the time dependent Mohr envelopes may be developed in terms of the compression:tension strength ratio.

A simiplified analysis of a simply supported beam was presented to illustrate flexural analysis concepts pertaining to the time dependent rupture and deflection of the beam. The analysis also serves to illustrate the ability of frozen sand to resist flexural deformation and the application of constitutive creep equations (and corresponding temperature corrections) for design or analysis of a frozen soil structural element.

7.4 Recommended Additional Research

Additional research is needed in several areas related to the mechanical properties of frozen sand and the design of frozen soil structures. Several specific problems are outlined below:

1. Due to uncertainty and difficulties in interpreting results for the split cylinder tests, additional tensile tests on sand-ice materials are needed. Direct tensile tests would help verify the results of indirect test methods. Constant strain rate and/or constant stress uniaxial tension tests would seem appropriate.

2. The influence of confining pressure on the volumetric strain of frozen soils should also be investigated. It is suspected that confining pressures would reduce the dilatancy of frozen sand during creep or constant strain rate compression tests, resulting in a decrease

in the value of Poisson's ratio. Data obtained from unconfined compression tests in this investigation suggest that Poisson's ratio may be significantly greater than 0.5 due to dilatancy effects. Data related to the interaction of confining pressure, strain, , and Poisson's ratio would permit a more realistic evaluation of current methods of considering creep under multi-axial stress conditions.

3. The ability of frozen sand to function as a structural element (even temporarily) suggests an analogy to concrete. Steel reinforcement is normally used in concrete structures to compensate for the low tensile strength of the material. Similar use of reinforcement may also be helpful in many applications of frozen soil structures. The bond strength as a function of time and temperature would be required to define the interaction between the reinforcement and the frozen sand for structural design.

4. Laboratory investigation of the performance of simple beams would provide verification of the analysis presented in this investigation. Properly instrumented beams would help define strain distribution in the beam and permit computation of the creep parameters in tension (provided the compression creep parameters are known in advance). Laboratory tests on model beams could also be extended to consider the effect of reinforcement on the time dependent response. Such information would be a valuable contribution to developing design procedures for field application of reinforced frozen earth structural elements for construction purposes.

APPENDIX

Table A-1: Constant Strain Rate Uniaxial Compression Test Data

SAMPLE NO. 1

Temperature = -6.08°C
Nom. Strain Rate = 1.19×10^{-4} sec^{-1}
Ave. Strain Rate = 9.46×10^{-5} sec^{-1}
Sample Diameter = 1.405"
Initial Length = 2.81"
Percent Sand (by Vol.) = 63.26
Degree Ice Saturation (%) = 98.27
Time to Failure = 310 sec

Strain (%)	Stress (psi)
0.027	77
0.049	192
0.092	301
0.131	435
0.179	492
0.192	543
0.229	684
0.326	945
0.625	1241
1.036	1382
1.474	1464
1.952	1525
2.431	1574
2.934	1585
3.423	1565
3.933	1519
4.429	1450
4.943	1376
5.496	1295
6.013	1204
6.547	1131
7.346	1032

SAMPLE NO. 2

Temperature = -6.05°C
Nom. Strain Rate = 1.19×10^{-4} sec^{-1}
Ave. Strain Rate = 1.02×10^{-4} sec^{-1}
Sample Diameter = 1.405"
Initial Length = 2.81"
Percent Sand (by Vol.) = 63.17
Degree Ice Saturation (%) = 99.22
Time to Failure = 335 sec

Strain (%)	Stress (psi)
0.083	83
0.135	109
0.224	147
0.241	179
0.307	230
0.374	294
0.399	389
0.442	491
0.480	625
0.597	878
0.755	1099
0.924	1237
1.114	1311
1.376	1358
1.613	1405
1.961	1457
2.310	1501
2.680	1527
3.033	1540
3.220	1543
3.407	1546
3.784	1521
4.181	1485
4.561	1442
4.979	1387
5.379	1333
5.777	1291
6.311	1218
6.862	1151
7.431	1091

SAMPLE NO. 3

Temperature = -6.05°C
Nom. Strain Rate = 1.19×10^{-4} sec^{-1}
Ave. Strain Rate = 9.76×10^{-5} sec^{-1}
Sample Diameter = 1.405"
Initial Length = 2.81"
Percent Sand (by Vol.) = 63.97
Degree Ice Saturation (%) = 98.83
Time to Failure = 282 sec

Strain (%)	Stress (psi)
0.069	44
0.122	236
0.194	428
0.261	651
0.380	912
0.521	1145
0.672	1298
0.906	1377
1.143	1418
1.305	1473
1.844	1508
2.213	1547

Table A-1 (cont'd.)

SAMPLE NO. 3 (cont'd.)

2.566	1565
2.752	1569
2.939	1566
3.316	1548
3.676	1498
4.210	1410
4.803	1304
5.358	1200
5.911	1108
6.618	987
7.307	866

SAMPLE NO. 4

Temperature = -6.05°C
Nom. Strain Rate = 1.19×10^{-4} sec^{-1}
Ave. Strain Rate = 9.29×10^{-5} sec^{-1}
Sample Diameter = 1.405"
Initial Length = 2.81"
Percent Sand (by Vol.) = 64.44
Degree Ice Saturation (%) = 97.03
Time to Failure = 290 sec

Strain (%)	Stress (psi)
0.027	89
0.063	262
0.133	461
0.202	677
0.271	888
0.343	1072
0.456	1224
0.685	1342
1.032	1413
1.491	1483
1.970	1544
2.452	1580
2.695	1582
2.939	1572
3.449	1527
3.945	1440
4.499	1339
5.171	1196
5.881	1054
6.609	909

SAMPLE NO. 5

Temperature = -6.05°C
Nom. Strain Rate = 1.19 x 10 sec
Ave. Strain Rate = 9.92 x 10 sec
Sample Diameter = 1.405"
Initial Length = 2.81"
Percent Sand (by Vol.) = 63.39
Degree Ice Saturation (%) = 99.99
Time to Failure = 370 sec

Strain (%)	Stress (psi)
0.011	96
0.087	211
0.159	403
0.230	594
0.319	798
0.409	982
0.575	1165
0.841	1289
1.112	1368
1.567	1475
2.023	1575
2.481	1649
3.053	1707
3.558	1716
3.668	1727
4.175	1700
4.819	1627
5.484	1543
6.322	1415
7.254	1289

SAMPLE NO. 6

Temperature = -6.08°C
Nom. Strain Rate = 1.34×10^{-3} sec^{-1}
Ave. Strain Rate = 3.69×10^{-4} sec^{-1}
Sample Diameter = 1.405"
Initial Length = 2.81"
Percent Sand (by Vol.) = 63.69
Degree Ice Saturation (%) = 98.56
Time to Failure = 11.1 sec

Strain (%)	Stress (psi)
0.009	83
0.003	134
---	---
0.017	332
---	---
0.033	678
0.080	921

Table A-1 (cont'd.)

SAMPLE NO. 6 (cont'd.)

0.107	1170
0.171	1423
0.244	1597
0.290	1685
0.360	1723
0.414	1741
0.489	1739
0.624	1705
0.823	1600
1.136	1482
1.579	1374
2.096	1272
2.593	1178
3.375	1051
4.268	938

SAMPLE NO. 7

Temperature = -6.05°C
Nom. Strain Rate = 5.93×10^{-4} sec^{-1}
Ave. Strain Rate = 2.68×10^{-4} sec^{-1}
Sample Diameter = 1.405"
Initial Length = 4.81"
Percent and (by Vol.) = 63.69
Degree Ice Saturation (%) = 98.79
Time to Failure = 28 sec

Strain (%)	Stress (psi)
0.037	83
0.074	166
0.120	333
0.172	531
0.240	754
0.298	977
0.366	1193
0.463	1403
0.568	1541
0.749	1589
0.928	1586
1.249	1556
1.617	1525
1.996	1481
2.628	1359
3.281	1214
4.303	956

SAMPLE NO. 8

Temperature = -6.10°C
Nom. Strain Rate = 2.77×10^{-4} sec^{-1}
Ave. Strain Rate = 2.04×10^{-4} sec^{-1}
Sample Diameter = 1.405"
Initial Length = 2.81"
Percent Sand (by Vol.) = 63.78
Degree Ice Saturation (%) = 98.16
Time to Failure = 143 sec

Strain (%)	Stress (psi)
0.098	205
0.186	492
0.229	684
0.301	868
0.373	1052
0.449	1199
0.621	1330
0.811	1391
1.012	1426
1.213	1468
1.414	1502
1.624	1544
1.826	1578
2.028	1606
2.287	1633
2.592	1659
2.917	1679
3.396	1658
3.979	1617
4.553	1516
5.201	1415
6.134	1274
6.893	1180
7.729	1076

SAMPLE NO. 9

Temperature = -6.05°C
Nom. Strain Rate = 5.34×10^{-5} sec^{-1}
Ave. Strain Rate = 2.57×10^{-5} sec^{-1}
Sample Diameter = 1.41"
Initial Length = 2.81"
Percent Sand (by Vol.) = 64.91
Degree Ice Saturation (%) = 98.39
Time to Failure = 1317 sec

Strain (%)	Stress (psi)
0.007	64
0.063	103
0.110	179

Table A-1 (cont'd.)

SAMPLE NO. 9 (cont'd.)

0.157	288
0.208	467
0.263	632
0.336	804
0.450	975
0.582	1107
0.774	1220
0.990	1293
1.223	1379
1.458	1451
1.746	1542
2.073	1624
2.419	1699
2.785	1761
3.175	1785
3.379	1795
3.587	1778
4.098	1719
4.616	1612
5.369	1411
6.183	1183
7.059	904

SAMPLE NO. 10

Temperature = -6.05°C
Nom. Strain Rate = 5.34×10^{-5} sec^{-1}
Ave. Strain Rate = 4.36×10^{-5} sec^{-1}
Sample Diameter = 1.405"
Initial Length = 2.81"
Percent Sand (by Vol.) = 63.50
Degree Ice Saturation (%) = 98.50
Time to Failure = 753 sec

Strain (%)	Stress (psi)
0.069	211
0.154	448
0.263	716
0.382	976
0.546	1172
0.747	1297
0.963	1364
1.201	1411
1.438	1464
1.822	1527
2.217	1584
2.614	1628
3.031	1658
3.280	1660
3.715	1646

SAMPLE NO. 10 (cont'd.)

4.184	1632
4.619	1588
5.054	1544
5.396	1497
0.018	83
0.103	320
0.195	575
0.039	147
0.465	1071
0.633	1234

SAMPLE NO. 11

Temperature = -6.05°C
Nom. Strain Rate = 1.07 x 10 sec
Ave. Strain Rate = 9.23 x 10 sec
Sample Diameter = 1.405"
Initial Length = 2.81"
Percent Sand (by Vol.) = 63.73
Degree Ice Saturation (%) = 97.91
Time to Failure = 4590 sec

Strain (%)	Stress (psi)
0.023	39
0.031	57
0.055	86
0.079	119
0.126	205
0.219	374
0.339	536
0.455	676
0.600	793
0.811	911
1.095	1036
1.434	1174
1.784	1299
2.032	1336
2.331	1420
2.650	1483
2.961	1541
3.338	1603
3.809	1638
4.237	1656
4.649	1642
5.139	1616
5.649	1571
6.159	1520
6.917	1442

Table A-1 (cont'd.)

SAMPLE NO. 12

Temperature = -6.05°C
Nom. Strain Rate = 2.37 x 10^{-5} sec^{-1}
Ave. Strain Rate = 2.01 x 10^{-5} sec^{-1}
Sample Diameter = 1.405"
Initial Length = 2.81"
Percent Sand (by Vol.) = 63.37
Degree Ice Saturation (%) = 98.80
Time to Failure = 1950 sec

Strain (%)	Stress (psi)
0.004	32
0.019	96
0.067	233
0.139	381
0.198	495
0.255	600
0.352	740
0.506	911
0.734	1068
0.996	1182
1.258	1271
1.536	1343
1.891	1426
2.378	1500
2.987	1572
3.558	1606
3.924	1618
4.850	1597
5.655	1528
6.498	1455
7.434	1363
7.415	1346

SAMPLE NO. 13

Temperature = -6.05
Nom. Strain Rate = 1.78 x 10^{-3} sec^{-1}
Ave. Strain Rate = 6.46 x 10^{-4} sec^{-1}
Sample Diameter = 1.405"
Initial Length = 2.81"
Percent Sand (by Vol.) = 63.01
Degree Ice Saturation (%) = 99.03
Time to Failure = 7.85 sec

Strain (%)	Stress (psi)
0.002	67
0.002	224
0.003	393
0.054	582
0.096	780
0.138	985
0.179	1195
0.238	1406
0.303	1577
0.382	1697
0.507	1746
0.693	1673
1.036	1458
1.402	1288
2.075	1129
2.812	989
3.733	875
4.755	780
5.659	725

SAMPLE NO. 14

Temperature = -6.10°C
Nom. Strain Rate = 4.75 x 10^{-6} sec^{-1}
Ave. Strain Rate = 4.05 x 10^{-6} sec^{-1}
Sample Diameter = 1.405"
Initial Length = 2.81"
Percent Sand (by Vol.) = 63.62
Degree Ice Saturation (%) = 97.88
Time to Failure = 11,280 sec

Strain (%)	Stress (psi)
0.026	16
0.042	42
0.066	73
0.107	128
0.153	211
0.246	303
0.310	391
0.375	474
0.586	659
0.916	809
1.359	954
1.599	1119
2.066	1286
2.455	1399
2.889	1511
3.422	1596
4.051	1647
4.293	1655
4.572	1662
4.986	1643
5.477	1604
5.761	1569
5.987	1559
6.366	1517

Table A-1 (cont'd.)

SAMPLE NO. 15

Temperature = -6.05°C
Nom. Strain Rate = 1.42 x 10^{-6} sec^{-1}
Ave. Strain Rate = 1.23 x 10^{-6} sec^{-1}
Sample Diameter = 1.405"
Initial Length = 2.81"
Percent Sand (by Vol.) = 63.39
Degree Ice Saturation (%) = 97.24
Time to Failure = 37,080 sec

Strain (%)	Stress (psi)	Time (min)
0.077	61	8
0.118	112	18
0.133	144	25
0.166	243	48
0.296	351	73
0.545	465	108
1.010	646	173
1.565	851	248
2.123	1047	323
2.719	1215	398
3.357	1356	478
4.022	1432	558
4.561	1442	618
5.162	1421	683
5.936	1355	768
6.714	1272	848
7.377	1204	913
7.534	1143	993

SAMPLE NO 16

Temperature = -0.06°C
Nom. Strain Rate = 5.69 x 10^{-7} sec^{-1}
Ave. Strain Rate = 4.90 x 10^{-7} sec^{-1}
Sample Diameter = 1.405"
Initial Length = 2.81"
Percent Sand (by Vol.) = 63.73
Degree Ice Saturation (%) = 97.78
Time to Failure = 93,540 sec

Strain (%)	Stress (psi)
0.017	10
0.033	39
0.049	61
0.084	83
0.135	131
0.202	192
0.359	294
0.737	426

SAMPLE NO. 16 (cont'd.)

1.133	560
1.582	712
2.123	887
2.593	1023
3.103	1138
3.707	1242
4.337	1289
4.580	1292
4.767	1290
5.219	1266
5.709	1229
6.333	1170
6.921	1111
7.470	1052
8.019	1001

SAMPLE NO. 17

Temperature = -6.13°C
Nom. Strain Rate = 4.45 x 10^{-4} sec^{-1}
Ave. Strain Rate = 2.26 x 10^{-4} sec^{-1}
Sample Diameter = 1.405"
Initial Length = 2.81"
Percent Sand (by Vol.) = 63.40
Degree Ice Saturation (%) = 97.75
Time to Failure = 36 sec

Strain (%)	Stress (psi)
0.043	51
0.059	137
0.085	237
0.143	445
0.222	732
0.310	1031
0.399	1263
0.479	1415
0.575	1521
0.651	1572
0.731	1589
0.812	1600
0.997	1585
1.322	1561
1.682	1530
2.287	1471
2.944	1374
3.611	1265
4.392	1145
5.31	995

Table A-1 (cont'd.)

SAMPLE NO. 18

Temperature = -6.06°C
Nom. Strain Rate = 2.14 x 10^{-6} sec^{-1}
Ave. Strain Rate = 1.87 x 10^{-6} sec^{-1}
Sample Diameter = 1.405"
Initial Length = 2.81"
Percent Sand (by Vol.) = 63.61
Degree Ice Saturation (%) = 98.23
Time to Failure = 2.622 x 10^{4} sec

Strain (%)	Stress (psi)
0.003	10
0.015	32
0.032	51
0.055	74
0.070	106
0.167	239
0.557	522
1.007	672
1.654	900
2.284	1101
2.699	1227
3.080	1328
3.607	1451
4.104	1517
4.548	1552
4.903	1559
5.522	1537
6.086	1509
6.692	1446
7.792	1322
0.105	160
0.224	326
0.291	396
0.379	447
0.449	478

SAMPLE NO. 19

Temperature = -6.08°C
Nom. Strain Rate = 1.42 x 10^{-5} sec^{-1}
Ave. Strain Rate = 1.16 x 10^{-5} sec^{-1}
Sample Diameter = 1.405"
Initial Length = 2.81"
Percent Sand (by Vol.) = 63.94
Degree Ice Saturation (%) = 98.99
Time to Failure = 3456 sec

Strain (%)	Stress (psi)
0.063	23
0.131	83
0.185	182
0.255	306
0.398	463
0.415	612
0.589	802
0.913	996
1.197	1126
1.482	1249
2.101	1467
2.921	1641

SAMPLE NO. 19 (cont'd.)

SAMPLE NO. 20

Temperature = -6.08°C
Nom. Strain Rate = 1.19 x 10^{-4} sec^{-1}
Ave. Strain Rate = 8.88 x 10^{-5} sec^{-1}
Sample Diameter = 1.405"
Initial Length = 2.81"
Percent Sand (by Vol.) = 63.88
Degree Ice Saturation (%) = 98.88
Time to Failure = 354 sec

Strain (%)	Stress (psi)
0.049	137
0.091	262
0.159	396
0.225	559
0.297	747
0.379	918
0.472	1090
0.639	1260
0.889	1358
1.161	1430
1.427	1477
1.701	1523
1.985	1569
2.317	1614
2.779	1650
3.144	1656
3.567	1630
4.209	1576
4.837	1487
5.712	1358
6.908	1216

Table A-1 (cont'd.)

SAMPLE NO. 21

Temperature = -6.08°C
Nom. Strain Rate = 1.19×10^{-4} sec^{-1}
Ave. Strain Rate = 9.59×10^{-5} sec^{-1}
Sample Diameter = 1.405"
Initial Length = 2.81"
Percent Sand (by Vol.) = 63.80
Degree Ice Saturation (%) = 97.78
Time to Failure = 335 sec

Strain (%)	Stress (psi)
0.019	70
0.095	233
0.168	406
0.259	587
0.341	772
0.441	953
0.553	1114
0.678	1249
0.819	1391
1.099	1476
1.395	1509
1.797	1584
2.194	1629
2.729	1682
3.212	1705
3.839	1694
4.538	1638
5.315	1546
6.132	1443
7.195	1308

SAMPLE NO. 22

Data Invalid - Membrane Leak

SAMPLE NO. 23

Temperature = -6.08°C
Nom. Strain Rate = 1.11×10^{-4} sec^{-1}
Ave. Strain Rate = 1.13×10^{-4} sec^{-1}
Sample Diameter = 1.13"
Initial Length = 2.26"
Percent Sand (by Vol.) = 63.54
Degree Ice Saturation = 98.29
Time to Failure = 243 sec

Strain (%)	Stress (psi)
0.133	109
0.201	194
0.287	307
0.403	524
0.487	794
0.549	973
0.615	1144
0.698	1271
0.798	1369
0.917	1421
1.186	1486
1.541	1514
1.882	1558
2.318	1590
2.756	1606
3.281	1594
3.893	1541
4.832	1412
6.073	1226
7.833	992

SAMPLE NO. 24

Temperature = -6.08°C
Nom. Strain Rate = 1.11×10^{-4} sec^{-1}
Ave. Strain Rate = 9.32×10^{-5} sec^{-1}
Sample Diameter = 1.13"
Initial Length = 2.26"
Percent Sand (by Vol.) = 63.39
Degree Ice Saturation (%) = 97.82
Time to Failure = 341 sec

Strain (%)	Stress (psi)
0.048	89
0.078	179
0.152	322
0.235	485
0.320	643
0.395	841
0.465	1037
0.554	1199
0.661	1316
0.793	1398
1.221	1481
1.689	1532
1.835	1559
2.096	1594
2.450	1631
2.634	1643
3.177	1658
3.821	1622
4.696	1532
5.621	1419
7.002	1223

Table A-1 (cont'd.)

SAMPLE NO. 25

Temperature = -6.09°C
Nom. Strain Rate = 1.11×10^{-4} sec^{-1}
Ave. Strain Rate = 8.23×10^{-5} sec^{-1}
Sample Diameter = 1.13"
Initial Length = 2.26"
Percent Sand (by Vol.) = 63.37
Degree Ice Saturation (%) = 98.14
Time to Failure = 341 sec

Strain (%)	Stress (psi)
0.027	174
0.057	303
0.094	392
0.134	490
0.189	664
0.225	782
0.303	960
0.364	1068
0.468	1200
0.606	1297
0.838	1353
1.196	1407
1.663	1479
2.175	1589
2.807	1582
3.426	1558
4.195	1473
5.193	1341
6.397	1226
7.880	987

SAMPLE NO. 26

Temperature = -6.08°C
Nom. Strain Rate = 1.11×10^{-4} sec^{-1}
Ave. Strain Rate = 9.78×10^{-5} sec^{-1}
Sample Diameter = 1.13"
Initial Length = 2.26"
Percent Sand (by Vol.) = 63.34
Degree Ice Saturation (%) = 98.06
Time to Failure = 382 sec

Strain (%)	Stress (psi)
0.030	101
0.050	162
0.082	238
0.117	318
0.228	456
0.304	502
0.369	574
0.416	682
0.493	835
0.574	992
0.707	1148
1.141	1260
1.472	1369
1.822	1428
2.458	1510
3.146	1567
3.735	1582
4.343	1557
5.310	1466
6.498	1317
7.966	1160

SAMPLE NO. 27

Temperature = -6.03°C
Nom. Strain Rate = 1.29×10^{-4} sec^{-1}
Ave. Strain Rate = 1.00×10^{-4} sec^{-1}
Sample Diameter = 1.94"
Initial Length = 3.88"
Percent Sand (by. Vol.) = 64.81
Degree Ice Saturation (%) = 98.75
Time to Failure = 247 sec

Strain (%)	Stress (psi)
0.034	133
0.077	260
0.119	406
0.155	574
0.193	752
0.274	1028
0.402	1220
0.570	1331
0.825	1411
1.118	1474
1.472	1558
1.830	1624
2.326	1682
2.579	1694
2.908	1678
3.452	1570
4.011	1414
4.838	1134
5.355	946

Table A-1 (cont'd.)

SAMPLE NO. 28

Temperature = -6.00°C
Nom. Strain Rate = 1.29 x 10^{-4} sec^{-1}
Ave. Strain Rate = 1.01 x 10^{-4} sec^{-1}
Sample Diameter = 1.94"
Initial Length = 3.88"
Percnet Sand (by Vol.) = 63.35
Degree Ice Saturation (%) = 98.48
Time to Failure = 267 sec

Strain (%)	Stress (psi)
0.046	93
0.068	234
0.092	398
0.117	564
0.147	741
0.183	936
0.219	1132
0.284	1295
0.438	1473
0.631	1571
1.093	1653
1.619	1722
2.161	1785
2.696	1802
3.382	1762
4.477	1618
5.418	1361
6.893	1130

SAMPLE NO. 29

Temperature = -6.05°C
Nom. Strain Rate = 1.29 x 10^{-4} sec^{-1}
Ave. Strain Rate = 9.30 x 10^{-5} sec^{-1}
Sample Diameter = 1.94"
Initial Length = 3.88"
Percent Sand (by Vol.) = 64.28
Degree Ice Saturation (%) = 98.11
Time to Failure - 273 sec

Strain (%)	Stress (psi)
0.027	79
0.043	147
0.079	283
0.145	325
0.142	601
0.168	792
0.201	989
0.266	1166

SAMPLE NO. 29 (cont'd.)

0.344	1311
0.505	1427
0.726	1497
0.956	1544
1.299	1616
1.692	1704
2.179	1790
2.539	1783
2.990	1764
3.611	1671
4.643	1378
5.117	1018
6.291	624

SAMPLE NO. 30

Temperature = -6.00°C
Nom. Strain Rate = 1.29 x 10^{-4} sec^{-1}
Ave. Strain Rate = 1.02 x 10^{-4} sec^{-1}
Sample Diameter = 1.94"
Initial Length = 3.88"
Percent Sand (by Vol.) = 64.16
Degree Ice Saturation (%) = 99.07
Time to Failure = 303 sec

Strain (%)	Stress (psi)
0.031	53
0.056	182
0.078	322
0.105	473
0.131	637
0.164	806
0.208	972
0.265	1115
0.335	1227
0.461	1315
0.637	1380
0.817	1426
1.039	1464
1.327	1521
1.684	1593
2.004	1654
2.438	1713
2.915	1743
3.088	1751
3.527	1727
4.071	1668
4.615	1519
5.599	1301

Table A-1 (cont'd.)

SAMPLE NO. 31

Temperature = -6.05°C
Nom. Strain Rate = 1.29×10^{-4} sec^{-1}
Ave. Strain Rate = 9.39×10^{-5} sec^{-1}
Sample Diameter = 1.94"
Initial Length = 3.88"
Percent Sand (by Vol.) = 63.44
Degree Ice Saturation (%) = 98.38
Time to Failure = 282 sec

Strain (%)	Stress (psi)
0.003	96
0.009	274
0.016	426
0.033	649
0.053	860
0.082	1069
0.180	1319
0.270	1425
0.382	1496
0.636	1554
0.970	1610
1.441	1686
2.075	1758
2.649	1775
3.402	1740
4.596	1578
5.339	1352
6.761	1121
8.243	787

SAMPLE NO. 32

Temperature = -6.02°C
Nom. Strain Rate = 1.29×10^{-4} sec^{-1}
Ave. Strain Rate = 1.04×10^{-4} sec^{-1}
Sample Diameter = 1.94"
Initial Length = 3.88"
Percent Sand (by Vol.) = 63.38
Degree Ice Saturation (%) = 98.53
Time to Failure = 275 sec

Strain (%)	Stress (psi)
0.014	56
0.027	149
0.046	245
0.072	412
0.097	579
0.133	821
0.224	935

SAMPLE NO. 32 (cont'd.)

0.216	1188
0.309	1374
0.483	1494
0.663	1531
0.895	1567
1.162	1602
1.505	1652
1.928	1706
2.391	1736
2.849	1738
3.389	1691
3.810	1591
4.717	1447
6.079	1230

SAMPLE NO. 33

Temperature = -6.08°C
Nom. Strain Rate = 1.29×10^{-4} sec^{-1}
Ave. Strain Rate = 9.67×10^{-5} sec^{-1}
Sample Diameter = 1.94"
Initial Length = 3.88"
Percent Sand (by Vol.) = 63.38
Degree Ice Saturation (%) = 98.53
Time to Failure = 268 sec

Strain (%)	Stress (psi)
0.020	90
0.033	234
0.054	398
0.073	567
0.091	748
0.117	939
0.155	1122
0.223	1324
0.330	1452
0.540	1539
0.984	1610
1.492	1696
1.895	1750
2.298	1776
2.592	1788
3.224	1749
4.276	1567
4.741	1366
5.671	1150
6.661	917
7.449	732

Table A-1 (cont'd.)

SAMPLE NO. 34

Temperature = -6.08°C
Nom. Strain Rate = 1.11×10^{-4} sec^{-1}
Ave. Strain Rate = 8.63×10^{-5} sec^{-1}
Sample Diameter = 1.13"
Initial Length = 2.26"
Percent Sand (by Vol.) = 63.42
Degree Ice Saturation (%) = 98.04
Time to Failure = 379 sec

Strain (%)	Stress (psi)
0.009	87
0.013	173
0.039	296
0.066	421
0.095	553
0.121	684
0.150	758
0.208	917
0.308	1074
0.451	1191
0.703	1296
1.196	1466
1.845	1637
2.707	1762
3.272	1780
4.000	1729
4.699	1646
5.748	1487
6.986	1315

SAMPLE NO. 35

Data Invalid - Membrane Leak

SAMPLE NO. 36

Temperature = -6.06°C
Nom. Strain Rate = 1.11×10^{-4} sec^{-1}
Ave. Strain Rate = 9.12×10^{-5} sec^{-1}
Sample Diameter = 1.13"
Initial Length = 2.26"
Percent Sand (by Vol.) = 63.62
Degree Ice Saturation (%) = 98.27
Time to Failure = 350 sec

Strain (%)	Stress (psi)
0.001	46
0.001	113
0.021	266
0.046	431

SAMPLE NO. 36 (cont'd.)

0.076	586
0.121	741
0.169	868
0.255	1054
0.368	1186
0.506	1278
0.707	1360
0.907	1411
1.113	1463
1.482	1534
2.181	1645
2.682	1700
3.191	1711
3.836	1670
5.256	1514
6.757	1296
8.018	1128

SAMPLE NO. 37

Temperature = -6.08°C
Nom. Strain Rate = 1.11×10^{-4} sec^{-1}
Ave. Strain Rate = 8.62×10^{-5} sec^{-1}
Sample Diameter = 1.13"
Initial Length = 2.26"
Percent Sand (by Vol.) = 64.51
Degree Ice Saturation (%) = 98.60
Time to Failure = 331 sec

Strain (%)	Stress (psi)
0.003	64
0.010	137
0.015	218
0.032	343
0.058	468
0.088	599
0.123	728
0.145	817
0.179	867
0.208	946
0.279	1079
0.409	1221
0.603	1312
0.904	1406
1.785	1609
2.358	1691
2.852	1721
3.805	1647
5.129	1446
6.425	1202
8.172	916

Table A-1 (cont'd.)

SAMPLE NO. 38

Temperature = -6.05°C
Nom. Strain Rate = 1.11 x 10^{-4} sec^{-1}
Ave. Strain Rate = 8.66 x 10^{-5} sec^{-1}
Sample Diameter = 1.13"
Initial Length = 2.26"
Percent Sand (by Vol.) = 63.83
Degree Ice Saturation (%) = 98.36
Time to Failure = 345 sec

Strain (%)	Stress (psi)
0.025	103
0.041	262
0.069	405
0.122	620
0.158	765
0.205	876
0.259	1004
0.361	1147
0.612	1317
0.902	1416
1.302	1528
1.856	1641
2.387	1725
2.986	1757
3.715	1701
4.879	1544
6.000	1362
7.096	1212
8.615	1034

SAMPLE NO. 39

Temperature = -6.08°C
Nom. Strain Rate = 1.11 x 10^{-4} sec^{-1}
Ave. Strain Rate = 8.43 x 10^{-5} sec^{-1}
Sample Diameter = 1.13"
Initial Length = 2.26"
Percent Sand (by Vol.) = 63.45
Degree Ice Saturation (%) = 98.04
Time to Failure = 345 sec

Strain (%)	Stress (psi)
0.021	181
0.045	322
0.071	447
0.110	575
0.153	712
0.253	956
0.347	1118
0.549	1273
0.828	1383
1.313	1508
1.848	1622
2.369	1701
2.907	1745
3.819	1704
5.016	1556
6.026	1339
7.484	1125
8.765	851

SAMPLE NO. 40

Temperature = -6.03°C
Nom. Strain Rate = 1.11 x 10 sec
Ave. Strain Rate = 8.88 x 10 sec
Sample Diameter = 1.13"
Initial Length = 2.26"
Percent Sand (by Vol.) = 63.92
Degree Ice Saturation (%) = 99.15
Time to Failure = 354 sec

Strain (%)	Stress (psi)
0.035	143
0.084	268
0.142	408
0.167	541
0.225	683
0.285	814
0.351	910
0.455	1052
0.677	1188
1.003	1327
1.523	1481
2.236	1664
3.145	1778
4.134	1693
5.376	1493
6.579	1247
7.807	1007
8.862	827

Table A-1 (cont'd.)

SAMPLE NO. 41

Temperature = -6.06°C
Nom. Strain Rate = 1.19×10^{-4} sec^{-1}
Ave. Strain Rate = 9.42×10^{-5} sec^{-1}
Sample Diameter = 1.405"
Initial Length = 2.81"
Percent Sand (by Vol.) = 63.81
Degree Ice Saturation (%) = 99.71
Time to Failure = 347 sec

Strain (%)	Stress (psi)
0.012	154
0.040	299
0.075	448
0.125	598
0.167	748
0.203	856
0.344	1031
0.385	1193
0.522	1299
0.729	1386
1.157	1494
1.845	1647
2.627	1758
3.279	1778
4.347	1672
5.470	1501
6.693	1291
7.686	1123

SAMPLE NO. 42

Temperature = -6.10°C
Nom. Strain Rate = 1.19×10^{-4} sec^{-1}
Ave. Strain Rate = 9.02×10^{-5} sec^{-1}
Sample Diameter = 1.405"
Initial Length = 2.81"
Percent Sand (by Vol.) = 63.93
Degree Ice Saturation (%) = 97.32
Time to Failure = 320 sec

Strain (%)	Stress (psi)
0.019	122
0.047	268
0.087	412
0.125	566
0.172	713
0.218	856
0.341	1117
0.498	1284
0.696	1380

SAMPLE NO. 42 (cont'd.)

1.122	1476
1.602	1576
2.209	1659
2.886	1698
3.667	1653
4.513	1535
5.385	1436
6.213	1237
7.226	1064

SAMPLE NO. 43

Temperature = -6.06°C
Nom. Strain Rate = 1.19×10^{-4} sec^{-1}
Ave. Strain Rate = 9.13×10^{-5} sec^{-1}
Sample Diameter = 1.405"
Initial Length = 2.81"
Percent Sand (by Vol.) = 63.68
Degree Ice Saturation (%) = 98.19
Time to Failure = 335 sec

Strain (%)	Stress (psi)
0.018	129
0.051	270
0.083	412
0.125	566
0.167	719
0.214	863
0.239	936
0.328	1139
0.443	1301
0.579	1419
1.056	1533
1.597	1619
2.151	1673
3.059	1732
4.071	1640
5.256	1419
6.636	1148

Table A-1 (cont'd.)

SAMPLE NO. 44

Temperature = -6.06°C
Nom. Strain Rate = 1.19×10^{-4} sec^{-1}
Ave. Strain Rate = 9.59×10^{-5} sec^{-1}
Sample Diameter = 1.405"
Initial Length = 2.81"
Percent Sand (by Vol.) = 63.54
Degree Ice Saturation (%) = 97.03
Time to Failure = 343 sec

Strain (%)	Stress (psi)	Time (sec)
0.006	105	8
0.035	246	18
0.075	386	28
0.125	536	38
0.169	668	48
0.253	878	63
0.343	1076	78
0.419	1189	88
0.503	1274	98
0.703	1354	118
1.035	1419	148
1.490	1495	188
2.049	1587	238
2.639	1652	288
3.290	1678	343
3.957	1648	393
4.717	1549	453
5.476	1453	513
6.615	1316	603
7.941	1173	703

SAMPLE NO. 45

Temperature = -6.09°C
Nom. Strain Rate = 8.90×10^{-4} sec^{-1}
Ave. Strain Rate = 3.80×10^{-4} sec^{-1}
Sample Diameter = 1.405"
Initial Length = 2.81"
Percent Sand (by Vol.) = 64.07
Degree Ice Saturation (%) = 97.43
Time to Failure = 16.4 sec

Strain (%)	Stress (psi)	Time (sec)
0.019	157	1.4
0.035	275	2.4
0.055	400	3.4
0.077	531	4.4
0.096	659	5.4
0.120	800	6.4
0.147	927	7.4

SAMPLE NO. 45 (cont'd.)

0.209	1198	9.4
0.288	1449	11.4
0.337	1570	12.4
0.387	1659	13.4
0.453	1734	14.4
0.527	1771	15.4
0.623	1781	16.4
0.809	1747	18.4
1.353	1629	23.4
2.096	1511	31.4
3.278	1313	43.4
4.658	1111	55.4
6.386	899	73.4

SAMPLE NO. 46

Temperature = -6.09°C
Nom. Strain Rate = 1.04×10^{-4} sec^{-1}
Ave. Strain Rate = 8.62×10^{-5} sec^{-1}
Sample Diameter = 2.40"
Initial Length = 4.80"
Percent Sand (by Vol.) = 64.33
Degree Ice Saturation (%) = 98.15
Time to Failure = 368 sec

Strain (%)	Stress (psi)
0.001	66
0.027	177
0.040	294
0.056	416
0.078	557
0.105	696
0.133	845
0.175	981
0.229	1100
0.299	1195
0.389	1263
0.552	1324
0.813	1403
1.285	1501
1.807	1610
2.552	1721
3.170	1754
3.658	1733
4.483	1623
5.249	1497
6.225	1339
7.243	1182

Table A-1 (cont'd.)

SAMPLE NO. 47

Temperature = -6.06°C
Nom. Strain Rate = 1.04×10^{-4} sec^{-1}
Ave. Strain Rate = 8.71×10^{-4} sec^{-1}
Sample Diameter = 2.40"
Initial Length = 4.80"
Percent Sand (by Vol.) = 63.91
Degree Ice Saturation (%) = 98.13
Time to Failure = 354 sec

Strain (%)	Stress (psi)
0.008	50
0.010	114
0.018	183
0.024	254
0.032	329
0.046	443
0.062	577
0.093	756
0.122	889
0.161	1007
0.206	1126
0.287	1256
0.362	1326
0.497	1434
0.724	1483
0.957	1519
1.209	1561
1.518	1595
1.944	1653
2.513	1709
3.082	1731
3.788	1705
4.281	1639
5.906	1487
7.787	1298

SAMPLE NO. 48

Temperature = -6.09°C
Nom. Strain Rate = 1.04×10^{-2} sec^{-1}
Ave. Strain Rate = 8.72×10^{-5} sec^{-1}
Sample Diameter = 2.40"
Initial Length = 4.80"
Percent Sand (by Vol.) = 63.98
Degree Ice Saturation (%) = 97.57
Time to Failure = 395 sec

Strain (%)	Stress (psi)
0.019	76
0.034	176
0.054	280
0.071	398
0.089	532
0.121	756
0.157	895
0.199	1030
0.257	1142
0.325	1247
0.424	1316
0.602	1414
0.959	1481
1.374	1541
1.961	1636
2.560	1697
3.035	1708
3.443	1725
3.880	1661
4.829	1569
6.109	1410
7.990	1223

SAMPLE NO. 49

Temperature = -6.03°C
Nom. Strain Rate = 1.04×10^{-4} sec^{-1}
Ave. Strain Rate = 9.24×10^{-5} sec^{-1}
Sample Diameter = 2.40"
Initial Length = 4.80"
Percent Sand (by Vol.) = 63.99
Degree Ice Saturation (%) = 98.36
Time to Failure = 361 sec

Strain (%)	Stress (psi)
0.018	42
0.033	161
0.055	282
0.083	407
0.119	548
0.184	756
0.239	892
0.305	1014
0.381	1119
0.515	1243
0.661	1324
0.872	1374
1.124	1446
1.382	1488
1.653	1523
1.996	1570
2.384	1609

Table A-1 (cont'd.)

SAMPLE NO. 49 (cont'd.)

2.856	1633
3.337	1656
3.612	1621
4.641	1490
6.617	1310
7.697	1135

SAMPLE NO. 50

Temperature = -6.00°C
Nom. Strain Rate = 1.04×10^{-4} sec^{-1}
Ave. Strain Rate = 8.95×10^{-5} sec^{-1}
Sample Diameter = 2.40"
Initial Length = 4.80"
Percent Sand (by Vol.) = 63.86
Degree Ice Saturation (%) = 98.66
Time to Failure = 335 sec

Strain (%)	Stress (psi)
0.019	80
0.042	184
0.069	297
0.099	428
0.130	571
0.169	713
0.217	849
0.305	1034
0.421	1185
0.560	1286
0.713	1347
0.903	1410
1.106	1453
1.479	1520
1.936	1584
2.472	1640
2.998	1662
3.570	1615
4.680	1502
6.296	1321
7.542	1199

SAMPLE NO. 51

Temperature = -6.05°C
Nom. Strain Rate = 1.04×10^{-4} sec^{-1}
Ave. Strain Rate = 8.74×10^{-5} sec^{-1}
Sample Diameter = 2.40"
Initial Length = 4.80"
Percent Sand (by Vol.) = 64.05
Degree Ice Saturation (%) = 98.42
Time to Failure = 354 sec

SAMPLE NO. 51 (cont'd.)

Strain (%)	Stress (psi)
0.004	50
0.008	105
0.014	170
0.028	243
0.037	322
0.039	402
0.058	490
0.061	580
0.076	668
0.105	797
0.132	929
0.173	1041
0.226	1157
0.279	1259
0.349	1331
0.418	1410
0.588	1457
0.748	1497
1.041	1559
1.372	1593
1.592	1669
2.452	1724
3.095	1724
3.847	1661
4.182	1611
5.053	1553
8.171	1434

SAMPLE NO. 52

Temperature = -5.99°C
Nom. Strain Rate = 1.29×10^{-4} sec^{-1}
Ave. Strain Rate = 1.02×10^{-4} sec^{-1}
Sample Diameter = 1.94"
Initial Length = 3.88"
Percent Sand (by Vol.) = 64.23
Degree Ice Saturation (%) = 98.27
Time to Failure = 315 sec

Strain (%)	Stress (psi)
0.065	42
0.104	132
0.142	241
0.184	370
0.228	512
0.275	674
0.364	929
0.502	1127

Table A-1 (cont'd.)

SAMPLE NO. 52 (cont'd.)

0.711	1291
1.047	1367
1.465	1461
1.978	1559
2.416	1650
2.881	1677
3.218	1677
3.754	1592
4.002	1492
4.991	1255

SAMPLE NO. 53

Temperature = -6.03°C
Nom. Strain Rate = 1.29×10^{-4} sec^{-1}
Ave. Strain Rate = 1.04×10^{-4} sec^{-1}
Sample Diameter = 1.94"
Initial Length = 3.88"
Percent Sand (by Vol.) = 64.31
Degree Ice Saturation (%) = 98.33
Time to Failure = 270 sec

Strain (%)	Stress (psi)
0.034	127
0.061	277
0.096	437
0.140	578
0.176	794
0.236	978
0.305	1145
0.398	1280
0.516	1369
0.641	1424
0.787	1452
0.908	1475
1.139	1517
1.445	1557
1.878	1620
2.335	1652
2.817	1664
3.286	1631
3.835	1554
4.543	1397
4.894	1218
5.605	1012

SAMPLE NO. 54

Temperature = -6.06°C
Nom. Strain Rate = 1.29×10^{-4} sec^{-1}
Ave. Strain Rate = 1.04×10^{-4} sec^{-1}
Sample Diameter = 1.94"
Initial Length = 3.88"
Percent Sand (by Vol.) = 64.27
Degree Ice Saturation (%) = 96.11
Time to Failure = 296 sec

Strain (%)	Stress (psi)
0.035	132
0.062	274
0.098	431
0.133	601
0.174	789
0.229	973
0.296	1140
0.386	1275
0.490	1375
0.617	1439
0.731	1478
0.857	1511
1.041	1554
1.280	1590
1.526	1626
1.769	1671
2.020	1707
2.283	1738
2.696	1755
3.088	1753
3.641	1709
4.264	1610
4.785	1403
5.838	1134

SAMPLE NO. 55

Temperature = -6.16°C
Nom. Strain Rate = 1.04×10^{-4} sec^{-1}
Ave. Strain Rate = 1.08×10^{-4} sec^{-1}
Sample Diameter = 1.94"
Initial Length = 3.88"
Percent Sand (by Vol.) = 64.29
Degree Ice Saturation (%) = 99.41
Time to Failure = 333 sec

Strain (%)	Stress (psi)
0.049	101
0.082	195
0.119	342

Table A-1 (cont'd.)

SAMPLE NO. 55 (cont'd.)

0.159	512
0.212	697
0.308	954
0.433	1160
0.593	1291
0.779	1362
0.959	1414
1.142	1460
1.325	1501
1.561	1552
1.879	1619
1.898	1692
2.776	1759
3.226	1789
3.601	1796
4.129	1744
4.756	1633
4.983	1460
5.998	1142
7.023	797

SAMPLE NO. 56

Temperature = -6.16°C
Nom. Strain Rate = 1.04×10^{-4} sec^{-1}
Ave. Strain Rate = 1.10×10^{-4} sec^{-1}
Sample Diameter = 1.94"
Initial Length = 3.88"
Percent Sand (by Vol.) = 63.96
Degree Ice Saturation (%) = 98.04
Time to Failure = 331 sec

Strain (%)	Stress (psi)
0.090	130
0.115	243
0.149	403
0.200	586
0.288	853
0.364	1016
0.403	1085
0.450	1147
0.555	1252
0.676	1329
1.138	1451
1.451	1514
1.799	1592
2.155	1669
2.775	1762
3.290	1802
3.641	1798

SAMPLE NO. 56 (cont'd.)

4.230	1766
4.429	1689
5.147	1542
6.002	1306
6.804	1068

SAMPLE NO. 57

Temperature = -10.05°C
Nom. Strain Rate = 1.78×10^{-3} sec^{-1}
Ave. Strain Rate = 7.20×10^{-4} sec^{-1}
Sample Diameter = 1.405"
Initial Length = 2.81"
Percent Sand (by Vol.) = 64.03
Degree Ice Saturation (%) = 97.41
Time to Failure = 9.9 sec

Strain (%)	Stress (psi)
0.003	66
0.021	207
0.056	448
0.086	611
0.141	883
0.203	1185
0.264	1495
0.336	1800
0.422	2092
0.514	2325
0.645	2456
0.713	2480
0.849	2400
1.139	2064
1.618	1600
2.041	1418
2.449	1287
2.873	1182
3.671	999
4.633	855
6.035	710
7.622	592

Table A-1 (cont'd.)

SAMPLE NO. 58

Temperature = -10.05°C
Nom. Strain Rate = 5.93 x 10^{-4} sec^{-1}
Ave. Strain Rate = 2.52 x 10^{-4} sec^{-1}
Sample Diameter = 1.405"
Initial Length = 2.81"
Percent Sand (by Vol.) = 64.12
Degree Ice Saturation (%) = 96.69
Time to Failure = 28.8 sec

Strain (%)	Stress (psi)
0.004	57
0.011	224
0.037	388
0.056	544
0.094	701
0.131	870
0.175	1071
0.219	1265
0.269	1475
0.360	1659
0.384	1837
0.452	1995
0.539	2114
0.627	2195
0.727	2231
0.914	2202
1.117	2089
1.371	1952
1.830	1779
2.586	1553
3.686	1265
4.971	998
6.724	741

SAMPLE NO. 59

Temperature = -10.05°C
Nom. Strain Rate = 1.19 x 10^{-4} sec^{-1}
Ave. Strain Rate = 9.06 x 10^{-5} sec^{-1}
Sample Diameter = 1.405"
Initial Length = 2.81"
Percent Sand (by Vol.) = 64.17
Degree Ice Satruation (%) = 97.39
Time to Failure = 324 sec

Strain (%)	Stress (psi)
0.006	112
0.022	259
0.049	413

SAMPLE NO. 59 (cont'd.)

0.091	569
0.124	735
0.168	904
0.211	1077
0.266	1252
0.359	1474
0.430	1607
0.511	1714
0.603	1795
0.856	1892
1.137	1918
1.603	1959
2.054	2019
2.516	2060
2.945	2063
3.381	2011
4.116	1879
4.894	1626
5.688	1401
6.592	1196

SAMPLE NO. 60

Temperature = -10.05°C
Nom. Strain Rate = 2.37 x 10^{-5} sec^{-1}
Ave. Strain Rate = 2.15 x 10^{-5} sec^{-1}
Sample Diameter = 1.405"
Initial Length = 2.81"
Percent Sand (by Vol.) = 63.56
Degree Ice Saturation (%) = 97.06
Time to Failure = 1914 sec

Strain (%)	Stress (psi)
0.010	43
0.024	114
0.029	196
0.050	277
0.075	349
0.102	440
0.132	537
0.179	652
0.253	820
0.348	992
0.452	1128
0.612	1263
0.869	1397
1.199	1518
1.613	1638
1.974	1751

Table A-1 (cont'd.)

SAMPLE NO. 60 (cont'd.)

2.325	1864
2.784	2004
3.147	2090
3.764	2163
4.113	2210
4.244	2213
4.786	2210
5.183	2167
5.582	2116
6.019	2052
6.517	1951
6.993	1882

SAMPLE NO. 61

Temperature = -10.05°C
Nom. Strain Rate = 4.75×10^{-6} sec^{-1}
Ave. Strain Rate = 4.35×10^{-6} sec^{-1}
Sample Diameter = 1.405"
Initial Length = 2.81"
Percent Sand (by Vol.) = 64.18
Degree Ice Saturation (%) = 97.40
Time to Failure = 12,204 sec

Strain (%)	Stress (psi)
0.007	44
0.013	109
0.029	172
0.048	233
0.071	292
0.109	380
0.132	441
0.161	480
0.188	505
0.239	584
0.404	740
0.722	900
1.480	1179
2.709	1688
4.021	2053
5.313	2177
6.771	2012
7.897	1817

SAMPLE NO. 62

Temperature = -10.05°C
Nom. Strain Rate = 1.42×10^{-6} sec^{-1}
Ave. Strain Rate = 1.28×10^{-6} sec^{-1}
Sample Diameter = 1.405"
Initial Length = 2.81"

SAMPLE NO. 62 (cont'd.)

Percent Sand (by Vol.) = 64.18
Degree Ice Saturation (%) = 97.05
Time to Failure = 37,920 sec

Strain (%)	Stress (psi)
0.008	60
0.019	95
0.031	154
0.041	197
0.062	240
0.083	284
0.105	325
0.126	366
0.144	406
0.180	442
0.329	581
0.613	710
1.425	1016
2.531	1466
3.898	1828
4.843	1894
6.261	1759
7.769	1500

SAMPLE NO. 63

Temperature = -10.00°C
Nom. Strain Rate = 5.69×10^{-7} sec^{-1}
Ave. Strain Rate = 4.82×10^{-7} sec^{-1}
Sample Diameter = 1.405"
Initial Length = 2.81"
Percent Sand (by Vol.) = 63.60
Degree Ice Saturation (%) = 96.96
Time to Failure = 91,680 sec

Strain (%)	Stress (psi)
0.016	19
0.024	47
0.049	93
0.071	134
0.099	174
0.129	214
0.169	281
0.223	336
0.379	440
0.616	531
0.992	672
1.489	870
2.259	1151
3.144	1414

Table A-1 (cont'd.)

SAMPLE NO. 63 (cont'd.)

4.419	1542
5.136	1488

SAMPLE NO. 64

Temperature = -10.05°C
Nom. Strain Rate = 2.14×10^{-6} sec^{-1}
Ave. Strain Rate = 1.84×10^{-6} sec^{-1}
Sample Diameter = 1.405"
Initial Length = 2.81"
Percent Sand (by Vol.) = 64.10
Degree Ice Saturation (%) = 98.90
Time to Failure = 25,680 sec

Strain (%)	Stress (psi)
0.007	36
0.013	116
0.027	188
0.052	259
0.190	294
0.202	358
0.251	415
0.283	466
0.334	504
0.439	574
0.705	699
1.275	942
2.361	1400
3.674	1832
4.728	1916
6.151	1743
7.449	1517

SAMPLE NO. 65

Temperature = -10.00°C
Nom. Strain Rate = 1.07×10^{-5} sec^{-1}
Ave. Strain Rate = 8.77×10^{-6} sec^{-1}
Sample Diameter = 1.405"
Initial Length = 2.81"
Percent Sand (by Vol.) = 64.10
Degree Ice Saturation = 98.06
Time to Failure = 4872 sec

Strain (%)	Stress (psi)
0.001	92
0.006	174
0.018	260
0.031	339
0.076	506

SAMPLE NO. 65 (cont'd.)

0.149	652
0.178	722
0.216	792
0.378	1014
0.575	1165
0.965	1351
1.795	1685
2.966	2051
4.275	2188
6.044	2004

SAMPLE NO. 66

Temperature = -10.09°C
Nom. Strain Rate = 5.34×10^{-5} sec^{-1}
Ave. Strain Rate = 4.18×10^{-5} sec^{-1}
Sample Diameter = 1.405"
Initial Length = 2.81"
Percent Sand (by Vol.) = 63.28
Degree Ice Saturation (%) = 99.43
Time to Failure = 322 sec

Strain (%)	Stress (psi)
0.003	36
0.013	138
0.025	236
0.047	338
0.068	442
0.123	649
0.179	873
0.255	1092
0.343	1296
0.564	1547
0.845	1669
1.396	1819
2.349	2044
3.437	2170
5.222	2003
7.244	1663

Table A-1 (cont'd.)

SAMPLE NO. 67

Temperature = -10.06°C
Nom. Strain Rate = 2.67 x 10^{-4} sec^{-1}
Ave. Strain Rate = 1.30 x 10^{-4} sec^{-1}
Sample Diameter = 1.405"
Initial Length = 2.81"
Percent Sand (by Vol.) = 63.08
Degree Ice Saturation (%) = 99.30
Time to Failure = 67.40 sec

Strain (%)	Stress (psi)
0.003	63
0.014	137
0.020	214
0.033	292
0.047	369
0.064	447
0.097	481
0.116	675
0.141	783
0.196	987
0.251	1188
0.378	1569
0.452	1740
0.518	1841
0.614	1947
0.873	2038
1.777	1906
4.096	1277

SAMPLE NO. 68

Temperature = -10.00°C
Nom. Strain Rate = 1.34 x 10^{-3} sec^{-1}
Ave. Strain Rate = 5.04 x 10^{-4} sec^{-1}
Sample Diameter = 1.405"
Initial Length = 2.81"
Percent Sand (by Vol.) = 64.00
Degree Ice Saturation (%) = 96.99
Time to Failure = 13 sec

Strain (%)	Stress (psi)
0.019	61
0.028	175
0.036	306
0.053	442
0.068	570
0.085	717
0.102	860
0.163	1202
0.231	1584

SAMPLE NO. 68 (cont'd.)

0.309	1902
0.379	2169
0.479	2403
0.655	2500
1.063	2173
1.553	1753
2.435	1406

SAMPLE NO. 69

Temperature = -15.00°C
Nom. Strain Rate = 1.34 x 10^{-3} sec^{-1}
Ave. Strain Rate = 4.75 x 10^{-4} sec^{-1}
Sample Diameter = 1.405"
Initial Length = 2.81"
Percent Sand (by Vol.) = 63.57
Degree Ice Saturation (%) = 98.96
Time to Failure = 13.60 sec

Strain (%)	Stress (psi)
0.003	68
0.004	190
0.015	324
0.023	415
0.042	538
0.059	682
0.086	870
0.112	1062
0.146	1253
0.189	1489
0.266	1897
0.355	2316
0.468	2626
0.646	2863
1.008	2384
1.512	1703
2.011	1355
3.237	954

SAMPLE NO. 70

Temperature = -15.00°C
Nom. Strain Rate = 5.93 x 10^{-4} sec^{-1}
Ave. Strain Rate = 1.95 x 10^{-4} sec^{-1}
Sample Diameter = 1.405"
Initial Length = 2.81"
Percent Sand (by Vol.) = 64.45
Degree Ice Saturation (%) = 98.39
Time to Failure = 23 sec

Table A-1 (cont'd.)

SAMPLE NO. 70 (cont'd.)

Strain (%)	Stress (psi)
0.021	73
0.029	163
0.037	259
0.044	364
0.053	474
0.064	576
0.073	691
0.085	809
0.095	921
0.107	1039
0.119	1158
0.139	1279
0.152	1394
0.187	1636
0.230	1878
0.272	2101
0.321	2317
0.383	2494
0.545	2700
1.047	2180
2.291	1514

SAMPLE NO. 71

Temperature = -15.00°C
Nom. Strain Rate = 2.67×10^{-4} sec^{-1}
Ave. Strain Rate = 1.14×10^{-4} sec^{-1}
Sample Diameter = 1.405"
Initial Length = 2.81"
Percent Sand (by Vol.) = 64.80
Degree Ice Saturation (%) = 97.66
Time to Failure = 67 sec

Strain (%)	Stress (psi)
0.005	53
0.008	126
0.013	205
0.019	289
0.031	374
0.036	458
0.053	538
0.066	624
0.082	713
0.098	800
0.123	937
0.171	1169
0.224	1386
0.276	1616

SAMPLE NO. 71 (cont'd.)

0.339	1838
0.422	2060
0.565	2343
0.765	2453
1.439	2083
2.820	1779

SAMPLE NO. 72

Temperature = -15.00°C
Nom. Strain Rate = 7.12×10^{-5} sec^{-1}
Ave. Strain Rate = 5.32×10^{-5} sec^{-1}
Sample Diameter = 1.405"
Initial Length = 2.81"
Percent Sand (by Vol.) = 64.70
Degree Ice Saturation (%) = 97.00
Time to Failure = 549 sec

Strain (%)	Stress (psi)
0.004	64
0.011	163
0.018	266
0.038	374
0.049	484
0.071	582
0.076	633
0.088	694
0.112	803
0.128	860
0.152	975
0.176	1093
0.224	1259
0.329	1545
0.458	1745
0.733	1990
1.437	2102
2.248	2266
2.920	2350
4.295	2102
6.599	1435

SAMPLE NO. 73

Temperature = -15.00°C
Nom. Strain Rate = 5.34×10^{-5} sec^{-1}
Ave. Strain Rate = 4.02×10^{-5} sec^{-1}
Sample Diameter = 1.405"
Initial Length = 2.81"
Percent Sand (by Vol.) = 63.81
Degree Ice Saturation (%) = 97.22
Time to Failure = 789 sec

Table A-1 (cont'd.)

SAMPLE NO. 73 (cont'd.)

Strain (%)	Stress (psi)
0.005	81
0.012	152
0.017	233
0.027	315
0.036	402
0.045	485
0.068	608
0.091	732
0.117	857
0.142	994
0.197	1198
0.271	1424
0.381	1646
0.483	1791
0.745	1951
1.446	2108
2.201	2273
3.171	2362
4.338	2205
6.096	1732

SAMPLE NO. 74

Temperature = -14.98°C
Nom. Strain Rate = 3.56×10^{-5} sec^{-1}
Ave. Strain Rate = 2.86×10^{-5} sec^{-1}
Sample Diameter = 1.405"
Initial Length = 2.81"
Percent Sand (by Vol.) = 64.18
Degree Ice Saturation (%) = 97.88
Time to Failure = 1297 sec

Strain (%)	Stress (psi)
0.004	60
0.003	132
0.013	210
0.015	292
0.028	374
0.040	458
0.052	543
0.073	659
0.097	771
0.122	882
0.150	994
0.179	1093
0.407	1550
0.963	1877
1.786	2151

SAMPLE NO. 74 (cont'd.)

2.772	2422
3.703	2522
4.803	2378
6.149	2055

SAMPLE NO. 75

Temperature = -15.00°C
Nom. Strain Rate = 2.38×10^{-5} sec^{-1}
Ave. Strain Rate = 1.79×10^{-5} sec^{-1}
Sample Diameter = 1.405"
Initial Length = 2.81"
Percent Sand (by Vol.) = 64.20
Degree Ice Saturation (%) = 97.22
Time to Failure = 1971 sec

Strain (%)	Stress (psi)
0.008	95
0.018	200
0.031	310
0.046	422
0.057	529
0.089	707
0.127	873
0.165	1029
0.214	1182
0.307	1411
0.426	1575
0.559	1681
0.880	1847
1.352	2028
1.881	2218
2.393	2388
3.004	2503
3.530	2558
4.249	2477
5.094	2285
5.907	2049
7.267	1781

Table A-1 (cont'd.)

SAMPLE NO. 76

Temperature = -15.00°C
Nom. Strain Rate = 1.42×10^{-5} sec^{-1}
Ave. Strain Rate = 1.15×10^{-5} sec^{-1}
Sample Diameter = 1.405"
Initial Length = 2.81"
Percent Sand (by Vol.) = 63.96
Degree Ice Saturation (%) = 98.51
Time to Failure = 3345 sec

Strain (%)	Stress (psi)
0.004	64
0.005	147
0.013	242
0.024	337
0.036	433
0.055	526
0.070	617
0.094	707
0.121	796
0.148	882
0.263	1175
0.758	1582
1.763	1950
2.885	2332
3.878	2462
4.479	2428
5.164	2326

SAMPLE NO. 77

Temperature = -14.98°C
Nom. Strain Rate = 2.14×10^{-6} sec^{-1}
Ave. Strain Rate = 1.82×10^{-6} sec^{-1}
Sample Diameter = 1.405"
Initial Length = 2.81"
Percent Sand (by Vol.) = 64.26
Degree Ice Saturation (%) = 98.98
Time to Failure = 25,260 sec

Strain (%)	Stress (psi)
0.001	83
0.009	173
0.022	263
0.042	349
0.062	433
0.090	513
0.142	550
0.189	620
0.295	683
0.356	798

SAMPLE NO. 77 (cont'd.)

0.459	880
0.741	1030
1.239	1240
2.003	1581
2.428	1781
2.838	1948
3.485	2151
4.088	2266
4.607	2297
5.038	2280
5.589	2207
6.162	2103
6.872	1950

SAMPLE NO. 78

Temperature = -15.00°C
Nom. Strain Rate = 1.07×10^{-5} sec^{-1}
Ave. Strain Rate = 8.53×10^{-6} sec^{-1}
Sample Diameter = 1.405"
Initial Length = 2.81"
Percent Sand (by Vol.) = 64.02
Degree Ice Saturation (%) = 96.16
Time to Failure = 4452 sec

Strain (%)	Stress (psi)
0.013	336
0.032	429
0.052	518
0.071	614
0.093	707
0.149	873
0.209	1029
0.283	1172
0.411	1320
0.556	1427
0.818	1549
1.260	1701
1.645	1845
2.209	2048
2.733	2199
3.318	2303
3.799	2341
4.324	2322
5.256	2184
6.156	2001
7.567	1769

Table A-1 (cont'd.)

SAMPLE NO. 79

Temperature = -15.00°C
Nom. Strain Rate = 1.42 x 10^{-6} sec^{-1}
Ave. Strain Rate = 1.21 x 10^{-6} sec^{-1}
Sample Diameter = 1.405"
Initial Length = 2.81"
Percent Sand (by Vol.) = 64.25
Degree Ice Saturation (%) = 98.98
Time to Failure - 34,080 sec

Strain (%)	Stress (psi)
0.002	207
0.027	311
0.053	417
0.082	517
0.106	565
0.336	811
0.403	874
0.505	962
0.628	1031
0.770	1099
1.015	1242
1.384	1439
1.810	1635
2.272	1833
2.775	2005
3.321	2124
3.781	2181
4.115	2198
4.697	2173
5.383	2060
6.322	1872
7.488	1659

SAMPLE NO. 80

Temperature = -14.98°C
Nom. Strain Rate = 5.69 x 10^{-7} sec^{-1}
Ave. Strain Rate = 4.83 x 10^{-7} sec^{-1}
Sample Diameter = 1.405"
Initial Length = 2.81"
Percent Sand (by Vol.) = 64.85
Degree Ice Saturation (%) = 97.37
Time to Failure = 90,900 sec

Strain (%)	Stress (psi)
0.003	68
0.004	96
0.009	151
0.053	192
0.066	237

SAMPLE NO. 80 (cont'd.)

0.071	275
0.073	333
0.104	390
0.157	499
0.222	588
0.483	752
0.858	908
1.335	1144
1.829	1389
2.308	1608
2.839	1779
3.382	1930
3.856	2019
4.394	2051
4.848	2010
5.437	1926
6.067	1801
6.699	1684
7.540	1539

SAMPLE NO. 81

Temperature = -14.98°C
Nom. Strain Rate = 4.75 x 10^{-6} sec^{-1}
Ave. Strain Rate = 3.77 x 10^{-6} sec^{-1}
Sample Diameter = 1.405"
Initial Length = 2.81"
Percent Sand (by Vol.) = 63.56
Degree Ice Saturation (%) = 98.77
Time to Failure = 9240 sec

Strain (%)	Stress (psi)
0.005	54
0.015	129
0.016	214
0.025	297
0.045	416
0.076	538
0.108	652
0.192	761
0.235	875
0.279	977
0.343	1072
0.455	1237
0.674	1438
0.954	1598
1.273	1751
1.789	1968
2.343	2176
2.742	2279

Table A-1 (cont'd.)

SAMPLE NO. 81 (cont'd.)

3.126	2345
3.479	2361
4.081	2322
4.750	2196
5.424	2029
6.518	1790

SAMPLE NO. 82

Temperature = -14.96°C
Nom. Strain Rate = 1.19×10^{-4} sec^{-1}
Ave. Strain Rate = 8.34×10^{-5} sec^{-1}
Sample Diameter = 1.405"
Initial Length = 2.81"
Percent Sand (by Vol.) = 64.10
Degree Ice Saturation (%) = 97.30
Time to Failure = 307 sec

Strain (%)	Stress (psi)	Δ Vol. (cm^3)
0.039	274	-0.01
0.064	579	-0.02
0.101	873	-0.03
0.155	1176	-0.06
0.220	1482	-0.09
0.302	1743	-0.09
0.409	1951	-0.11
0.528	2109	-0.11
0.678	2207	-0.08
0.839	2235	-0.04
1.021	2237	-0.01
1.291	2231	+0.05
1.366	2230	+0.12
1.543	2232	+0.18
1.710	2241	+0.24
1.885	2262	+0.30
2.219	2286	+0.43
2.561	2309	+0.60
2.930	2269	+0.78
3.714	2115	+1.02
4.507	1896	+1.49
6.470	1426	+2.84

SAMPLE NO. 83

Temperature = -14.96°C
Nom. Strain Rate = 7.12×10^{-6} sec^{-1}
Ave. Strain Rate = 5.63×10^{-6} sec^{-1}
Sample Diameter = 1.405"
Initial Length = 2.81"
Percent Sand (by Vol.) = 64.32
Degree Ice Saturation = 96.40

SAMPLE NO. 83 (cont'd.)

Time to Failure = 7200 sec

Strain (%)	Stress (psi)	Δ Vol. (cm^3)
0.035	246	-0.01
0.073	495	-0.01
0.166	828	-0.02
0.298	1105	-0.03
0.438	1282	-0.02
0.572	1388	-0.02
0.759	1481	-0.01
0.936	1567	+0.01
1.128	1646	+0.04
1.323	1725	+0.06
1.553	1828	+0.08
1.655	1920	+0.10
1.907	1998	+0.12
2.433	2206	+0.18
2.926	2381	+0.30
3.299	2458	+0.40
4.054	2550	---
4.675	2509	+0.79
5.363	2376	+1.25
6.707	2079	+1.85

SAMPLE NO. 84

Temperature = -5.96°C
Nom. Strain Rate = 1.19×10^{-4} sec^{-1}
Ave. Strain Rate = 9.64×10^{-5} sec^{-1}
Sample Diameter = 1.405"
Initial Length = 2.81"
Percent Sand (by Vol.) = 63.89
Degree Ice Saturation (%) = 96.69
Time to Failure = 330 sec

Strain (%)	Stress (psi)	Δ Vol. (cm^3)
0.003	73	-0.01
0.016	220	-0.01
0.053	509	-0.02
0.107	752	-0.04
0.191	994	-0.05
0.304	1178	-0.06
0.440	1294	-0.04
0.586	1362	-0.02
0.739	1430	+0.01
0.897	1479	+0.03
1.053	1527	+0.06
1.212	1569	+0.09
1.418	1622	+0.13
1.736	1705	+0.20

Table A-1 (cont'd.)

SAMPLE NO. 84 (cont'd.)

2.055	1775	+0.29
2.394	1831	+0.40
2.744	1875	+0.50
3.199	1890	+0.64
3.556	1877	+0.79
4.274	1808	+1.19
5.053	1702	+1.64
5.948	1566	+2.22
6.557	1484	+2.58

SAMPLE NO. 85

Temperature = -5.95°C
Nom. Strain Rate = 7.12×10^{-6} sec^{-1}
Ave. Strain Rate = 6.10×10^{-6} sec^{-1}
Sample Diameter = 1.405"
Initial Length = 2.81"
Percent Sand (by Vol.) = 64.41
Degree Ice Saturation (%) = 96.39
Time to Failure = 7380 sec

Strain (%)	Stress (psi)	Δ Vol. (cm^3)
0.037	294	+0.03
0.121	508	+0.07
0.269	610	+0.10
0.434	708	+0.13
0.613	780	+0.15
0.787	855	+0.17
0.976	932	+0.19
1.166	1006	+0.19
1.350	1064	+0.20
1.605	1153	+0.21
1.748	1208	+0.22
1.927	1275	+0.23
2.198	1353	+0.24
2.725	1483	+0.27
2.997	1553	+0.30
3.178	1606	+0.32
3.579	1686	+0.40
4.506	1749	+0.83
5.296	1704	+1.46
6.456	1539	+2.32
7.218	1426	+2.84

SAMPLE NO. 86

Temperature = -5.95°C
Nom. Strain Rate = 9.94×10^{-7} sec^{-1}
Ave. Strain Rate = 8.12×10^{-7} sec^{-1}
Sample Diameter = 1.405"
Initial Length = 2.81"
Percent Sand (by Vol.) = 64.16
Degree Ice Saturation (%) = 99.69
Time to Failure = 53,340 sec

Strain (%)	Stress (psi)	Δ Vol. (cm^3)
0.002	14	-0.01
0.004	33	-0.01
0.005	56	-0.01
0.008	91	-0.01
0.022	168	-0.01
0.093	292	+0.01
0.184	346	+0.01
0.401	415	+0.02
0.517	446	+0.03
0.770	524	+0.07
0.914	574	+0.07
1.051	615	+0.08
1.149	652	+0.08
1.331	698	+0.11
1.690	828	+0.15
1.797	871	+0.17
2.024	929	+0.19
2.096	953	+0.19
3.182	1259	+0.30
4.433	1426	+0.52
5.635	1378	+1.12
6.354	1307	+1.61
7.341	1187	+2.30

SAMPLE NO. 87

Temperature = -2.03°C
Nom. Strain Rate = 1.19×10^{-4} sec^{-1}
Ave. Strain Rate = 9.42×10^{-5} sec^{-1}
Sample Diameter = 1.405"
Initial Length = 2.81"
Percent Sand (by Vol.) = 64.22
Degree Ice Saturation (%) = 96.13
Time to Failure = 351 sec

Strain (%)	Stress (psi)	Δ Vol. (cm^3)
0.033	101	-0.01
0.096	303	-0.01
0.154	479	-0.01

Table A-1 (cont'd.)

SAMPLE NO. 87 (cont'd.)

0.241	696	-0.02
0.336	839	-0.01
0.468	959	-0.01
0.607	1018	+0.01
0.745	1058	+0.04
1.037	1119	+0.10
1.308	1166	+0.15
1.691	1221	+0.26
2.033	1252	+0.36
2.377	1269	+0.47
2.729	1296	+0.60
3.063	1316	+0.72
3.306	1319	---
3.437	1317	+0.88
3.830	1306	+1.06
4.169	1289	+1.26
4.907	1218	+1.70
5.305	1176	+1.93
5.663	1148	+2.18
6.440	1066	+2.87

SAMPLE NO. 88

Temperature = -2.02°C
Nom. Strain Rate = 7.12 x 10 sec
Ave. Strain Rate = 6.19 x 10 sec
Sample Diameter = 1.405"
Initial Length = 2.81"
Percent Sand (by Vol.) = 64.05
Degree Ice Saturation (%) = 98.30
Time to Failure = 7248 sec

Strain (%)	Stress (psi)	Δ Vol. (cm^3)
0.031	88	-0.01
0.082	199	-0.01
0.245	342	+0.01
0.394	411	+0.03
0.589	468	+0.03
0.766	527	+0.05
0.949	590	+0.05
1.133	652	+0.07
1.346	733	+0.11
1.472	779	+0.12
1.661	834	+0.14
1.860	896	+0.16
2.049	950	+0.19
2.230	1002	+0.22
2.430	1056	+0.25
2.819	1161	+0.32
3.232	1233	+0.43

SAMPLE NO. 88 (cont'd.)

3.609	1284	+0.55
4.054	1315	+0.70
4.483	1321	+0.88
4.897	1297	+1.10
6.411	1148	+1.93
6.734	1111	+2.14

SAMPLE NO. 89

Temperature = -2.02°C
Nom. Strain Rate = 9.94 x 10^{-7} sec^{-1}
Ave. Strain Rate = 8.74 x 10^{-7} sec^{-1}
Sample Diameter = 1.405"
Initial Length = 2.81"
Percent Sance (by Vol.) = 64.10
Degree Ice Saturation (%) = 98.90
Time to Failure = 98.90

Strain (%)	Stress (psi)	Δ Vol. (cm^3)
0.019	29	-0.01
0.035	50	-0.01
0.055	67	-0.01
0.069	82	-0.01
0.104	107	+0.01
0.236	164	+0.02
0.366	199	+0.03
0.519	232	+0.03
0.669	265	+0.07
0.823	298	+0.08
1.023	343	+0.12
1.231	388	+0.13
1.456	437	+0.18
1.706	456	+0.21
1.796	481	+0.22
2.163	548	+0.29
2.586	614	+0.40
3.213	688	+0.58
3.807	730	+0.80
4.311	738	+1.02
4.968	718	+1.37
6.493	638	+2.31
7.569	562	+3.05

Table A-1 (cont'd.)

SAMPLE NO. 90

Temperature = -2.02°C
Nom. Strain Rate = 3.56×10^{-6} sec^{-1}
Ave. Strain Rate = 3.02×10^{-6} sec^{-1}
Sample Diameter = 1.405"
Initial Length = 2.81"
Percent Sand (by Vol.) = 64.92
Degree Ice Saturation (%) = 96.20
Time to Failure = 13,380 sec

Strain (%)	Stress (psi)
0.007	38
0.018	70
0.029	104
0.052	131
0.067	159
0.095	183
0.136	219
0.161	253
0.303	294
0.444	337
0.669	391
0.925	476
1.169	563
1.531	672
2.065	825
2.562	967
3.147	1085
3.645	1142
4.035	1161
4.597	1155
5.293	1116
6.259	1020
6.998	941
7.718	868

Table A-2: Constant Stress Uniaxial Compression Creep Test Data

SAMPLE NO. 1c

Stress = 1350 psi
Temperature = -6.10°C
Sample Diameter = 1.13"
Initial Length = 2.26"
Percent Sand (by Vol.) = 63.69
Degree Ice Saturation (%) = 98.22

Strain (%)	Time (min)
0.876	1.00
1.239	2.00
1.489	3.00
1.702	4.00
1.845	5.00
1.987	6.00
2.194	8.00
2.358	10.00
2.643	12.00
2.928	17.00
3.184	22.00
3.384	27.00
3.711	37.00
4.039	47.00
4.324	57.00
4.595	67.00
4.922	87.00
5.236	97.00
6.048	107.00
6.361	117.00
6.789	127.00
7.245	137.00
7.815	147.00
8.580	157.00
9.496	166.33

SAMPLE NO. 2c

Stress = 1350 psi
Temperature = -6.03°C
Sample Diameter = 1.13"
Initial Length = 2.26"
Percent Sand (by Vol.) = 63.08
Degree Ice Saturation (%) = 97.47

Strain (%)	Time (min)
0.491	0.13
0.783	0.50
1.118	1.00
1.524	2.00
1.795	3.00
2.173	5.00
2.629	8.00
3.027	11.00
3.426	16.00
3.783	21.00
4.096	26.00
4.395	31.00
4.851	36.00
5.393	46.00
5.677	51.00
6.076	56.00
6.931	66.00
7.729	76.00
8.613	86.00
9.354	96.00
9.553	106.00
10.978	114.67

SAMPLE NO. 3c

Stress = 1140 psi
Temperature = -6.08°C
Sample Diameter = 1.13"
Initial Length = 2.26"
Percent Sand (by Vol.) = 63.62
Degree Ice Saturation (%) = 97.30

Strain (%)	Time (min)	Δ Vol. (cm^3)
0.000	0.00	+0.00
0.119	1.00	+0.01
0.283	2.00	+0.01
0.639	5.00	+0.02
1.024	11.00	+0.03
1.388	20.00	+0.04
1.644	30.00	+0.06
1.794	39.00	+0.06
2.029	59.00	+0.07
2.199	79.00	+0.07
2.392	99.00	+0.09
2.663	129.00	+0.11
2.833	159.00	+0.13
2.948	189.00	+0.15
3.048	219.00	+0.16
3.233	249.00	+0.18
3.318	279.00	+0.18
3.461	309.00	+0.18
3.660	339.00	+0.23

Table A-2 (cont'd.)

SAMPLE NO. 4c

Stress = 1503 psi
Temperature = -6.10°C
Sample Diameter = 1.13"
Initial Length = 2.26"
Percent Sand (by Vol.) = 63.74
Degree Ice Saturation (%) = 97.30

Strain (%)	Time (min)
0.466	0.167
0.922	0.333
1.777	0.399
2.169	0.499
2.497	0.599
2.604	0.799
3.173	0.999
3.601	1.199
4.028	1.399
4.684	1.599
4.969	1.799
5.325	1.999
5.667	2.199
7.020	2.332
7.875	2.399

SAMPLE NO. 5c

Stress = 1244 psi
Temperature = -6.10°C
Sample Diameter = 1.13"
Initial Length = 2.26"
Percent Sand (by Vol.) = 63.58
Degree Ice Saturation (%) = 96.87

Strain (%)	Time (min)	Δ Vol. (cm^3)
0.068	0.00	---
0.417	0.50	-0.03
0.538	1.00	-0.01
0.730	2.00	-0.01
1.008	4.00	+0.01
1.464	9.00	+0.04
1.806	15.00	+0.05
2.148	25.00	+0.09
2.476	35.00	+0.12
2.689	45.00	+0.13
2.903	60.00	+0.15
3.159	80.00	+0.18
3.501	110.00	+0.22
3.786	140.00	---
3.915	160.00	+0.32

SAMPLE NO. 5c (cont'd.)

4.099	185.00	---
4.428	215.00	+0.41
4.641	236.00	---
5.083	290.00	+0.56
5.781	327.00	---
6.152	357.00	+0.71
6.519	387.00	---
8.431	500.00	+1.26
10.141	557.00	+1.66

SAMPLE NO. 6c

Stress = 1296 psi
Temperature = -6.03°C
Sample Diameter = 1.13"
Initial Length = 2.26"
Percent Sand (by Vol.) = 63.57
Degree Ice Saturation (%) = 97.16

Strain (%)	Time (min)	Δ Vol. (cm^3)
0.022	0.00	---
0.485	1.00	+0.04
0.799	2.00	+0.05
1.176	4.00	+0.08
1.561	7.00	+0.09
1.832	10.00	+0.13
2.152	15.00	+0.17
2.437	20.00	+0.19
2.822	30.00	+0.24
3.121	40.00	+0.27
3.363	50.00	+0.32
3.691	65.00	+0.38
4.005	80.00	+0.44
4.446	100.00	+0.53
4.973	120.00	+0.63
5.439	140.00	+0.73
5.999	160.00	+0.85
6.655	180.00	+1.00
7.481	200.00	+1.15
8.564	220.00	+1.37
10.160	237.33	+1.58

Table A-2 (cont'd.)

SAMPLE NO. 7c

Stress = 1100 psi
Temperature = -6.03°C
Sample Diameter = 1.13"
Initial Length = 2.26"
Percent Sand (by Vol.) = 63.89
Degree Ice Saturation (%) = 98.36

Strain (%)	Time (min)
0.091	0.00
0.454	2.00
0.896	7.00
1.380	17.00
1.815	37.00
2.142	67.00
2.370	97.00
2.598	137.00
2.698	160.00
3.068	249.00
3.239	300.00
3.453	359.00
3.667	411.00
3.852	472.00
4.094	533.00
4.237	583.00
4.365	615.00
4.507	667.00
5.030	734.00
5.092	806.00
5.319	865.00
5.576	923.00
5.804	975.00
6.231	1033.00
6.601	1069.00

Table A-3: Split Cylinder Test Data

SAMPLE NO. 1s

Vertical Def. Rate = 0.250 in/min
Temperature = -6.06°C
Sample Height = 2.00"
Sample Diameter = 4.00"
Percent Sand (by Vol.) = 64.57
Degree Ice Saturation (%) = 97.90

Load (lbs.)	Vert. Def. (in.)	Horiz. Def. (in.)	Time (sec)
1.70	0.0800	---	---

Recorder Malfunction - No Additional Data Points.

SAMPLE NO. 2s

Vertical Def. Rate = 0.250 in/min
Temperature = -5.96°C
Sample Height = 2.00"
Sample Diameter = 4.00"
Percent Sand (by Vol.) = 63.68
Degree Ice Saturation (%) = 96.57

Load (lbs.)	Vert. Def. (in.)	Horiz. Def. (in.)	Time (sec)
276	0.0045	0.00000	0.60
539	0.0071	0.00000	1.20
843	0.0097	0.00000	1.80
1189	0.0113	0.00000	2.40
1617	0.0138	0.00000	3.00
1907	0.0161	0.00010	3.60
2474	0.0189	0.00010	4.20
2902	0.0213	0.00030	4.80
3317	0.0235	0.00040	5.40
3718	0.0258	0.00070	6.00
4229	0.0289	0.00080	6.76

SAMPLE NO. 3s

Vertical Def. Rate = 0.050 in/min
Temperature = -5.99°C
Sample Height = 2.00"
Sample Diameter = 4.00"
Percent Sand (by Vol.) = 65.21
Degree Ice Saturation (%) = 97.10

Load (lbs.)	Vert. Def. (in.)	Horiz. Def. (in.)	Time (sec)
76	0.0059	0.00007	6.00
228	0.0101	0.00007	10.00
553	0.0123	0.00013	14.00
898	0.0146	0.00013	18.00
1410	0.0172	0.00019	22.00
1935	0.0201	0.00027	26.00
2405	0.0232	0.00047	30.00
2723	0.0256	0.00060	34.00
3137	0.0283	0.00079	38.00
3510	0.0319	0.00113	42.00
3787	0.0361	0.00139	46.00
4119	0.0444	0.00233	53.00

SAMPLE NO. 4s

Vertical Def. Rate = 0.002 in/min
Temperature = -5.96°C
Sample Height = 2.00"
Sample Diameter = 4.00"
Percent Sand (by Vol.) = 65.27
Degree Ice Saturation (%) = 97.66

Load (lbs.)	Vert. Def. (in.)	Horiz. Def. (in.)	Time (sec)
54	0.0004	0.00027	32.00
256	0.0033	0.00087	152.00
408	0.0063	0.00133	242.00
492	0.0121	0.00220	292.00
871	0.0213	0.00373	517.00
1382	0.0339	0.00733	742.00
1714	0.0469	0.01092	967.00
1824	0.0552	0.01239	1092.00
2211	0.0798	0.02224	1892.00
2681	0.1143	0.04229	2342.00
3096	0.1771	0.08658	2792.00
2764	0.2366	0.11655	3172.00

-- No Tensile Split Developed --

SAMPLE NO. 5s

Vertical Def. Rate = 0.002 in/min
Temperature = -5.99°C
Sample Height = 2.00"
Sample Diameter = 4.00"
Percent Sand (by Vol.) = 64.58
Degree Ice Saturation (%) = 97.18

Load (lbs.)	Vert. Def. (in.)	Horiz. Def. (in.)	Time (sec)
55	0.0004	0.00020	32.00
253	0.0034	0.00073	151.00
409	0.0063	0.00140	241.00

Table A-2 (cont'd.)

SAMPLE NO. 5s (cont'd.)

477	0.0123	0.00206	293.00
871	0.0214	0.00366	516.00
1409	0.0337	0.00733	741.00
1699	0.0468	0.01079	966.00
1838	0.0551	0.01252	1093.00
2267	0.0794	0.02211	1894.00
2654	0.1139	0.04196	2340.00
3096	0.1765	0.08725	2791.00
2792	0.2359	0.11790	3170.00

-- No Tensile Split Developed --

SAMPLE NO. 6s

Vertical Def. Rate = 0.083 in/min
Temperature = -5.99°C
Sample Height = 2.00"
Sample Diameter = 4.00"
Percent Sand (by Vol.) = 64.53
Degree Ice Saturation (%) = 97.63

Load (lbs.)	Vert. Def. (in.)	Horiz. Def. (in.)	Time (sec)
202	0.0003	0.00036	1.00
663	0.0018	0.00073	3.00
1265	0.0036	0.00102	5.00
1831	0.0058	0.00113	7.00
2370	0.0083	0.00128	9.00
2930	0.0107	0.00135	11.00
3497	0.0137	0.00135	13.00
4036	0.0171	0.00139	15.00
4464	0.0214	0.00146	17.00
4671	0.0250	0.00154	18.40

SAMPLE NO. 7s

Vertical Def. Rate = 0.143 in/min
Temperature = -5.96°C
Sample Height = 2.00"
Sample Diameter = 4.00"
Percent Sand (by Vol.) = 65.29
Degree Ice Saturation (%) = 97.49

Load (lbs.)	Vert. Def. (in.)	Horiz. Def. (in.)	Time (sec)
380	0.0010	---	1.00
843	0.0033	---	2.00
1424	0.0050	---	3.00
1976	0.0070	---	4.00
2640	0.0092	---	5.00
3206	0.0116	---	6.00

SAMPLE NO. 7s (cont'd.)

3842	0.0143	---	7.00
4312	0.0174	---	8.00
4948	0.0217	---	9.10

--- LADT Not Operating ---

SAMPLE NO. 8s

Vertical Def. Rate = 0.144 in/min
Temperature = -5.93°C
Sample Height = 2.00"
Sample Diameter = 4.00"
Percent Sand (by Vol.) = 65.70
Degree Ice Saturation (%) = 97.58

Load (lbs.)	Vert. Def. (in.)	Horiz. Def. (in.)	Time (sec)
58	0.0018	---	0.74
130	0.0044	---	1.82
224	0.0069	---	2.88
423	0.0080	---	3.36
830	0.0096	---	4.02
1189	0.0109	---	4.54
1652	0.0126	---	5.28
2156	0.0147	---	6.14
2778	0.0172	---	7.19
3372	0.0198	---	8.28
3980	0.0228	---	9.55
4450	0.0253	---	10.56
4782	0.0275	---	11.50
5058	0.0296	---	12.40

--- LADT Not Operating ---

SAMPLE NO. 9s

Vertical Def. Rate = 0.092 in/min
Temperature = -5.93°C
Sample Height = 2.00"
Sample Diameter = 4.00"
Percent Sand (by Vol.) = 65.21
Degree Ice Saturation (%) = 97.48

Load (lbs.)	Vert. Def. (in.)	Horiz. Def. (in.)	Time (sec)
102	0.0031	---	2.00
213	0.0081	---	4.00
539	0.0108	---	6.00
1030	0.0128	---	8.00
1589	0.0147	---	10.00
2211	0.0170	---	12.00

Table A-3 (cont'd.)

SAMPLE NO. 9s (cont'd.)

2792	0.0192	---	14.00
3399	0.0220	---	16.00
3953	0.0251	---	18.00
4395	0.0293	---	20.00
4699	0.0335	---	21.80

--- LADT Not Operating ---

SAMPLE NO. 10s

Vertical Def. Rate = -0.053 in/min
Temperature = -6.00°C
Sample Height = 2.00"
Sample Diameter = 4.00"
Percent Sand (by Vol.) = 63.86
Degree Ice Saturation (%) = 97.14

Load (lbs.)	Vert. Def. (in.)	Horiz. Def. (in.)	Time (sec)
91	0.0045	---	4.00
362	0.0076	---	9.00
658	0.0100	---	13.00
961	0.0118	---	17.00
1299	0.0146	---	21.00
1659	0.0178	---	25.00
2128	0.0220	---	29.00
2626	0.0272	---	34.00
3054	0.0319	---	39.00
3455	0.0368	---	44.00
3897	0.0425	---	49.00
4146	0.0466	---	54.00
4174	0.0489	---	55.00

--- LADT Not Operating ---

SAMPLE NO. 11s

Vertical Def. Rate = 0.100 in/min
Temperature = -5.90°C
Sample Height = 2.00"
Sample Diameter = 4.00"
Percent Sand (by Vol.) = 64.17
Degree Ice Saturation (%) = 96.65

Load (lbs.)	Vert. Def. (in.)	Horiz. Def. (in.)	Time (sec)
160	0.0046	---	3.40
362	0.0100	---	7.40
636	0.0153	---	11.40
1126	0.0204	---	15.40
1652	0.0262	---	19.40

SAMPLE NO. 11s (cont'd.)

2169	0.0352	---	23.40
2688	0.0434	---	27.40
3441	0.0500	---	31.41
4146	0.0564	---	35.41
4824	0.0646	---	39.41
4948	0.0671	---	40.41

--- LADT Not Operating ---

SAMPLE NO. 12s

Vertical Def. Rate = 0.192 in/min
Temperature = -5.90°C
Sample Height = 2.00"
Sample Diameter = 4.00"
Percent Sand (by Vol.) = 64.49
Degree Ice Saturation(%) = 97.01

Load (lbs.)	Vert. Def. (in.)	Horiz. Def. (in.)	Time (sec)
66	0.0031	---	0.72
196	0.0067	---	1.52
547	0.0077	---	2.32
974	0.0089	---	3.12
1548	0.0107	---	3.92
2128	0.0134	---	4.72
2750	0.0158	---	5.52
3372	0.0179	---	6.32
3939	0.0206	---	7.12
4478	0.0239	---	7.92
4920	0.0277	---	8.64

--- LADT Not Operating ---

SAMPLE NO. 13s

Vertical Def. Rate = 0.256 in/min
Temperature = -6.09°C
Sample Height = 2.00"
Sample Diameter = 4.00"
Percent Sand (by Vol.) = 64.58
Degree Ice Saturation (%) = 97.00

Load (lbs.)	Vert. Def. (in.)	Horiz. Def. (in.)	Time (sec)
332	0.0028	---	0.54
815	0.0040	---	0.99
1306	0.0051	---	1.45
1838	0.0064	---	1.90
2335	0.0080	---	2.36

Table A-3 (cont'd.)

SAMPLE NO. 13s (cont'd.)

2861	0.0098	---	2.81
3552	0.0118	---	3.26
4063	0.0138	---	3.72
4644	0.0165	---	4.17
5114	0.0196	---	4.59

---LADT Not Operating ---

SAMPLE NO. 14s

Vertical Def. Rate = 0.250 in/min
Temperature = -10.09°C
Sample Height = 2.00"
Sample Diameter = 4.00"
Percent Sand (by Vol.) = 64.63
Degree Ice Saturation (%) = 97.23

Load (lbs.)	Vert. Def. (in.)	Horiz. Def. (in.)	Time (sec)
166	0.0038	0.00036	0.60
357	0.0071	0.00089	1.07
699	0.0093	0.00089	1.54
1126	0.0114	0.00080	2.02
1652	0.0126	0.00071	2.49
2211	0.0142	0.00062	2.96
2737	0.0159	0.00062	3.92
3289	0.0180	0.00071	4.39
3870	0.0201	0.00089	4.86
4395	0.0223	0.00098	5.33
4699	0.0234	0.00107	5.62

SAMPLE NO. 15s

Vertical Def. Rate = 0.185 in/min
Temperature = -10.09°C
Sample Height = 2.00"
Sample Diameter = 2.00"
Percent Sand (by Vol.) = 64.54
Degree Ice Saturation (%) = 97.53

Load (lbs.)	Vert. Def. (in.)	Horiz. Def. (in.)	Time (sec)
464	0.0011	0.00009	0.67
1030	0.0025	0.00018	1.29
1603	0.0040	0.00036	1.91
2198	0.0053	0.00053	2.52
2819	0.0071	0.00071	3.14
3441	0.0091	0.00089	3.76
4174	0.0107	0.00098	4.37
4754	0.0130	0.00116	4.98

SAMPLE NO. 15s (cont'd.)

5363	0.0153	0.00124	5.60
5888	0.0178	0.00133	6.22
6164	0.0194	0.00169	6.56

SAMPLE NO. 16s

Vertical Def. Rate = 0.146 in/min
Temperature = -10.10°C
Sample Height = 2.00"
Sample Diameter = 4.00"
Percent Sand (by Vol.) = 64.67
Degree Ice Saturation (%) = 97.19

Load (lbs.)	Vert. Def. (in.)	Horiz. Def. (in.)	Time (sec)
235	0.0002	0.00044	1.10
500	0.0002	0.00071	2.10
1009	0.0011	0.00089	3.10
1506	0.0028	0.00098	4.10
2128	0.0045	0.00133	5.10
2889	0.0065	0.00160	6.10
3524	0.0086	0.00160	7.10
4132	0.0112	0.00160	8.10
4948	0.0138	0.00160	9.10
5473	0.0245	0.00160	10.10
5860	0.0263	0.00160	10.80

SAMPLE NO. 17s

Vertical Def. Rate = 0.100 in/min
Temperature = -9.99°C
Sample Height = 2.00"
Sample Diameter = 4.00"
Percent Sand (by Vol.) = 64.93
Degree Ice Saturation (%) = 98.45

Load (lbs.)	Vert. Def. (in.)	Horiz. Def. (in.)	Time (sec)
246	0.0036	0.00009	1.80
556	0.0051	0.00018	3.30
1057	0.0064	0.00027	4.80
1652	0.0088	0.00053	6.30
2529	0.0112	0.00080	7.80
3262	0.0137	0.00089	9.30
3967	0.0164	0.00098	10.80
4865	0.0192	0.00116	12.30
5501	0.0227	0.00124	13.80
5832	0.0242	0.00133	14.50

Table A-3 (cont'd.)

SAMPLE NO. 18s

Vertical Def. Rate = 0.072 in/min
Temperature = -9.99°C
Sample Height = 2.00"
Sample Diameter = 4.00"
Percent Sand (by Vol.) = 64.18
Degree Ice Saturation (%) = 97.42

Load (lbs.)	Vert. Def. (in.)	Horiz. Def. (in.)	Time (sec)
268	0.0012	0.00000	2.30
603	0.0022	0.00000	4.30
962	0.0038	0.00009	6.30
1569	0.0064	0.00018	8.30
2170	0.0085	0.00027	10.30
2999	0.0110	0.00036	12.30
3455	0.0137	0.00044	14.30
4050	0.0165	0.00071	16.30
4754	0.0198	0.00089	18.30
5252	0.0240	0.00098	20.30
5528	0.0261	0.00107	21.60

SAMPLE NO. 19s

Vertical Def. Rate = 0.043 in/min
Temperature = -10.08°C
Sample Height = 2.00"
Sample Diameter = 4.00"
Percent Sand (by Vol.) = 64.95
Degree Ice Saturation (%) = 98.37

Load (lbs.)	Vert. Def. (in.)	Horiz. Def. (in.)	Time (sec)
340	0.0011	0.00000	5.30
702	0.0041	0.00000	10.30
1189	0.0069	0.00009	15.30
1721	0.0100	0.00027	20.30
2253	0.0135	0.00036	25.30
2778	0.0171	0.00071	30.30
3317	0.0211	0.00089	35.30
3842	0.0248	0.00098	40.30
4298	0.0294	0.00116	45.30
4658	0.0325	0.00142	49.20

SAMPLE NO. 20s

Vertical Def. Rate = 0.230 in/min
Temperature = -10.01°C
Sample Height = 2.00"
Sample Diameter = 4.00"
Percent Sand (by Vol.) = 64.45

SAMPLE NO. 20s (cont'd.)

Degree Ice Saturation (%) = 97.13

Load (lbs.)	Vert. Def. (in.)	Horiz. Def. (in.)	Time (sec)
254	0.0019	0.00044	0.48
586	0.0029	0.00062	0.76
1106	0.0047	0.00080	1.21
1728	0.0056	0.00080	1.46
2336	0.0069	0.00089	1.80
2902	0.0084	0.00098	2.20
3455	0.0102	0.00107	2.64
4036	0.0119	0.00116	3.09
4561	0.0137	0.00142	3.58
5667	0.0179	0.00160	4.66

SAMPLE NO. 21s

Vertical Def. Rate = 0.222 in/min
Temperature = -15.05°C
Sample Height = 2.00"
Sample Diameter = 4.00"
Percent Sand (by Vol.) = 64.15
Degree Ice Saturation (%) = 96.89

Load (lbs.)	Vert. Def. (in.)	Horiz. Def. (in.)	Time (sec)
177	0.0034	0.00009	0.92
608	0.0059	0.00018	1.59
1099	0.0077	0.00027	2.08
1797	0.0093	0.00027	2.52
2571	0.0112	0.00036	3.11
3359	0.0132	0.00044	3.56
4146	0.0152	0.00053	4.11
5058	0.0173	0.00071	4.66
5750	0.0198	0.00080	5.35
6634	0.0236	0.00089	6.37

SAMPLE NO. 22s

Vertical Def. Rate = 0.133 in/min
Temperature = -15.05°C
Sample Height = 2.00'
Sample Diameter = 4.00"
Percent Sand (by Vol.) = 64.81
Degree Ice Saturation (%) = 98.09

Load (lbs.)	Vert. Def. (in.)	Horiz. Def. (in.)	Time (sec)
149	0.00184	0.00009	0.80
470	0.00254	0.00018	1.60

Table A-3 (cont'd.)

SAMPLE NO. 22s (cont'd.)

961	0.0034	0.00018	2.40
1500	0.0046	0.00027	3.20
2377	0.0070	0.00036	4.20
3220	0.0091	0.00044	5.20
4050	0.0115	0.00053	6.20
5031	0.0141	0.00062	7.20
5998	0.0174	0.00080	8.40
6828	0.0212	0.00098	9.60

SAMPLE NO. 23s

Vertical Def. Rate = 0.160 in/min
Temperature = -15.05°C
Sample Height = 2.00"
Sample Diameter 4.00"
Percent Sand (by Vol.) = 64.58
Degree Ice Saturation (%) = 97.61

Load (lbs.)	Vert. Def. (in.)	Horiz. Def. (in.)	Time (sec)
304	0.0056	0.00018	1.31
967	0.0078	0.00027	2.13
1520	0.0096	0.00044	2.94
2080	0.0113	0.00071	3.76
3013	0.0131	0.00089	4.58
3455	0.0149	0.00107	5.39
4008	0.0172	0.00116	6.21
4602	0.0192	0.00124	7.03
5667	0.0212	0.00142	7.85
6496	0.0240	0.00169	8.99

SAMPLE NO. 24s

Vertical Def. Rate = 0.106 in/min
Temperature = -14.95°C
Sample Height = 2.00"
Sample Diameter = 4.00"
Percent Sand (by Vol.) = 64.75
Degree Ice Saturation (%) = ∿100.00

Load (lbs.)	Vert. Def. (in.)	Horiz. Def. (in.)	Time (sec)
207	0.0030	0.00000	1.00
504	0.0054	0.00000	1.80
1140	0.0077	0.00000	3.00
1769	0.0089	0.00000	4.20
2709	0.0100	0.00000	5.40
3869	0.0118	0.00000	6.60
4948	0.0141	0.00000	7.80
5943	0.0157	0.00000	8.80

SAMPLE NO. 24s (cont'd.)

6496	0.0172	0.00000	9.60
6634	0.0175	0.00000	9.92

SAMPLE NO. 25s

Vertical Def. Rate = 0.034 in/min
Temperature = -14.93°C
Sample Height = 2.00"
Sample Diameter = 4.00"
Percent Sand (by Vol.) = 64.69
Degree Ice Saturation (%) = 98.02

Load (lbs.)	Vert. Def. (in.)	Horiz. Def. (in.)	Time (sec)
111	0.0020	0.00009	3.60
243	0.0051	0.00027	7.60
451	0.0078	0.00036	11.60
829	0.0090	0.00044	15.60
1341	0.0106	0.00053	19.60
1852	0.0126	0.00062	21.70
2972	0.0164	0.00080	29.70
4050	0.0208	0.00098	37.70
5141	0.0251	0.00107	45.70
6026	0.0312	0.00124	54.30

SAMPLE NO. 26s

Vertical Def. Rate = 0.075 in/min
Temperature = -14.95°C
Sample Height = 2.00"
Sample Diameter = 4.00"
Percent Sand (by Vol.) = 64.67
Degree Ice Saturation (%) = 96.92

Load (lbs.)	Vert. Def. (in.)	Horiz. Def. (in.)	Time (sec)
80	0.0021	0.00036	1.00
285	0.0058	0.00053	3.00
1023	0.0081	0.00071	6.00
1935	0.0112	0.00080	9.00
2944	0.0141	0.00089	12.00
3967	0.0174	0.00089	15.00
4906	0.0212	0.00098	18.00
5832	0.0257	0.00107	21.00
6219	0.0283	0.00116	22.80

Table A-3 (cont'd.)

SAMPLE NO. 27s

Vertical Def. Rate = 0.002 in/min
Temperature = -14.95°C
Sample Height = 2.00"
Sample Diameter = 4.00"
Percent Sand (by Vol.) = 64.69
Degree Ice Saturation (%) = 98.44

Load (lbs.)	Vert. Def. (in.)	Horiz. Def. (in.)	Time (sec)
207	0.0000	0.00000	85.00
558	0.0003	0.00000	190.00
1216	0.0028	0.00000	305.00
1949	0.0059	0.00000	425.00
2902	0.0099	0.00062	590.00
3635	0.0142	0.00151	740.00
4533	0.0184	0.00409	905.00
4920	0.0243	0.00480	1025.00
5169	0.0317	0.00640	1155.00
5224	0.0394	0.00738	1275.00

SAMPLE NO. 28s

Vertical Def. Rate = 0,002 in/min
Temperature = -14.95°C
Sample Height = 2.00"
Sample Diameter = 4.00"
Percent Sand (by Vol.) =
Degree Ice Saturation (%) = 98.09

Load (lbs.)	Vert. Def. (in.)	Horiz. Def. (in.)	Time (sec)
210	0.0028	0.00044	85.00
556	0.0058	0.00089	191.00
1223	0.0092	0.00151	305.00
1956	0.0128	0.00213	426.00
2916	0.0180	0.00293	592.00
3607	0.0226	0.00373	742.00
4561	0.0273	0.00453	907.00
4920	0.0314	0.00616	1028.00
5197	0.0356	0.00587	1160.00
5252	0.0397	0.00622	1280.00
5197	0.0436	0.00702	1400.00
5141	0.0477	0.00782	1520.00

SAMPLE NO. 29s

Vertical Def. Rate = 0.016 in/min
Temperature = -1.96°C
Sample Height = 2.00"
Sample Diameter = 4.00"

SAMPLE NO. 29s (cont'd.)

Percent Sand (by Vol.) = 64.28
Degree Ice Saturation (%) = 96.95

Load (lbs.)	Vert. Def. (in.)	Horiz. Def. (in.)	Time (sec)
133	0.0012	0.00009	1.00
376	0.0031	0.00018	2.00
670	0.0055	0.00036	3.00
967	0.0084	0.00053	4.00
1272	0.0113	0.00071	5.00
1576	0.0140	0.00089	6.00
1852	0.0168	0.00098	7.00
2156	0.0207	0.00116	8.00
2460	0.0236	0.00142	9.00
2737	0.0270	0.00151	10.00
3040	0.0283	0.00160	10.44

SAMPLE NO. 30s

Vertical Def. Rate = 0.280 in/min
Temperature = -1.96°C
Sample Height = 2.00"
Sample Diameter = 4.00"
Percent Sand (by Vol.) = 65.31
Degree Ice Saturation (%) = 98.55

Load (lbs.)	Vert. Def. (in.)	Horiz. Def. (in.)	Time (sec)
188	0.0037	0.00009	1.11
406	0.0077	0.00018	2.23
545	0.0131	0.00027	3.35
643	0.0200	0.00053	4.47
967	0.0257	0.00071	5.58
1320	0.0324	0.00089	6.70
1755	0.0372	0.00098	7.82
2280	0.0443	0.00107	9.49
2806	0.0504	0.00124	10.88
3110	0.0560	0.00142	12.01

SAMPLE NO. 31s

Vertical Def. Rate = 0.058 in/min
Temperature = -1.96°C
Sample Height = 2.00"
Sample Diameter = 4.00"
Percent Sand (by Vol.) = 64.88
Degree Ice Saturation (%) =99.37

Table A-3 (cont'd.)

SAMPLE NO. 31s

Load (lbs.)	Vert. Def. (in.)	Horiz. Def. (in.)	Time (sec)
64	0.0021	0.00000	2.00
199	0.0049	0.00007	6.00
486	0.0073	0.00007	10.00
760	0.0097	0.00007	14.00
1050	0.0129	0.00013	18.00
1465	0.0185	0.00020	24.00
1886	0.0246	0.00033	30.00
2301	0.0311	0.00053	36.00
2640	0.0383	0.00067	42.00
2833	0.0469	0.00073	48.00
2902	0.0484	0.00073	49.40

SAMPLE NO. 32s

Vertical Def. Rate = 0.085 in/min
Temperature = -6.03°C
Sample Height = 1.20"
Sample Diameter = 2.40"
Percent Sand (by Vol.) = 64.42
Degree Ice Saturation (%) = 99.36

Load (lbs.)	Vert. Def. (in.)	Horiz. Def. (in.)	Time (sec)
55	0.0017	---	1.00
97	0.0029	---	2.00
366	0.0057	---	4.00
518	0.0072	---	5.00
677	0.0084	---	6.00
802	0.0093	---	7.00
926	0.0113	---	8.00
1223	0.0138	---	10.00
1499	0.0165	---	12.00
1811	0.0198	---	14.00

---LADT Not Used ---

SAMPLE NO. 33s

Vertical Def. Rate = 0.070 in/min
Temperature = -5.99°C
Sample Height = 1.20"
Sample Diameter = 2.40"
Percent Sand (by Vol.) = 64.07
Degree Ice Saturation (%) = 98.48

SAMPLE NO. 33s (cont'd.)

Load (lbs.)	Vert. Def. (in.)	Horiz. Def. (in.)	Time (sec)
283	0.0022	---	2.00
428	0.0032	---	3.00
539	0.0044	---	4.00
753	0.0058	---	5.50
954	0.0076	---	7.00
1133	0.0092	---	8.50
1340	0.0108	---	10.00
1527	0.0118	---	11.00
1672	0.0127	---	12.00
1817	0.0139	---	12.80

--- LADT Not Used ---

SAMPLE NO. 34s

Vertical Def. Rate = 0.069 in/min
Temperature = -5.96°C
Sample Height = 0.97"
Sample Diameter = 1.94"
Percent Sand (by Vol.) = 64.04
Degree Ice Saturation (%) = 97.72

Load (lbs.)	Vert. Def. (in.)	Horiz. Def. (in.)	Time (sec)
97	0.0014	---	1.00
200	0.0028	---	2.00
297	0.0043	---	3.00
401	0.0057	---	4.00
498	0.0072	---	5.00
594	0.0086	---	6.00
698	0.0100	---	7.00
795	0.0115	---	8.00
995	0.0143	---	10.00
1175	0.0137	---	11.90

--- LADT Not Used ---

SAMPLE NO. 35s

Vertical Def. Rate = 0.066 in/min
Temperature = -6.03°C
Sample Height = 0.97"
Sample Diameter = 1.94"
Percent Sand (by Vol.) = 64.10
Degree Ice Saturation (%) = 98.75

Table A-3 (cont'd.)

SAMPLE NO. 35 (cont'd.)

Load (lbs.)	Vert. Def. (in.)	Horiz. Def. (in.)	Time (sec)
97	0.0014	---	1.00
200	0.0028	---	2.00
297	0.0042	---	3.00
401	0.0056	---	4.00
498	0.0069	---	5.00
609	0.0083	---	6.00
698	0.0097	---	7.00
802	0.0111	---	8.00
1002	0.0139	---	10.00
1133	0.0125	---	11.33

BIBLIOGRAPHY

BIBLIOGRAPHY

Akazawa, T., "Tension Test Method for Concrete", Bulletin No. 16, Int. Assoc. of Testing and Research Lab. for Mat. and Struct., Paris, (November 1953), pp. 11-23.

Alkire, B. D., "Mechanical Properties of Sand-Ice Materials", Unpublished Ph.D. Dissertation, Michigan State University, East Lansing, 1972.

Alkire, B. D., and Andersland, O. B., "The Effect of Confining Pressure on the Mechanical Properties of Sand-Ice Materials", J. Glaciology, 12(16), 1972.

Anagnos, J. N., and Kennedy, T. W., "Practical Method of Conducting the Indirect Tensile Test", Research Report 98-10, Center for Highway Research, The University of Texas at Austin, August 1972.

Andersland, O. B., and AlNouri, I., "Time-Dependent Strength Behavior of Frozen Soil", J. Soil Mech. Found. Div. Am. Soc. Civ. Eng., 96(SM4), 1970.

Andersland, O. B., Sayles, F. H., and Ladanyi, B., "Chapter 5: Mechanical Properties of Frozen Ground", Geotechnical Engineering for Cold Regions, O. B. Andersland and D. M. Anderson, eds., New York: McGraw-Hill Book Co., Inc., 1978.

Anderson, D. M., "Ice Nucleation and the Substrate-Ice Interface," Nature, CCXVI (November, 1967).

Anderson, D. M., Pusch, R. and Penner, E., "Chapter 2; Physical and Thermal Properties of Frozen Ground", Geotechnical Engineering For Cold Regions, O.B. Andersland and D. M. Anderson, eds., New York: McGraw-Hill Book Co., Inc., 1978.

Anderson, D. M. and Tice, A . R., "Predicting Unfrozen Water Contents in Frozen Soils from Surface Area Measurements," Highway Research Record, No. 393, 1972, 12-18.

Baker, T. H. W., "Effect of End Conditions on the Uniaxial Compressive Strength of Frozen Sand", Proc. 3rd Int. Conf. on Permafrost, Ed mouton, Alberta, 1978a, Vol. 1: pp.608-614.

Baker, T. H. W., Strain Rate Effects on the Compressive Strength of Frozen Sand", Engineering Geology, 13 (1978b) 223-231.

Carniero, F. and Barcellos, A., "Concrete Tensile Strength", Bulletin No. 13, Int. Assoc. of Testing and Research Lab. for Mat. and Struct., Paris, (March 1953). pp. 97-127.

Chen, W. and Chang, T., "Plasticity Solution of Concrete Splitting Tests", J. Eng. Mech. Div. Am. Soc. Civ. Eng., 104(EM3), 1978.

Daniel, E. E., and Olson, R. E., "Stress-Strain Properties of Compacted Clays", J. Geotech. Eng. Div. Am. Soc. Civ. Eng., 100(GT10), 1974.

Dillion, H. B. and Andersland, O. B., "Predicting Unfrozen Water Contents in Frozen Soils," Canadian Geotechnical Journal, III, (February 1966), 53-60.

Duncan, J. M., and Chang, C. Y., "Nonlinear Analysis of Stress and Strain in Soils", J. Soil Mech. and Found. Div. Soc. Civ. Eng., 96(SM5), 1970.

Fairhurst, C., "On the Validity of the Brazilian Test for Brittle Mateirals", Int. J. Rock Mech. Mining Sci., 1 (1964) pp. 535-546.

Frocht, M. M., Photoelasticity, Vol. 2, New York: John Wiley and Sons, Inc., 1957.

Goughnour, R. R., "The Soil-Ice System and the Shear Strength of Frozen Soils", Unpublished Ph.D. Dissertation, Michigan State University, East Lansing, 1967.

Goughnour, R. R., and Andersland, O.B., "Mechanical Properties of a Sand-Ice System", J. Soil Mech. Found. Div. Am. Soc. Civ. Eng., 94(SM4), 1968.

Grieb, W. E. and Werner, G., "Comparison of the Splitting Tensile Strength of Concrete with Flexural and Compressive Strengths", Public Roads, Vol. 32 (December 1962). pp. 97-106.

Hadley, W. O., Hudson, W. R., and Kennedy, T. W., "Evaluation and Predication of the Tensile Properties of Asphalt-Treated Materials", Research Report 98-9, Center for Highway Research, The University Of Texas at Austin, May 1971.

Hawkes, I., and Mellor, M., "Deformation and Fracture of Ice Under Uniaxial Stress", J. of Glaciology, Vol. 11, No. 71, 1972.

Hawkes, I., and Mellor, M., "Uniaxial Testing in Rock Mechanics Laboratories", Eng. Geology, Vol, 4, 1970.

Haynes, F. D., "Tensile Strength of Ice Under Triaxial Stresses", Technical Note, U.S. Army Cold Regions Research and Engineering Laboratory, Hanover, New Hampshire, 1973.

Haynes, F. D., Karalius, J. A., and Kalafut, J., "Strain RAte Effect on the Strength of Frozen Silt", Research Report 350, U. S. Army Cold Region Research and Engineering Laboratory, Hanover, New Hampshire, 1975.

Houdros, G., "The Evaluation of Poisson's Ratio and the Modulus of Materials of a Low Tensile Resistance by the Brazilian Indirect Tensile Test with Particular Reference to Concrete", Australian J. Applied Sci., 10 (1959), pp. 243-268.

Hudson, W. R. and Kennedy, T. W., "An Indirect Tensile Test for Stabilized Materials", Research Report 98-1, Center for Highway Research, The University of Texas at Austin, January 1968.

Hult, J. A. H., Creep in Engineering Structures. Waltham, Mass: Blaisdell Publishing Company, 1966.

Klein, J. and Jessberger, H. L., "Creep Stress Analysis of Frozen Soils under Multiaxial States of Stress", Proc. 1st Int. Symp: on Ground Freezing, Bochum, Germany, 1978.

Ladanyi, B., "An Engineering Theory of Creep of Frozen Soils," Canadian Geotechnical Journal, Vol. 9, No. 1 (February 1972), 63-80.

Ladanyi, B. and Arteau, J., "Effect of Specimen Shape on Creep Response of a Frozen Sand", Proc. 1st Int. Symp. on Ground Freezing, Bochum, Germany,1978.

Leonards, G. A. and Andersland, O. B., "The Clay-Water System and the Shearing Resistance of Clays", Proc. Conf. on Shear Strength of Cohesive Soils, ASCE, University of Colorado, Boulder, Colorado, 1960, pp. 793-818.

Lovell, C. S. "Temperature Effects on Phase Composition and Strength of Partially Frozen Soil", Bulletin 168, Highway Research Board, Washington, D.C., 1957.

Mellor, M. and Hawkes, I., "Measurements of Tensile Strength by Diametrical Compression of Disk and Annuli", Eng. Geology, Vol. 5, No. 3, (1971), pp. 173-225.

Mitchell, N. B., "The Indirect Tension Test for Concrete", Materials Research and Standards, (October 1961), pp. 780-787.

Offensend, F. L., "The Tensile Strength of Frozen Soils", Technicial Note, U.S. Army Cold Regions Research and Engineering Laboratory, Hanover, New Hampshire, 1966.

Odqvist, F. K. G., Mathematical Theory of Creep and Creep Rupture. London: Oxford University Press, 1966.

Parameswaran, V. R., "Deformation Behavior and Strength of Frozen Sand", Canadian Geotechnical J., 17 (1980), 74-88.

Perkins, T. K. and Ruedrich, R. A., "The Mechanical Behavior of Synthetic Permafrost", Soc. Petrol. Eng. J., (Aug 1973), 211-220.

Perloff, W. H. and Baron, W., Soil Mechanics, New York: The Ronald Press Company, 1976.

Popov, E. P., Introduction to Mechanics of Solids, Englewood Cliffs: Prentice-Hall, Inc., 1968.

Pounder, E. R., The Physics of Ice, Oxford: Pergamon Press, 1967.

Sayles, F. H., "Creep of Frozen Sand", Technical Report 190, U. S. Army Cold Regions Research and Engineering Laboratory, Hanover, New Hampshire, 1968.

Sayles, F. H., "Low Temperature Soil Mechanics", Technical Note, U.S. Army Cold Regions Research and Engineering Laboratory, Hanover, New Hampshire, 1966.

Sayles, F. H., "Triaxial and Creep Test on Frozen Ottawa Sand", Technical Report 253, U.S. Army Cold Regions Research and Engineering Laboratory, Hanover, New Hampshire, 1974.

Sayles, F. H. and Epanchin, N. V., "Rate of Strain Compression Tests on Frozen Ottawa Sand and Ice", Technical Note, U.S. Army Cold Regions Research and Engineering Laboratory, Hanover, New Hampshire, 1966.

Timoshenko, S. and Goodier, J. N., "Stresses in a Circular Disk", Theory of Elasticity, 2nd E., McGraw-Hill Book Co., Inc., New York, 1951.

Tsytovich, N. A., "Bases and Foundations on Frozen Soils", Highway Research Board, Tr. Spec. Rpt, 58, 1955.

Vyalov, S. S., "Rheological Properties and Bearing Capacity of Frozen Soils", Translation 74, U.S. Army Cold Regions Research and Engineering Laboratory, Hanover, New Hampshire, 1959.

Vyalov, S. S. "Rheology of Frozen Soils," Proc. 1st Int. Conf. Permafrost, Lafayette, Ind., 1963, NAS-NRC Pub. 1287, pp. 332-337.

Vyalov, S. S., "The Strength and Creep of Frozen Soils and Calculations for Ice-Soil Retaining Structures", Translation 76, Cold Regions Research and Engineering Laboratory, Hanover, New Hampshire, 1962.

Williams, P. J., "Unfrozen Water Content of Frozen Soils and Soil Moisture Suction", Geotechnique, XIV (March 1964), pp. 231-246.

Wright, P. J. F., "Comments on the Indirect Tensile Test on Concrete Cylinders", Magazine of Concrete Research, July 1955.

MICHIGAN STATE UNIV. LIBRARIES
31293102117201